AD-A111 012 CORNELL UNIV ITHACA N Y DEPT OF STRUCTURAL ENGINEERING F/G 12/1
FINITE ELEMENT ANALYSIS OF MAGNETOELASTIC PLATE PROBLEMS.(U)
AUG 81 K Y YUAN N00014-79-C-0224
UNCLASSIFIED 81-14 NL

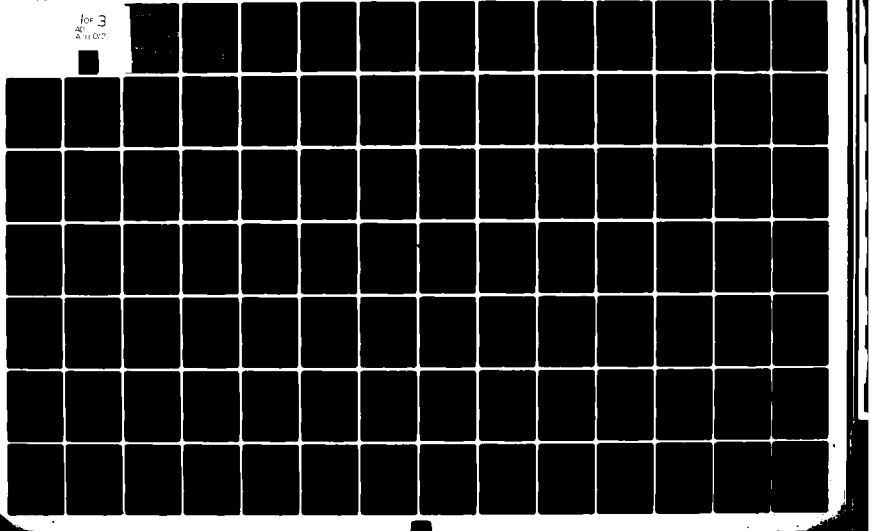

(12) LEVEL II

Cornell University

Magnetomechanics Research

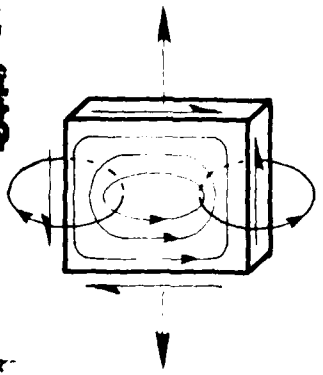

Departments of
Theoretical & Applied
Mechanics
and
Structural Engineering

(12) LEVEL II

Technical Report

FINITE ELEMENT ANALYSIS OF MAGNETOELASTIC PLATE PROBLEMS

K.Y. Yuan

Department of Structural Engineering Report
Number 81-14

submitted to the
Office of Naval Research
Structural Mechanics Program, Material Sciences Division
ONR Contract No. N00014-79-C-0224
Task No. NR 064-621

Departments of Structural Engineering
and Theoretical & Applied Mechanics
Cornell University
Ithaca, New York 14853

August 1981

ACKNOWLEDGEMENTS

This report is essentially a reproduction of the thesis submitted by the author in partial fulfillment for the degree of Doctor of Philosophy. However, Kosei Hara did the search coil and low inductance strain gage experiments as well as the parameter studies related to nondimensionalization. Tim Bond performed the infrared experiments. The research was supervised by Professors John F. Abel and Francis C. Moon.

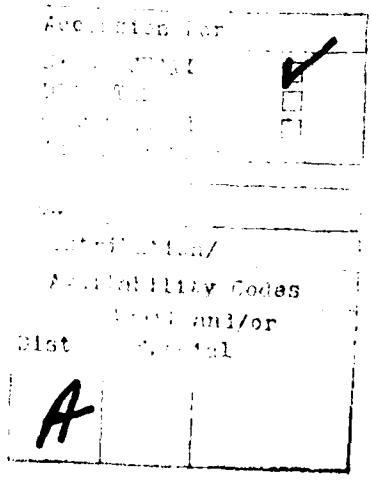

Unclassified

SECURITY CLASSIFICATION OF THIS PAGE (When Data Entered)

REPORT DOCUMENTATION PAGE	READ INSTRUCTIONS BEFORE COMPLETING FORM
1. REPORT NUMBER: 6	2. GOVT ACCESSION NO.: AD-A111612	3. RECIPIENT'S CATALOG NUMBER:
4. TITLE (and Subtitle): FINITE ELEMENT ANALYSIS OF MAGNETOELASTIC PLATE PROBLEMS	5. TYPE OF REPORT & PERIOD COVERED: Technical Report February 1979- August 1981
	6. PERFORMING ORG. REPORT NUMBER:
7. AUTHOR(s): K.Y. Yuan	8. CONTRACT OR GRANT NUMBER(s): ONR Contract Number N00014-79-C-0224
9. PERFORMING ORGANIZATION NAME AND ADDRESS: Departments of Structural Engineering and Theoretical & Applied Mechanics, Cornell University, Ithaca, NY 14853	10. PROGRAM ELEMENT, PROJECT, TASK AREA & WORK UNIT NUMBERS: NR 064-621
11. CONTROLLING OFFICE NAME AND ADDRESS: Director, Structural Mechanics Program, Material Sciences Division, Office of Naval Research, Arlington, VA 22217	12. REPORT DATE: August 1981
	13. NUMBER OF PAGES: XV + 230
14. MONITORING AGENCY NAME & ADDRESS(if different from Controlling Office)	15. SECURITY CLASS. (of this report)
	15a. DECLASSIFICATION/DOWNGRADING SCHEDULE

16. DISTRIBUTION STATEMENT (of this Report)

This document has been approved for public release and sale; distribution unlimited.

17. DISTRIBUTION STATEMENT (of the abstract entered in Block 20, if different from Report)

18. SUPPLEMENTARY NOTES

Eddy currents, Finite element method, Magnetic forces, Magnetomechanics, Nondestructive testing, Numerical methods, plates

19. KEY WORDS (Continue on reverse side if necessary and identify by block number)

20. ABSTRACT (Continue on reverse side if necessary and identify by block number)

Magnetic forces acting on conducting metal structures are significant in the design of such devices as fusion reactors, magnetohydrodynamic generators, magnetically levitated vehicles, magnetic forming devices, and various electric machines. The magnetic loads on these structures may be pulsed or cyclical and arise from the interaction between the induced eddy currents in the conductor and the externally applied magnetic fields. Moreover, the velocity and finite deformation of the conducting structure

DD FORM 1 JAN 73 1473 EDITION OF 1 NOV 65 IS OBSOLETE

S/N 0102-LF-014-6601

Unclassified

SECURITY CLASSIFICATION OF THIS PAGE (When Data Entered)

20. Abstract (continued)

may interact with the electromagnetic fields to yield a coupled problem.

This thesis presents an integrated study of magnetoelasticity problems for thin nonferrous conducting plates. Three phases of the study have been emphasized: theoretical modelling of interaction problems, finite element eddy current calculations for rigid conducting plates, and finite element numerical studies of coupled magnetoelastic problems. Experimental results by others and analytical solutions for limiting cases have been used to verify the numerical results obtained at each stage of the investigation. The Fortran programs developed for each part of the study are also described.

The electrodynamics and continuum mechanics bases of the problem are presented in the modelling part of the study. The Eulerian nature of the problem is emphasized. All the field relations are linearized in an updated Lagrangian sense. A stream function method is introduced for the eddy current calculations on thin moving plates. The couplings between the eddy current problem and the vibration of the plates are discussed in detail. Both linear and geometrically nonlinear problems are formulated for the coupled magnetomechanical systems.

Eddy current calculations on rigid conducting plates form the basis for later consideration of the coupled magnetoelastic problems. Steady state harmonic eddy current analyses are performed for both finite and infinitely long conducting plates. Transient time-integration analysis is also performed for infinitely-long plates. In all cases, the nonlocal effect of the self-field on the eddy current is included. Infrared and search coil experimental results by others are employed to verify the finite element numerical solutions.

Linear vibrations of infinitely long conducting plates excited by pulsed magnetic fields are studied via finite element time integration analysis. Low inductance strain gages are used for experimental verifications of the numerical results obtained. The effects of pulse duration and various kinds of interactions on the coupled systems are investigated. A finite element formulation for the induced nonlinear vibrations of infinitely long conducting plates is presented. Numerical difficulties and some limited results for nonlinear static problems are discussed.

TABLE OF CONTENTS

LIST OF TABLES

LIST OF FIGURES

Chapter 1

INTRODUCTION

Materials interact with electromagnetic fields in a variety of ways. Some electromagnetic interaction phenomena, such as photoelasticity and piezoelectricity, have found wide application in experimental mechanics and in industry. But it is only recently that a corresponding theory of sufficient generality has been developed for electromagnetic interaction phenomena of elastic solids. This field is generally called <u>electromagnetoelasticity</u>.

Special branches of the electromagnetoelasticity, such as piezoelectricity, have been well developed and applied widely in the electronic industry. Other branches of the general theory remain unnoticed and seldomly interest structural mechanicians. However, recent developments in the high energy industry are gradually changing this situation.

High energy devices such as fusion reactors, superconductive energy storage devices, MHD generators, and magnetically levitated vehicles are all subjected to strong electromagnetic fields. The design of these devices calls for an understanding of the nature of the electromagnetic forces and the interactions between the fields and the structure. Thus, although still relatively unnoticed, electromagnetoelasticity is gradually emerging as a new field-structure interaction theory for structural mechanicians.

The electromagnetoelastic materials of interest to structural mechanicians are conducting metals and superconducting materials. Both

types are used as major structural materials in the high energy industry and sometimes they appear in composite form. The electromagnetic phenomenon in such materials is basically a magnetic one. The interaction theory between the field and the elastic body is therefore called magnetoelasticity.

Scattered studies of magnetoelastic structural problems exist in the literature. Knowledge of this theory is still restricted to a relatively small group of specialists. In no small measure, this fact is due to the complexity of the subject, requiring knowledge of mechanics, electromagnetic theory, and thermodynamics. Even for relatively simple materials like nonferrous conductors, the interactions among these three fields are by no means trivial.

This chapter gives a brief introduction to the main features of magnetoelastic structural problems. Section 1.1 describes the multidisciplinary nature of the theory of magnetoelasticity for nonferrous conductors. Section 1.2 introduces the plate as a special structural form in the general theory and describes the modelling approach of magnetoelastic plate problems used in this thesis. Section 1.3 presents the organization and an overview of the later Chapters.

1.1 The Multidisciplinary Nature of Magnetoelasticity

Magnetoelasticity for nonferrous conductors encompasses three different fields: elasticity, electrodynamics, and thermodynamics. The coupling of these three fields is shown schematically in Figure 1.1 and occurs through the field equations, constitutive equations, and boundary conditions. The quantification of the mutual interactions and their effects on the behavior of the elastic structure is the purpose of this

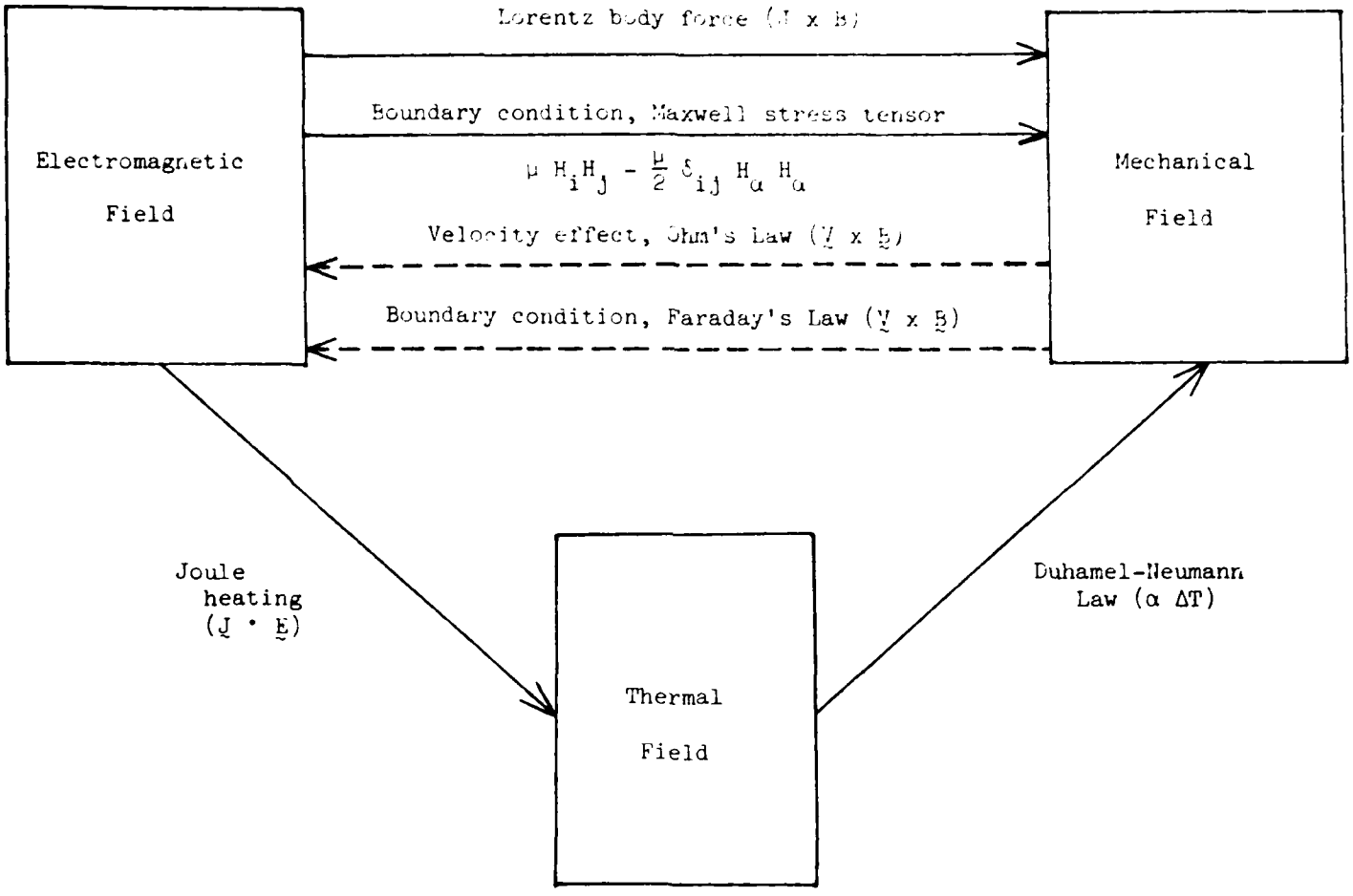

Figure 1.1 A schematic of one form of magnetothermomechanical coupling ($\underset{\sim}{E}$ = electric field, $\underset{\sim}{J}$ = electric current, $\underset{\sim}{B}$ = magnetic flux, $\underset{\sim}{V}$ = velocity field, μ = magnetic permeability, α = coefficient of thermal expansion, ΔT = change in temperature from reference temperature, $\underset{\sim}{H}$ = magnetic intensity.)

study.

Details of the theory of magnetoelasticity will be presented in Chapter Two. However, from the simple figure here, one notes that the electric current interacts with the magnetic field to create a magnetic body force on the conducting structure. The deformation and motion of the structure then perturb and change the electromagnetic field. The electric current generates Joule heating which diffuses through the conductor body and creates thermal stresses. The thermoelastic effects further change the motion of the conductor structure and affect the electromagnetic fields. During the whole process, the distributions of the magnetic body force and the electric heating depend on the variation of the magnetic field and all other field variables. The resulting body force distribution can be markedly different from the gravitational body force more familiar to structural mechanicians and may cause deformation gradients inside the structure that differ from the conventional kinematic simplifying assumptions of a particular structural form. Furthermore, coupled problems are three-dimensional as the magnetic fields can permeate through both the structure and the free space surrounding it. The coupled problem is also a dynamic one since the interactions come through the motion of the conductor and the time variation of the electric and thermal fields inside the conductor body. The solution of any but the simplest structural configurations is difficult, and one generally has to resort to numerical means.

1.2 Modelling of Magnetoelastic Plate Problems

All the above mentioned features of magnetoelasticity may be found for the problem of a conducting thin plate in a time-varying magnetic

field. But here the thinness of the plate may cause the electromagnetic and mechanical field variables to have certain restricted variations across the thickness. Simplifying assumptions regarding these variations may then be made to model the problem in a form more amenable to analysis. The study of the interactions between time-varying magnetic fields and the motion and deformation of thin conductor plates is the topic of this report. The thermoelastic effects are not considered in this work. The modelling approach is described in the following paragraphs.

The magnetoelastic problem of a thin nonferrous conductor is basically an electromagnetic induction problem coupled with a problem of dynamic elasticity. For structural problems, one considers low frequency theories in both subsystems. When the frequency of the electromagnetic field is sufficiently low, the penetration depth of the magnetic field into the conductor is large compared to the thickness of the plate, and the induced current (eddy current) is approximately uniform across the thickness and flows parallel to the mid-surface. One can therefore assume that

(1) the normal to the mid-surface remains unstretched and normal to the deflected mid-surface of the plate,

(2) the eddy current density is constant across the thickness of the plate, and, from this assumption,

(3) the normal component of the induced magnetic field is constant across the thickness of the plate.

The induced eddy current flow is therefore perpendicular to the normal and rotates with the normal when the plate is vibrating.

With these three basic assumptions, and a few others introduced in Section 2.3.2, the plate problem is modelled as an eddy current problem on a moving conducting sheet coupled to a vibration problem of the thin

elastic plate. The equations governing these two subproblems will all be referred to the mid-surface of the plate and coupled through velocity and the calculated magnetic force.

To achieve such a two-dimensional model, the current density is chosen as the primary variable in the induction problem. A stream function method is introduced to reduce the vector equation into a scalar equation. The Biot-Savart law is used to calculate the normal component of the induced magnetic field, which is basically the stream function for the induced current density. The singular nature of the Biot-Savart law is avoided at the mid-surface of the plate by transforming the volume integration into a surface integration. The expression obtained is then substituted into Faraday's law to obtain the desired governing equation.

The magnetic force calculated will have components normal and tangential to the plate. The equations of motion of the plate will contain the effects of both components.

1.3 Thesis Overview

The theoretical side of this thesis is treated in Chapter Two. To provide a proper background to the discussion of the stream function method, the theory of magnetoelasticity for nonferrous conducting materials is summarized, together with the linearization procedure of the various electromagnetic and mechanical field relations. The stream function method is then discussed in detail. Various assumptions used are examined and the electromagnetic field problem reduced to a single integro-differential equation for the stream function. A literature survey of magnetoelastic plate problems is also given.

Chapter Three is devoted to the eddy current calculation on rigid, stationary conducting plates since this subproblem is not trivial and is in itself a significant aspect of electromagnetic field computation. The governing equations for eddy currents derived in Chapter Two are applied to finite (two-dimensional) and infinitely long (one-dimensional) plates subjected to various exciting magnetic fields. The numerical results are compared to some experimental data obtained by using infrared sensing techniques. The finite element method is used to solve the integro-differential equation for the stream function.

Chapter Four is concerned with the linear vibration of infinitely long magnetoelastic plates. Small deformation linearizations are employed, and various types of coupling investigated. Forced vibrations induced by transient magnetic fields generated by pulsed currents in nearby coils are studied. A finite element staggered transient analysis procedure is used for the coupled set of equations. Parameter studies are presented to explore the effects of the different time characteristics of the magnetic and mechanical subsystems. Some comparisons of the calculations with experimental results are given.

Chapter Five discusses the nonlinear vibration of infinitely long magnetoelastic plates. The formulation and algorithm for solution are presented based on the linearized equations for the updated, incremental analysis procedure. A two-dimensional nonlinear beam element is proposed for the geometrically nonlinear problems. Some limited results for the uncoupled, static nonlinear elastic problems are presented, and difficulties in the convergence of solutions for the nonlinear dynamic cases are discussed. Some suggestions for the improvement of the numerical technique are also given.

Conclusions on the results of the present study on magnetoelastic plates are drawn in the last Chapter, together with some suggestions for further research in this area.

Chapter 2

GENERAL THEORY

Several features of the theory of electromagnetic interactions in elastic solids make it unique in continuum mechanics. In the first place, there is no generally agreed upon interpretation of some of the electric and magnetic vectors in continuous bodies. These differing interpretations, together with the fact that the laws of classical mechanics are Galilean-invariant while the Maxwell equations are Lorentz-invariant, give rise to a variety of formulations of electrodynamics in a moving medium. In the second place, the separation of total contact force into mechanical and electromagnetic parts is not unique. The definitions of the stress tensor and the electromagnetic body force thus become mutually dependent. Finally, for materials such as piezoelectric solids, the interaction energy is linear in strain. If the stress-strain relations are to be obtained to the first order in the strains by differentiation of an energy function, then that energy function must be correct to the second order (Ref. 1). Finite-strain theory with all the complications of the associated two-point tensors must then be used in some problems, even when the deformation is small. Such features, as the three mentioned, make the general theory much more complicated than a simple superposition of the Maxwell equations and the theory of linear elasticity.

Toupin (Refs. 2,3) was the first one to use finite-strain theory to clarify some problems in the theory of interaction of an electrostatic field with a perfectly elastic dielectric. Tiersten (Refs. 4,5) then

developed a similar theory for the deformation of magnetically saturated insulators. A rigorous treatment of the magnetoelastic interactions has been given by Brown in his monograph (Ref. 1). The treatment is mainly for saturated non-dissipative, and non-conductive materials under static magnetic fields. The model of electrodynamic theory used by Toupin and Tiersten is also criticized in Brown's work. The interest in all these studies has been toward an understanding of the phenomena of electrostriction and magnetostriction as physical problems.

Electrodynamics in a moving media has long been a controversial subject. Pao (Ref. 6) has given a detailed comparison of four different theories in the literature: the Minkowski formulation, the Lorentz formulation, the statistical formulation, and the Chu formulation. Field-matter interaction theories for stationary and moving media based on these different models are also presented. Discussed also are the constitutive equations and boundary conditions. It is shown that under appropriate transformations of the different definitions of the electric and magnetic vectors, the four models can be made equivalent to each other. However, the expressions for the electromagnetic body force, body couple, and energy supply for polarizable magnetizable moving media based on these models differ from each other. For nonferrous metals, however, the differences in these expressions vanish and the results are also much simpler.

Field-matter interaction theory is a special branch of continuum mechanics. The treatment of this subject in the literature basically follows two different procedures. The stress method uses the stress concept and the expression for the electromagnetic forces on a material volume. The energy method uses a stored energy function and a variational principle. Parallels exist between the two procedures, and in theory they should yield

equivalent models. However, since it is impossible to measure the field variables inside the material, some assumptions always have to be made in either method. Several self-consistent theories exist in the literature. Some classical monographs and articles on this subject include Brown (Ref. 1), Penfield and Hans (Ref. 7), and Truesdell and Toupin (Ref. 8). Some more recent ones include Parkus (Refs. 9, 10, 11) Hutter and Van de Ven (Ref. 12), Alblas (Ref. 13), and Eringen (Ref. 14). In each of these, extensive references to other papers may be found.

Beside the interest in pure theoretical studies, there has been research work on this subject toward its practical applications in diverse fields such as geophysics, optics, acoustics, solid-state devices, and so on. Knopoff (Ref. 15), Wilson (Ref. 16), Kaliski (Ref. 17), and Dunkin and Eringen (Ref. 18) studied the effects of magnetic fields on elastic wave propogation. The magnetoelasticity theory they use is a simple combination of Maxwell equations and the equations of linear elasticity. The influence of the electromagnetic field on the strain occurs solely by means of Lorentz forces appearing in the equations of motion. The motion of the material affects the electromagnetic field only through the velocity of the particles in Ohm's law. Electromagnetic wave propogation usually is not considered. The use of quasi-static theory further simplifies the field problem. Many papers of this type have been reviewed by Paria (Ref. 19).

On engineering aspects, Montgomery (Ref. 20) and Brechna (Ref. 21) discussed stress analysis in magnet design. Woodson and Melcher (Ref. 22) treated electromechanical problems in electric machines and other devices. Melcher's new book (Ref. 23) directs toward electromagnetic field-continuum interactions. The treatment in this book is general, but the problems

discussed are mainly fluid flow ones. Many other books on electric machines and energy conversion also include electromechanical problems. Quasi-static theory is generally used for analysis. The circuit analogy provides a convenient tool in such a case. Many of the studies are for the uncoupled cases only, where the knowledge of the magnetic field determines the body force and hence the motion and deformation of the solid. Becker and Pillsbury (Ref. 24) is one of the few cases where the mutual coupling is taken into account.

Moon's recent article (Ref. 25) provides a broad survey of possible engineering applications of magneto-solid mechanics. Many problems discussed find applications in high energy technology. Design of fusion reactors, superconductive energy storage devices, MHD generators, etc., all involve considerations of strong magnetic forces imposed on the structural components. Moon and his co-works (Refs. 26, 27) have studied the stability and vibrations of superconducting magnet systems extensively. Miya, et al (Ref. 28) studied conductive cylindrical shells in pulsed axisymmetrical magnetic fields. A new monograph edited by Moon (Ref. 29) has addressed the mechanics of superconducting structures. Papers published in the nuclear engineering literature on the structural considerations of the devices are also numerous. However, apart from the few studies already cited, they are all limited to the uncoupled cases. The mutual interaction between the field and the response of the structure has received little attention.

The purpose of this report is to study the mutual interactions between the time-varying magnetic field and the induced motion of thin, nonferrous conducting plates on a rigorous continuum mechanic basis. The dynamics of the coupled magneto-mechanical system is emphasized. The eddy current

problem and the deformation-dependent nature of the magnetic force are given special attention. Both linear and nonlinear deformations of the conducting plate are considered.

In this chapter the theory of magnetoelastic plates and the formulation approach used in this thesis are presented. Section 2.1 summarizes the theory of magnetoelasticity for nonferrous conductors based on the Lorentz force concept. The Eulerian description is used. Section 2.2 discusses the linearization procedure of the field equations. The description of the coupled system is then referred to a known configuration of the conductor body. The approximation of the procedure is also discussed. Section 2.3 addresses thin nonferrous conducting plates. A stream function method for eddy current calculation is introduced. The problem is then modelled as an eddy current problem on a moving conducting sheet coupled to a vibration problem of a thin plate subjected to deformation-dependent load. The various coupling effects and the magnetic body force in the plate are discussed. A state-of-the-art survey of magnetoelastic plate problems is also given.

2.1 Magnetoelasticity for Nonferrous Conducting Materials

The material treated in this study is assumed to be homogeneous, isotropic, and possessing finite conductivity. Polarization and magnetization are not considered. Furthermore, no thermal effects are included. The theory presented below is basically a theory of the electrodynamics of a moving media coupled to the theory of nonlinear elasticity. The coupling effects come from the Lorentz force, the modification of the electromagnetic field relations by the velocity of the material, and the boundary conditions. The presentation follows that of Hutter and Pao (Ref.30). Details of some

derivations are omitted when the reader may be referred to this and other cited papers.

Consider first the kinematics of a material body in three-dimensional space. The position of a particle in the reference (material) configuration will be denoted by $\underset{\sim}{X}$, while its position in the present (spatial) configuration by $\underset{\sim}{x}$. Both $\underset{\sim}{X}$ and $\underset{\sim}{x}$ are referred to a common Cartesian coordinate system fixed in space, as shown in Figure 2.1. The component of $\underset{\sim}{X}$ and of all other vector and tensor quantities in the reference configuration are indicated by Greek subscripts (α, β = 1,2,3), and those in the present configuration by Latin subscripts (i, j = 1,2,3). The motion and deformation of the body are then described by

$$\underset{\sim}{x} = \underset{\sim}{x}\,(\underset{\sim}{X},t) \quad \text{or} \quad x_i = x_i\,(X_\alpha,t), \quad i, \alpha = 1,2,3 \tag{2.1}$$

The particle velocity and acceleration are

$$\underset{\sim}{v} = \frac{d}{dt}\,\underset{\sim}{x}\,(\underset{\sim}{X},t) = \frac{\partial}{\partial t}\,\underset{\sim}{x}\,(\underset{\sim}{X},t) \tag{2.2a}$$

$$\dot{\underset{\sim}{v}} = \frac{d^2}{dt^2}\,\underset{\sim}{x}\,(\underset{\sim}{X},t) = \frac{\partial}{\partial t}\,\underset{\sim}{v} + \underset{\sim}{v}\,\nabla \cdot \underset{\sim}{v} \tag{2.2b}$$

respectively. Introduce the displacement vector u with components

$$u_i = x_i - \delta_{i\alpha} X_\alpha, \quad \text{or} \quad u_\alpha = \delta_{i\alpha} x_i - X_\alpha \tag{2.3}$$

The particle velocity can then be calculated by

$$\underset{\sim}{v} = \frac{\partial}{\partial t}\,\underset{\sim}{u} + \underset{\sim}{v}\,\nabla \cdot \underset{\sim}{u} \tag{2.4}$$

The deformation may be measured by either the Green's strain tensor in the coordinate system X_α

$$E_{\alpha\beta} = \tfrac{1}{2}\,(u_{\alpha,\beta} + u_{\beta,\alpha} + u_{\gamma,\alpha}\,u_{\gamma,\beta}) \tag{2.5a}$$

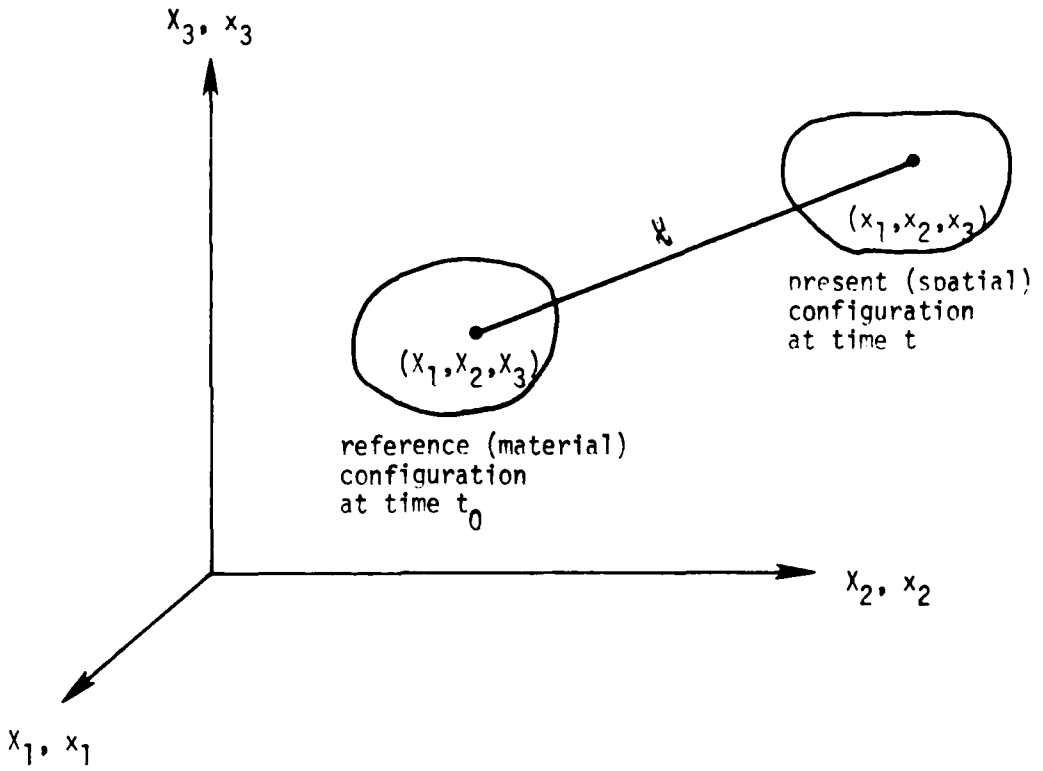

Figure 2.1 Motion of deformable body in Cartesian co-ordinate system.

or the Almansi's strain tensor in the coordinate system x_i

$$e_{ij} = \tfrac{1}{2} (u_{i,j} + u_{j,i} - u_{k,i}\, u_{k,j}) \tag{2.5b}$$

The balance laws will be applied to quantities measured in the coordinates x_i for the present configuration only.

2.1.1 Electromagnetic Field Equations, Constitutive Relations, and Boundary Conditions

The electromagnetic field equations for moving media may be derived from the following postulated global laws (Ref. 6).

Gauss - Faraday : $\oint_S \underset{\sim}{B} \cdot d\underset{\sim}{S} = 0$ (2.6a)

Faraday : $\oint_C \underset{\sim}{E}_e \cdot d\underset{\sim}{\ell} = - \frac{d}{dt} \int_S \underset{\sim}{B} \cdot d\underset{\sim}{S}$ (2.6b)

Gauss - Coulomb : $\oint_S \underset{\sim}{D} \cdot d\underset{\sim}{S} = \int_V q \, dV$ (2.6c)

Ampere - Maxwell : $\oint_C \underset{\sim}{H}_e \cdot d\underset{\sim}{\ell} = \frac{d}{dt} \int_S \underset{\sim}{D} \cdot d\underset{\sim}{S} + \int_S \underset{\sim}{J}_e \cdot d\underset{\sim}{S}$ (2.6d)

In addition, there is the law of conservation of charge

$$\oint_S \underset{\sim}{J}_e \cdot d\underset{\sim}{S} + \frac{d}{dt} \int_V \sigma \, dV = 0 \tag{2.6e}$$

In the above, $\underset{\sim}{B}$ is the magnetic induction, $\underset{\sim}{D}$ is the electric displacement, the $\underset{\sim}{E}_e$ and $\underset{\sim}{H}_e$ are the effective electric field and magnetic field, respectively, and $\underset{\sim}{J}_e$ is the effective current. q is the free charge density. All integrations are taken over material volume V, material surface S, or material circuit C, which vary with time. The time differentiations should be carried out by applying the transport theorem

$$\frac{d}{dt} \int_V \psi \, dV = \int_V \left[\frac{\partial \psi}{\partial t} + \nabla \cdot (\underset{\sim}{v} \psi) \right] dV \tag{2.7a}$$

$$\frac{d}{dt} \int_S \underset{\sim}{A} \cdot d\underset{\sim}{S} = \int_S \overset{*}{\underset{\sim}{A}} \cdot d\underset{\sim}{S} \tag{2.7b}$$

in which $\overset{*}{\underset{\sim}{A}} \equiv \frac{\partial}{\partial t}\underset{\sim}{A} + \underset{\sim}{v}\,\nabla\cdot\underset{\sim}{A} + \nabla\times(\underset{\sim}{A}\times\underset{\sim}{v})$. (2.7c)

For nonferrous metals with good (but finite) conductivity, the free charge density q can often be dropped. Also, since the frequencies related to vibrations and mechanical waves are much smaller than the frequencies of electromagnetic waves with the same wave length, one can regard the electromagnetic fields as quasistatic when investigating the dynamic response of the conductor structures. Mathematically it means that the electric displacement $\underset{\sim}{D} = 0$ and $\frac{\partial}{\partial t}\underset{\sim}{D} = 0$. The field equations so derived will be of the diffusion type rather than the wave type. All the electromagnetic variables inside the material are then treated as convected quantities.

The electromagnetic field equations in local form may be obtained by substitution of Eqs. (2.6) into Eqs. (2.7) and application of the divergence and Stokes theorems to the moving volume V and surface S. With the above simplifications, Eqs. (2.6) become

$$\nabla\cdot\underset{\sim}{B} = 0 \tag{2.8a}$$

$$\nabla\times\underset{\sim}{E}_e = -\overset{*}{\underset{\sim}{B}} = -\frac{\partial}{\partial t}\underset{\sim}{B} - \nabla\times(\underset{\sim}{B}\times\underset{\sim}{v}) \tag{2.8b}$$

$$\underset{\sim}{D} = 0 \tag{2.8c}$$

$$\nabla\times\underset{\sim}{H}_e = \underset{\sim}{J}_e \tag{2.8d}$$

$$\nabla\cdot\underset{\sim}{J}_e = 0 \tag{2.8e}$$

The $\underset{\sim}{B}$, $\underset{\sim}{D}$, $\underset{\sim}{H}_e$, $\underset{\sim}{E}_e$, and $\underset{\sim}{J}_e$ in Eqs. (2.6) are fields in the moving body as measured by an observer following each material particle. After the application of the transport theorem, the $\underset{\sim}{B}$ and $\underset{\sim}{D}$ in Eqs. (2.8) are those in the moving body measured by an observer in a reference frame fixed in space. The effective fields $\underset{\sim}{H}_e$ and $\underset{\sim}{E}_e$ can also be expressed in terms of the corresponding fixed-frame quantities $\underset{\sim}{H}$ and $\underset{\sim}{E}$, respectively. The expressions are different in various formulations for general materials.

However, for nonferrous metals the same results may be obtained and are

$$\underset{\sim}{E}_e = \underset{\sim}{E} + \underset{\sim}{v} \times \underset{\sim}{B} \qquad \underset{\sim}{H}_e = \underset{\sim}{H} - \underset{\sim}{v} \times \epsilon \underset{\sim}{E} \tag{2.9a}$$

The effective current density measured by an observer moving with the charged particle is

$$\underset{\sim}{J}_e = \underset{\sim}{J} - q \underset{\sim}{v} \tag{2.9b}$$

In the usual case of quasistatic field problems, no free charge can exist inside the conductor and one has $\underset{\sim}{J}_e = \underset{\sim}{J}$. In problems that involve conductors with slits or cracks, free charge may be accumulated on the two sides of the narrow opening, and electric arcing may occur when the voltage across the opening becomes too high. In such problems, the effect of the free charge cannot be neglected. In the present study, however, free charge accumulation and electric arcing are not considered, and thus the relation $\underset{\sim}{J}_e = \underset{\sim}{J}$ is assumed.

Note also that since $\underset{\sim}{D} = \epsilon \underset{\sim}{E}$, the quasistatic approximation effectively implies that the permittivity $\epsilon = 0$ and hence $\underset{\sim}{H}_e = \underset{\sim}{H}$.

The electromagnetic constitutive relations in this study are limited to the classical linear relations for homogeneous, isotropic materials. For slowly moving media these relations are invariant with respect to the transformation of reference frames. Namely,

$$\underset{\sim}{D} = \epsilon \underset{\sim}{E}, \quad \underset{\sim}{B} = \mu \underset{\sim}{H}, \quad \underset{\sim}{J} = \sigma \underset{\sim}{E} \tag{2.10a}$$

in the fixed frame, and

$$\underset{\sim}{D} = \epsilon \underset{\sim}{E}_e, \quad \underset{\sim}{B} = \mu \underset{\sim}{H}_e, \quad \underset{\sim}{J}_e = \sigma \underset{\sim}{E}_e \tag{2.10b}$$

in the moving frame. In the above μ is the magnetic permeability and σ the electric conductivity of the material. In view of Eqs. (2.9), one has

$$\underset{\sim}{D} = \epsilon (\underset{\sim}{E} + \underset{\sim}{v} \times \underset{\sim}{B}) \tag{2.11a}$$

$$\underset{\sim}{B} = \mu (\underset{\sim}{H} - \underset{\sim}{v} \times \underset{\sim}{D}) \tag{2.11b}$$

$$\underset{\sim}{J} = \sigma\,(\underset{\sim}{E} + \underset{\sim}{v} \times \underset{\sim}{B}) \tag{2.11c}$$

Again, because of the quasi-static approximation, only Eq. (2.11c) and Eq. (2.11b) with $\rho = 0$ will be needed. For nonferrous metals μ can be replaced by μ_0 of the free space without introducing any significant error.

The electromagnetic boundary conditions may be derived by applying the global laws, Eqs. (2.6), to volumes and surfaces which contain singular surfaces and lines across which the field quantities may not be continuous or may suffer a jump. The transport theorem, Eqs. (2.7), in such cases should be modified to account for the discontinuities of the field quantities. The modified transport theorem is then applied to global laws for the small volume or "pillbox" and for the circuit shown in Fig. 2.2. By taking the limits of vanishing volume for the pillbox and vanishing enclosed area for the circuit, one may derive the jump conditions. For nonferrous metals with finite conductivity in a quasi-static field, they are

$$\underset{\sim}{n} \cdot [\![\, \underset{\sim}{B} \,]\!] = 0 \tag{2.12a}$$

$$\underset{\sim}{n} \times [\![\, \underset{\sim}{E} + \underset{\sim}{v} \times \underset{\sim}{B} \,]\!] = 0 \tag{2.12b}$$

$$\underset{\sim}{n} \times [\![\, \underset{\sim}{H} \,]\!] = 0 \tag{2.12c}$$

$$\underset{\sim}{n} \cdot [\![\, \underset{\sim}{J} \,]\!] = \underset{\sim}{n} \cdot [\![\, \sigma(\underset{\sim}{E} + \underset{\sim}{v} \times \underset{\sim}{B}) \,]\!] = 0 \tag{2.12d}$$

in which $\underset{\sim}{n}$ is the unit vector normal to the boundary surface of the body in the present configuration, $[\![\, \underset{\sim}{A} \,]\!] = \underset{\sim}{A}^{+} - \underset{\sim}{A}^{-}$ denotes the jump of the quantity $\underset{\sim}{A}$ from the positive side (positive direction of $\underset{\sim}{n}$) to the negative side of the boundary surface.

The modified transport theorem and the details of the derivations may be found in Hutter (Ref. 31). Dunkin and Eringen (Ref. 18) used a different approach of derivation. Equations (2.12c,d) have the following form in

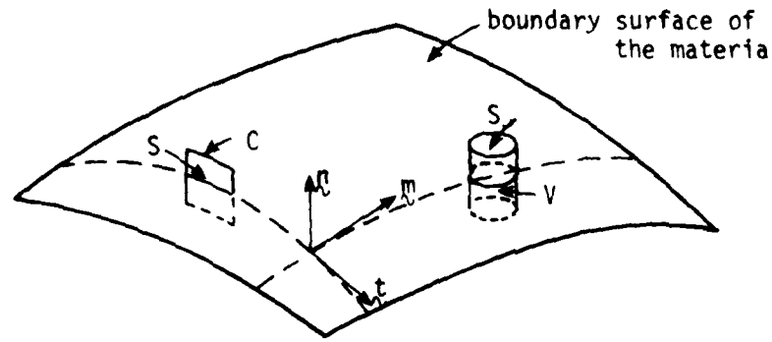

Figure 2.2 Pillbox and Circuit for the derivation of the jump conditions.

Hutter (Ref. 31):

$$\underset{\sim}{n} \times [\![\underset{\sim}{H} - \underset{\sim}{\chi} \times \underset{\sim}{B}]\!] = \underset{\sim}{\mathcal{J}}_s - q_s \underset{\sim}{\chi} \tag{2.13a}$$

$$\underset{\sim}{n} \cdot [\![\underset{\sim}{\mathcal{J}}]\!] - (\underset{\sim}{\chi} \cdot \underset{\sim}{n}) [\![\rho]\!] + \underset{\sim}{n} \cdot \nabla \times (\underset{\sim}{n} \times \underset{\sim}{\mathcal{J}}_s) + (\underset{\sim}{\chi} \cdot \underset{\sim}{n}) \nabla \cdot (\underset{\sim}{n}\, q_s)$$

$$= - \frac{\partial}{\partial t} q_s \tag{2.13b}$$

in which q_s and $\underset{\sim}{\mathcal{J}}_s$ are the free surface charge density and free surface current density, respectively. For good conductors the free surface charge and current densities, although achievable in high frequency cases, can only be an idealization that occurs in conjunction with the assumption of a perfect conductor ($\sigma = \infty$) (Ref. 32).

Equations (2.8), (2.9), (2.11), and (2.12) complete the description of the electromagnetic field inside moving nonferrous metals in quasi-static cases.

2.1.2 Mechanical Field Equations, Magnetic Body Force, Constitutive Relations, and Boundary Conditions

The mechanical field of a nonpolar material is governed by the following balance laws of continuum mechanics.

Mass : $$\frac{d}{dt} \int_V \rho \, dV = 0 \tag{2.14a}$$

Linear Momentum : $$\frac{d}{dt} \int_V \rho \underset{\sim}{v} \, dV = \oint_S \underset{\sim}{t}^{(n)} \, dS + \int_V \rho \underset{\sim}{f} \, dV \tag{2.14b}$$

Angular Momentum: $$\frac{d}{dt} \int_V \underset{\sim}{\chi} \times \rho \underset{\sim}{v} \, dV$$

$$= \oint_S \underset{\sim}{\chi} \times \underset{\sim}{t}^{(n)} \, dS + \int_V \underset{\sim}{\chi} \times \rho \underset{\sim}{f} \, dV \tag{2.14c}$$

Energy : $$\frac{d}{dt} \int_V (\tfrac{1}{2} \rho \underset{\sim}{v} \cdot \underset{\sim}{v} + \rho U) \, dV$$

$$= \oint_S \underset{\sim}{t}^{(n)} \cdot \underset{\sim}{v} \, dS + \int_V (\rho \underset{\sim}{f} \cdot \underset{\sim}{v} + \phi) \, dV \tag{2.14d}$$

in which ρ is the mass density, $\underset{\sim}{t}^{(n)}$ the stress vector at the surface with unit vector $\underset{\sim}{n}$, $\underset{\sim}{f}$ the body force per unit mass, U the strain energy, and ϕ the energy supply. The integrations are over the material volume V and material surface S, both moving with the material contained in them.

Thermodynamic processes are not considered in this study. The heat flux and heat energy supply terms have been dropped in the balance law of energy. Introducing the Cauchy stress tensor $\underset{\sim}{\tau}$ with

$$\underset{\sim}{t}^{(n)} = \underset{\sim}{n} \cdot \underset{\sim}{\tau} \quad \text{or} \quad t_i^{(n)} = n_j \tau_{ij} \tag{2.15}$$

and applying the divergence and transport theorems to Eqs. (2.14), one obtains the mechanical field equations in local form,

$$\frac{d}{dt} \rho + \rho \nabla \cdot \underset{\sim}{v} = 0 \tag{2.16a}$$

$$\rho \frac{d}{dt} \underset{\sim}{v} = \nabla \cdot \underset{\sim}{\tau} + \rho \underset{\sim}{f} \tag{2.16b}$$

$$\underset{\sim}{\tau} - \underset{\sim}{\tau}^t = 0 \tag{2.16c}$$

$$\rho \frac{d}{dt} U = \underset{\sim}{\tau} : \nabla \underset{\sim}{v} + \phi \tag{2.16d}$$

in which $\underset{\sim}{\tau}^t$ is the transpose of the stress tensor $\underset{\sim}{\tau}$, and $\underset{\sim}{\tau} : \nabla \underset{\sim}{v} = \tau_{ij} v_{j,i}$ is the trace of the tensor product of τ_{ij} and $v_{j,i}$.

The body force $\rho \underset{\sim}{f}$ and energy supply ϕ arise from the electromagnetic fields. For nonferrous metals they have the following expressions:

$$\rho \underset{\sim}{f} = \underset{\sim}{J} \times \underset{\sim}{B} \tag{2.17}$$

$$\phi = \underset{\sim}{J} \cdot \underset{\sim}{E} - \rho \underset{\sim}{f} \cdot \underset{\sim}{v} \tag{2.18}$$

Applying the electromagnetic field equations (2.8) and some vector operations to Eq. (2.17), one obtains another form for the body force,

$$\rho \underset{\sim}{f} = \nabla \cdot \underset{\sim}{T} \quad \text{or} \quad \rho f_i = T_{ij,j} \tag{2.17a}$$

in which $\underset{\sim}{T}$ is the Maxwell stress tensor for the magnetic system (Ref. 6),

$$T_{ij} = T_{ji} = \frac{1}{\mu_o} B_i B_j - \frac{1}{2\mu_o} \delta_{ij} B_k B_k \tag{2.19}$$

Substitution of Eq. (2.17) into Eq. (2.18) gives

$$\phi = \underset{\sim}{J}_e \cdot \underset{\sim}{E}_e \tag{2.18a}$$

Equations (2.16d) and (2.18) represent a conversion of electromagnetic energy into mechanical energy. Substitution of Eq. (2.17a) into Eq. (2.14b) and application of the divergence theorem yields the balance law of linear momentum:

$$\frac{d}{dt} \int_V \rho \underset{\sim}{v} \, dV = \oint_S \underset{\sim}{T} \cdot \underset{\sim}{n} \, dS + \oint_S \underset{\sim}{I} \cdot \underset{\sim}{n} \, dS \tag{2.20}$$

which states that the flow of electromagnetic momentum into the material body is completely converted into a kinetic momentum which affects the motion of the body. Detailed discussions of the electromagnetic momentum flow and force density and of the transfer of these into mechanical momentum and body force are given in Pao (Ref. 6), Penfeld and Hans (Ref. 7), Jackson (Ref. 32), and Landau and Lifshitz (Ref. 33). Here, it is only noted that the force acting on the material body is equal and opposite to the "force" (transfer of the electromagnetic momentum) acting on the electromagnetic field.

No useful boundary conditions follow from the global laws Eqs. (2.14a,c). By applying the same technique as used in Subsection 2.1.1, one may derive two more boundary conditions from Eqs. (2.20) and (2.14d).

$$\underset{\sim}{n} \cdot [\![\underset{\sim}{T} + \underset{\sim}{I}]\!] = 0 \tag{2.21a}$$

$$\underset{\sim}{n} \cdot [\![\underset{\sim}{T} \cdot \underset{\sim}{v} + \frac{1}{2\mu_o} (\underset{\sim}{B} \cdot \underset{\sim}{B}) \underset{\sim}{v} - \frac{1}{\mu_o} \underset{\sim}{E} \times \underset{\sim}{B}]\!] = 0 \tag{2.21b}$$

in which the Poynting vector in Eq. (2.21b)

$$\frac{1}{\mu_o} \underset{\sim}{E} \times \underset{\sim}{B} = \underset{\sim}{S} \tag{2.22}$$

represents a density of energy flow by the electromagnetic field across the boundary surfaces.

The mechanical constitutive equations are assumed to be unaffected by the presence of the electromagnetic fields. For isotropic, homogeneous, linear elastic materials, they are the usual Hooke's Law

$$\tau_{ij} = \lambda \delta_{ij} e_{kk} + 2G e_{ij} \tag{2.23}$$

in which λ and G are the elastic constants independent of the spatial coordinates and e_{ij} is the Almansi's strain tensor, (Eq.(2.5b).

2.1.3 Summary of Equations

For convenience of future reference the pertinent equations in this section are grouped together and listed below.

Electromagnetic Subsystem

Field Equations

$$\nabla \cdot \underset{\sim}{B} = 0 \tag{2.24a}$$

$$\nabla \times \underset{\sim}{E} = - \frac{\partial}{\partial t} \underset{\sim}{B} \tag{2.24b}$$

$$\nabla \times \underset{\sim}{H} = \underset{\sim}{J} \tag{2.24c}$$

together with

$$\nabla \cdot \underset{\sim}{J} = 0 \tag{2.24d}$$

Constitutive Equations

$$\underset{\sim}{B} = \mu \underset{\sim}{H} \qquad \underset{\sim}{J} = \sigma (\underset{\sim}{E} + \underset{\sim}{v} \times \underset{\sim}{B}) \tag{2.25a,b}$$

Jump Conditions

$$\underset{\sim}{n} \cdot [\![\underset{\sim}{B}]\!] = 0 \tag{2.26a}$$

$$\underset{\sim}{n} \times [\![\underset{\sim}{E} + \underset{\sim}{v} \times \underset{\sim}{B}]\!] = 0 \tag{2.26b}$$

$$\underset{\sim}{n} \times [\![\underset{\sim}{H}]\!] = 0 \tag{2.26c}$$

$$\underset{\sim}{n} \cdot [\![\underset{\sim}{J}]\!] = \underset{\sim}{n} \cdot [\![\sigma (\underset{\sim}{E} + \underset{\sim}{v} \times \underset{\sim}{B})]\!] = 0 \tag{2.26d}$$

Mechanical Subsystem

Field Equations

$$\frac{d}{dt}\rho + \rho\,\nabla\cdot\underset{\sim}{v} = 0 \tag{2.27a}$$

$$\rho\,\frac{d}{dt}\underset{\sim}{v} = \nabla\cdot\underset{\sim}{\tau} + \rho\,\underset{\sim}{f} \tag{2.27b}$$

$$\rho\,\frac{d}{dt}U = \tau_{ij}\,v_{j,i} + \phi \tag{2.27c}$$

where $\rho\,\underset{\sim}{f} = \underset{\sim}{J}\times\underset{\sim}{B} = \nabla\cdot\underset{\sim}{T}$

$$\phi = \underset{\sim}{J}_e\cdot\underset{\sim}{E}_e = \underset{\sim}{J}\cdot\underset{\sim}{E} - \rho\,\underset{\sim}{f}\cdot\underset{\sim}{v}$$

Constitutive Equations

$$\tau_{ij} = \lambda\,\delta_{ij}\,e_{kk} + 2G\,e_{ij} \tag{2.28a}$$

$$T_{ij} = \frac{1}{\mu_o}B_i\,B_j - \frac{1}{2\mu_o}\delta_{ij}\,B_k\,B_k \tag{2.28b}$$

where $e_{ij} = \tfrac{1}{2}\,(u_{i,j} + u_{j,i} - u_{k,i}\,u_{k,j})$

Jump Conditions

$$\underset{\sim}{n}\cdot[\![\,\underset{\sim}{\tau} + \underset{\sim}{T}\,]\!] = 0 \tag{2.29a}$$

$$\underset{\sim}{n}\cdot[\![\,\underset{\sim}{\tau}\cdot\underset{\sim}{v} + \frac{1}{2\mu_o}(\underset{\sim}{B}\cdot\underset{\sim}{B})\,\underset{\sim}{v} - \frac{1}{\mu_o}\underset{\sim}{E}\times\underset{\sim}{B}\,]\!] = 0 \tag{2.29b}$$

2.2 Linearization Procedures

The field relations and boundary conditions presented in the last subsection are formulated in Eulerian coordinates and refer to the as yet unknown deformed configuration. To render the equations amenable to analysis, one needs a known, given reference configuration about which one linearizes all the field relations and boundary conditions. For small deformation cases, the undeformed initial configuration of the conductor is a natural choice. For geometrically nonlinear problems, one can choose for reference the last known configuration of the conductor during the solution process.

Such a procedure is standard for nonlinear mechanical problems and is called the "updated Lagrangian formulation" in the literature (Ref. 34).

The initial undeformed configuration or any known intermediate configuration during the solution process can also be used for reference for the mechanical subsystem. To have a consistent linearization for the coupled problem, however, the same procedure should be applied to the electromagnetic subsystem. Since a purely Lagrangian description is not available for the Maxwell equations, the updated Lagrangian formulation is a more natural choice.

Hutter and Pao (Ref. 30) have developed a linearization procedure for moving magnetizable elastic solids. Alblas (Ref. 13), Van de Ven (Ref. 35), and some Russian authors (Ref. 36) also suggested similar procedures. In all these studies, it is assumed that the deformation is small even with very large electromagnetic fields, and that the deformation has only a minor influence on the fields. The dominant effect on the field is the presence of the undeformed body. The linearization of the Maxwell equations is then carried out as a perturbation on the undeformed body. All the authors considered polarizable magnetizable materials. The constitutive equations and other field relations must therefore also be linearized.

For the geometrically nonlinear problems in this thesis, the deformation is allowed to be finite, but the displacement increment within each incremental solution is assumed to be small enough to allow the field equations to be linearized in a similar way. The approximations made in the linearization procedure will be discussed.

For the purpose of linearization, three configurations of the body are distinguished as shown in Figure 2.3,

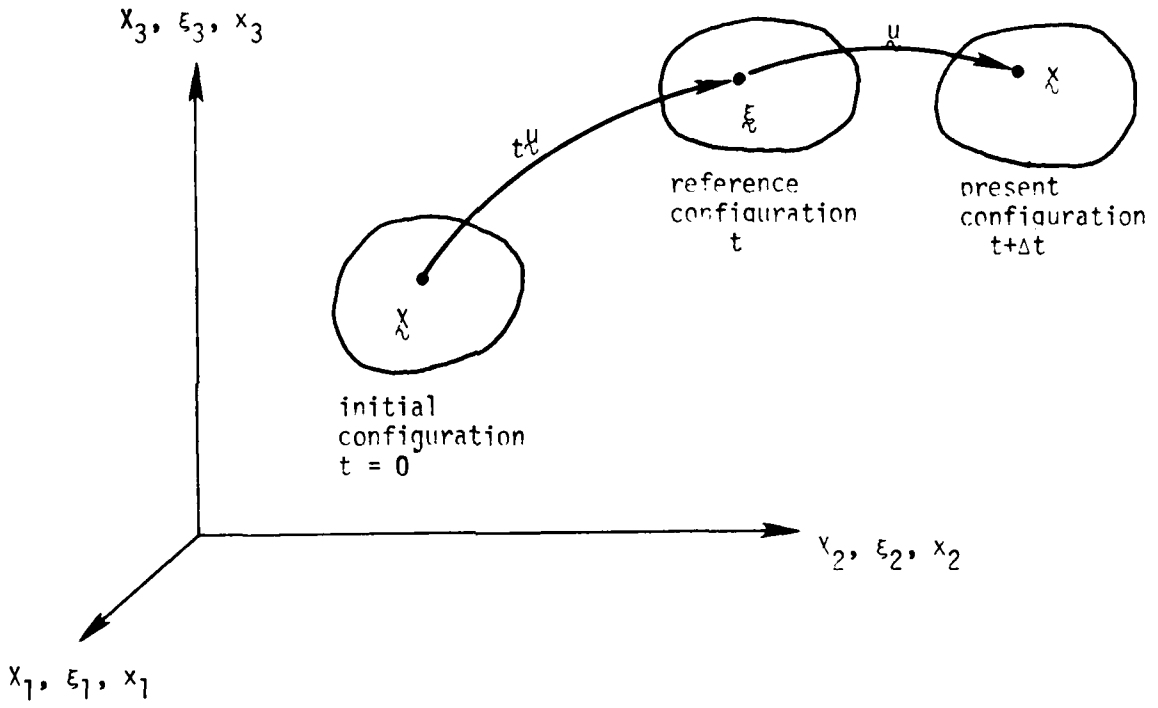

Figure 2.3 Initial, reference, and present configurations of a deformable body in electromagnetic field.

(a) the initial undeformed configuration with coordinates $\underset{\sim}{X}$,

(b) the intermediate reference configuration with coordinates $\underset{\sim}{\xi}$,

(c) the present configuration with coordinates $\underset{\sim}{x}$.

All $\underset{\sim}{X}$, $\underset{\sim}{\xi}$, and $\underset{\sim}{x}$ are measured in the same Cartesian coordinate system. The intermediate state can either be the initial undeformed state in the small deformation cases, or the last known moving, deformed state in the non-linear cases. All the field vectors and tensors in this state are assumed to be known and are denoted by a left subscript t.

The displacement of a particle from its intermediate configuration to its present configuration is denoted by

$$u_i = x_i - \delta_{\alpha i}\,\xi_\alpha, \qquad \xi_\alpha = \delta_{i\alpha}\,x_i - u_\alpha \tag{2.30}$$

u_i is assumed to be small such that $|u_{i,\alpha}| \ll 1$ and $|\dot{u}_i| \ll v_o$, where v_o is some characteristic wave speed, e.g., $v_o = \sqrt{E/\rho}$

The derivatives in the present configuration referred to the intermediate configuration then become

$$\frac{\partial}{\partial x_i} = \frac{\partial}{\partial \xi_\alpha}\frac{\partial \xi_\alpha}{\partial x_i} = \left(\delta_{i\alpha} - \frac{\partial u_\alpha}{\partial x_i}\right)\frac{\partial}{\partial \xi_\alpha} \tag{2.31}$$

In view of the small displacement assumptions, Eq. (2.31) may be replaced by

$$\frac{\partial}{\partial x_i} \approx \delta_{i\alpha}\frac{\partial}{\partial \xi_\alpha} \quad . \tag{2.32}$$

However, if coupling terms that are linear in the deformation gradient $u_{\alpha,\beta}$ are important, Eq. (2.32) must be replaced by the more accurate relation

$$\frac{\partial}{\partial x_i} = \left(\delta_{i\alpha} - u_{\alpha,\beta}\,\delta_{i\beta}\right)\frac{\partial}{\partial \xi_\alpha} \tag{2.33}$$

2.2.1 Electromagnetic Field Equations and Boundary Conditions

The electromagnetic field variables are decomposed into two parts. The first part corresponds to the intermediate state and satisfies Eqs. (2.24) - (2.26). The second part represents the perturbation which accounts for the changes of the externally applied field and the effect of deformation. These perturbations are denoted by lower case letters and are assumed to be small so that all the equations may be linearized with respect to them.

With $\underset{\sim}{B} = {}_t\underset{\sim}{B} + \underset{\sim}{b}$, $\underset{\sim}{E} = {}_t\underset{\sim}{E} + \underset{\sim}{e}$, and $\underset{\sim}{J} = {}_t\underset{\sim}{J} + \underset{\sim}{j}$, one obtains, using Eqs. (2.33) and (2.24),

$$b_{\alpha,\alpha} - u_{\alpha,\beta}\,({}_tB_\beta + b_\beta)_{,\alpha} = 0 \tag{2.34a}$$

$$\epsilon_{\alpha\beta\gamma}\,({}_tE_\gamma + e_\gamma)_{,\beta} - \epsilon_{\alpha\beta\gamma}\,u_{\delta,\beta}\,({}_tE_\gamma + e_\gamma)_{,\delta} + \frac{\partial}{\partial t}\,b_\alpha = 0 \tag{2.34b}$$

$$\epsilon_{\alpha\beta\gamma}\,b_{\gamma,\beta} - \epsilon_{\alpha\beta\gamma}\,u_{\delta,\beta}\,({}_tB_\gamma + b_\gamma)_{,\delta} - \mu_o\,j_\alpha = 0 \tag{2.34c}$$

$$j_{\alpha,\alpha} - u_{\alpha,\beta}\,({}_tJ_\beta + j_\beta)_{,\alpha} = 0 \tag{2.34d}$$

For the small deformation cases, one obtains, using Eq. (2.32) instead of (2.33),

$$b_{\alpha,\alpha} = 0 \tag{2.35a}$$

$$\epsilon_{\alpha\beta\gamma}\,({}_tE_\gamma + e_\gamma)_{,\beta} + \frac{\partial}{\partial t}\,b_\alpha = 0 \tag{2.35b}$$

$$\epsilon_{\alpha\beta\gamma}\,b_{\gamma,\beta} - \mu_o\,j_\alpha = 0 \tag{2.35c}$$

$$j_{\alpha,\alpha} = 0 \tag{2.35d}$$

which are the same as Eqs. (2.24).

For the small deformation cases, it is assumed that the boundary conditions may be satisfied on the surface

$$S\,(\xi_\alpha,\ t) = 0 \tag{2.36}$$

with unit normal vector $\underset{\sim}{N}$

$$N_\alpha = \frac{S_{,\alpha}}{\sqrt{S_{,\beta}\, S_{,\beta}}} \tag{2.37}$$

in the intermediate state. The boundary conditions are then

$$\underset{\sim}{N} \cdot [\![\underset{\sim}{b}]\!] = 0 \tag{2.38a}$$

$$\underset{\sim}{N} \times [\![{}_t\underset{\sim}{E} + \underset{\sim}{e} + \dot{\underset{\sim}{\chi}} \times {}_t\underset{\sim}{B}]\!] = 0 \tag{2.38b}$$

$$\underset{\sim}{N} \times [\![\underset{\sim}{b}/\mu_0]\!] = 0 \tag{2.38c}$$

$$\underset{\sim}{N} \cdot [\![\underset{\sim}{j}]\!] = 0 \tag{2.38d}$$

When the second order theory must be used, for example, in elastic stability problems, $\underset{\sim}{N}$ must be replaced by the unit vector $\underset{\sim}{n}$ normal to the deformed surface $S(x_j, t)$. n_i is connected to N_α by the following relation

$$n_i = N_\alpha \left(\delta_{i\alpha} + N_\beta N_\gamma e_{\beta\gamma} \delta_{i\alpha} - u_{\alpha,i}\right) \tag{2.39}$$

This derivation is given by Parkus (Ref. 11) and Hutter and Pao (Ref. 30).

The reduction of Eqs. (2.34) to (2.35) in small deformation cases is obvious since $u_{\alpha,\beta} \underset{\sim}{\approx} 0$ in such cases. The nonlinear terms in the perturbed quantities in Eqs. (2.34) should be dropped to have a linearized set of equations. The linearized equations also allow for the inclusion of transport current. In such cases ${}_t\underset{\sim}{B}$, ${}_t\underset{\sim}{E}$, and ${}_t\underset{\sim}{\chi}$ are generated by some external electromotive sources connected to the conductor body (Ref. 37).

2.2.2 Mechanical Field Equations, Magnetic Body Force, and Boundary Conditions

The mechanical field equations (2.27) may be linearized by the same procedure as used for the electromagnetic equations. For the small deformation case, one has, using Eq. (2.32),

$$\underset{\sim}{v} = \frac{\partial}{\partial t}\underset{\sim}{u}, \qquad \frac{d}{dt}\underset{\sim}{v} = \frac{\partial}{\partial t}\underset{\sim}{v} \tag{2.40}$$

$$e_{\alpha\beta} = \tfrac{1}{2}\,(u_{\alpha,\beta} + u_{\beta,\alpha}) \tag{2.41}$$

The equations of motion in this case become the usual Navier's equation,

$$\rho\,\frac{\partial^2}{\partial t^2}\,u_\alpha = G\,u_{\alpha,\beta\beta} + (\lambda + G)\,u_{\beta,\beta\alpha} + \rho\,f_\alpha \tag{2.42}$$

which is the basis of the magnetoelasticity theory used by Paria (Ref. 14) and Knopoff (Ref. 15). The boundary conditions in this case refer to the surface S and unit normal vector $\underset{\sim}{N}$ in the original configuration.

For geometrically nonlinear problems, the principle of virtual work provides a more convenient formulation method. In the updated Lagrangian formulation, the principle of virtual work gives

$$\int_{t_V} {}^{t+\Delta t}S_{\alpha\beta}\;\delta\,{}^{t+\Delta t}\varepsilon_{\alpha\beta}\;{}^{t}dV = {}^{t+\Delta t}R \tag{2.43}$$

where ${}^{t+\Delta t}R$ is the external virtual work expression,

$${}^{t+\Delta t}R = \int_{t+\Delta t_A} {}^{t+\Delta t}t_i\;\delta u_i\;{}^{t+\Delta t}dA + \int_{t+\Delta t_V} {}^{t+\Delta t}\rho({}^{t+\Delta t}f_i - \ddot{u}_i)\;\delta u_i\;{}^{t+\Delta t}dV \tag{2.44}$$

In Eq. (2.43), ${}^{t+\Delta t}S$ are the Cartesian components of the 2nd Piola-Kirchhoff stress tensor corresponding to the configuration x_i at time $t+\Delta t$ but measured in the configuration ξ_α which occurs at time t,

$${}^{t+\Delta t}S_{\alpha\beta} = \frac{{}^{t}\rho}{{}^{t+\Delta t}\rho}\,\xi_{\alpha,i}\;{}^{t+\Delta t}\tau_{ij}\;\xi_{\beta,j} \tag{2.45}$$

and $\delta\,{}^{t+\Delta t}\varepsilon_{\alpha\beta}$ are the virtual variations in the Cartesian components of the Green-Lagrange strain tensor in the configuration x_i (at time $t+\Delta t$) referred to the configuration ξ_α (at time t),

$$\delta\,{}^{t+\Delta t}\varepsilon_{\alpha\beta} = \tfrac{1}{2}\,\delta\,(u_{\alpha,\beta} + u_{\beta,\alpha} + u_{\gamma,\alpha}\;u_{\gamma,\beta}) \tag{2.46}$$

The integral of Piola-Kirchhoff stresses times variations in the Green-Lagrange strains is defined over the configuration ξ_α (at time t) of the body.

In Eq. (2.44) u_i is a virtual variation in the current displacement increment components u_i. When measured in the configuration ξ_α,

$$\delta u_\alpha = \delta u_i \, \delta_{i\alpha} \tag{2.47}$$

$\ddot{u}_i$ is the acceleration in the configuration x_i. ${}^{t+\Delta t}t_i$, ${}^{t+\Delta t}f_i$, and ${}^{t+\Delta t}\rho$ are the surface traction, the body force per unit mass, and the specific mass in the configuration x_i at time $t+\Delta t$. The integrations are defined over the unknown configuration x_i of the body.

When referred to the configuration ξ_α of the body at time t, the applied forces are evaluated using (Ref. 38)

$$\int_{{}^{t+\Delta t}t_\alpha} {}^{t}dA = \xi_{\alpha,i} \int_{{}^{t+\Delta t}t_i} {}^{t+\Delta t}dA \tag{2.48a}$$

$$\int ({}^{t+\Delta t}f_\alpha - \ddot{u}_\alpha) \, {}^{t}dV = \frac{{}^{t+\Delta t}\rho}{{}^{t}\rho} \int ({}^{t+\Delta t}f_i - \ddot{u}_i) \, \delta_{i\alpha} \, {}^{t+\Delta t}dV \tag{2.48b}$$

The surface traction ${}^{t+\Delta t}t_i$ and body force ${}^{t+\Delta t}f_i$ are generated by the electromagnetic fields and depend on the deformation of the conductor.

To linearize Eq. (2.43), the Piola-Kirchhoff stress tensor is first decomposed into two parts,

$${}^{t+\Delta t}S_{\alpha\beta} = {}^{t}\tau_{\alpha\beta} + S_{\alpha\beta} \tag{2.49}$$

where ${}^{t}\tau_{\alpha\beta}$ are the Cartesian components of the Cauchy stress tensor that satisfy Eq. (2.27) - (2.29) at time t, and $S_{\alpha\beta}$ are the Cartesian components of the 2nd Piola-Kirchhoff stress increment tensor referred to the configuration ξ_α at time t. The strain increment ${}^{t+\Delta t}\varepsilon_{\alpha\beta}$ is separated into linear and nonlinear parts

$$ {}^{t+\Delta t}\varepsilon_{\alpha\beta} = \varepsilon_{\alpha\beta} \tag{2.50a} $$

$$ \varepsilon_{\alpha\beta} = e_{\alpha\beta} + \eta_{\alpha\beta} \tag{2.50b} $$

where

$$ e_{\alpha\beta} = \tfrac{1}{2}\,(u_{\alpha,\beta} + u_{\beta,\alpha}) \tag{2.51} $$

$$ \eta_{\alpha\beta} = \tfrac{1}{2}\,u_{\gamma,\alpha}\,u_{\gamma,\beta} \tag{2.52} $$

The constitutive relation between stress and strain increments used now is

$$ S_{\alpha\beta} = C_{\alpha\beta\gamma\delta}\,\varepsilon_{\gamma\delta} \tag{2.53} $$

Eq. (2.43) can then be rewritten as

$$ \int_{{}^{t}V} C_{\alpha\beta\gamma\delta}\,\varepsilon_{\gamma\delta}\,\delta\varepsilon_{\alpha\beta}\,{}^{t}dV + \int_{{}^{t}V} {}^{t}\tau_{\alpha\beta}\,\delta\eta_{\alpha\beta}\,{}^{t}dV = {}^{t+\Delta t}R - \int_{{}^{t}V} {}^{t}\tau_{\alpha\beta}\,\delta e_{\alpha\beta}\,{}^{t}dV \tag{2.54} $$

which is a nonlinear equation in the incremental displacements u_α.

Linearization of Eq. (2.54) may be obtained by assuming that $\varepsilon_{\alpha\beta} = e_{\alpha\beta}$, $\delta\varepsilon_{\alpha\beta} = \delta e_{\alpha\beta}$ and that $S_{\alpha\beta} = C_{\alpha\beta\gamma\delta}\,e_{\gamma\delta}$. The equation then becomes

$$ \int_{{}^{t}V} C_{\alpha\beta\gamma\delta}\,e_{\gamma\delta}\,\delta e_{\alpha\beta}\,{}^{t}dV + \int_{{}^{t}V} {}^{t}\tau_{\alpha\beta}\,\delta\,\eta_{\alpha\beta}\,{}^{t}dV = {}^{t+\Delta t}R - \int_{{}^{t}V} {}^{t}\tau_{\alpha\beta}\,\delta e_{\alpha\beta}\,{}^{t}dV \tag{2.55} $$

The electromagnetic body force may be calculated from the linearized Maxwell equations (2.34) or (2.35). Whichever set of equations is used, one has

$$ \rho f_\alpha = ({}^{t}\underline{J} \times {}^{t}\underline{B})_\alpha + ({}^{t}\underline{J} \times \underline{b})_\alpha + (\underline{j} \times {}^{t}\underline{B})_\alpha + (\underline{j} \times \underline{b})_\alpha \tag{2.56} $$

The last term in Eq. (2.56) is of the second order in the perturbed quantities and should be dropped to have a consistent linearization. However, in some problems this last term is not small. This point will be discussed in the next section.

The mechanical boundary condition, when referred to the boundary surface S and the unit normal vector $\underset{\sim}{N}$ in the configuration ξ_α, is

$$N_\beta \cdot [\![{}^{t+\Delta t}S_{\alpha\beta} + T_{\alpha\beta}]\!] = 0 \tag{2.57}$$

When second order theory needs to be used, $\underset{\sim}{N}$ should be replaced by $\underset{\sim}{n}$ in Eq. (2.39).

The elasticity material tensor $C_{\alpha\beta\gamma\delta}$ and the specific mass ρ are deformation dependent in the theory of finite elasticity. However, for small strain and finite deformation problems for conducting metals, the deformation effects will be very small, i.e., $\xi_{\alpha,i} \approx \delta_{\alpha i}$ in these cases. In this study, the constitutive tensor is taken the same as in the undeformed original configuration of the material.

2.2.3 Summary of Equations

The linearized equations of the theory of magnetoelasticity are summarized below.

Electromagnetic Subsystem

$$\underset{\sim}{B} = {}_t\underset{\sim}{B} + \underset{\sim}{b}, \qquad \underset{\sim}{E} = {}_t\underset{\sim}{E} + \underset{\sim}{e}, \qquad \underset{\sim}{J} = {}_t\underset{\sim}{J} + \underset{\sim}{j}$$

Field Equations

(i) small deformation cases

$$b_{\alpha,\alpha} = 0 \tag{2.58a}$$

$$\epsilon_{\alpha\beta\gamma} ({}_tE_\gamma + e_\gamma)_{,\beta} + \frac{\partial}{\partial t} b_\alpha = 0 \tag{2.58b}$$

$$\epsilon_{\alpha\beta\gamma} b_{\gamma,\beta} - \mu_o j_\alpha = 0 \tag{2.58c}$$

$$j_{\alpha,\alpha} = 0 \tag{2.58d}$$

(ii) large deformation cases

$$b_{\alpha,\alpha} - u_{\alpha,\beta} {}^tB_{\beta,\alpha} = 0 \tag{2.59a}$$

$$\epsilon_{\alpha\beta\gamma}\,({}_tE_\gamma + e_\gamma)_{,\beta} - \epsilon_{\alpha\beta\gamma}\,u_{\delta,\beta}\,{}_tE_{\gamma,\delta} + \frac{\partial}{\partial t}\,b_\alpha = 0 \tag{2.59b}$$

$$\epsilon_{\alpha\beta\gamma}\,b_{\gamma,\beta} - \epsilon_{\alpha\beta\gamma}\,u_{\delta,\beta}\,{}_tB_{\gamma,\delta} - \mu_o\,j_\alpha = 0 \tag{2.59c}$$

$$j_{\alpha,\alpha} - u_{\alpha,\beta}\,{}_tJ_{\beta,\alpha} = 0 \tag{2.59d}$$

Constitutive Equations

$${}_tJ_\alpha + j_\alpha = \sigma\,[{}_tE_\alpha + e_\alpha + \epsilon_{\alpha\beta\gamma}\,\dot{u}_\beta\,{}_tB_\gamma] \tag{2.60}$$

Boundary Conditions

$$\underset{\sim}{N}\cdot[\![\,\underset{\sim}{b}\,]\!] = 0 \tag{2.61a}$$

$$\underset{\sim}{N}\times[\![\,{}_t\underset{\sim}{E} + \underset{\sim}{e} + \dot{\underset{\sim}{u}}\times{}_t\underset{\sim}{B}\,]\!] = 0 \tag{2.61b}$$

$$\underset{\sim}{N}\times[\![\,\underset{\sim}{b}/\mu_o\,]\!] = 0 \tag{2.61c}$$

$$\underset{\sim}{N}\cdot[\![\,\underset{\sim}{j}\,]\!] = 0 \tag{2.61d}$$

where $\underset{\sim}{N}$ is the unit vector normal to the boundary surface

$$S(\xi_\alpha,\ t) = 0,$$

$$N_\alpha = S_{,\alpha} \,/\, \sqrt{S_{,\beta}\,S_{,\beta}} \tag{2.62}$$

In the second order theory, $\underset{\sim}{N}$ is replaced by $\underset{\sim}{n}$ given by

$$n_i = N_\alpha\,(\delta_{i\alpha} + N_\beta\,N_\gamma\,e_{\beta\gamma}\,\delta_{i\alpha} - u_{\alpha,i}) \tag{2.63}$$

Mechanical Subsystem

Equations of Motion

(i) small deformation cases

$$\rho\,\frac{\partial^2}{\partial t^2}\,u_\alpha = G u_{\alpha,\beta\beta} + (\lambda + G)\,u_{\beta,\beta\alpha} + \rho f_\alpha \tag{2.64}$$

$$\rho f_\alpha = ({}_t\underset{\sim}{J}\times{}_t\underset{\sim}{B})_\alpha + ({}_t\underset{\sim}{J}\times\underset{\sim}{b})_\alpha + (\underset{\sim}{j}\times{}_t\underset{\sim}{B})_\alpha \tag{2.65a}$$

(ii) large deformation cases (U.L. formulation)

$$\int_{t_V} C_{\alpha\beta\gamma\delta}\, e_{\gamma\delta}\, \delta e_{\alpha\beta}\, {}^{t}dV + \int_{t_V} {}^{t}\tau_{\alpha\beta}\, \delta\, \eta_{\alpha\beta}\, {}^{t}dV = {}^{t+\Delta t}R - \int_{t_V} {}^{t}\tau_{\alpha\beta}\, \delta e_{\alpha\beta}\, {}^{t}dV$$

$${}^{t+\Delta t}R = \int_{t_A} {}^{t+\Delta t}t_\alpha\, \delta\, u_\alpha\, {}^{t}dA + \int_{t_V} {}^{t}\rho\, ({}^{t+\Delta t}f_\alpha - \ddot{u}_\alpha)\, \delta\, u_\alpha\, {}^{t}dV \qquad (2.66a,b)$$

where

$$e_{\alpha\beta} = \tfrac{1}{2}\,(u_{\alpha,\beta} + u_{\beta,\alpha})$$

$$\eta_{\alpha\beta} = \tfrac{1}{2}\; u_{\gamma,\alpha}\, u_{\gamma,\beta}$$

$${}^{t}\rho\; {}^{t+\Delta t}f_\alpha = ({}^{t}\ddot{\mathcal{U}} \times {}^{t}\mathcal{B})_\alpha + ({}^{t}\ddot{\mathcal{U}} \times \mathcal{b})_\alpha + (\ddot{\mathcal{u}} \times {}^{t}\mathcal{B})_\alpha \qquad (2.65b)$$

Constitutive Equations

$$S_{\alpha\beta} = C_{\alpha\beta\gamma\delta}\, e_{\gamma\delta} \qquad (2.67)$$

where

$$S_{\alpha\beta} = {}^{t+\Delta t}S_{\alpha\beta} - {}^{t}\tau_{\alpha\beta}$$

$$C_{\alpha\beta\gamma\delta} = \lambda\, \delta_{\alpha\beta}\, \delta_{\gamma\delta} + 2G\, \delta_{\alpha\gamma}\, \delta_{\beta\delta}$$

Boundary Conditions

$$N_\beta \cdot [\![\, {}^{t+\Delta t}S_{\alpha\beta} + T_{\alpha\beta}\,]\!] = 0 \qquad (2.68)$$

N_β is replaced by n_j, Eq. (2.63), in the second order theory.

2.3 Magnetoelastic Plates

The linearized equations of magnetoelasticity presented in the previous section are specialized for thin plate problems in this section. In addition, some simplifying assumptions are introduced.

2.3.1 Literature Survey

There are two types of studies of magnetoelastic plates in the literature. The first one deals with the interaction of magnetic fields

with soft ferromagnetic plates. The magnetic force and body couple are generated from the magnetization of the material in this case. Eddy currents are usually not considered. The second one deals with conducting materials. In this case the eddy currents can be generated from both the time variation of the magnetic field and the motion of the plates. Most studies of this type consider the effect of motion only. A few studies consider transient magnetic fields but assume that the electric and magnetic fields are uncoupled and that the eddy current can have no reaction to the applied field. For the analytic treatment of the subject in both types, almost all authors consider strong and uniform static external magnetic fields.

Panovko and Gubanova (Ref. 39) first discussed the buckling of a cantilever ferromagnetic plate in a uniform static transverse magnetic field using a negative foundation type of magnetic force distribution. Moon and Pao (Ref. 40) recognized that in a uniform magnetic field there can be no net force on a magnetized body. A model based on a distribution of magnetic couple along the length of the plate was built, with the jump conditions of the magnetic field calculated on the surfaces of the deformed plate. The calculated critical magnetic fields agree well qualitatively with the experimental data, but the experimental data are lower than the theoretical values by a factor of about 1.8. Since then, a number of theoretical and experimental studies have been conducted trying to resolve this discrepancy, including the development of a self-consistent theory of linear ferroelastic continua by Pao and Yeh (Ref. 41). A detailed review of many of these papers may be found in Moon (Ref. 25).

More general boundary value problems have been studied by Van de Ven (Ref. 35) and Parkus (Ref. 11). In Parkus (Ref. 11), rectangular and

circular plates of an elastic, soft ferromagnetic material in a uniform, static transverse magnetic field are discussed. The linearized magnetoelastic theory based on Hutter and Pao's procedure (Ref. 30) is used for analysis. The equation of motion of the plate is derived by assuming uniform tangential induced electric fields and uniform normal induced magnetic fields across the thickness of the plates. The classic Kirchhoff assumption is used for the kinematics of the plate. Eddy current is not considered, and the effect of the in-plane deformation on the flexural deformation is also neglected. The influence of the magnetic field on the deformation of the plate is modelled as a surface effect. The critical magnetic field that causes the buckling of a clamped circular plate has been calculated. The resulting expression contains the 3/2 power of the thickness to radius ratio for an axisymmetric buckling mode, the same as in the Moon and Pao model for a periodically pinned beam-plate in sinusoidal deformation. No comparison to experimental data of this result is reported in this work. However, it shows unusual completeness of derivation, starting from the dipole-Amperian current model of electrodynamics in a moving body, through the linearization of the various field equations and boundary conditions, to the modelling of the specific boundary value problem of magnetoelastic plates.

Kaliski (Ref. 42) and Dunkin and Eringen (Ref.18) studied the vibrations and wave propagations in ferromagnetic plates under the action of uniform, static magnetic fields. The theories included conducting currents, but did not predict any instability phenomena. Moon and Pao (Ref. 43) in another paper showed that the frequency of vibration of the beam plate decreases as the magnetic field increases. The vibration and stability problems are then connected to each other, and the critical

magnetic field can be determined from the relation between the frequency and the field. In two-dimensional ferromagnetic plates, Moon (Ref. 44) and Srinivasan (Ref. 45) found that the magnetic field can either decrease or increase the natural frequencies, depending on its direction. To achieve buckling and a decrease in frequency, the field has to be nearly parallel to the plate normal. In Moon (Ref. 44), the buckling theory of beam-plates has also been extended to two-dimensional ferroelastic plates in oblique magnetic fields.

For nonferrous conducting materials, Dunkin and Eringen (Ref. 18) discussed the vibration of an infinite beam-plate in a static, tangential magnetic field and showed that the eddy current acts as a damping force. Their treatment of the interaction terms, however, is not complete. Ambartsumyan, et al. (Ref. 36) have published a monograph (in Russian) on magnetoelasticity of thin shells and plates under the action of static magnetic field. In a recent paper, Ambartsumyan (Ref. 46) discussed the oscillations of thin conducting plates in static, uniform transverse magnetic field. The linearized magnetoelastic equations (Ref. 36) were used for analysis. The induced tangential electric field and the induced normal magnetic field are assumed uniform across the thickness of the plate. An improved bending theory of plates (Ref. 47) is used, and the shear deformations of the plate considered. The electromagnetic boundary conditions are imposed on the surfaces of the undeformed plate. The calculated electromagnetic body force is in-plane and includes the effects of both the rotation of the plate normal and the shear deformations. The equations of motion are then integrated and averaged over the plate's thickness. The equations derived are applied to infinitely long plates, simply supported on the edges. The comparison of the results to the

predictions based on the assumption of undeformable normals shows very different behavior. The latter indicates the classical phenomena of decreasing frequency and buckling with increasing field in all modes. The former indicates damping without oscillations in the first mode for all values of the transverse shear effect. For the higher modes, the deformable normal theory shows decreasing frequencies and increasing damping for small thickness-to-length ratios at the beginning, and increasing frequencies at larger thickness-to-length ratios. No experimental data are reported to verify these results. However, it clearly indicates the importance of magnetic shear forces in such problems.

In an unpublished report, Moon (Ref. 37) presented some preliminary studies of the vibrations of conducting plates carrying strong transport currents. Edelen's nonlocal variational calculus (Ref. 48) was applied to the Lagrangian function of the coupled electromechanical system. Electrical heating was not considered. The results indicate stiffening of the system; however, further studies are needed for confirmation.

Moon (Ref. 25) has conducted experiments on circular aluminum plates levitated above a neighboring coil with sinusoidal currents. Circulating currents of up to 10^3A were induced in the plate together with the associated Joule heating. To minimize the thermal effects, resonance and free vibration techniques were used within 10 seconds after the current was turned on. The changes in frequency squared were found to be linearly related to the squares of the exciting coil currents. The frequencies of the diameter modes were found decreased and that of the symmetrical mode increased. However, thermoelastic effects cannot be separated from the observed changes in frequency. Further studies have been abandoned because of the inevitable complications of Joule heating. Clearly, all the

magnetoelastic studies of conducting bodies have to be subjected to the same limitation (Ref. 25).

2.3.2 Stream Function Method for Eddy Current Problem on a Moving Plate

In the last subsection some research on the vibrations of thin conducting plates under the action of a uniform, static field have been reviewed. The discussions there serve to reveal some aspects of the physical nature of the problem. In this subsection, forced vibrations of plates induced by time-dependent, nonuniform magnetic fields will be considered. Eddy currents can be generated by both the motion of the plate and the time variation of the magnetic field. Practical non-uniform fields such as those generated by current-carrying coils are of special interest. The tangential component of such a field will exert a normal force on the plate and cause a forced vibration. The induced vibration and the mutual interactions between the fields and the motion are the object of the study.

The linearized electromagnetic field relations, Eqs. (2.58), (2.60), and (2.61) will be used for analysis. They are referred to the configuration and boundary surfaces of the undeformed plate in the small deformation cases, and to the configuration and boundary surfaces of the last known position of the plate in large deformation cases. The unit normal vector to the boundary surface is defined by Eq. (2.62). In making such a choice, one loses the coupling terms in Eqs. (2.59). An iterative procedure will be suggested for the simultaneous satisfaction of both the electromagnetic and mechanical field equations. This procedure is basically an extension of the iteration scheme for the out-of-balance forces widely used in geometrically nonlinear elastic analysis.

Eqs. (2.64) and (2.66) will be applied to the mechanical subsystem in the small deformation and in the incremental large deformation analysis, respectively. The classical Kirchhoff assumption of the undeformable normal to the midsurface is adapted. Transverse and in-plane shear deformations are not considered.

The following two basic assumptions are made in this study:

(1) the induced current density $\underset{\sim}{J}$ is constant across the thickness of the plate and is parallel to the midsurface of the plate;

(2) the normal component of the induced magnetic field B_n^I is constant across the thickness of the plate.

These assumptions differ slightly from what other investigators have used in that one neglects the normal component of the current inside the plate.

The first assumption is a good approximation when the penetration depth of the magnetic field is large compared to the thickness of the plate, since the boundary condition Eq. (2.61d) will force the current to flow parallel to the surface. The second assumption is a valid one for such a current distribution, since the induced current is related to the normal component of the induced magnetic field through Eq. (2.58c). The penetration depth (skin depth) δ is large when the frequency of the magnetic field is low. It is expressed by the following formula (Ref. 49)

$$\delta^2 = \frac{2}{\mu\sigma\omega} \tag{2.69}$$

in which ω is the frequency of the magnetic field and σ the conductivity of the material.

Except for these two assumptions, the applied external magnetic field is assumed unaffected by the generation of the induced eddy current. That is, the power supply of the external driving coil is assumed to be

current controlled instead of voltage controlled. The generation of the eddy currents in the external coil thus does not need to be considered.

With the above assumption, the spatial and time variations of the applied field can be calculated directly from the driving current and geometry of the external coil. Only the induced parts of the electromagnetic field variables need to be determined.

To solve for the induced field variables, if Eqs. (2.58) in their present form are used, the electromagnetic field equations in regions outside the plate need to be considered. Boundary conditions for the induced field at infinity also have to be imposed. To avoid solving such a three-dimensional problem, the current density is chosen as the primary variable in this study. The electromagnetic field problem will be reformulated by using a generalization of the stream function method suggested by Moon (Ref. 25). Since Eqs. (2.58) and (2.60) are the same as Eqs. (2.24) and (2.25), respectively, in the following derivation the notation employed is that of the total $\underset{\sim}{B}$, $\underset{\sim}{E}$, and $\underset{\sim}{J}$ in the present configuration, but referred to the reference configuration.

Since the current density $\underset{\sim}{J}$ is uniform across the thickness, one defines

$$\underset{\sim}{I} = h\underset{\sim}{J} \tag{2.70}$$

where h is the thickness of the plate. From the continuity condition Eq. (2.24d):

$$\nabla \cdot \underset{\sim}{I} = h \nabla \cdot \underset{\sim}{J} = 0 \tag{2.71}$$

a stream function ψ is introduced for the current

$$\underset{\sim}{I} = \nabla \times (\psi \underset{\sim}{N}) = - \underset{\sim}{N} \times \nabla \psi \tag{2.72}$$

where $\underset{\sim}{N}$ is given by Eq. (2.62). Comparing Eq. (2.71) to (2.24c), one

finds that ψ is basically the normal component of the induced magnetic field B_N^I,

$$\psi = \frac{h}{\mu_o} B_N^I \tag{2.73}$$

The total magnetic field is separated into the applied external part $\underset{\sim}{B}^o$ and the induced part $\underset{\sim}{B}^I$,

$$\underset{\sim}{B} = \underset{\sim}{B}^o + \underset{\sim}{B}^I \tag{2.74}$$

The induced part is related to the eddy current distribution, under the quasi-static assumption, through the Biot-Savart law

$$\underset{\sim}{B}^I (\underset{\sim}{r}) = \frac{\mu_o}{4\pi h} \int_V \frac{\underset{\sim}{J}(\underset{\sim}{r}') \times (\underset{\sim}{r} - \underset{\sim}{r}')}{|\underset{\sim}{r} - \underset{\sim}{r}'|^3} dV' \tag{2.75}$$

Eq. (2.24a) is automatically satisfied here where $\underset{\sim}{r}$ is at the mid-surface of the plate.

The stream function may now be determined by substitution of Eqs. (2.72), (2.74) and (2.75) into the Faraday's law, Eq. (2.24b),

$$\nabla \times \nabla \times (\psi \underset{\sim}{N}) = - \sigma h \frac{\partial}{\partial t} (\underset{\sim}{B}^o + \underset{\sim}{B}^I) + \sigma h \nabla \times (\dot{\underset{\sim}{u}} \times \underset{\sim}{B}^o) \tag{2.76}$$

Only the normal component of the vector equation will be used because the in-plane current is of primary interest. Note also that the last term in Eq. (2.76) has been linearized by dropping the self-induced field. The variation of $\dot{\underset{\sim}{u}} \times \underset{\sim}{B}^o$ across the thickness contains all the shear deformation effects. However, since the flexural motion of the plate is of primary interest in this research, this term will refer to $\dot{\underset{\sim}{u}} \times \underset{\sim}{B}^o$ on the mid-surface of the plate only. In small deformation cases, it is the original mid-plane of the plate. In the large deformation cases, it is the curved mid-surface in the reference configuration of the deformed plate.

To have a general description, let an orthogonal curvilinear coordinate system ζ_α be introduced on the mid-surface, Fig. 2.4, with unit base vectors $\underset{\sim}{e}_\alpha$ (α=1,2,3). $\underset{\sim}{e}_\zeta$ is the same unit normal vector $\underset{\sim}{N}$ defined by Eq. (2.62). One has, on the mid-surface,

$$\xi_1 = \xi_1 (\zeta_1, \zeta_2), \quad \xi_2 = \xi_2 (\zeta_1, \zeta_2), \quad \xi_3 = \xi_3 (\zeta_1, \zeta_2) \tag{2.77}$$

The infinitesimal line element on the mid-surface is given by

$$dS^2 = a_{\alpha\beta}\, d\zeta_\alpha\, d\zeta_\beta \tag{2.78}$$

where

$$a_{\alpha\beta} = \frac{\partial \xi_\gamma}{\partial \zeta_\alpha} \frac{\partial \xi_\gamma}{\partial \zeta_\beta} \tag{2.79a}$$

$$a_{12} = \frac{\partial \xi_\gamma}{\partial \zeta_1} \frac{\partial \xi_\gamma}{\partial \zeta_2} \equiv 0 \tag{2.79b}$$

The unit tangent vector $\underset{\sim}{e}_\alpha$ (α=1,2) is given by

$$\underset{\sim}{e}_\alpha = \frac{1}{a_{\alpha\alpha}} \left[\frac{\partial \xi_1}{\partial \zeta_\alpha}, \frac{\partial \xi_2}{\partial \zeta_\alpha}, \frac{\partial \xi_3}{\partial \zeta_\alpha}\right]$$

The current density on the surface can be written in the form

$$\underset{\sim}{I} = I_1 (\zeta_1, \zeta_2)\, \underset{\sim}{e}_1 + I_2 (\zeta_1, \zeta_2)\, \underset{\sim}{e}_2 \tag{2.81}$$

Then,

$$\nabla \cdot \underset{\sim}{I} = \frac{1}{a_{11}\, a_{22}} \left[\frac{\partial}{\partial \zeta_1} (a_{22}\, I_1) + \frac{1}{\partial \zeta_2} (a_{11}\, I_2)\right] = 0 \tag{2.82}$$

and

$$I_1 = \frac{1}{a_{22}} \frac{\partial \psi}{\partial \zeta_2}, \quad I_2 = -\frac{1}{a_{11}} \frac{\partial \psi}{\partial \zeta_1} \tag{2.83}$$

The normal component of the left hand side of Eq. (2.76) becomes

$$\underset{\sim}{e}_3 \cdot [\nabla \times \nabla \times (\psi\, \underset{\sim}{e}_3)] = -\frac{1}{a_{11}\, a_{22}} \left[\frac{\partial}{\partial \zeta_1} \left(\frac{a_{22}}{a_{11}} \frac{\partial \psi}{\partial \zeta_1}\right) + \frac{\partial}{\partial \zeta_2} \left(\frac{a_{11}}{a_{22}} \frac{\partial \psi}{\partial \zeta_2}\right)\right] \tag{2.84}$$

Let $\underset{\sim}{R} = \underset{\sim}{r} - \underset{\sim}{r}'$, $R = |\underset{\sim}{R}| = |\underset{\sim}{r} - \underset{\sim}{r}'|$. Note that $\underset{\sim}{R}/R^3 = \nabla_1 \left(\frac{1}{R}\right)$, where ∇_1 is the gradient and operates on the $\underset{\sim}{r}'$ variables. One has, by

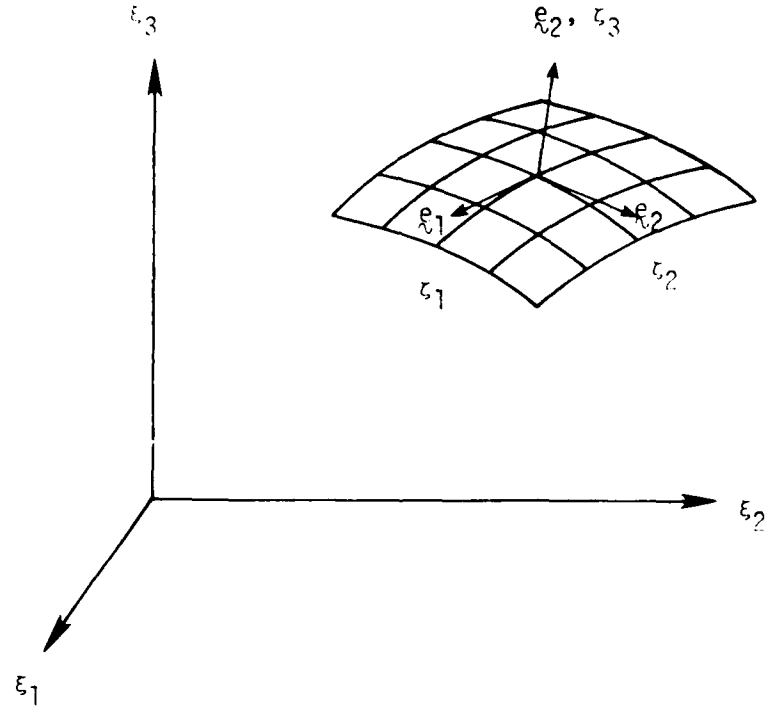

Figure 2.4 Orthogonal curvilinear coordinate system $\underset{\sim}{\xi}_\alpha$ on the mid-surface of the deformed plate; $\underset{\sim}{\xi}_\alpha$ is the Cartesian coordinate of the reference configuration of the deformed plate.

substituting Eq. (2.77) into (2.75),

$$\underset{\sim}{B}^{I}(\underset{\sim}{r}) = -\frac{\mu_o}{4\pi h}\int_{V'}(\underset{\sim}{e}_3' \times \nabla_1 \psi) \times \nabla_1 \left(\frac{1}{R}\right) dV' \tag{2.85}$$

$$= \frac{\mu_o}{4\pi h}\int_{V'}[\nabla_1 \psi \cdot \nabla_1 \left(\frac{1}{R}\right)]\underset{\sim}{e}_3' \, dV' - \frac{\mu_o}{4\pi h}\int_{V'}[\underset{\sim}{e}_3' \cdot \nabla_1 \left(\frac{1}{R}\right)] \nabla_1 \psi \, dV'$$

The normal component of which is

$$B_N^I(\underset{\sim}{r}) = \frac{\mu_o}{4\pi h}\int_{V'}[\nabla_1 \psi \cdot \nabla_1 \left(\frac{1}{R}\right)] (\underset{\sim}{e}_3' \cdot \underset{\sim}{N}) \, dV'$$

$$- \frac{\mu_o}{4\pi h}\int_{V'}[\underset{\sim}{e}_3' \cdot \nabla_1 \left(\frac{1}{R}\right)] (\nabla_1 \psi \cdot \underset{\sim}{N}) \, dV' \tag{2.86}$$

Note that because

$$[\nabla_1 \psi \cdot \nabla_1 \left(\frac{1}{R}\right)] (\underset{\sim}{e}_3' \cdot \underset{\sim}{N}) = \nabla_1 \cdot \{(\underset{\sim}{e}_3' \cdot \underset{\sim}{N}) \psi \nabla_1 \left(\frac{1}{R}\right)\} - (\underset{\sim}{e}_3' \cdot \underset{\sim}{N}) \psi \nabla_1^2 \left(\frac{1}{R}\right)$$

$$- \psi \nabla_1 (\underset{\sim}{e}_3' \cdot \underset{\sim}{N}) \cdot \nabla_1 \left(\frac{1}{R}\right), \tag{2.87}$$

one has

$$B_N^I(\underset{\sim}{r}) = \frac{\mu_o}{4\pi h}\int_{V'}\{\nabla_1 \cdot [(\underset{\sim}{e}_3' \cdot \underset{\sim}{N}) \psi \nabla_1 \left(\frac{1}{R}\right)] - (\underset{\sim}{e}_3' \cdot \underset{\sim}{N}) \psi \nabla_1^2 \left(\frac{1}{R}\right)\} dV'$$

$$- \frac{\mu_o}{4\pi h}\int_{V'}[(\nabla_1 \psi \cdot \underset{\sim}{N}) \underset{\sim}{e}_3' + \psi \nabla_1 (\underset{\sim}{e}_3' \cdot \underset{\sim}{N})] \cdot \nabla_1 \left(\frac{1}{R}\right) dV' \tag{2.88}$$

Let

$$\underset{\sim}{Q} = (\nabla_1 \psi \cdot \underset{\sim}{N}) \underset{\sim}{e}_3' + \psi \nabla_1 (\underset{\sim}{e}_3' \cdot \underset{\sim}{N}) \tag{2.89}$$

By using the following relations,

$$\int_V \nabla \cdot \underset{\sim}{\bar{\phi}} \, dV = \int_S \underset{\sim}{\bar{\phi}} \cdot dS \tag{2.90a}$$

$$\int_{V'} f(\underset{\sim}{r}') \nabla^2 \frac{1}{|\underset{\sim}{r} - \underset{\sim}{r}'|} dV' = -4\pi f(\underset{\sim}{r}) \tag{2.90b}$$

$$\underset{\sim}{Q} \cdot \nabla_1 \left(\frac{1}{R}\right) = \nabla_1 \cdot \left(\frac{1}{R}\underset{\sim}{Q}\right) - \frac{1}{R}\nabla_1 \cdot \underset{\sim}{Q} \tag{2.90c}$$

one has

$$B_N^I(\underset{\sim}{r}) = \frac{\mu_o}{h}\psi(\underset{\sim}{r}) + \frac{\mu_o}{4\pi h}\int_{S'}(\underset{\sim}{e}_3' \cdot \underset{\sim}{N})\,\psi\,\nabla_1\left(\frac{1}{R}\right)\cdot\underset{\sim}{e}_3'\,dS'$$

$$- \frac{\mu_o}{4\pi h}\int_{S'}[(\nabla_1\psi \cdot \underset{\sim}{N})\,\underset{\sim}{e}_3' + \psi\,\nabla_1(\underset{\sim}{e}_3' \cdot \underset{\sim}{N})]\frac{1}{R}\cdot\underset{\sim}{e}_3'\,dS'$$

$$+ \frac{\mu_o}{4\pi h}\int_{V'}\frac{1}{R}\nabla_1 \cdot \underset{\sim}{Q}\,dV' \tag{2.91}$$

under the assumption of undeformable normals, $\nabla_1(\underset{\sim}{e}_3' \cdot \underset{\sim}{N}) \cdot \underset{\sim}{e}_3' = 0$. The second surface integral becomes

$$- \frac{\mu_o}{4\pi h}\int_{S'}\frac{1}{R}\nabla_1\psi \cdot \underset{\sim}{N}\,dS'$$

The volume integral contains the 1/R singularity and diverges at the mid-surface as R approaches 0. However, for flate plates, $\underset{\sim}{e}_3' \cdot \underset{\sim}{N} = 1$ and $\nabla_1\psi \cdot \underset{\sim}{N} = 0$ for all $\underset{\sim}{r}'$. Eq. (2.91) becomes

$$B_N^I(\underset{\sim}{r}) = \frac{\mu_o}{h}\psi(\underset{\sim}{r}) + \frac{\mu_o}{4\pi h}\int_{S'}(\underset{\sim}{e}_3' \cdot \underset{\sim}{N})\,\psi\,\nabla_1\left(\frac{1}{R}\right)\cdot\underset{\sim}{e}_3'\,dS' \tag{2.92}$$

which is free from the singular nature of the Biot-Savart law at the mid-plane of the plate.

It is observed that the $\nabla_1 \cdot \underset{\sim}{Q}$ term in Eq. (2.91) is related to the curvatures and their derivatives of the deformed plate and is therefore of the second order in magnitude. Furthermore, the type of singularity associated with it has been reduced by the order of one. One must assume finite deflections but small rotations in nonlinear problems to neglect the last term. Eq. (2.91) then takes the following form

$$B_N^I(\underset{\sim}{r}) = \frac{\mu_o}{h}\psi(\underset{\sim}{r}) + \frac{\mu_o}{4\pi h}\int_{S'}(\underset{\sim}{e}_3' \cdot \underset{\sim}{N})\,\psi\,\nabla_1\left(\frac{1}{R}\right)\cdot\underset{\sim}{e}_3'\,dS'$$

$$- \frac{\mu_o}{4\pi h}\int_{S'}\frac{1}{R}\nabla_1\psi\cdot\underset{\sim}{N}\,dS' \qquad (2.93)$$

The time rate of change of which is

$$\frac{\partial}{\partial t}B_N^I = \frac{\mu_o}{h}\frac{\partial}{\partial t}\psi + \frac{\mu_o}{4\pi h}\int_{S'}(\underset{\sim}{e}_3' \cdot \underset{\sim}{N})\frac{\partial}{\partial t}\psi\,\nabla_1\left(\frac{1}{R}\right)\cdot\underset{\sim}{e}_3'\,dS'$$

$$- \frac{\mu_o}{4\pi h}\int_{S'}\frac{1}{R}\frac{\partial}{\partial t}(\nabla_1\psi)\cdot\underset{\sim}{N}\,dS'$$

$$+ \frac{\mu_o}{4\pi h}\int_{S'}\frac{\partial}{\partial t}(\underset{\sim}{e}_3' \cdot \underset{\sim}{N})\,\psi\,\nabla_1\left(\frac{1}{R}\right)\cdot\underset{\sim}{e}_3'\,dS'$$

$$+ \frac{\mu_o}{4\pi h}\int_{S'}(\underset{\sim}{e}_3' \cdot \underset{\sim}{N})\,\psi\frac{\partial}{\partial t}\left[\nabla_1\left(\frac{1}{R}\right)\cdot\underset{\sim}{e}_3'\right]dS'$$

$$- \frac{\mu_o}{4\pi h}\int_{S'}\frac{\partial}{\partial t}\left(\frac{1}{R}\underset{\sim}{N}\right)\cdot\nabla_1\psi\,dS' \qquad (2.94)$$

The first three terms obviously correspond to the rigid body state. The other terms represent the perturbation caused by the relative rotation, transverse deflection, and stretching of the plate elements. The rigid body terms are expected to have the dominant effect. The coupling terms will be discussed in the next subsection.

For rigid flat plates, Fig. 2.5a, one has (Ref.25)

$$\frac{\partial}{\partial t}B_N^I = \frac{\mu_o}{h}\frac{\partial}{\partial t}\psi - \frac{\mu_o}{4\pi}\int_{S'}\frac{\frac{\partial}{\partial t}\psi(x', y')}{\left[(x-x')^2 + (y-y')^2 + \frac{h^2}{4}\right]^{3/2}}\,dS' \qquad (2.95)$$

In the derivation of the above equation, the boundary condition on the narrow edges of the plate is $\psi = o$. For a rigid plate infinitely long in the y-direction and of finite width ℓ in the x-direction, Fig. 2.5b, with fields independent of the y-coordinate, one can integrate the second

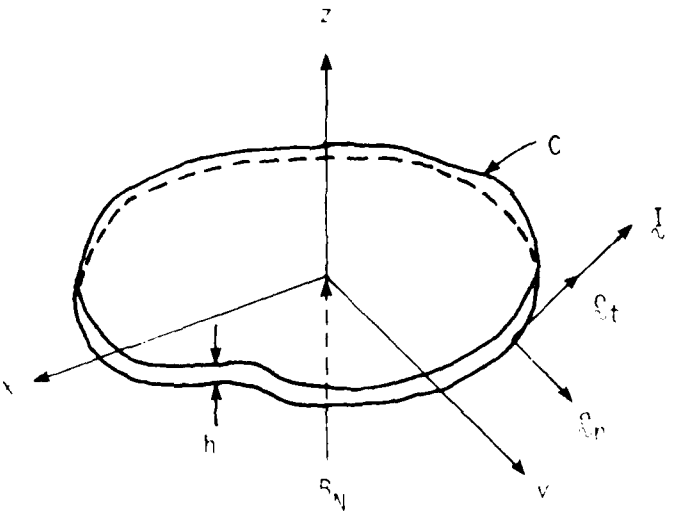

(a)

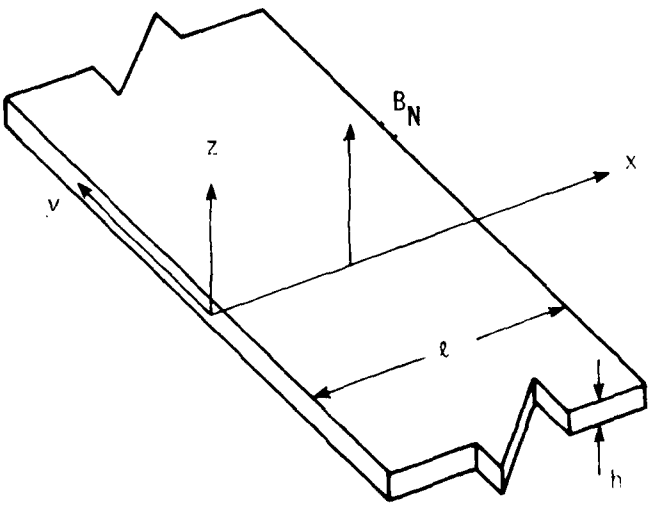

(b)

Figure 2.5 (a) Finite (two-dimensional) conducting plate;
(b) Infinitely-long (one-dimensional) conducting plate.

term in Eq. (2.95) with respect to y' and obtain

$$\frac{\partial}{\partial t} B_N^I = \frac{\mu_o}{h} \frac{\partial}{\partial t} \psi - \frac{\mu_o}{2\pi} \int_o^{\ell} \frac{\frac{\partial}{\partial t} \psi (x')}{(x-x')^2 + \frac{h^2}{4}} dx' \tag{2.96}$$

Eqs. (2.95) and (2.96) will be used in Chapter Three for eddy current calculations on rigid plates.

The normal component of the last term in Eq. (2.76) is

$$\sigma h \, \underset{\sim}{N} \cdot \nabla \times (\dot{\underset{\sim}{\mu}} \times \underset{\sim}{B}^o) = \sigma h \frac{1}{a_{11} a_{22}} \left[\frac{\partial}{\partial \zeta_1} (a_{22} A_2) - \frac{\partial}{\partial \zeta_2} (a_{11} A_1)\right] \tag{2.97}$$

where

$$A_1 = \dot{u}_2 B_3^o - \dot{u}_3 B_2^o, \qquad A_2 = \dot{u}_3 B_1^o - \dot{u}_1 B_3^o \tag{2.98}$$

in the ζ_α - coordinate system.

The three-dimensional transient field problem thus reduces to a two-dimensional one on the mid-surface of the plate. To the above equations, one needs to add the boundary conditions for ψ described in the following.

Assume a simply connected plate. At the boundary curve C, Fig. 2.5a, the current density I should be tangent:

$$\underset{\sim}{I} \cdot \underset{\sim}{e}_n = 0 \tag{2.99}$$

or

$$(\nabla \psi \times \underset{\sim}{N}) \cdot \underset{\sim}{e}_n = \nabla \psi \cdot \underset{\sim}{e}_t = 0 \tag{2.100}$$

By integrating the above equation along the boundary, one can replace Eq. (2.99) by

$$\psi = 0 \qquad \text{on C} \tag{2.101}$$

2.3.3 Coupling Effects

The kinematic nature of the Biot-Savart law has been recognized in the last subsection. Eq. (2.94) has been derived based on the assumption

of nondeformable normal and small rotation of the plate element. The divergence property of the Biot-Savart law on the mid-surface has been avoided by transforming the volume integral into a surface integral. The normal component of the self-field on the mid-surface of the plate has therefore been modelled as caused by a distribution of singularities on the top and the bottom surfaces of the plate.

The coupling terms in Eq. (2.94), however, are too complicated. The effects of the motion on the field come through the relative rotational and translational velocities of the whole plate in a global way. However, these terms correspond to the interaction between the motion of the plate and the self magnetic field and are of the second order in the theory of the coupled problem. One therefore drops these coupling terms and considers only the local coupling effect, i.e., the last term in Eq. (2.76), which has already been linearized. The coupling terms in Eq. (2.94) might be important for transport current problems, however (Ref. 37).

With the above linearization, the eddy current problem is formulated as follows. For finite deformation incremental analysis, one has

$$\frac{1}{a_{11}\,a_{22}}\left[\frac{\partial}{\partial\zeta_1}\left(\frac{a_{22}}{a_{11}}\frac{\partial\psi}{\partial\zeta_1}\right)+\frac{\partial}{\partial\zeta_2}\left(\frac{a_{11}}{a_{22}}\frac{\partial\psi}{\partial\zeta_2}\right)\right]-\mu_0\sigma\frac{\partial\psi}{\partial t}$$

$$-\frac{\mu_0\sigma}{4\pi}\left(\int_{\text{top}}+\int_{\text{bottom}}\right)\left[\left(\underset{\sim}{e}'_3\cdot\underset{\sim}{N}\right)\frac{\partial\psi}{\partial t}\nabla_1\left(\frac{1}{R}\right)\cdot\underset{\sim}{e}'_3-\frac{1}{R}\frac{\partial}{\partial t}\left(\nabla_1\psi\right)\cdot\underset{\sim}{N}\right]dS'$$

$$+\sigma h\frac{1}{a_{11}\,a_{22}}\left\{\frac{\partial}{\partial\zeta_1}\left[a_{22}\left(\dot{\underset{\sim}{\mu}}\times\underset{\sim}{\beta}^0\right)_2\right]-\frac{\partial}{\partial\zeta_2}\left[a_{11}\left(\dot{\underset{\sim}{\mu}}\times\underset{\sim}{\beta}^0\right)_1\right]\right\}$$

$$=\sigma h\frac{\partial}{\partial t}B_N^0 \qquad (2.102)$$

In the small deformation cases, it reduces to

$$\left(\frac{\partial^2}{\partial x^2} + \frac{\partial^2}{\partial y^2}\right) \psi - \mu_o \sigma \frac{\partial \psi}{\partial t} \quad \frac{\mu_o \sigma h}{4\pi} \iint \frac{\frac{\partial}{\partial t} \psi\ (x', y')}{\left[(x-x')^2 + (y-y')^2 + \frac{h^2}{4}\right]^{3/2}} dx'\ dy$$

$$+ \sigma h \frac{\partial}{\partial x} (\dot{w} B_x^o - \dot{u} B_z^o) - \frac{\partial}{\partial y} (\dot{v} B_z^o - \dot{w} B_y^o)$$

$$= h \frac{\partial}{\partial t} B_z^o \tag{2.103}$$

where $\dot{u}$, $\dot{v}$, and $\dot{w}$ are the in-plane x-direction velocity, the in-plane y-direction velocity, and the transverse velocity, respectively. In the small deformation of infinitely long plates, it is

$$\frac{\partial^2 \psi}{\partial x^2} - \sigma \mu_o \frac{\partial \psi}{\partial t} + \frac{\sigma \mu_o h}{2\pi} \int_0^{\ell} \frac{\frac{\partial}{\partial t} \psi\ (x')}{(x-x')^2 + \frac{h^2}{4}} dx' + \sigma h \frac{\partial}{\partial x} (\dot{w} B_x^o - \dot{u} B_z^o)$$

$$= h \frac{\partial}{\partial t} B_z^o \tag{2.104}$$

The effect of in-plane deformation has been included in Eqs. (2.102) to (2.104). The corresponding equations of motion are provided by Eqs. (2.66) to (2.67) for the finite deformation incremental analysis. For small deformation cases, they can be obtained by applying the nondeformable normal assumption to Eq. (2.64). In the present study, they are taken to be the classical equations for plates subjected to both in-plane and out-of-plane loads, and are

$$\frac{Eh}{1-\nu^2}\left(\frac{\partial^2 u}{\partial x^2}+\frac{H\nu}{2}\frac{\partial^2 v}{\partial x\partial y}+\frac{1-\nu}{2}\frac{\partial^2 u}{\partial y^2}\right)+I_y B_z^o=\rho h\frac{\partial^2 u}{\partial t^2} \tag{2.105a}$$

$$\frac{Eh}{1-\nu^2}\left(\frac{\partial^2 v}{\partial y^2}+\frac{H\nu}{2}\frac{\partial^2 u}{\partial x\partial y}+\frac{1-\nu}{2}\frac{\partial^2 v}{\partial x^2}-I_x B_z^o=\rho h\frac{\partial^2 v}{\partial t^2}\right. \tag{2.105b}$$

$$D\left(\frac{\partial^4 w}{\partial x^4}+2\frac{\partial^4 w}{\partial x^2\partial y^2}+\frac{\partial^4 w}{\partial y^4}+I_y B_z^o\frac{\partial w}{\partial x}-I_x B_z^o\frac{\partial w}{\partial y}\right.$$

$$\left.=I_x B_y^o-I_y B_x^o-\rho h\frac{\partial^2 w}{\partial t^2}\right. \tag{2.105c}$$

For small deformations of infinitely long plates, Eqs. (2.105) reduce to

$$\frac{Eh}{1-\nu^2}\frac{\partial^2 u}{\partial x^2}+I_y B_z^o=\rho h\frac{\partial^2 u}{\partial t^2} \tag{2.106a}$$

$$D\frac{\partial^4 w}{\partial x^4}+I_y B_z^o\frac{\partial w}{\partial x}+\rho h\frac{\partial^2 w}{\partial t^2}=-I_y B_x^o \tag{2.106b}$$

where

$$I_x = \frac{\partial \psi}{\partial y} , \qquad I_y = - \frac{\partial \psi}{\partial x} \tag{2.107}$$

2.3.4. Magnetic Body Forces in Plates

Equations (2.102) to (2.107) will be the basis for the later chapters. Their derivations have been based on several assumptions. Except for the undeformable normal of the plate and the constant eddy current density and constant normal component of the induced magnetic field across the thickness of the plate, every variable has been referred to the mid-surface of the plate. Specifically, the magnetic force density has been treated as constant across the thickness and equals in magnitude to its value at the mid-surface. In these calculations, the equation has also been linearized by dropping the effect of the induced magnetic field. In this subsection, the implications of these assumptions will be considered.

The assumptions of constant current and constant normal component of the induced magnetic field across the thickness average the induced current distribution. In the calculation of the normal force, the tangential component of the applied field is evaluated at the mid-surface, and the contribution from the induced field B_t^I, is not included, Figure 2.6a. Since the tangential component of the induced field will vary approximately linearly across the thickness and have zero value at the mid-surface, the normal force ρf_n^I corresponding to it will have the same variation and be self-equilibrating. The result for the normal force should therefore be a good representation for the total force across the thickness.

The same approach is used for the calculation of the in-plane force. Again, good results should be obtained for the total force by averaging

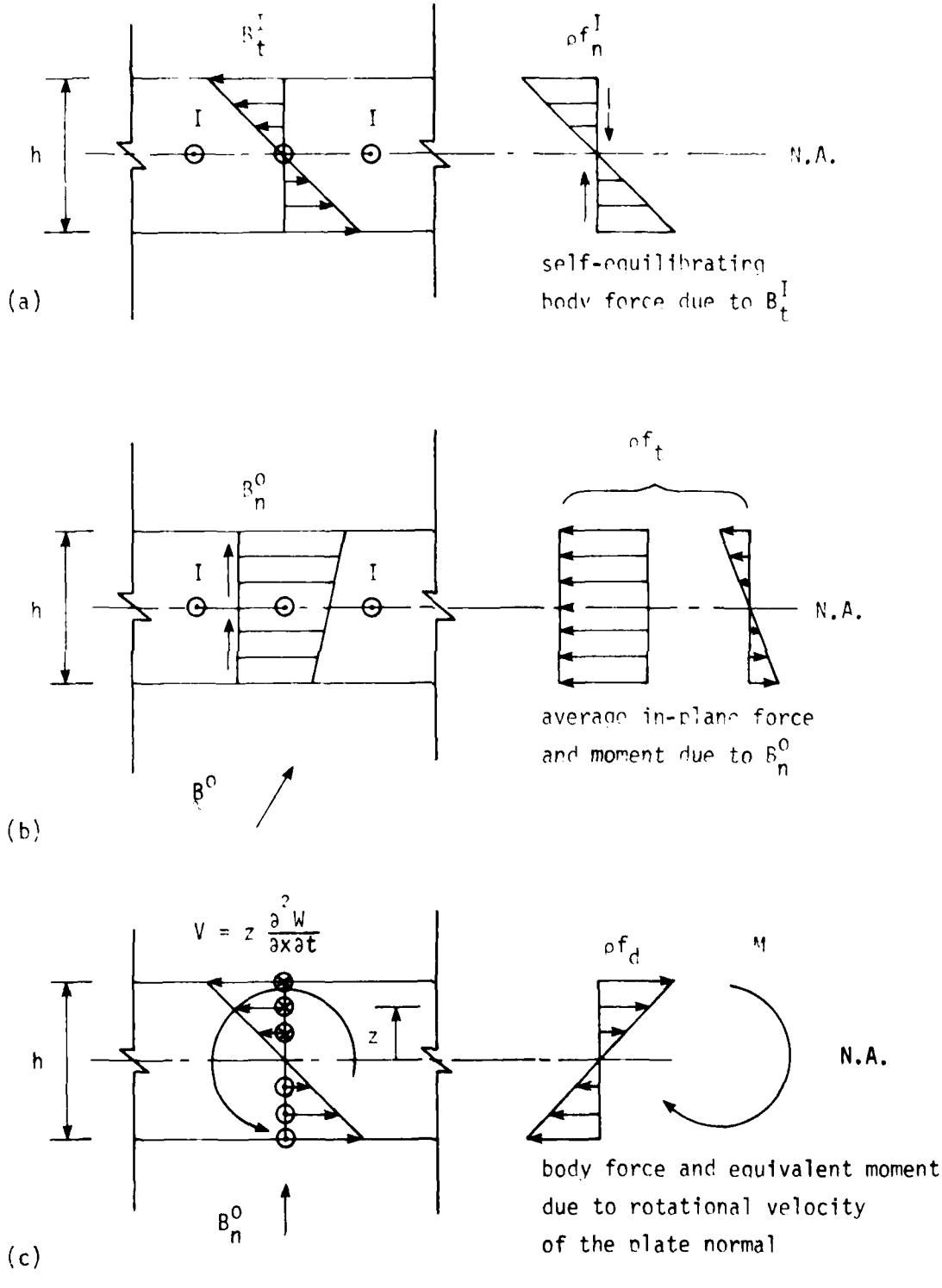

Figure 2.6 Body forces and moments in conducting plate.

across the thickness. Here, however, the variation of the normal component of the applied field B_n^o gives a variation of the in-plane force across the thickness, which creates a body moment distributed over the whole plate, Fig. 2.6b. This effect is not included in the present model since all the variables have been evaluated on the mid-surface. The body moment can be easily included, however. Moon (Ref. 25) has derived the following equation for the plate which includes such an effect, but neglects the in-plane force in the plate.

$$D \nabla^4 w + \rho h \frac{\partial^2 w}{\partial t^2} = F + \underset{\sim}{N} \cdot \nabla \times \underset{\sim}{C} \tag{2.108}$$

where

$$F = \int_{-h/2}^{h/2} \underset{\sim}{N} \cdot (\underset{\sim}{J} \times \underset{\sim}{B}) \, dz \tag{2.109a}$$

$$\underset{\sim}{C} = \int_{-h/2}^{h/2} \underset{\sim}{N} \times (\underset{\sim}{J} \times \underset{\sim}{B}) \, z dz \tag{2.109b}$$

When the plate is thin, and the driving coil far away from the plate, the applied magnetic field will have only a small variation across the thickness. The magnetic moment in such cases can be neglected without introducing much error.

A coupling effect not considered in the present model comes from the rotational velocity of the plate normal, Fig. 2.6 (c). The rotational velocity gives an effective tangential current

$$J = B_n^o \, z \frac{\partial^2 w}{\partial x \partial t}$$

in a normal direction across the thickness. This causes a tangential body force distribution

$$\rho f = J B_n^o = (B_n^o)^2 \, z \frac{\partial^2 w}{\partial x \partial t}$$

Integrating over the thickness, one obtains the body moment distribution

$$M = \int_{-h/2}^{h/2} \rho f\, z\, dz = (B_n^o)^2 \frac{\partial^2 w}{\partial x \partial t} \int_{-h/2}^{h/2} z^2\, dz$$

$$= \frac{1}{12} h^3 (B_n^o)^2 \frac{\partial^2 w}{\partial x \partial t} \qquad (2.110)$$

which is opposite to the rotational velocity and thus has a rotational damping effect. This is the "classical" coupling term reported by Ambartsumyan et al. (Ref. 36). To consider this effect, one needs to add the rotational inertia force term in the equation of motion. In the present study, one is limited to the stretching and the transverse flexural deflection of the plate. The rotational effect is not considered.

A visualization of the magnetic body force in an infinitely long plate may be obtained from Faraday's concept of the magnetic line of force. The magnetic line of force is the magnetic field line to which certain amount of electromotive tension has been applied. The force depends solely upon the strength of the magnet producing it. A compressive force is also developed between the field lines and is at a right angle to them (Ref. 50). When the line of force is cut, due to either the time-variation of the field or the motion of the plate, exactly the same amount of force is released. The mechanical stress must then be developed to equilibrate the above-mentioned tension and pressure.

In Fig. 2.7a, the applied field is varying at a relatively low frequency. Eddy current is induced in the plate and the generated self field is added to the applied field. The total magnetic field lines are distorted from straight but still penetrate through the plate. The tension and pressure associated with the magnetic field lines are exerted on the plate. It is to this case that the theory developed in this chapter is

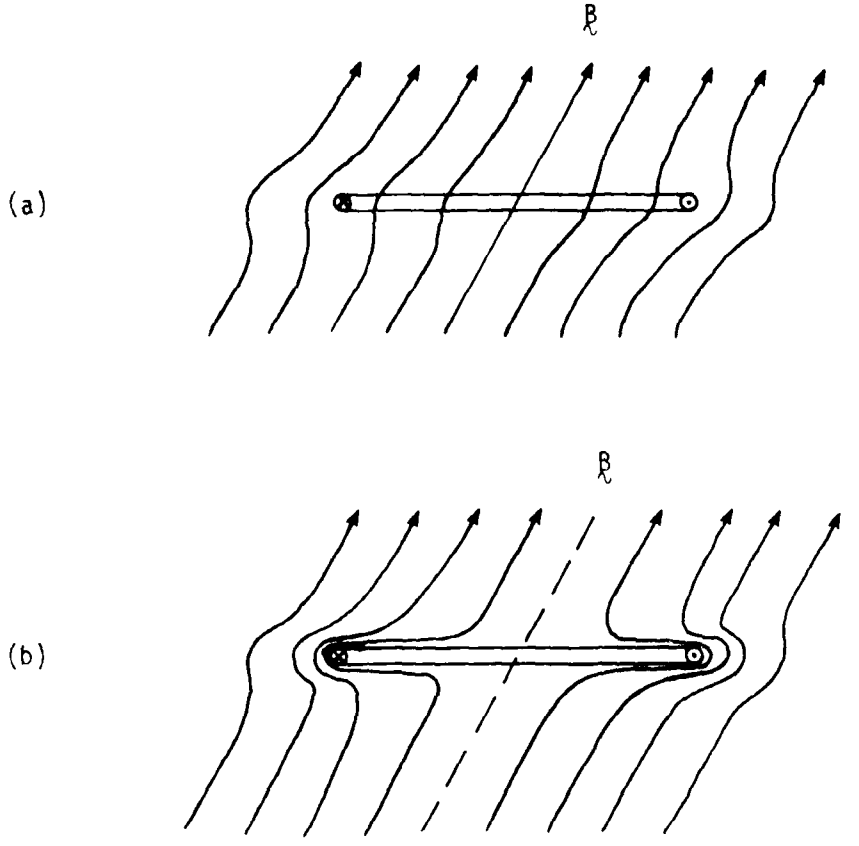

Figure 2.7 Magnetic lines of force (magnetic field lines) in and around an infinitely long conducting plate; (a) low frequency case, (b) high frequency case.

applied under the two basic magnetoelastic assumptions.

When the frequency of the applied field is high, the generated self field completely screens the applied field from penetrating the plate. This situation is shown in Fig. 2.7b. The skin depth in this case is limited to a very thin layer on the top and bottom surfaces of the plate, and the eddy current is basically a surface current on the plate. The same situation may be obtained at low frequencies for conductors with very large conductivity ($\sigma \tilde{\sim} \infty$). The magnetic force in this case acts like a surface force. Boundary conditions Eqs. (2.13a) and (2.13b) should be used for the electromagnetic field conditions in such problems. The magnetic force is usually called the magnetic pressure in such cases.

Chapter 3

EDDY CURRENT CALCULATION ON RIGID CONDUCTORS

The governing equations derived in Chapter Two for the calculation of eddy currents are applied to rigid conducting plates in this chapter as a first step in the study of the coupling of eddy currents and deformations. The one-and two-dimensional equations for steady state eddy current problems are nondimensionalized and solved by the finite element method. The role of the nondimensional parameters in these equations are investigated. Finite element transient analysis is also applied to the one-dimensional problems. The results of the analysis are verified by comparing with analytic solutions in the high and low frequency extreme cases and with experimental data. The capability, input, and output of the computer programs developed are briefly described.

A literature survey of the eddy current calculation on conducting plates is given in the first section. The intimate relation between the quasi-static field equations and the circuit equations is the basis of many studies and provides another point of view to the stream function formulation of the eddy current calculation used in this work. This subject is discussed in the second section of this chapter.

3.1 Literature Survey

Because of the importance of the eddy current calculation in the present research, a brief literature survey on this subject is given in this section. The purpose of the survey is to provide a background for

the comparison of the stream function method with other approaches to this problem. Some key features of eddy current calculation and recent advances are also highlighted.

As discussed in Chapter Two, eddy currents are found in any conducting material which is subjected to time-varying magnetic field. Its existence is manifested by (1) induced Joule heating, (2) a magnetic reaction field, and (3) a magnetic force resulting from the interaction of the inducing and reaction fields. It is possible to put the eddy currents to good use. Examples are induction furnaces, which use the ohmic losses of high frequency eddy currents; electromagnetic nondestructive testing, which uses the magnetic reaction field of eddy current; and magnetic forming and levitation, which use the magnetic force generated by eddy currents. It is sometimes necessary to take steps to reduce the effect of eddy currents. An example is the need to minimize losses to enable the cores of transformers and rotating electrical machines to carry the required magnetic flux; one way this is achieved is by laminating the cores. Studies of the effects of eddy currents may be found in the technical literature related to all of these applications.

Rigorous analytic solutions to eddy current problems can seldomly be obtained and are usually limited to infinitely extended conductors or closed conductor shapes such as spheres or ellipsoids. Many such problems and some solutions may be found in Smythe (Ref. 51). Conductors with finite length and more general shape are more difficult to handle. The solutions are usually obtained by either analytic techniques such as iterative approximation and Rayleigh-Ritz method, or by numerical means such as finite difference, finite element, and boundary integral equation methods. The choice of the solution method depends to a large extent on

the formulation of the problem. The magnetic energy and variational principle are the basis of many studies. The circuit analogy provides another model more intuitively appealing to electrical engineers.

The analytic techniques have the advantage that the problem parameters appear as variables in the solutions. The effect of altering one or more such parameters can therefore be fairly readily appreciated. The numerical methods have wider application but the disadvantage that the parameters are concealed in the numerical results produced from a given set of data. Dimensional analysis in this case can be used to reduce the excessive computation with numerous sets of data. Some illustrations of the application of dimensional analysis in the present study are given in sections 3 and 4 of this chapter. A brief introduction to the use of dimensional analysis in eddy current problems is given in Stoll (Ref. 52); this is one of the few references which deals with this specific application of dimensional analysis.

Books and monographs addressing the analysis of eddy currents are scarce in the literature. Two monographs on this subject are Stoll (Ref. 52) and Lammeraner and Stasl (Ref. 53). The problems discussed are mostly two-dimensional ones solved by analytical methods or finite difference techniques. The application of finite element and boundary integral equation methods in this area has recently been developing rapidly. A new monograph edited by Chari and Silvester (Ref. 54) contains many discussions of these methods in eddy current problems.

The eddy current problems studied most in the literature are the two-dimensional ones. Taking rectangular coordinates to illustrate these, one may have problems in which (1) the currents flow in the z-direction only, and J_z, H_x, and H_y are functions of x and y; and (2) the magnetic

field has a single component in the z-direction only, and H_z, J_x, and J_y are functions of x and y. In the first case, it is convenient to use the magnetic vector potential which is parallel to the current density to formulate the problem. The magnetic vector potential $\underset{\sim}{A}$ is defined as

$$\nabla \times \underset{\sim}{A} = \underset{\sim}{B} \tag{3.1a}$$

$$\nabla \cdot \underset{\sim}{A} = 0 \tag{3.1b}$$

In case (1), $A_x = A_y = 0$ and A_z is related to current density through (Ref. 52)

$$A_z(\underset{\sim}{r}) = \int\int_{\text{area}} \frac{\mu}{2\pi} J_z(\underset{\sim}{r}') \ln|\underset{\sim}{r}-\underset{\sim}{r}'| \, d(\text{area}') \tag{3.2}$$

A two-dimensional diffusion equation may then be derived for A_z with appropriate boundary conditions.

Silvester and Haslam (Ref. 55) first presented a finite element Galerkin analysis of eddy current fields in magnetotelluric problems using such a formulation. Chari (Ref. 56) showed a similar formulation using a variational approach for the eddy current problem in magnetic structures. Since the magnetic vector potential must be calculated both inside and outside the conductor, the discretization of space must be extended to regions sufficiently far away from the conductor. Chari's study concerns the highly permeable iron part of the electrical machines where significant skin effects and ohmic loss are developed. The eddy current problem on infinitely long plates in the present research belongs to the same class of two-dimensional problems but is directed to conducting materials with small relative permeability. For such material the skin effect is not well developed in the low and intermediate frequency range. The stream function method used has the advantage of limiting the discretization to the conductor body only, at the expense of solving a system of linear

equations with a full coefficient matrix.

For the case in which the magnetic field has only a single component H_z, many authors use the electrical vector potential $\underset{\sim}{T}$ to formulate the problem. The electrical vector potential $\underset{\sim}{T}$ is defined such that

$$\nabla \times \underset{\sim}{T} = \underset{\sim}{J} \tag{3.3}$$

For strictly two-dimensional problems, $\underset{\sim}{T}$ has only one nonzero component T_z, which equals H_z. A two-dimensional diffusion equation for T_z can again be derived. The problem may then be solved either by finite element method through a variational formulation (Ref. 57), or by boundary integral equation method through a transformation of the differential equation into anintegral equation (Ref. 58).

Silvester (Ref. 59) developed the useful concept of eddy current modes from the eigenfunction expansion of the solution for this class of problems. The orthogonality of the eigenfunctions enables an equivalent circuit representation of the eddy current distribution to be developed. Each eigenfunction, or mode, forms a separate R-L circuit and there is no magnetic coupling between the modal circuits. In a subsequent paper (Ref. 60), Silvester extends the modal network theory to infinitely long flat conducting plates. The current density J_z is used to formulate the problem, and consideration is limited to the conductor itself. The plate is subdivided into N parallel strips of equal width. Each strip is assumed to carry a uniformly distributed current at all times. The thickness of the plate comes into the calculation of the resistance R of the strips. The inductances are calculated using the geometric mean distance theory of linear conductors. The solutions are then found by solving the matrix circuit equations. This eddy current modal theory has later been applied to the studies of many other eddy current problems (Refs. 61, 62).

For the case in which the eddy current flows in z-direction only, Silvester (Ref. 63) developed an integral equation essentially of the Fredholm type which treats current density directly. This equation has been solved with various methods by Schaffer and Bandevet (Ref. 64), by Silvester (Ref. 65), by Gopinath and Silvester (Ref. 66), and by Silvester, Wong and Burke (Ref. 61). Trowbridge (Ref. 54) and Biddlecombe et al. (Ref. 67) also developed an integral equation formulation for eddy currents using the magnetic vector potential.

For two-dimensional eddy current problems in cylindrical coordinate systems, the only nonzero components of current and the magnetic vector potential are in the circumferential direction. A two-dimensional diffusion equation can be constructed for the magnetic vector potential. Donea, Giuliani and Philippe (Ref. 68) presented a finite element formulation using a variational method. Becker and Pillsbury (Ref. 24), and Miya, et al. (Ref. 28) solved it by using a finite element Galerkin technique. Both studies consider coupled electromagnetic-mechanical effects. Many electromagnetic NDT studies also consider problems with cylindrical symmetry. Most of them use a variational, or energy functional, formulation. Examples are Palanisamy and Lord (Ref. 69), Nehl and Demerdash (Ref. 70), and Hwang and Lord (Ref. 71).

All the two-dimensional problems discussed assume the conductors to be infinitely long. For conductor plates with finite length, the eddy current problem becomes three-dimensional. To simplify the problem, it is usually assumed that the skin depth is large compared to the thickness so that the current density can be taken as constant across the thickness. The network analogy, in many respects equivalent to eddy current modal theory, plays an important role in such problems. This analogy will be

discussed in more detail in the subsequent section of this chapter.

Turner (Refs. 72, 73, 74) has developed computer programs for two- and three-dimensional transient eddy currents. The conducting materials are represented by a network of current-carrying line elements in order that Maxwell's field equations may be replaced by Kirchoff's circuit rules. Loop currents are used as the variables in the analysis so that the Kirchoff's mode equations are satisfied automatically. Thin conducting plates and shells are treated as two-dimensional problems by such a network model.

Kameari and Suzuki (Ref. 75) developed a finite element circuit method for the analysis of transient eddy currents on thin conducting plates and shells. The electric vector potential is used to formulate the problem. Unlike the two-dimensional problems such as long prismatic bars, the electric vector potential now is not equal to the magnetic field but differs by an additional scalar potential ϕ, i.e.

$$\underset{\sim}{B} = \mu \underset{\sim}{T} + \nabla \phi \qquad (3.4)$$

A set of circuit equations are formulated in this method from the balance of the magnetic energy and Joule loss of the system. Eddy current modal analysis is then performed through an eigenvalue analysis of the derived finite element circuit equations. This formulation gives a set of linear equations with fully symmetric matrices. The effect of the thickness comes into the calculation of the resistance matrix. The inductance and resistance matrices in this method are all calculated by numerical integration.

Compter and Hamels (Ref. 76) studied a coupled mechanical-eddy current problem for a movable conducting disk using a network circuit model. Carpenter (Refs. 77, 78) described a finite element network model and its application to eddy currents in thin plates. Thus most eddy current studies for thin conducting plates use a circuit model for analysis. The applica-

tion of variational methods is difficult because the dissipation term affects the variational formulation. Hammond and Penman (Ref. 79) studied the upper and lower bounds of the resistances and inductances of thick and thin conducting plates using a variational approach, but the problems they treated are for the classical skin effect of current carrying conductors, not the induction problems treated in the present research. De Mey (Ref. 80) presented a variational, integral equation study of eddy currents in plates using a stream function representation. But he neglects the reaction of the eddy currents on the magnetic field and therefore only obtains a local solution of the problem.

3.2 Quasi-static Field Equations and Circuit Equations

As discussed in the last section, there is an intimate relation between the circuit model and the various formulations for eddy currents in thin plates. This relation is examined in this section through the correlations between the quasi-static Maxwell's equations and the rules of circuit theory. The comparison provides a point of view alternative to the stream function method used in this study.

The scalar potential ϕ and the vector potential $\underset{\sim}{A}$ are first introduced for time varying fields. They are defined as (Ref. 32)

$$\underset{\sim}{B} = \nabla \times \underset{\sim}{A} \tag{3.1a}$$

$$\underset{\sim}{E} = -\frac{\partial}{\partial t}\underset{\sim}{A} - \nabla \phi \tag{3.5}$$

and

$$\nabla \cdot \underset{\sim}{A} = -\mu \epsilon \frac{\partial}{\partial t}\phi \quad \text{(Lorentz condition)} \tag{3.6}$$

These relations come from Equations (2.24). The electromagnetic field can be completely described by

$$\nabla^2 \underset{\sim}{A} - \mu \epsilon \frac{\partial^2}{\partial t^2} \underset{\sim}{A} = - \mu \underset{\sim}{J} \tag{3.7a}$$

$$\nabla^2 \phi - \mu \epsilon \frac{\partial^2}{\partial t^2} \phi = - \frac{\rho}{\epsilon} \tag{3.7b}$$

Neglecting retardation in the quasi-static case, one obtains the general solution

$$\underset{\sim}{A} = \frac{\mu}{4\pi} \int_V \frac{1}{r} \underset{\sim}{J} \, dV \tag{3.8a}$$

$$\phi = \frac{1}{4\pi\epsilon} \int_V \frac{1}{r} \rho \, dV \tag{3.8b}$$

The relations between quasi-static field equations and circuit equations will be discussed in terms of these two potentials.

The circuit theory includes the two following Kirchoff's laws:

(1) the current law: At any point in a circuit, the current flow is equal to the rate at which charge is passing through a cross-section of the conductor at that point;

(2) the voltage law: Around a closed circuit, the algebraic sum of the potential difference is zero.

These two laws may be put into the following equation form when there is no capacitor in the circuit, Fig. 3.1, which is the case in the present study since eddy current arcing is not considered.

$$\Sigma I_{in} = \Sigma I_{out} \tag{3.9a}$$

$$e = IR + L \frac{dI}{dt} \tag{3.9b}$$

In which I is the total current across the cross section of the conductor, e is the applied electromotive force; R is the resistance per unit length; and L the inductance of the circuit.

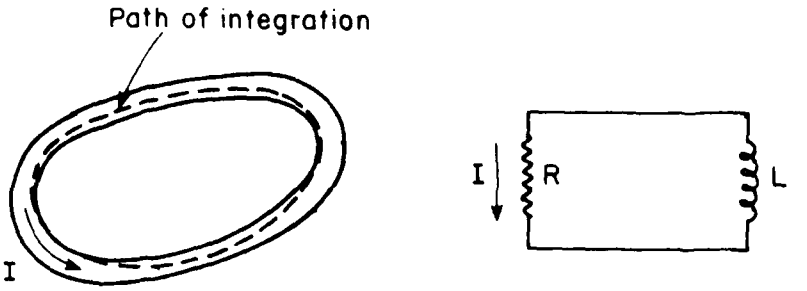

Figure 3.1 Metallic conductor wire showing path of integration lying on surface and the equivalent RL circuit.

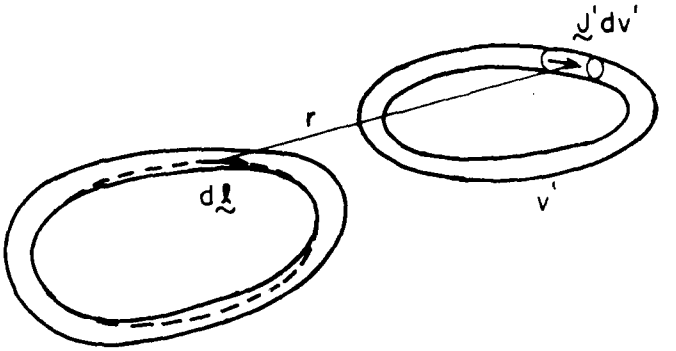

Figure 3.2 Mutual inductance between circuits. Variation of $\underset{\sim}{J}'dv'$ induces an emf in $d\underset{\sim}{\ell}$.

Eq. (3.9a) comes from the equation of continuity of current and is automatically satisfied by the potentials $\underset{\sim}{A}$ and ϕ defined before. The relation between Eq. (3.9b) and the quasi-static field equations is discussed below.

A circuit is defined as any closed path. For the one shown in Fig. 3.1, one first separates the total electric field $\underset{\sim}{E}$ in the conductor into two parts: $\underset{\sim}{E}'$ is that due to charges and currents defined by Eq. (3.5), and $\underset{\sim}{E}^o$ is the impressed field due to energy sources such as the external exciting coil.

$$\underset{\sim}{E} = \underset{\sim}{E}' + \underset{\sim}{E}^o \tag{3.10}$$

Then

$$\underset{\sim}{E}^o = \underset{\sim}{E} - \underset{\sim}{E}'$$

$$= \frac{1}{\sigma} \underset{\sim}{J} + \frac{\partial}{\partial t} \underset{\sim}{A} + \nabla \phi \tag{3.11}$$

Integrating around the circuit along a path on the surface of the conductor one has

$$\oint \underset{\sim}{E}^o \cdot d\underset{\sim}{\ell} = \oint \frac{1}{\sigma} \underset{\sim}{J} \cdot d\underset{\sim}{\ell} + \oint \frac{\partial}{\partial t} \underset{\sim}{A} \cdot d\underset{\sim}{\ell} + \oint \nabla\phi \cdot d\underset{\sim}{\ell} \tag{3.12}$$

The term on the left-hand side of the above equation is the applied electromotive force, which is designated e as in Eq. (3.9b). The last term is zero since without retardation one has

$$\oint \nabla\phi \cdot d\underset{\sim}{\ell} = \oint \frac{\partial\phi}{\partial \ell} d\ell = \oint d\phi = 0 \tag{3.13}$$

The second term on the right-hand side of Eq. (3.12) may be written as $\frac{d}{dt} \oint \underset{\sim}{A} \cdot d\underset{\sim}{\ell}$ for a rigid stationary conductor, in which $\underset{\sim}{A}$ is determined by Eq. (3.8a) in the quasi-static case. Assume that the conductor is a wire with small cross-sectional dimensions so that $\underset{\sim}{J}'\, dV'$ in Eq. (3.8a) may be replaced by $I\, d\underset{\sim}{\ell}'$ where I is the total current across the cross section of

the wire. One has

$$\underset{\sim}{A} = \frac{\mu I}{4\pi} \oint \frac{1}{r} \, d\underset{\sim}{\ell}' \tag{3.14}$$

and

$$\frac{d}{dt} \oint \underset{\sim}{A} \cdot d\underset{\sim}{\ell} = L \frac{dI}{dt} \tag{3.15}$$

in which

$$L = \frac{\mu}{4\pi} \oint \oint \frac{1}{r} \, d\underset{\sim}{\ell}' \cdot d\underset{\sim}{\ell}$$

is the inductance of the circuit and is a function only of the geometry of the circuit. Another way of defining L is the following:

$$\begin{aligned} LI &= \oint \underset{\sim}{A} \cdot d\underset{\sim}{\ell} \\ &= \int_S \nabla \times \underset{\sim}{A} \cdot d\,\underset{\sim}{a} \\ &= \int_S \underset{\sim}{B} \cdot d\,\underset{\sim}{a} \end{aligned} \tag{3.16}$$

or

$$L = \frac{1}{I} \int_S \underset{\sim}{B} \cdot d\,\underset{\sim}{a} \tag{3.17}$$

in which $\underset{\sim}{B}$ is the total magnetic induction.

The first term on the right-hand side of Eq. (3.12) involves $\underset{\sim}{J}/\sigma$ which represents the total electric field $\underset{\sim}{E}$ at the surface of the conductor. For sinusoidal time variations $\underset{\sim}{J}$ is related to the total current $\underset{\sim}{I}$ by

$$\underset{\sim}{J} = \frac{1}{A_c} \underset{\sim}{I} \tag{3.18}$$

in which A_c is a complex number having the dimensions of area, but not actually equal to the cross-section area of the conductor. It is complex because the current density at the surface of a conductor is not in phase with the total current when a skin effect exists. In such cases $1/\sigma A_c$, designated by Z, is called the impedance (per unit length) of the conductor.

When the frequency is sufficiently low that the skin effect is not well developed, the current is essentially uniform over the entire cross-

section of the conductor. In such cases A_c is the actual cross-sectional area A of the wire and

$$\oint \frac{1}{\sigma} \underset{\sim}{J} \cdot d\underset{\sim}{\ell} = I \oint \frac{1}{\sigma A} d\ell = IR \tag{3.19}$$

in which

$$R = \oint \frac{1}{\sigma A} d\ell \tag{3.20}$$

is the usual resistance per unit length of the wire.

The quasi-static field equations are therefore related to the equilibrium equation (3.9b) for a closed circuit. In the induction problem, the emf e is generated by the varying magnetic field due to the exciting coil, Fig. 3.2. Assume that the induced current in the exciting coil b is zero, i.e., that I^o is voltage-controlled or that the exciting coil has infinite conductivity. One has

$$e = - \oint \frac{\partial}{\partial t} \underset{\sim}{A}^o \cdot d\underset{\sim}{\ell} \tag{3.21}$$

in which $\underset{\sim}{A}^o$ is the component of vector potential due to the magnetic field of the exciting coil and is given by

$$\underset{\sim}{A}^o = \frac{\mu}{4\pi} \int_{V_b} \frac{1}{r} \underset{\sim}{J}^o \, dV_b$$

$$= \frac{\mu I^o}{4\pi} \oint_b \frac{1}{r} d\underset{\sim}{\ell}' \tag{3.22}$$

Substituting Eq. (3.22) into Eq. (3.21), one has

$$e = - M \frac{dI^o}{dt} \tag{3.23}$$

in which

$$M = \frac{\mu}{4\pi} \oint_a \oint_b \frac{1}{r} d\underset{\sim}{\ell}' \cdot d\ell \tag{3.24}$$

is the mutual inductance between the coils a and b.

The relationships established above for a single discrete current loop use exactly the same assumptions applied in the present work for a thin conducting plate, i.e., the skin effect is not significant and the current is constant across the thickness of the plate. A further similarity occurs between the circuit equation that describes the discrete circuit and that for the eddy current modes on the conducting plates. The eddy current modes are certain distribution patterns of the current density that are electrically and magnetically uncoupled from each other. The modal distribution can be obtained by decomposing the total current distribution into components orthonormal to both resistance and inductance operators. The derivation is briefly described below.

The law of conservation of magnetic energy, or the Poynting's theorem, for the induction problems states that (Ref. 52)

$$\frac{dU}{dt} + W = \frac{dU_m}{dt} \tag{3.25}$$

in which U is the total magnetic energy due to the current distribution, W is the total ohmic loss, and U_m the mutual magnetic energy between the external magnetic field and the induced current. Assuming constant current across the thickness of the plate, one has (Ref. 49)

$$U = \frac{\mu}{8\pi} \int_S \int_S \frac{1}{r_{PQ}} \underline{J}_P \cdot \underline{J}_Q \, dS_P \, dS_Q \tag{3.26a}$$

$$W = \int_S \eta \underline{J} \cdot \underline{J} \, dS \tag{3.26b}$$

$$U_m = \int_S \underline{J} \cdot \underline{A}^0 \, dS \tag{3.26c}$$

in which η is the area electrical resistivity, $\underline{A}^0$ is the magnetic vector potential of the externally applied field, and $\underline{J}$ is the total induced current density across the thickness of the plate.

By using an electric vector potential T for the current density, and the finite element technique Kameari and Suzuki (Ref.75) obtained the following coupled circuit equations for the plate

$$[L] \frac{d}{dt} \{V\} + [R] \{V\} = \frac{d}{dt} \{e\} \tag{3.27}$$

in which [L] and [R] are the time-independent inductance and resistance matrices, respectively. Both [L] and [R] are positive-definite and fully-populated; however, for a uniform mesh they are also symmetric. Applying the generalized eigenvalue analysis to the coupled system of equations, Kameari and Suzuki obtained the eddy current modes $\{E_n\}$, n = 1,2, ..., N, where N is the total number of the nodal points. Since

$$[L] \{E_n\} = \lambda_n [R] \{E_n\} \tag{3.28}$$

one has

$$\{E_m\}^T [R] \{E_n\} = \delta_{mn} \tag{3.29a}$$

$$\{E_m\}^T [L] \{E_n\} = \lambda_n \delta_{mn} \tag{3.29b}$$

The modes are therefore electrically and magnetically uncoupled. By expanding the potential T by the eddy current mode,

$$\{T\} = \sum_{n=1}^{N} P_n \{E_n\} \tag{3.30}$$

one obtains the uncoupled equation for each mode

$$P_n + \lambda_n \frac{d}{dt} P_n = \frac{d}{dt} e_n \qquad n=1,2, \ldots, N \tag{3.31}$$

in which

$$e_n = \{E_n\}^T \{e\} \tag{3.32}$$

The modal equations (3.31) are electrically and magnetically uncoupled to each other and are linked magnetically to the driving field through Eq.

(3.32). Eq. (3.31) is completely equivalent to the circuit equation (3.9b) with resistance, inductance, and decay time constant 1, λ_n, and λ_n, respectively. The full analogy between the circuit theory and the quasi-static description of eddy currents on thin plates is thus completed.

3.3 Eddy Currents on Infinitely Long Plates

The finite element Galerkin technique is applied to solve steady state and transient eddy current equations for infinitely long conducting plates. The formulations and the Fortran codes developed are described in subsection 3.3.1. To facilitate parameter studies for this problem, the steady state eddy current equation is nondimensionalized. A study of the relevant nondimensional parameters is presented in subsection 3.3.2, together with other examples which provide analytical and experimental verifications of the numerical results.

3.3.1. Finite Element Formulations for Steady State and Transient Problems

The transient eddy current equation is given by Eq. (2.104), without the coupling terms,

$$\frac{\partial^2 \psi}{\partial X^2} - \sigma\mu \frac{\partial \psi}{\partial t} + \frac{1}{2\pi} \sigma\mu h \int_0^L \frac{\frac{\partial \psi(X')}{\partial t}}{(X-X')^2 + \frac{h^2}{4}} dX' = \sigma h \frac{\partial B_z^o}{\partial t} \qquad (3.33)$$

in which X is used to denote the position in physical units, and L is the total width or span.

3.3.1.a Formulation and Implementation for Steady State Problems

For steady-state harmonic currents in the plate, Eq. (3.33) may be nondimensionalized into

$$\frac{d^2\phi}{dx^2} - iR\phi + i\frac{R}{2\pi}\int_0^{\ell} \frac{\phi(\xi)}{(\xi-x)^2 + \frac{1}{4}}\, d\xi = iRB(x) \tag{3.34}$$

in which x and ξ are distances across the width nondimensionalized with respect to the thickness h; $\psi = \phi I^o e^{i\omega t}$; $B_z^o = (\mu/\Lambda)B(x)I^o e^{i\omega t}$; the magnetic Reynolds number $R = \omega\mu\sigma h^2$, which is related to the skin depth δ through $R = 2(h/\delta)^2$; I^o is the current in a nearby exciter coil; and ℓ is the nondimensionalized width.

The finite element (FE) Galerkin method is used to solve the integro-differential equation (3.34). φ is approximated globally and locally by piecewise linear models

$$\phi = \sum_{k=1}^{G} M_k \phi_k \tag{3.35a}$$

$$\phi^E = \sum_{k=1}^{2} N_E^k \phi_k \tag{3.35b}$$

in which G is the total number of nodal points, the superscript E denotes the E-th element, and M_k are the global interpolation functions generated from the local linear element shape functions N_k^E. The linear algebraic equations for each element are

$$-\sum_{k=1}^{2} S_{jk}^E \phi_k - i\sum_{k=1}^{2} P_{jk}^E \phi_k + i\sum_{k=1}^{G} Q_{jk}^E \phi_k = iR_j^E \tag{3.36}$$

in which

$$S_{jk}^E = \int_E \frac{dN_j^E}{dx}\frac{dN_k^E}{dx}\, dx \; ; \; P_{jk}^E = R\int_E N_j^E N_k^E\, dx$$

$$Q_{jk}^E = \frac{R}{2\pi}\int_0^{\ell} M_k(\xi) W_j^E(\xi)\, d\xi \; ; \; R_j^E = R\int_E N_j^E B dx \tag{3.37}$$

the weighting functions W_j^E used in calculating the integral term is

$$W_j^E(\xi) = \int_E \frac{N_j^E(x)}{(\xi-x)^2 + \frac{1}{4}} dx \tag{3.38}$$

Both Eqs. (3.37) and (3.38) are integrated analytically. The resulting element matrices are shown in Appendix A for both the local and nonlocal terms. The assembled global matrix is complex, generally nonsymmetric, and fully populated. The usual limited connectivity (banded matrix) finite element representation is lost due to the nonlocal nature of the problem.

When the frequency of the external magnetic field is low, the effect of the self field is small. The solution in this case will approach the local solution obtained by dropping the second and third terms on the left hand side of Eq. (3.34). When the frequencies are high, the distribution of the eddy current is primarily influenced by the self field. The solution will approach the one obtained by dropping the first term on the left of Eq. (3.34). The solution so obtained is an asymptotic value for the high frequency limit, and is called the "image solution" in the literature.

A Fortran program EDDY1 has been developed based on Eqs. (3.36)-(3.38). It is designed to perform the following calculations:

(1) Steady state local solutions of stream function, current, temperature, and pressure,

(2) Steady state nonlocal solutions of stream function, current, temperature, and pressure, and

(3) Steady state image solution of stream function, current, temperature, and pressure.

To perform the calculations necessary to construct a spectrum, EDDY1 performs the above calculations for any number of magnetic Reynolds numbers in one run. Multiple load cases (up to 10) are allowed. Each load case will be solved for all the magnetic Reynolds numbers specified for that run.

Presently, EDDY1 can handle uniform magnetic field cases and cases where the fields are generated by any number of conductor wires parallel to the plate. The strengths and senses of the currents and the positions of the wires may be different. Space has also been left to include other types of exciting fields in the program.

Program EDDY1 takes the geometric information of the plate and magnetic field source information as input. The total numbers of nodal points, load cases, parameter sets, and the plotting option of the output must be specified on the master input card. Nodal point information may be generated for portions of the mesh that are uniform.

The type of source of magnetic field is specified. No other information is needed for a uniform magnetic field. For the parallel wire cases, the positions, senses, and the relative strengths of the currents in each wire must be input subsequently.

All the input data must be nondimensionalized according to the conventions presented in the formulation.

Values of the stream function, eddy current, temperature induced in a half-cycle of the current, and time-averaged magnetic pressure exerted on the plate are produced as output of the program. The stream function and eddy current are calculated in complex form. The stream function values are calculated at the nodal points of the mesh, while the current, temperature, and pressure are evaluated at the centroids of the elements. The stream function and eddy current are given in complex form, and the modulus

and phase angle are calculated for the eddy current. Values of the modulus and phase angle for different frequencies may be used to generate the spectrum of the current any any point on the plate. These curves and the spectrum of the exciting current may be used to calculate the transient current at the point by fast Fourier transform techniques.

All the outputs of the program may be plotted using a printer-plotter subroutine. This capability is optional and can be specified in the input.

In this program the local solutions are printed out and plotted parallel to the nonlocal solutions for comparison. When there are several load cases, the results are printed out in groups in the sequence of the load numbers. In the multiple parameter (frequency) cases, this is done for each Reynolds number. Title lines will be printed for each parameter to distinguish the different groups of output. Image solutions, which are independent of the Reynolds number, are printed out last in the sequence of load cases.

3.3.1.b Formulation and Implementation for Transient Problems

The Galerkin finite element (FE) version of the transient equation (3.33) is formulated in a way similar to the steady state problem. It is integrated with respect to time by an implicit scheme. ψ is approximated in physical units globally and locally by

$$\psi = \sum_{k=1}^{G} M_k \psi_k \tag{3.39a}$$

$$\psi^E = \sum_{k=1}^{2} N_k^E \psi_k \tag{3.39b}$$

The linear equations for each element are

AD-A111 012 CORNELL UNIV ITHACA N Y DEPT OF STRUCTURAL ENGINEERING F/G 12/1
FINITE ELEMENT ANALYSIS OF MAGNETOELASTIC PLATE PROBLEMS.(U)
AUG 81 K Y YUAN N00014-79-C-0224
UNCLASSIFIED 81-14 NL

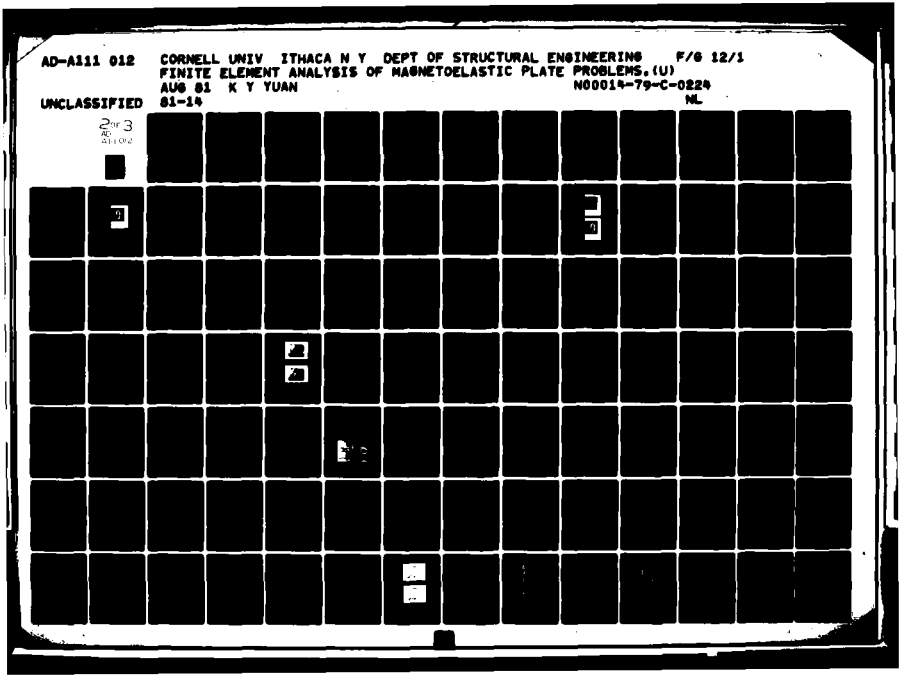

$$-\sum_{k=1}^{2} S^E_{jk}\psi_k - \sum_{k=1}^{2} P^E_{jk}\dot{\psi}_k + \sum_{k=1}^{G} Q^E_{jk}\dot{\psi}_k = R^E_j \tag{3.40}$$

in which

$$S^E_{jk} = \int_E \frac{dN^E_j}{dX}\frac{dN^E_k}{dX}\,dZ \quad ; \quad P^E_{jk} = \sigma\mu \int_E N^E_j N^E_k\,dX$$

$$Q^E_{jk} = \frac{\sigma\mu}{2\pi}\int_0^L M_k(X')W^E_j(X')dX \quad ; \quad R_j = \sigma h \int_E N^E_j \dot{B}^o_z\,dX \tag{3.41}$$

where the weighting function is:

$$W^E_j\,(X') = \int_E \frac{h\,N^E_j\,(X)}{(X-X')^2 + \frac{h^2}{4}}\,dX \tag{3.42}$$

Equations (3.41) and (3.42) are again integrated analytically, and the resulting expressions are those given in Appendix A. The global matrix form of Eq. (3.40) is

$$[A]\,\{\dot{\psi}\} - [S]\,\{\psi\} = \{R\} \tag{3.43}$$

in which

$$[A] = [Q] - [P] \tag{3.44}$$

Again, [A] is full and generally nonsymmetric.

The transient equations (3.43) are integrated using the following scheme

$$\left\{\frac{1}{\Delta t}[A] - (1-\theta)\,[S]\right\}\quad \{\psi\}_{t+\Delta t}$$

$$= \left\{\frac{1}{\Delta t}[A] + \theta\,[S]\right\}\{\psi\}_t + \theta\,\{R\}_t + (1-\theta)\,\{R\}_{t+\Delta t} \tag{3.45}$$

θ= 0.5 has been used in all the problems analyzed.

A Fortran program EDDY1T has been developed based on Eqs. (3.41)-(3.45) and has been built into a more general transient analysis program EDDYBEAM for the coupled electromagnetic-mechanical effects. The purely transient one-dimensional eddy current analyzer EDDY1T may be recovered from it by specifying the input parameter LINK to be zero. EDDY1T is designed to perform the following calculations for pure eddy current problems:

(1) transient local solutions of stream function, current, temperature, and magnetic force, and

(2) transient nonlocal solutions of stream function, current, temperature, and magnetic force.

EDDY1T handles one load case in one run only. The two types of magnetic fields included are a time-varying uniform magnetic field and a field generated by any number of conductor wires parallel to the plate. The strength and sense of the currents and the positions of the wires may be different, but the time variations of all the currents must be the same. The time function may either be analytic and calculated at each time step, or numerical and read in from the input data. Presently a half-sine function, a continual sinusoidal function, and a ramp function of time have been included in EDDY1T. Flexibility has been left for the user to create additional modules if other analytic forms of the time function are preferred. The temperature calculated is the instantaneous temperature rise; the effect of heat conduction is not included.

Geometric information of the plate, source information of the magnetic field, relevant physical constants, time integration parameters, and the numerical information (if any) describing the time function of the field must be input to the program EDDY1T. The units of all the input values must be consistent. The rationalized MKS system (Giorgi system) has been used

for all the problems in the present research.

Mesh generation and incremental plotting capabilities are also included in EDDY1T.Time history plots at selected points and spatial variation plots at selected time-steps for both current and magnetic force may be produced in the same scale for comparison. Appropriate mesh generation and plotting information must be input if these capabilities are used.

Values of the stream function, eddy current, magnetic force, and temperature at each time step are produced as output of the program. The stream function values are calculated at the nodal points of the mesh. The eddy current and temperature are evaluated at the centroids of the elements and are constant within each element. The magnetic forces are calculated at the integration points of each element and vary within each element with the tangential component of the applied field. The outputs may be plotted using a library subroutine. A short form of the output is provided as an option if long time solutions are needed. Local and nonlocal solutions are handled as different jobs and must be executed separately. The type of analysis (local or nonlocal) must be specified in the input.

3.3.2 Numerical Results and Experimental Verifications for Infinitely Long Plates

The programs EDDY1 and EDDY1T have been applied to a number of problems to test and verify the programs' validity and to demonstrate their utility for problems of scientific and practical interest. A portion of the verification process is the comparison of the computed results with experimental measurements. A summary of these numerical results is given below.

3.3.2.a Steady State Analysis by Program EDDY1

The first test of the numerical techniques discussed in this section is the calculation of induced currents in a long rectangular plate by a two-dimensional magnetic field using program EDDY1, Figure 3.3. Near the center of the plate, Section C-C in Figure 3.3, the end effects of the plate are negligible, and the currents are one-dimensional or are parallel to the long edges of the plate. The external magnetic field used in the test cases was that due to parallel current filaments above the plate and a uniform time dependent magnetic field. In addition to the induced current distribution across the plate, the induced temperatures and magnetic pressure distributions were calculated.

The following objectives were met with the program EDDY1.

a) Comparison of low magnetic Reynolds number (R) results with direct quadrature of local theory.

b) Comparison of high R results with the image method.

c) Demonstration of the importance of nonlocal theory for moderate frequencies or R.

d) Comparison of finite element calculations with experimental infrared measurements reported in Refs. 101 and 102.

e) Combination of the finite element (FE) results for different field frequencies with the fast Fourier transform (FFT) to predict dynamic currents and pressures.

f) Demonstration of the importance of the edge effect in increasing the current density and magnetic pressure.

g) Calculation of the magnetic forces on a long plate due to a tilted coil.

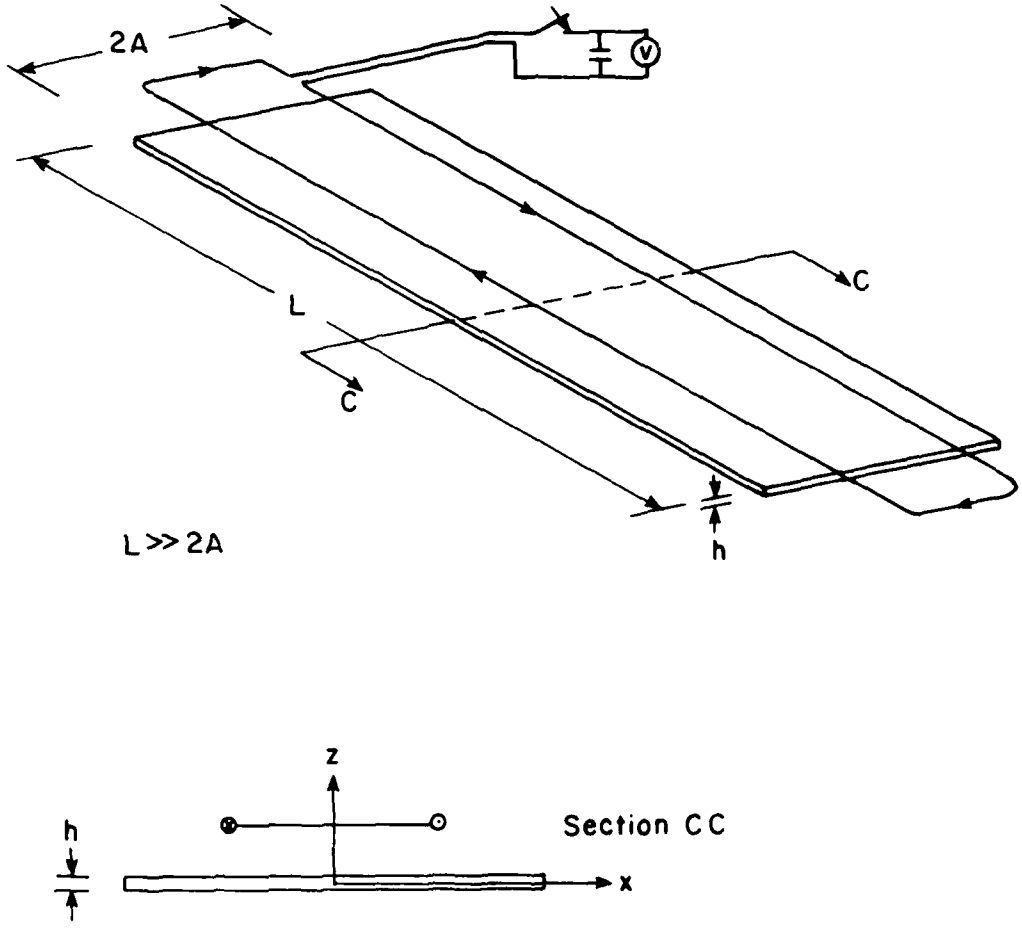

Figure 3.3 Induced currents in a long rectangular plate.

h) Examined the effect of a banded matrix as an approximation to the full matrix or complete nonlocal solution.

i) Demonstration of the size effect of the width on the induced current through a different nondimensional magnetic Reynolds number R_w.

Each of these will be described separately below.

a) Comparison of FEM with Direct Quadrature for R<<1. When R<<1 one may drop the nonlocal terms in Eq. (3.34) and obtain the local theory for the stream function, i.e.

$$\frac{d^2\phi}{dx^2} = iRB(x) \tag{3.46}$$

The solution for the one-dimensional case can be found by direct integration of a given B(x). Comparison of the low Reynolds number solution for the finite element method (FEM) and direct quadrature is shown in Figure 3.4 for a pair of current filaments centered above a long conducting plate. The results show excellent agreement.

b) *Comparison with the Image Method.* When the frequency is high, i.e., R>>1, the nonlocal effects act to prevent the magnetic field from penetrating the plate. In this limit the solution can be approximated by considering an image coil below the plate which serves to cancel out the normal component of the total magnetic field (Figure 3.5). The results of the one-dimensional FEM with the image coil calculation are shown in Figure 3.6 and again show excellent agreement.

c) Nonlocal vs. Local Theory for Eddy Currents. A comparison of the local and nonlocal theories for eddy current distribution is shown in Figure 3.7 for different R or frequencies. It is clear that even though the skin depth may be several times the thickness (R = 0.1, δ = 4.5h), the

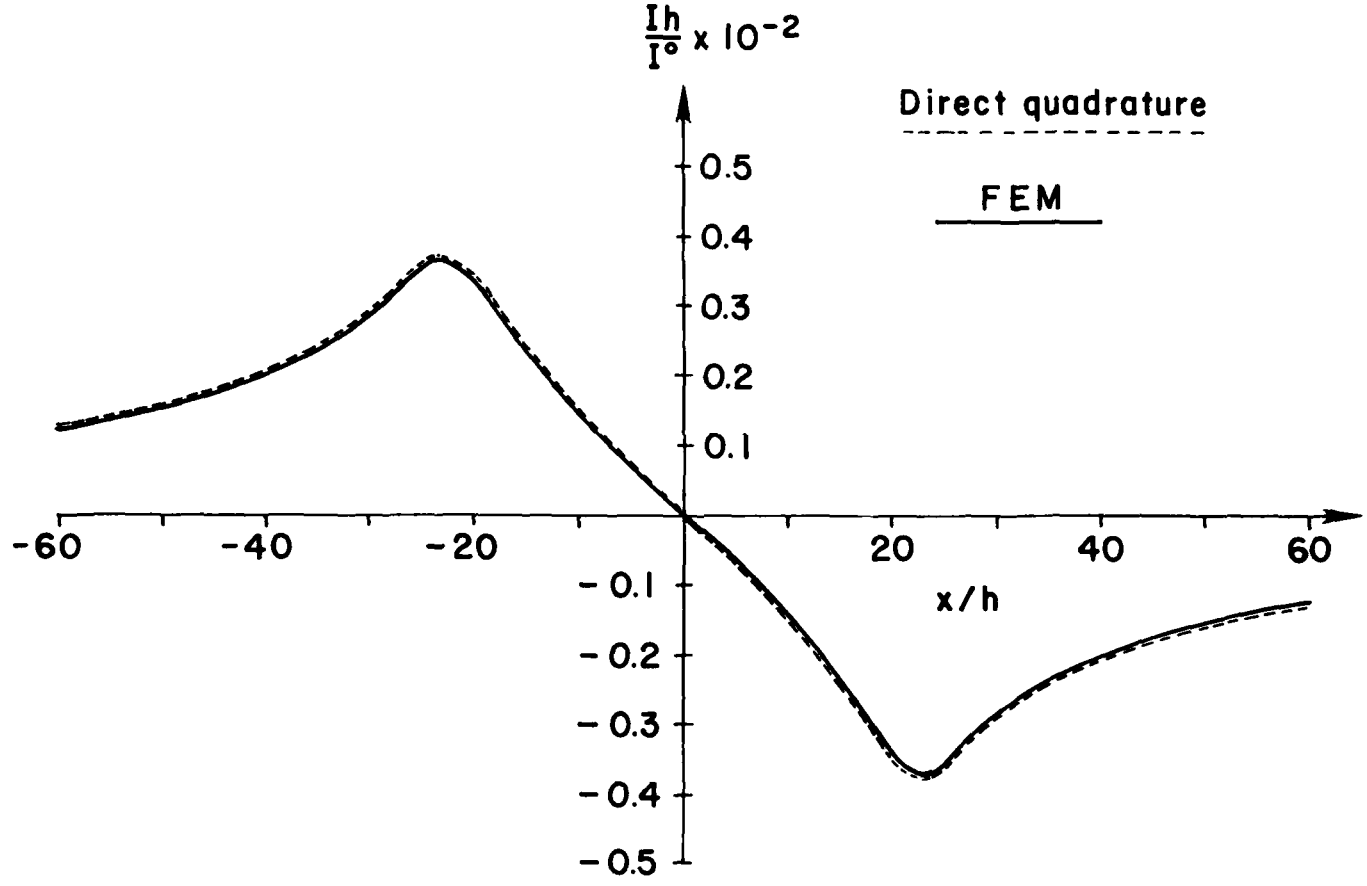

Figure 3.4 Comparison of FEM and Direct Quadrature Solutions for low R for a pair of current filaments centered above a long conducting plate ($R = 0.01$).

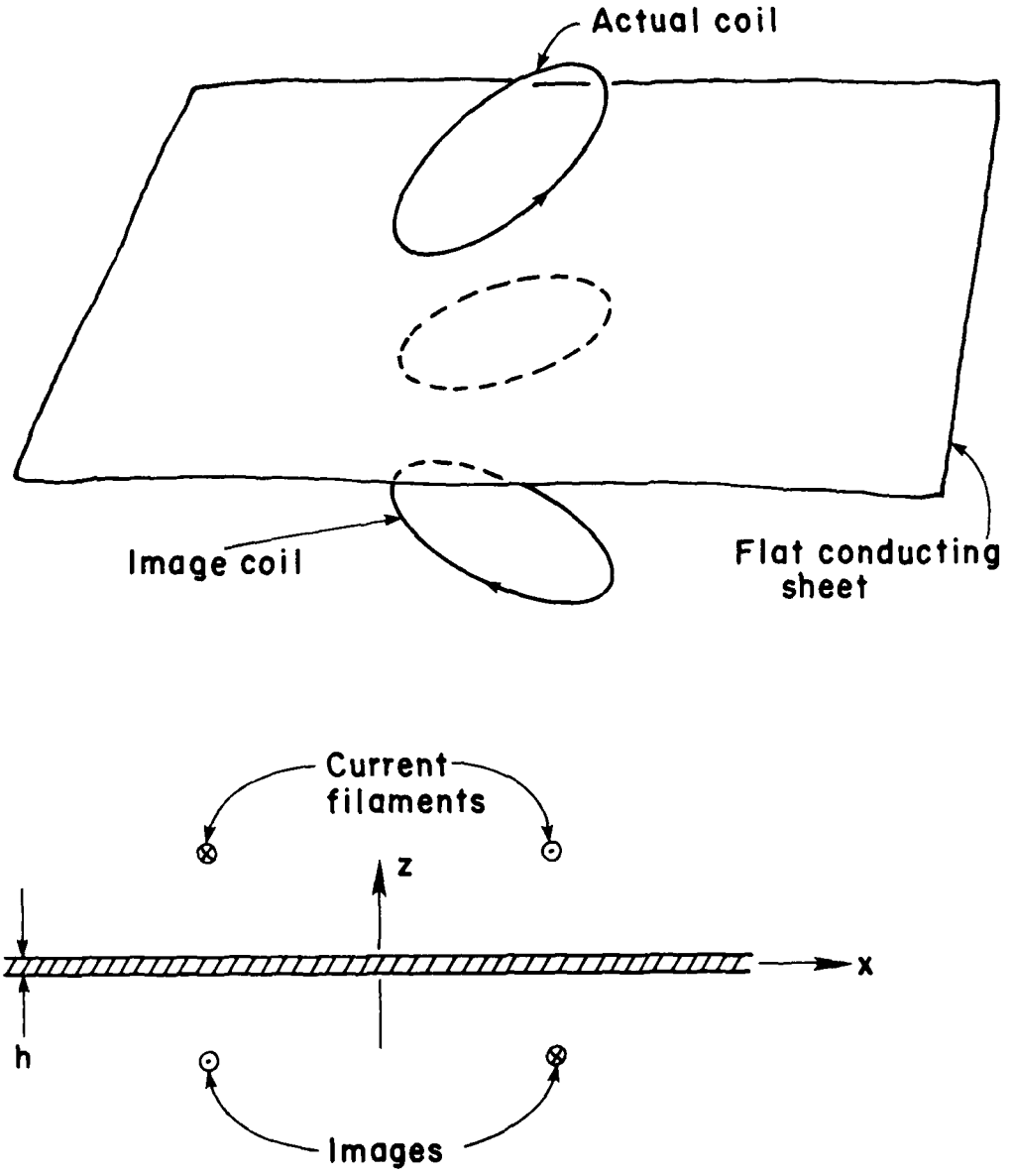

Figure 3.5 The image method for high R.

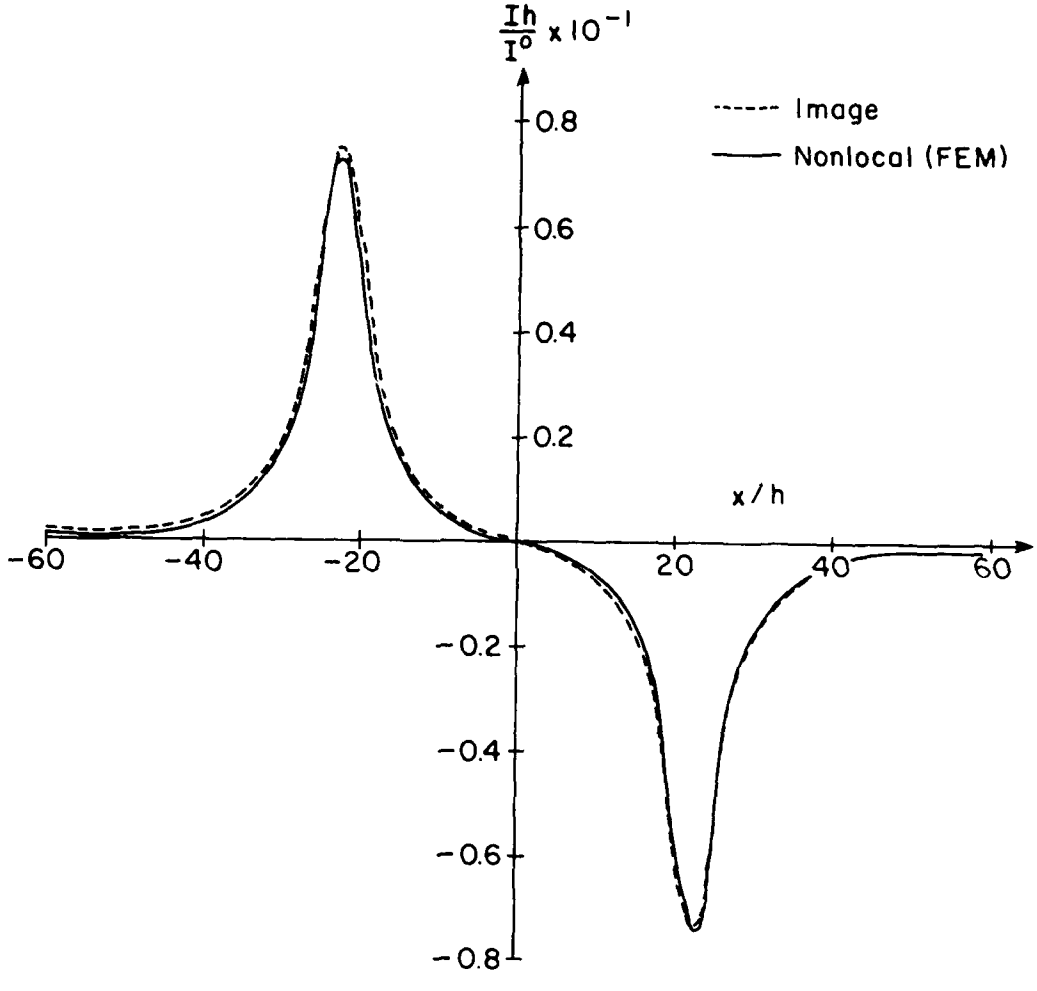

Figure 3.6 Comparison of FEM and image method solutions for high R for a pair of current filaments centered above a long conducting plate (R = 5).

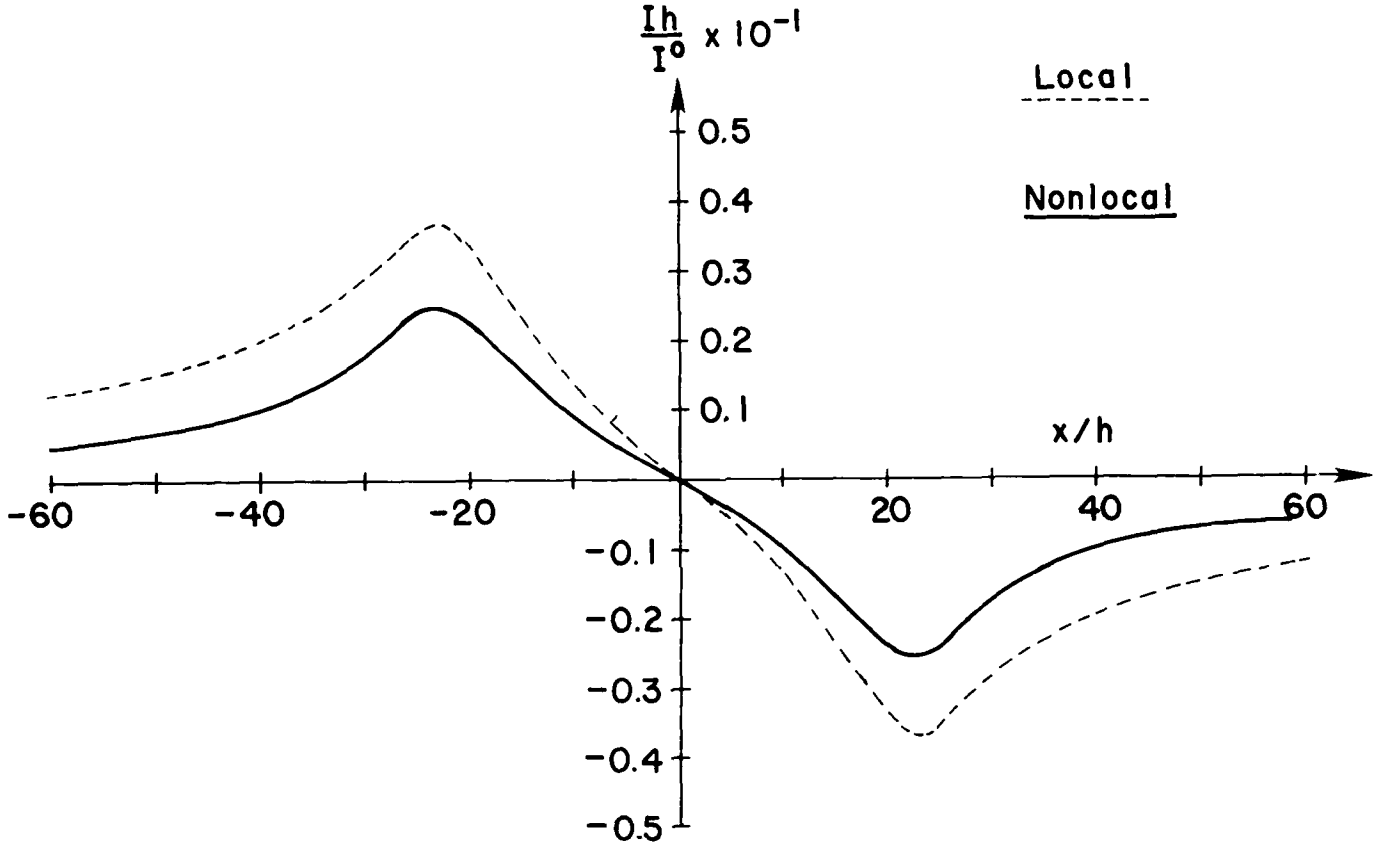

Figure 3.7 Comparison of nonlocal and local solutions for a pair of current filaments centered above a long conducting plate (R = 0.1).

nonlocal distribution differs significantly from the local theory. The importance of the nonlocal effects is not recognized by some eddy current calculations which neglect the reaction field of the induced current (Ref. 80).

A more fundamental difference between the nonlocal and local effects concern the magnetic pressure. When the nonlocal or self field of the induced currents is neglected, the average force on the plate for a sinusoidal current is zero. The nonlocal or self field effects are necessary to obtain a time-averaged force on the plate between the sources of the external field (such as coils or current filaments) and the currents in the plate.

The phase difference between the driving magnetic field and the induced eddy current is 90 degrees in the local theory, as is evidenced by Eq. (3.46). The phase difference is zero in the image solution. The induced current densities in Figures (3.4) and (3.6) therefore have the same phase across the width of the plate. For the intermediate case, the eddy current density has different phase angles at different locations of the plate. Figure 3.7 shows the modulus, or the maximum value, of the current density across the plate.

d) Comparison of FE Calculations with Experimental Measurements. An important feature of this research program has been the experimental verification of the numerical calculations. To check the calculations, measurements of one of several physical quantities along the surface of the plate must be made such as electric or magnetic fields, induced temperature, or magnetic pressure. Measurement of electric or magnetic fields associated with the induced currents in the plate involve taking data of a sufficient number of points to map out the current distribution.

It has the advantage that the time history of the electromagnetic field variables at such points may be more easily determined. Such a technique will be used in the experimental verification of the results of the transient analysis. To verify the current distribution, an infrared scanning technique which senses the incremental temperature distribution is used (Ref.102). This technique is based on the fact that for small times after the induced currents are generated, the heat conduction can be neglected and the induced temperature is proportional to the square of the current density. The heat equation is given by

$$-\kappa\nabla^2 T + c\,\frac{\partial T}{\partial t} = \frac{J^2}{\sigma} \tag{3.47}$$

in which κ is the thermal conductivity, and c is the heat capacity of the plate. Under appropriate conditions on the gradient of temperature and time, one may neglect the first term and write

$$T \approx \frac{1}{c\sigma}\int_0^t J^2 dt \tag{3.48}$$

To simulate a one-dimensional problem, a rectangular multiturn induction coil is placed parallel to a flat stainless steel plate and induced temperatures are measured across the plate under the middle of the coil, Figure 3.8. The two-dimensional infrared scanner used is described in Ref. 102. An infrared thermogram of the temperature or J^2 pattern in the plate due to a pulsed rectangular coil is shown in Figure 3.9. The induction coil has damped sinusoidal currents. Comparison of the qualitative behavior of the measured temperature and the calculated temperature distribution along the plate using an effective frequency is shown in Figures 3.10 and 3.11 for two different frequencies. Both calculated and

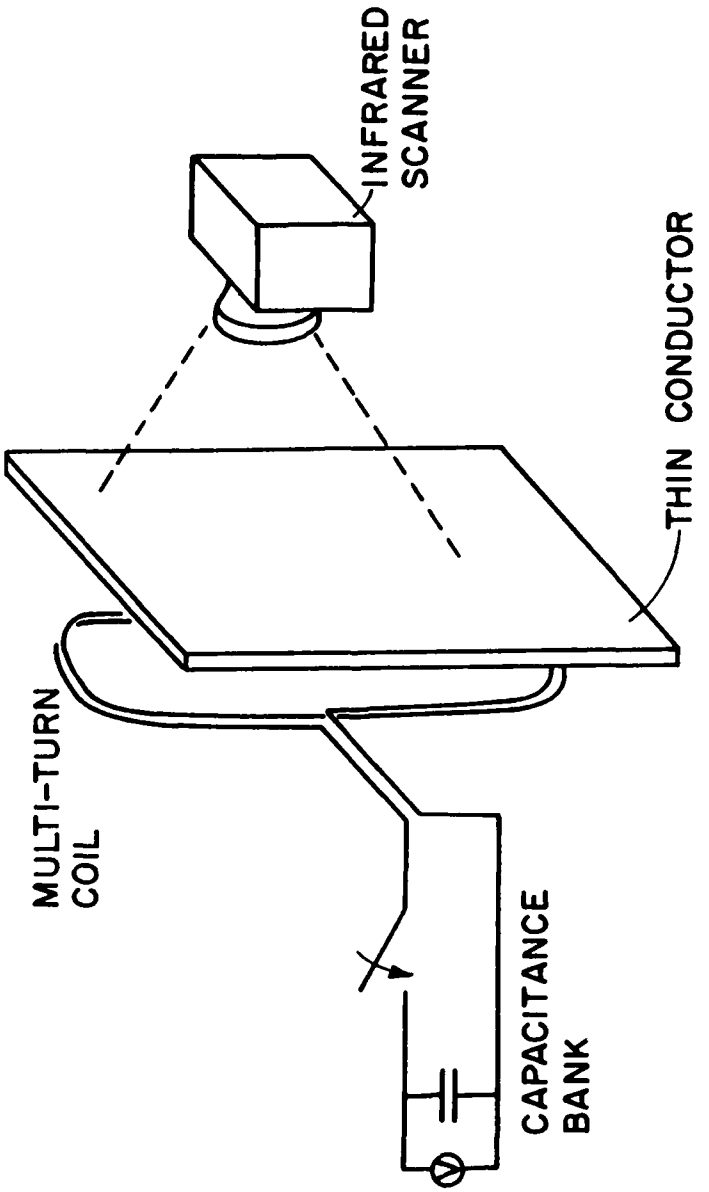

Figure 3.8 Method of detecting eddy current flow patterns in thin structures.

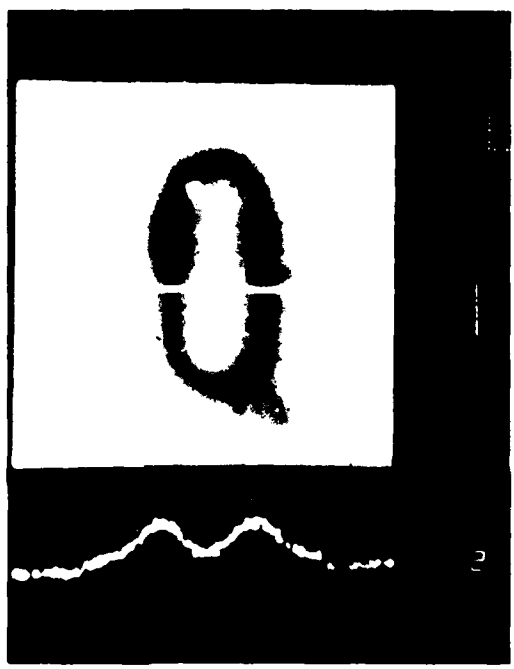

Figure 3.9 Photograph of an infrared thermogram for currents in a plate as induced by a pulsed rectangular coil.

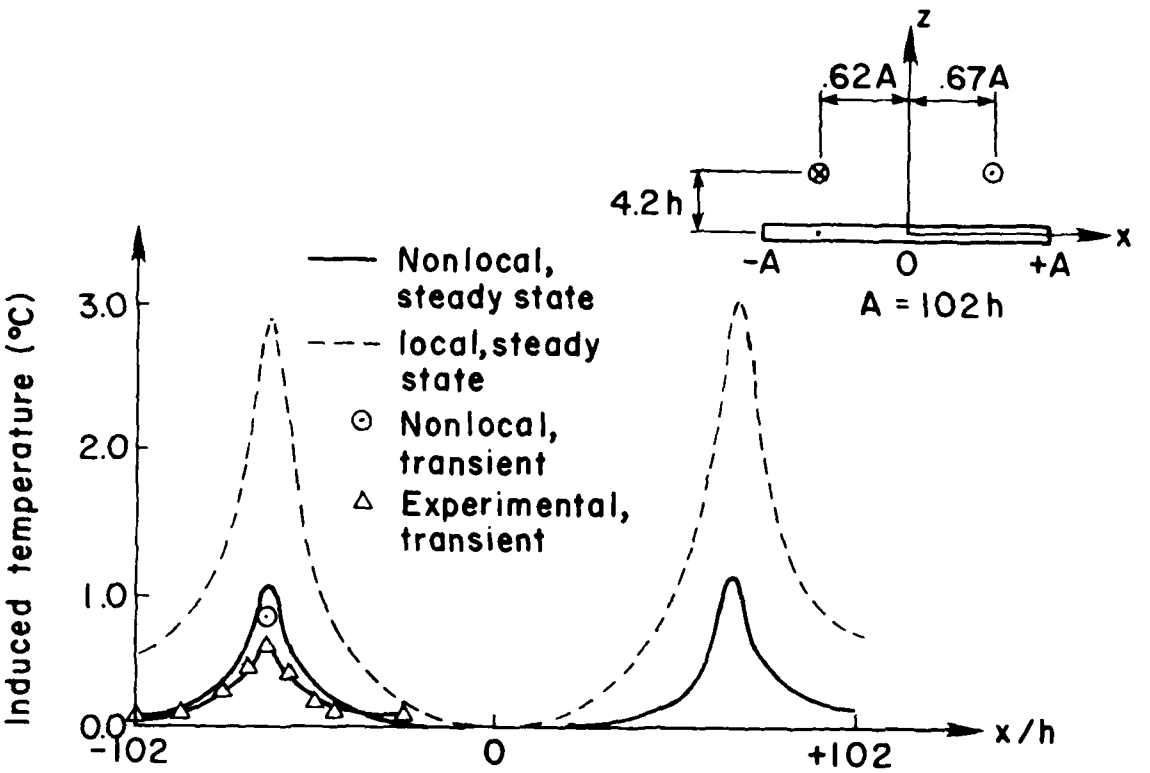

Figure 3.10 Comparison of FE solution and measured temperatures for a pair of current filaments centered above a long conducting plate (R = 0.071).

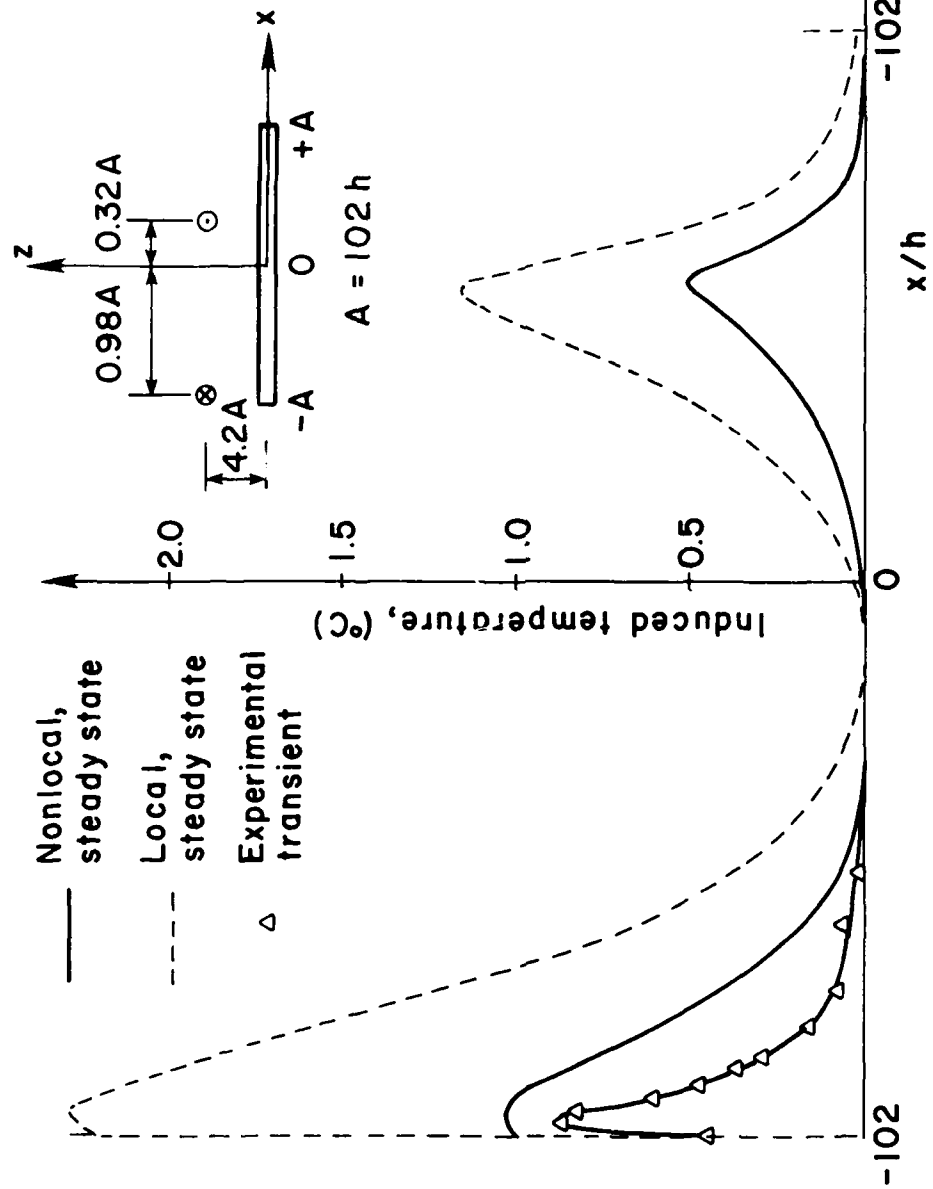

Figure 3.11 Comparison of FE solution and measured temperatures for a pair of current filaments nearer one edge of a long conducting plate ($R = 0.074$).

measured data have been normalized. Excellent qualitative agreement can be seen for the coil centered above the plate, Figure 3.10, and for the coil near the edge of the plate, Figure 3.11.

Quantitative agreement is difficult because the calculations are for a harmonic excitation field and the experiment uses pulsed current in the coil. This problem is solved by calculating the induced current density, as a function of frequency, and using a fast Fourier transform (FFT) to calculate the induced current as a function of time, as shown in Figure 3.12. This data is then integrated using Eq. (3.48) above to calculate the temperature as a function of time at the point of maximum temperature in the plate. Using the maximum temperature in time along with the calculated distribution as in Figure 3.12, a quantitative comparison of calculated and measured temperature were made as shown in Figure 3.10. The measured values are about 20% below the calculated values. A comparison of the FFT result and a subsequent transient analysis result for the same problem is given in sub-subsection 3.3.2.b. In light of this later comparison, the difference between the experimental result and the FFT analysis appears to arise partly from the rough calculation in the FFT, i.e., the cutoff frequency used may be too low and the number of terms used in the finite sum approximation of the Fourier integral may be insufficient. The crudeness of the FFT result is also evidenced by the late arrival of the peak value of the induced current in Figure 3.12. In the FFT analysis of the present problem a half-sine pulse of the driving current is used, while in the experiment the real driving current has a damped half-sine variation. The major cause of the difference between the calculated peak temperature and the measured one is probably heat conduction the effect of which is not included in the calculation. The infrared

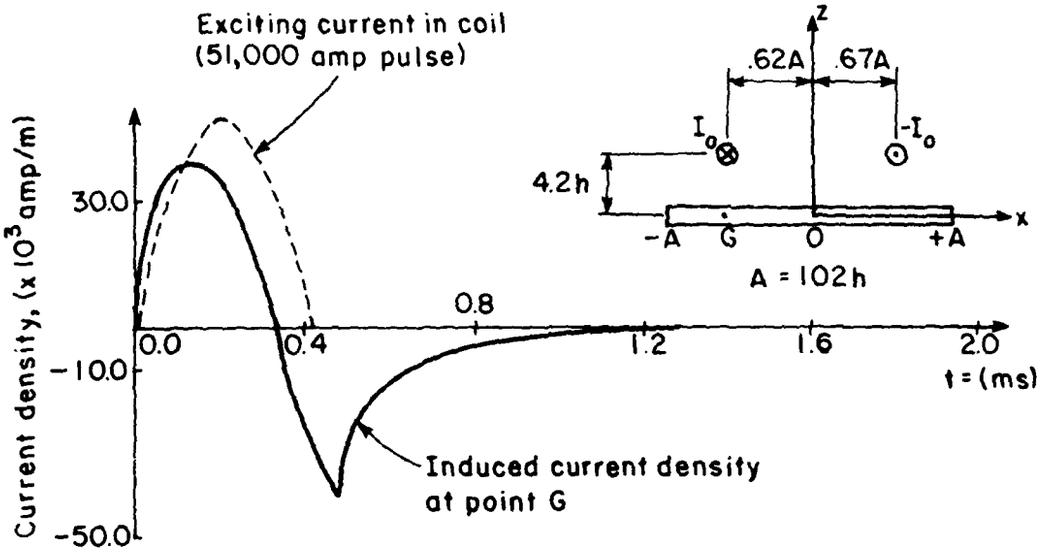

Figure 3.12 Transient exciting and induced currents as functions of time.

picture was taken approximately 160 ms after the pulse was applied. This may explain the loss of the sharp peak of the temperature curve under the wire. In sum, the FFT result obtained for this problem is satisfactory considering the approximations involved.

e) FE and FTT Methods for Pulsed Magnetic Fields. As discussed above, the distribution of current in the plate, as well as induced pressure and temperatures are for harmonic excitation. For pulsed or transient excitation fields $\underset{\sim}{B}^{o}(t)$, one may decompose the field into its spectral components

$$B_o f(\omega) = \frac{1}{2\pi} \int_{-\infty}^{\infty} B(t)\, e^{i\omega t} dt \tag{3.49}$$

If the induced current is calculated as a function of frequency $J(\omega)$, for an excitation $B_o e^{-i\omega t}$, the time variation of current can be found from the integral

$$J(t) = \int_{-\infty}^{\infty} J(\omega)\, f(\omega) e^{-i\omega t} d\omega \tag{3.50}$$

The function $J(\omega)$ is found by calculating the induced current for various frequencies using the nonlocal theory as shown in Figure 3.13. A polynomial is then fitted to these points over the significant frequency domain of $f(\omega)$. The Fourier integral is then approximated by a finite sum and the summation carried out using a fast Fourier transform algorithm. The resulting time history of current in the plate is shown in Figure 3.12. From this history the magnetic force and induced temperature histories in the plate can be calculated. A detailed discussion of the FFT method in the transient solution of the diffusion equation has been given in Chapter 8 of Reference 54.

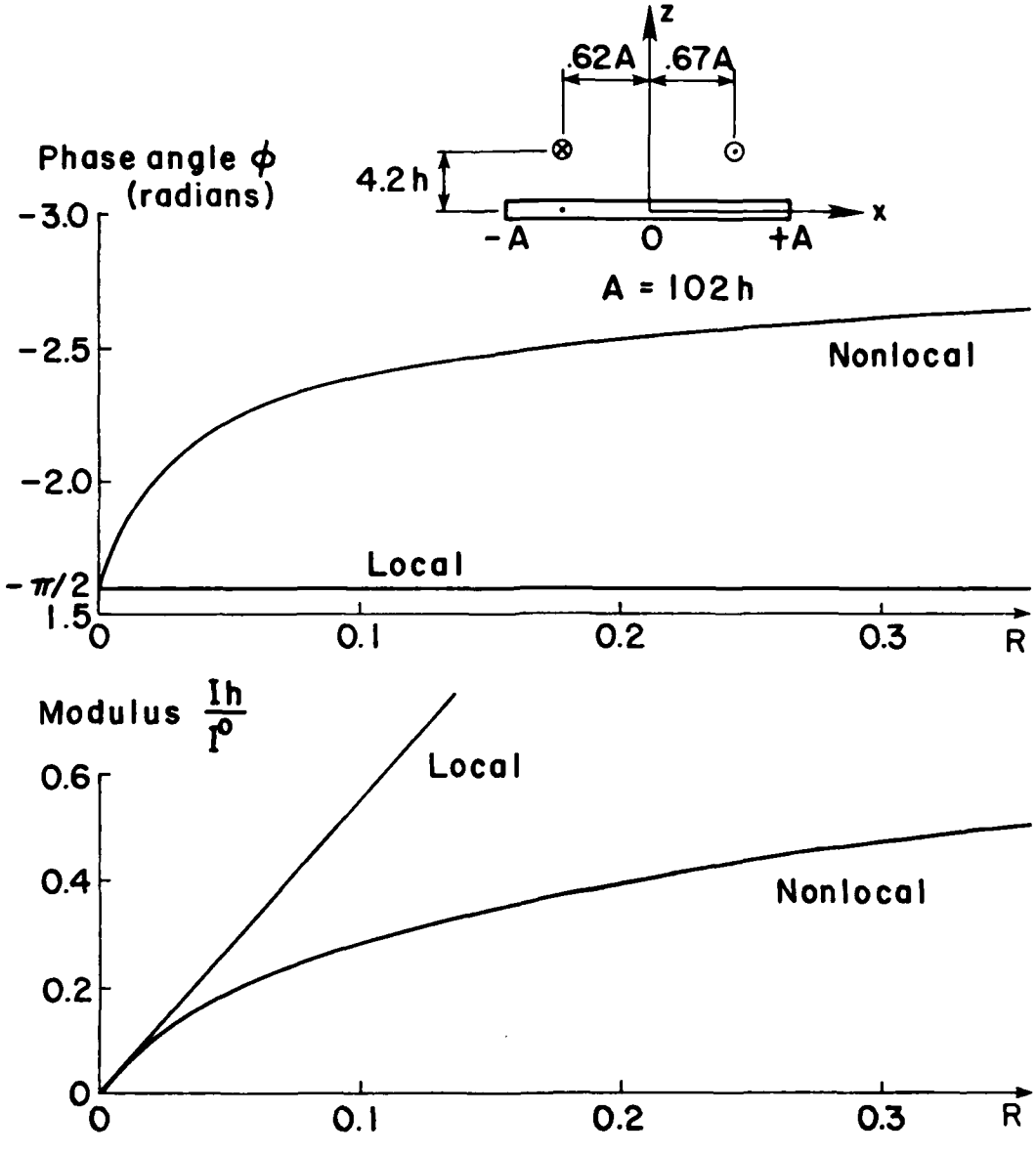

Figure 3.13 Spectrum for current at x = -0.62A for local and nonlocal solutions.

f) Effect of Edges on Induced Eddy Currents. One of the immediate results of infrared scan experiments on induced eddy currents in plates is the observation that high current densities will occur when the excitation field is concentrated near the edges of the plates. This can be seen in Figure 3.14a,b, where a coil is moved closer to the edge of a rectangular plate. The results of the one-dimensional program also show a distinct edge effect for both the paired current filament induction, Figure 3.4, and the uniform field induction, Figure 3.15.

g) Pressure Distributions Due to Tilted Induction Coils. Both magnetic forming devices and magnetic levitation devices use current carrying coils near plate-like conductors. The effect of tilting the induction coil has been calculated as shown in Figures 3.16 and 3.17. The increased magnetic pressure under the filament close to the plate produces a moment on the plate and a restoring moment on the coil. The effect of lateral movement of the coil can also be seen in Figure 3.17, and the effect of lateral movement on the restoring moment can be calculated.

h) Effect of Reduced Matrix Band on Nonlocal Solutions. One manifestation of the FE implementation of the nonlocal theory is that the algebraic FE equations become full rather than banded. Nevertheless, the nonlocal effects which cause this loss of banding are proportional to $1/r^2$ in which r is the distance from a self-field source point on the sheet conductor to the field point in question, Eq. (3.34). One method of restricting the nonlocal effect at any field point on the sheet would be to exclude source points at distances from the field point greater than some cut-off value of r. For a uniformly spaced finite element mesh, this would yield a banded matrix, but the size of the band would now be determined by the cut-off distance. The choice of an appropriate cut-off

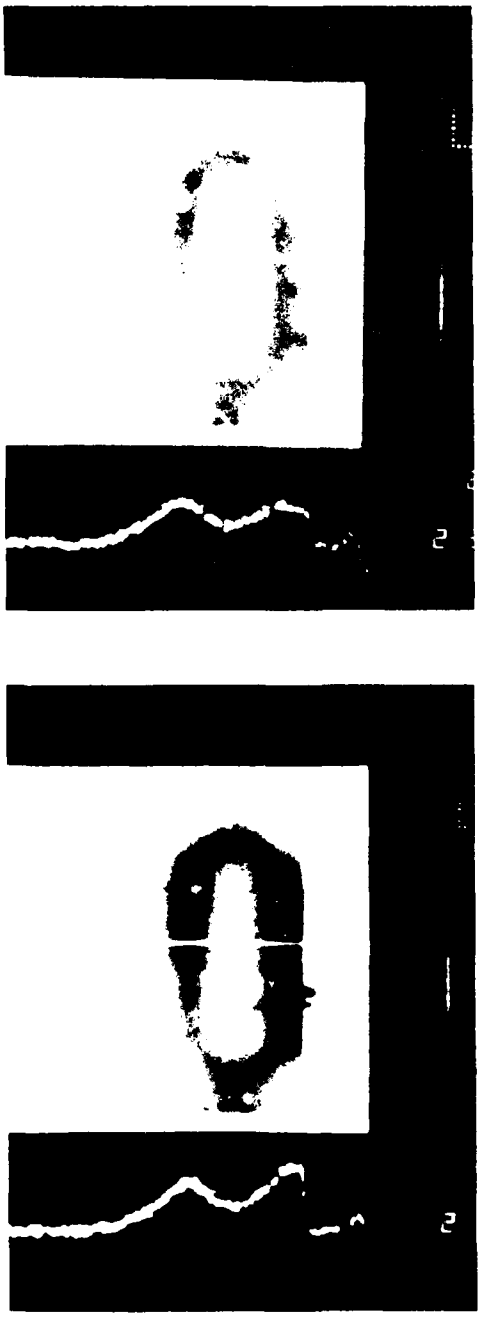

Figure 3.14 Photographs showing effects of edges on induced eddy currents.

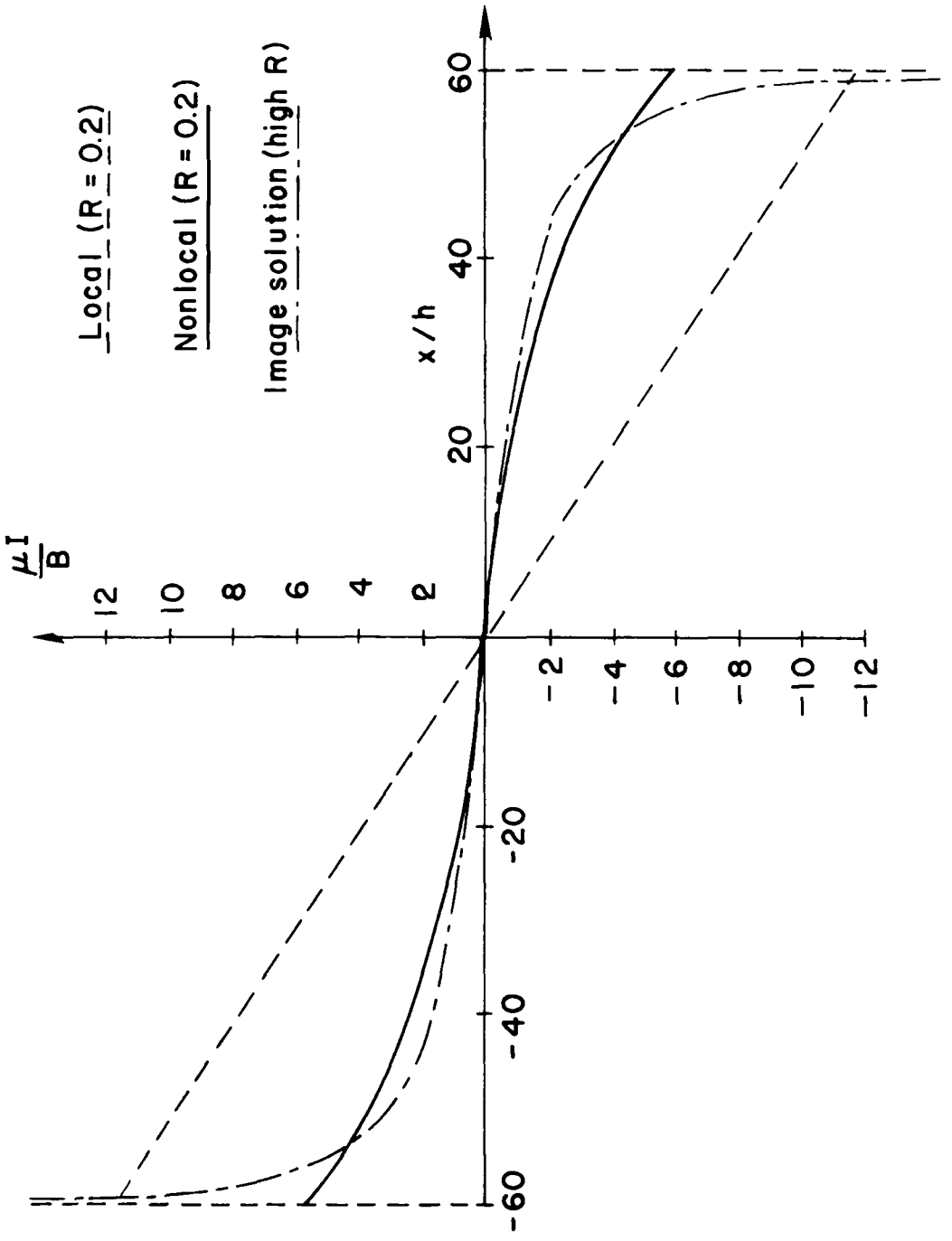

Figure 3.15 Calculated edge effects for uniform induction field.

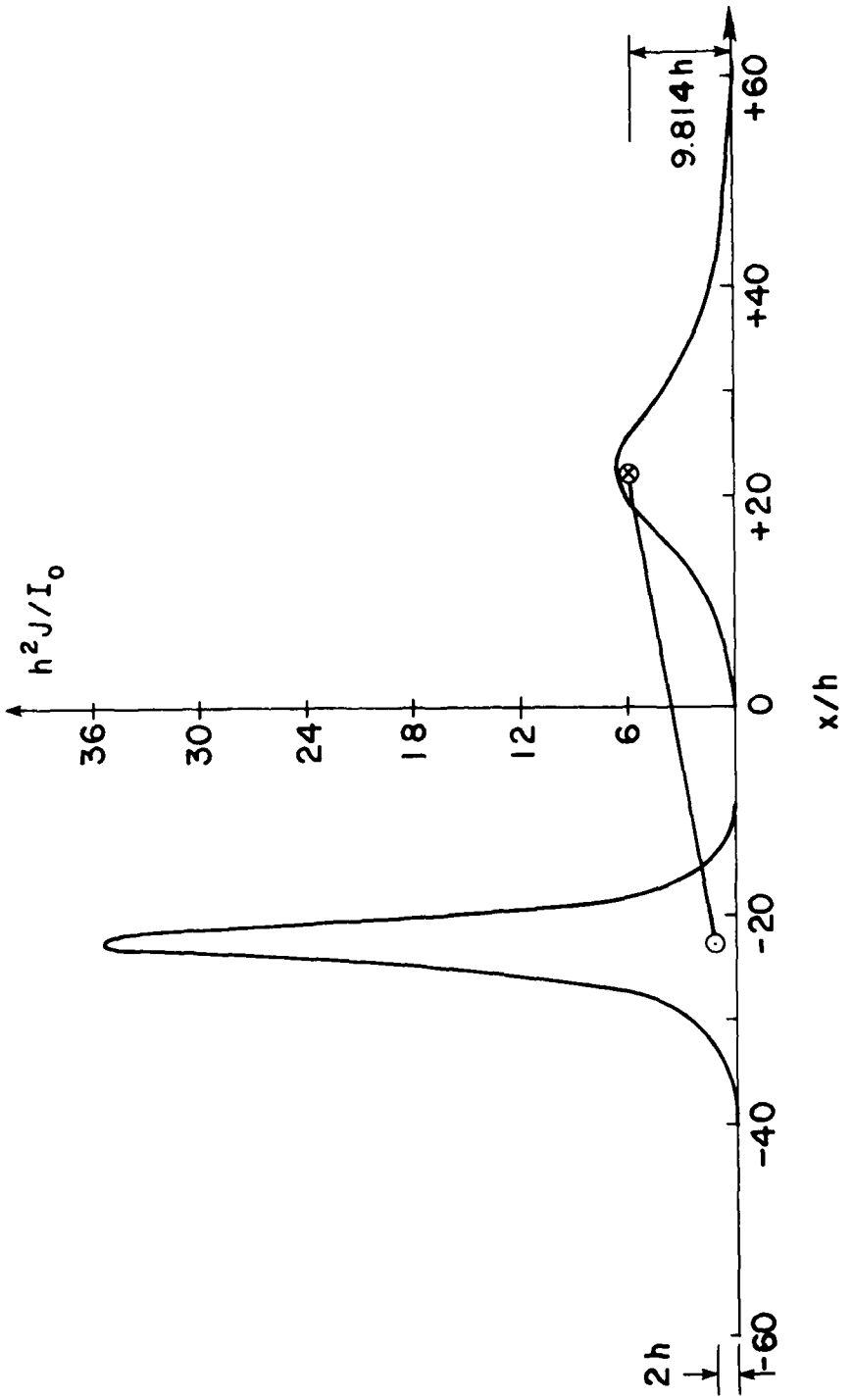

Figure 3.16 Magnetic pressures due to a tilted pair of current filaments centered above a long conducting plate (R = 0.07, tilt = 10 deg).

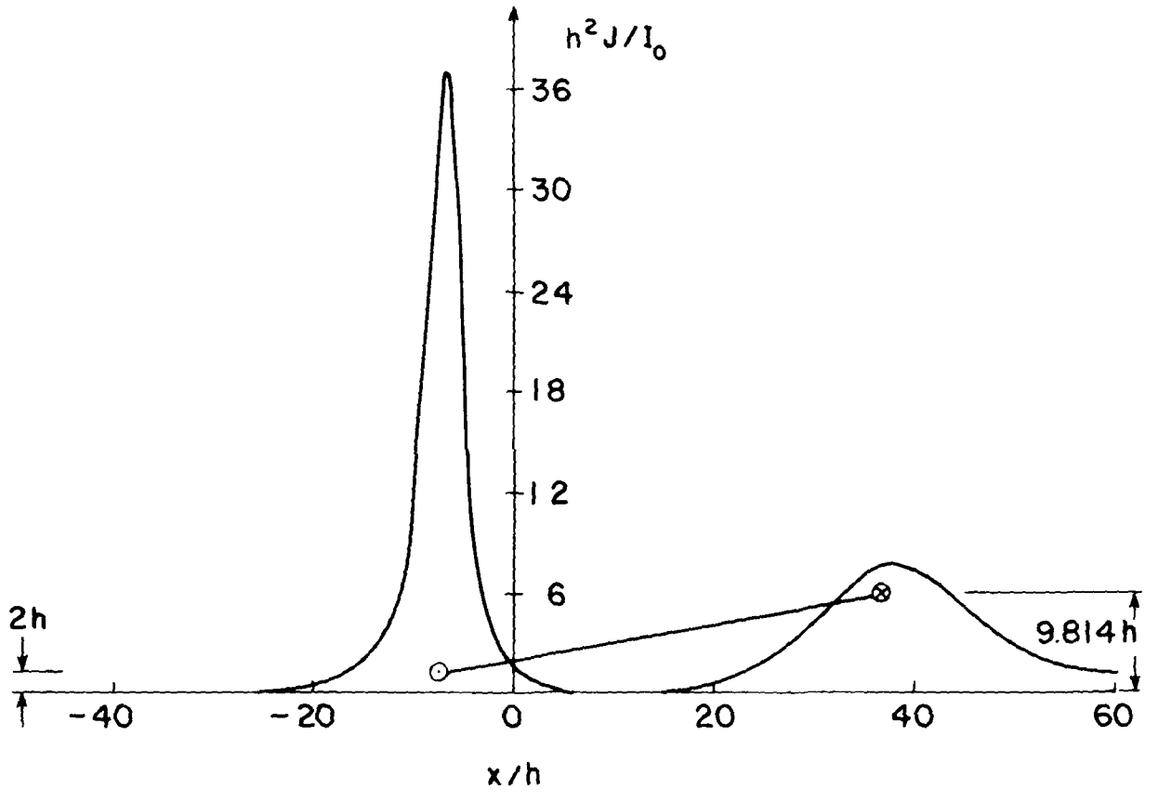

Figure 3.17 Magnetic pressures due to a tilted pair of current filaments nearer one edge of a long conducting plate (R = 0.07, tilt = 10 deg).

distance will be dependent upon the particular problem. The solution to the restricted nonlocal problem with an appropriate cutoff distance would be negligibly different from the full nonlocal solution, and considerable savings in computation would be achieved due to a reduction in the nonlocal integrations required, Eq. (3.34).

As a preliminary test of this strategy, the expedient of merely reducing the bandwidth of the FE equations was utilized by neglecting all terms outside of selected bandwidths. For the nonuniform mesh necessary for the eddy currents induced by a pair of external current filaments, this procedure is not equivalent to the selection of a cutoff distance. (A finer mesh is required under each filament). Nevertheless, as illustrated in Figure 3.18, the reduction in bandwidth provides a variation in the solution that approaches the full nonlocal solution. These results provide evidence that reduced nonlocal solutions will be efficient and useful in some situations. Further work will be needed to develop criteria for the selection of appropriate cutoff distances and to implement it in the computer program. For the efficient solution of large, dense matrix systems, Lachat and Watson (Ref. 81) presented a similar ad hoc approach for the numerical treatment of boundary integral equations in three-dimensional elastostatics. Jeng and Wexler (Ref. 82) described a successive element iterative scheme in their studies of three-dimensional static field problems using a boundary integral equation formulation.

i) Dimensional Analysis of the Size Effect of the Plate. The numerical results obtained from program EDDY1 presented so far have been based on a single nondimensional parameter: the magnetic Reynolds number R. R is defined as $R = \omega\mu\sigma h^2$ and is related to the skin depth δ through $R = 2(h/\delta)^2$, as discussed in connection with Eq. (3.34). For infinite

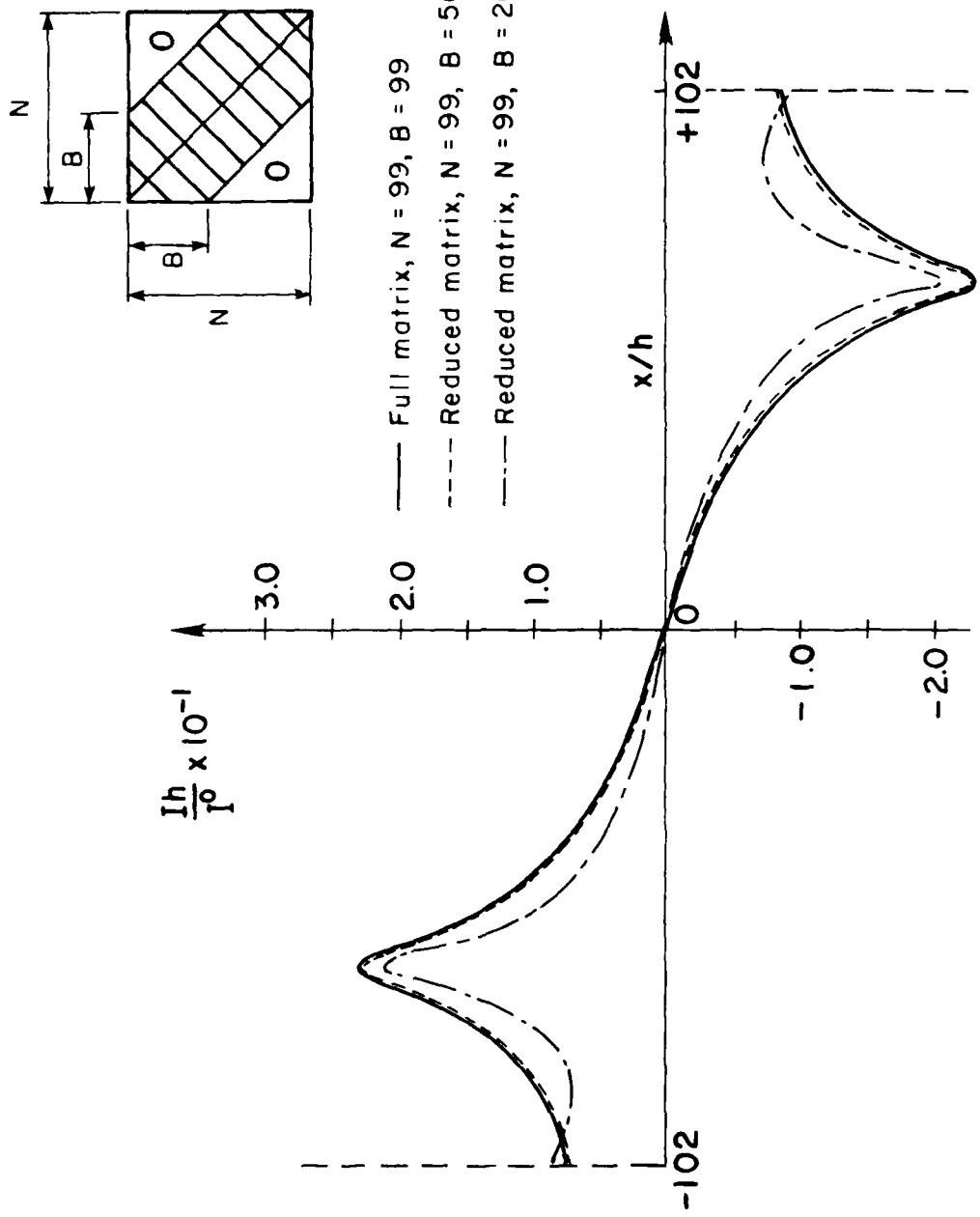

Figure 3.18 Effect of reduced matrix band on nonlocal solutions for a pair of current filaments centered above a long conducting plate ($R = 0.071$).

plates, except for the geometric parameters characterizing the positions of the exciting wires, this is the only possible nondimensional parameter characterizing the plate. For plates with finite width ℓ, the size effect of the width (span) comes in an another nondimensional parameter characterizing the effects of both the thickness and the width of the plate is possible. The new nondimensional parameter is designated by R_w and is defined and related to R as

$$R_w = \omega\mu\sigma h\ell = 2h\ell/\delta^2 = R\ell/h \qquad (3.51)$$

The role of R_w is illustrated through the one-dimensional plates with varying width/thickness ratio in a uniform, sinusoidally varying magnetic field. The analyses with EDDY1 have been performed by Hara (Ref. 83).

Figure 3.19 shows the maximum induced current at the edges of the plate versus the Reynolds number R using ℓ/h as a parameter. Figure 3.20 shows that the different curves can be collapsed to a single curve by using the new nondimensional parameter R_w.

Figure 3.21 shows the sum of the moduli of the induced currents through the width of the plate versus R for different ℓ/h values. Again, the different curves can be mapped to one by using the new parameter R_w as shown in Figure 3.22.

To determine the total torque and force on a conductor, one needs to know the real current distribution. Both the real and the imaginary parts of the induced currents therefore need to be considered (Ref. 33). Figure 3.23 shows the real and imaginary parts of the total induced current as functions of the Reynolds number R for two different ℓ/h values. The real part α' is the total current across the width in phase with the driving magnetic field, the imaginary part α'' is the total current 90 degrees out-of-phase with the driving field. These curves

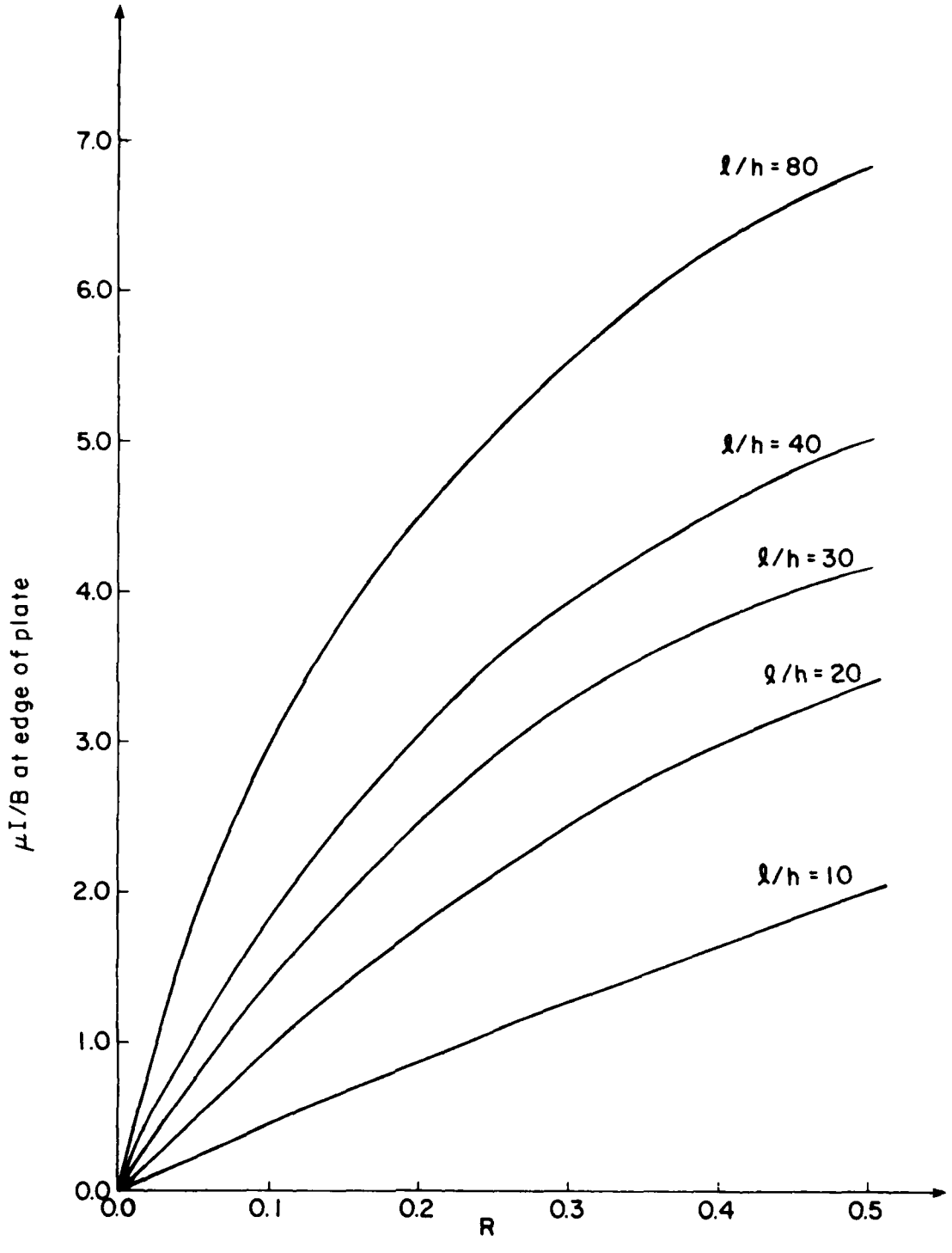

Figure 3.19 Maximum normalized current density at the edge of a plate subject to a uniform transverse field as a function of Reynolds number $R = 2(h/\delta)^2$.

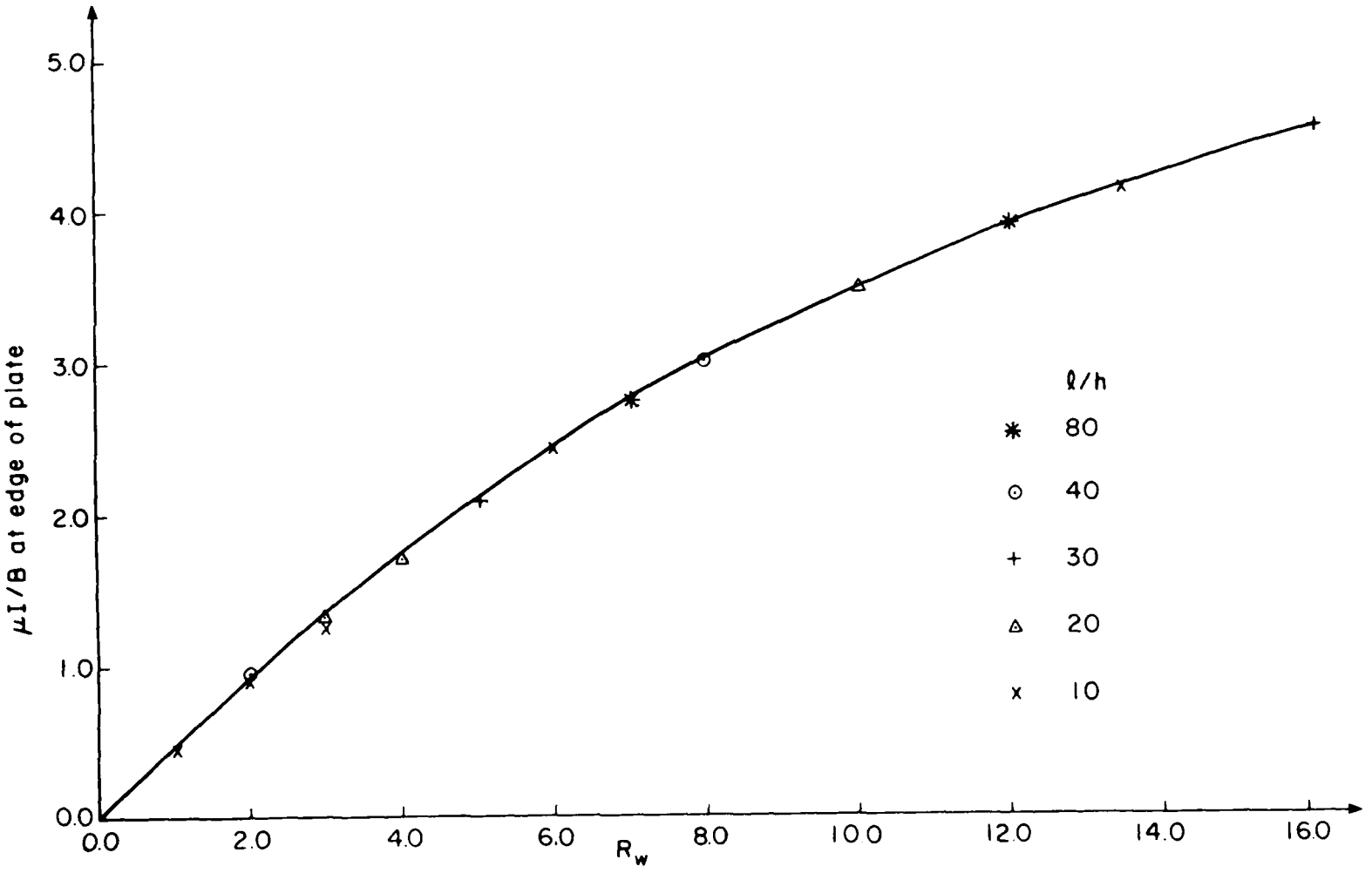

Figure 3.20 Maximum normalized current density at the edge of a plate subject to a uniform transverse field as a function of modified Reynolds number $R_w = R_i/h = 2h_i/\lambda^2$.

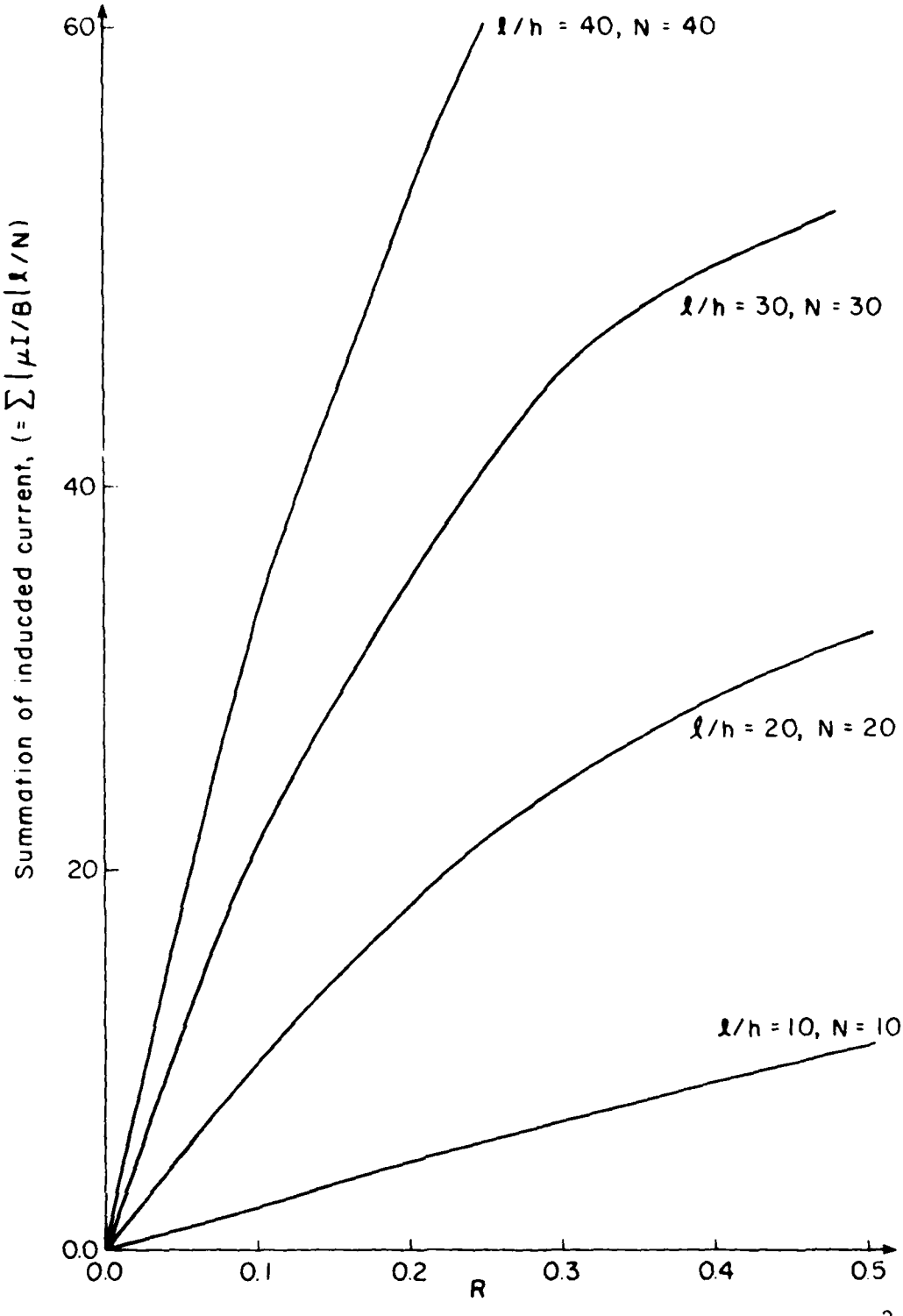

Figure 3.21 Total maximum current along the width vs. $R = 2(h/\delta)^2$ for a plate subject to a uniform transverse field. (N = number of equally spaced elements.)

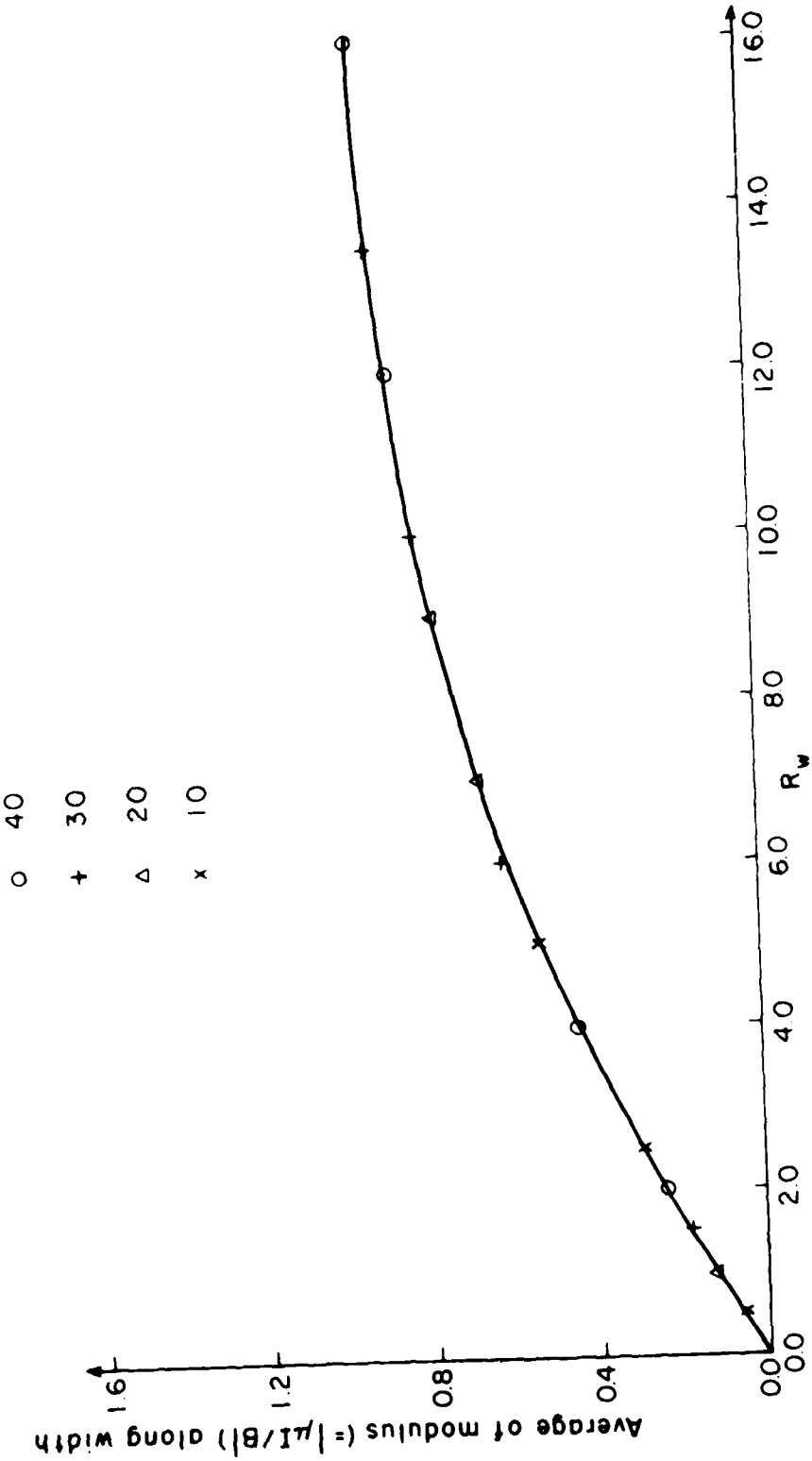

Figure 3.22 Averaged maximum current through the width vs. modified Reynolds number $R_w = 2h\ell/s2$ for a plate subject to a uniform transverse field.

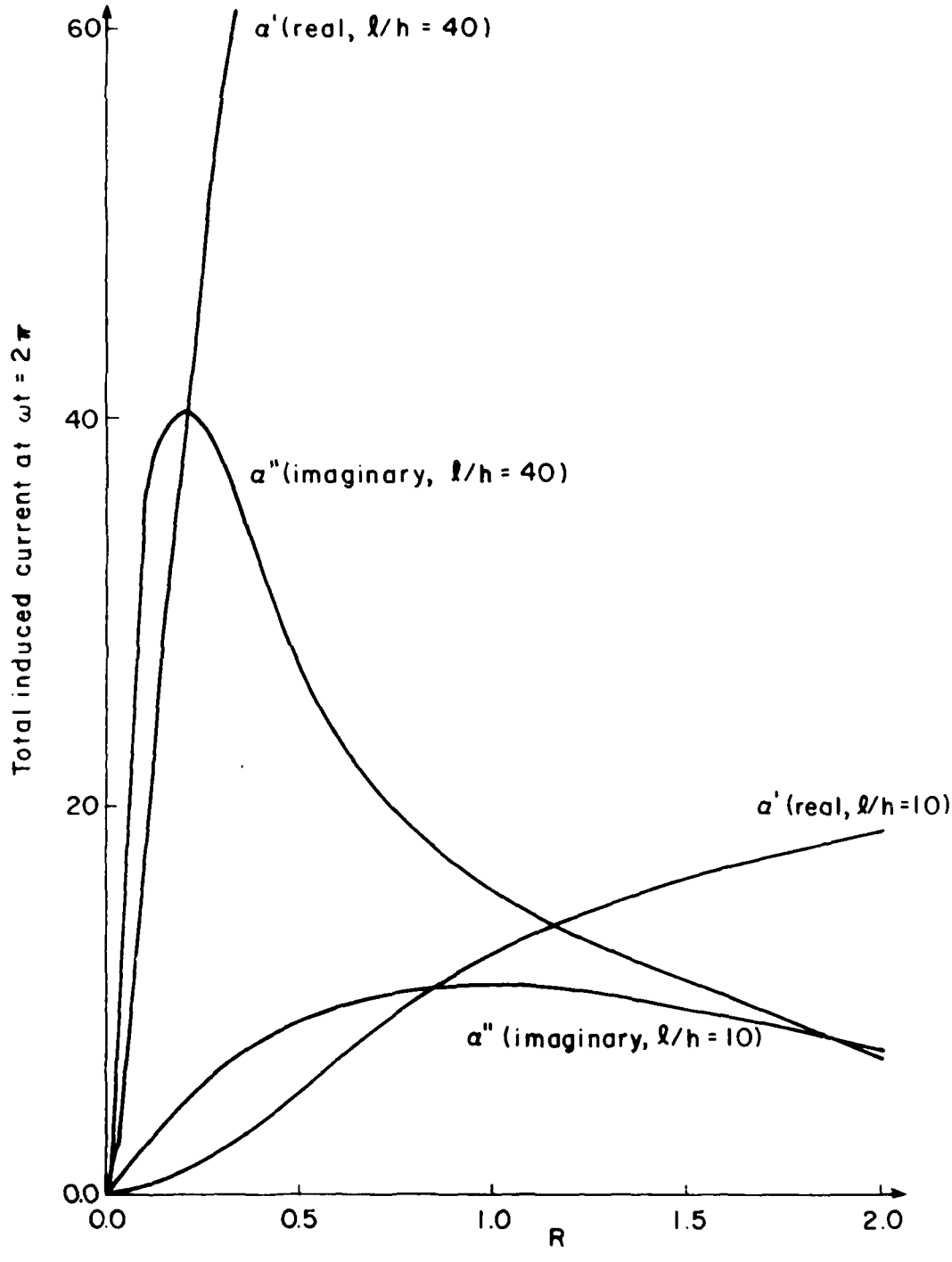

Figure 3.23 Total induced current vs. Reynolds number $R = 2(h/\delta)^2$ for a plate subject to a uniform transverse field.

are plotted in Figure 3.24 using the new parameter R_w. Again, good correlation is obtained although some differences occur at high Reynolds number cases.

3.3.2.b Transient Analysis by Program EDDY1T

The transient analysis program EDDY1T has been verified analytically and experimentally in various cases. The following is a summary of some of the results:

a) Comparison of the local solutions with the analytic results.

b) Comparison of the steady state nonlocal solution with the EDDY1 results.

c) Comparison of the transient solution with the FFT and infrared experimental results of Ref. 102.

d) Comparison of the transient solution and experimental measurements of eddy currents obtained with a search coil (Ref. 101).

All the cases analyzed use the physical parameters of the problem in the rationalized MKS system. Each of these problems is described in more detail below.

a) Comparison of the Local Solutions with the Analytic Results. The local solutions of the two-wire problem studied previously with the program EDDY1(Section 3.3.2.a; Figure 3.10)are calculated and presented in Figure 3.25. Since the reaction field is neglected, the solution may be obtained by direct integration and is the same for each cycle of excitation. A stainless steel plate is used in this problem. The FEM solutions obtained with two different time-step sizes do not differ significantly from the analytic results.

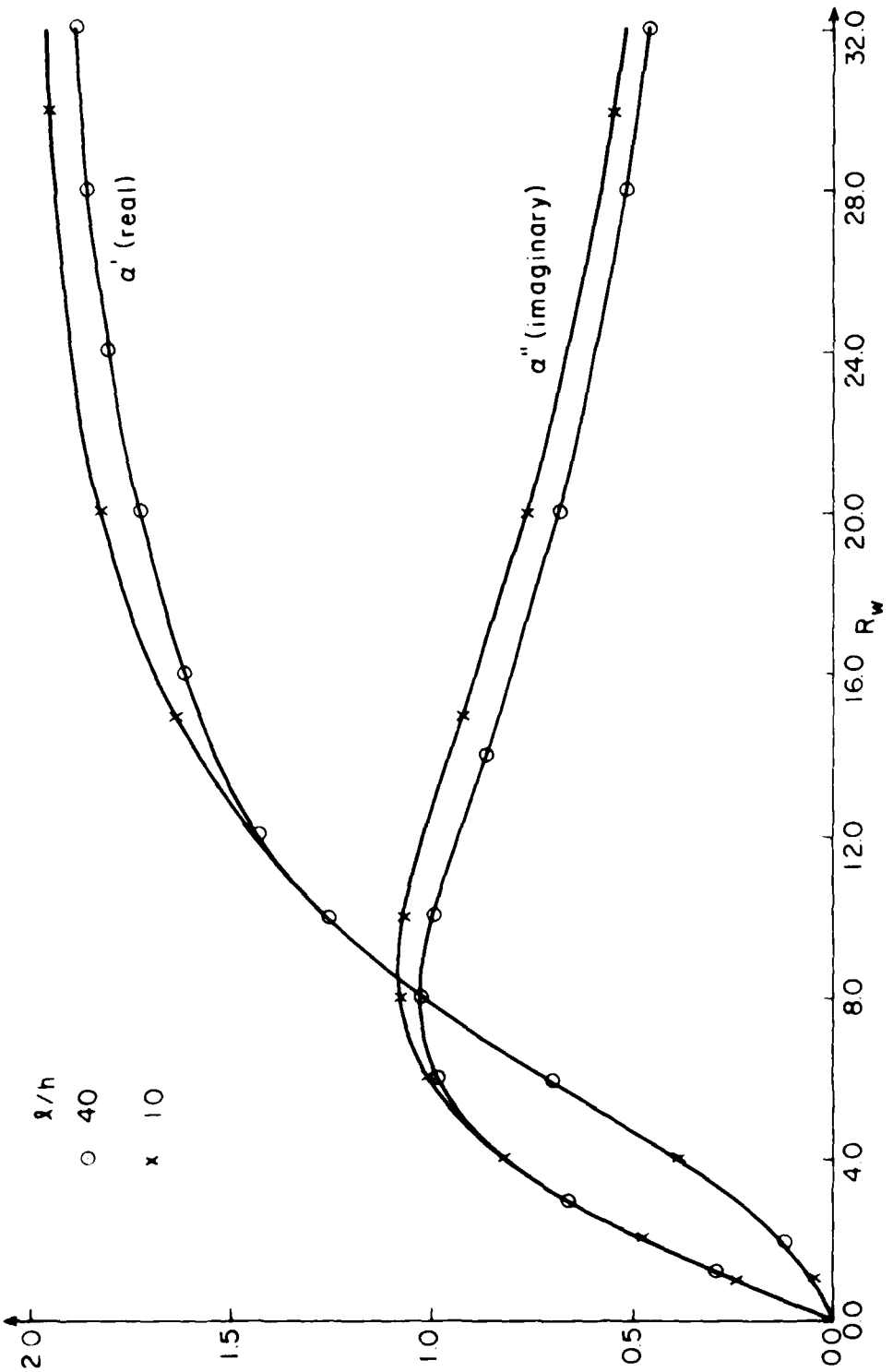

Figure 3.24 Averaged current vs. modified Reynolds number $R_w = 2(h/\delta)^2$ for a plate subject to a uniform transverse field.

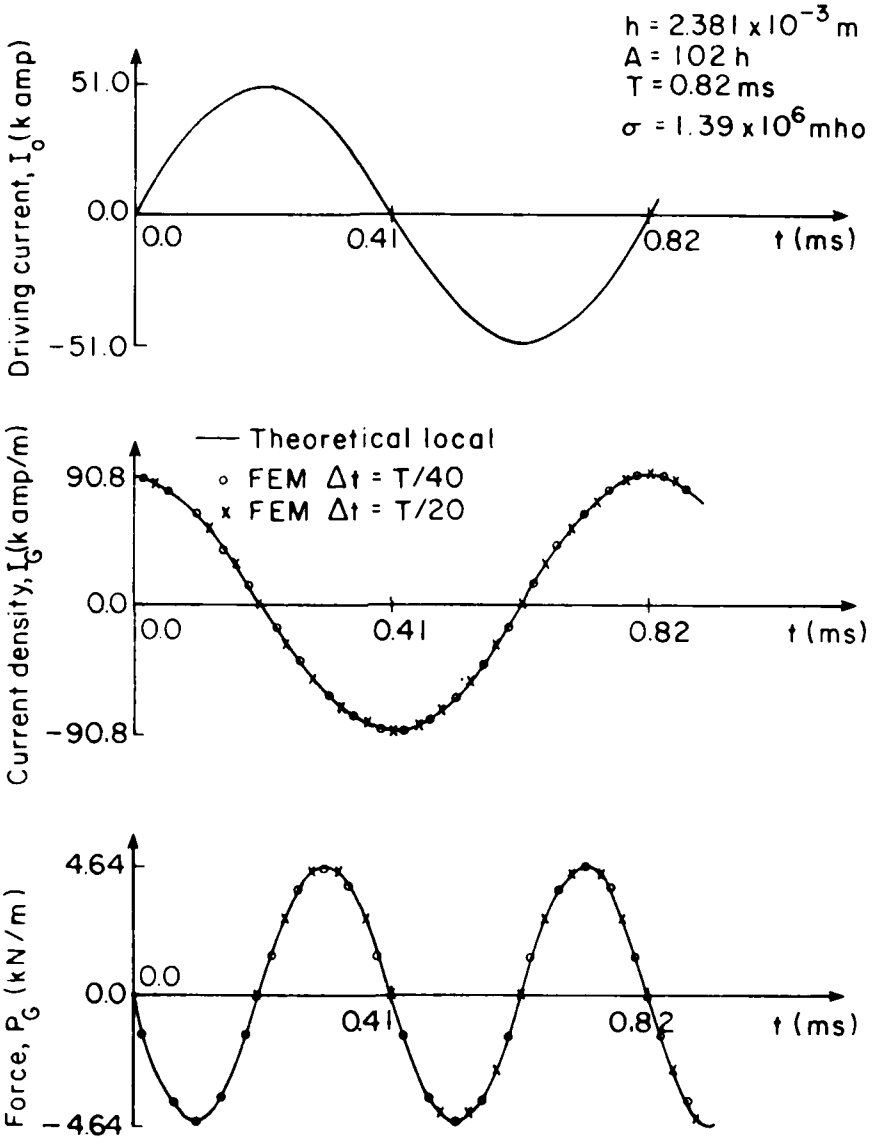

Figure 3.25 Comparison of theoretical and finite element method (FEM) predictions of local transient eddy current effects for the long plate in Figure 3.12 subject to a sinusoidally varying magnetic field.

b) Comparison of the Steady State Nonlocal Solutions with the EDDY1 Results. The nonlocal solution of the same problem with a continual sinusoidal exciting current is calculated by program EDDY1T. Figure 3.26 shows that the induced current at point G becomes nearly steady state after two cycles of excitation. The magnetic Reynolds number in this problem is R = 0.079. The modulus and phase angle of the induced current when it becomes steady state are the same as predicted in Figure 3.13. In Figure 3.26b, the magnetic pushing force is shown, and the fact that its average value is nonzero is clearly evident.

The size of the time step used in this problem is Δt = 0.041 ms, or one twentieth of the period of the driving current. Figure 3.27a shows the eddy current distribution at the 53-rd time step when the induced current at point G is almost at its maximum. Figure 3.27b shows the current distribution at the 57-th time step when the induced current at point G is nearly zero. Figure 3.27c shows the current distribution at the 60-th time step ($\omega t = 6\pi$) when the driving current in the wire is zero. Figure 3.27d shows the current distribution at the 65-th time step ($\omega t = 6\frac{1}{2}\pi$) when the driving current in the wire reaches its maximum value. The corresponding magnetic force distributions at these particular time steps are shown in Figure 3.28.

c) Comparison of the Transient Solution with the FFT and Infrared Experimental Results. The transient eddy current problem discussed in Figures 3.10, 3.12, and 3.13 is re-analyzed using program EDDY1T. The results are shown in Figures 3.29 and 3.30. The induced current density calculated at point G underneath the wire is presented in Figure 3.29 and compared with the FFT result from Figure 3.12. It is seen that the two results have nearly the same magnitude but the one calculated by EDDY1T

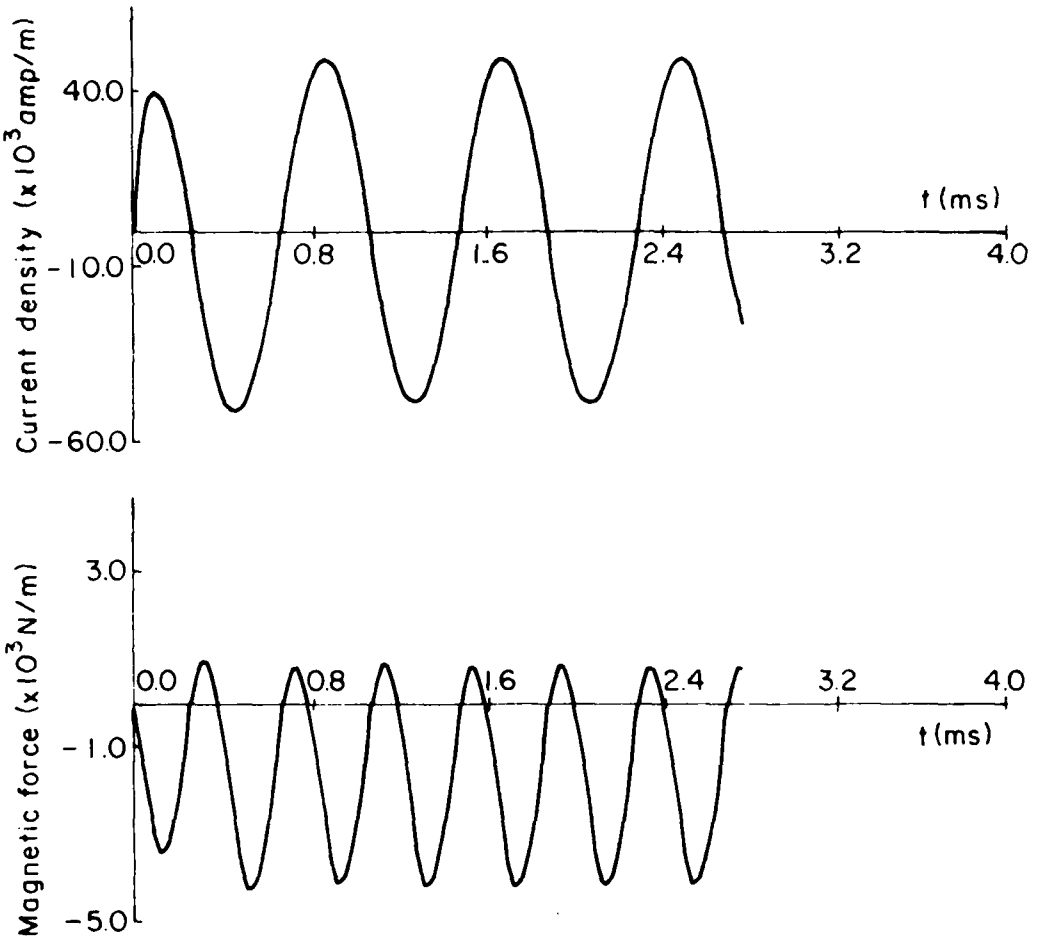

Figure 3.26 Induced current and force at point G (Figure 3.12) for a continual sinusoidal exciting current.

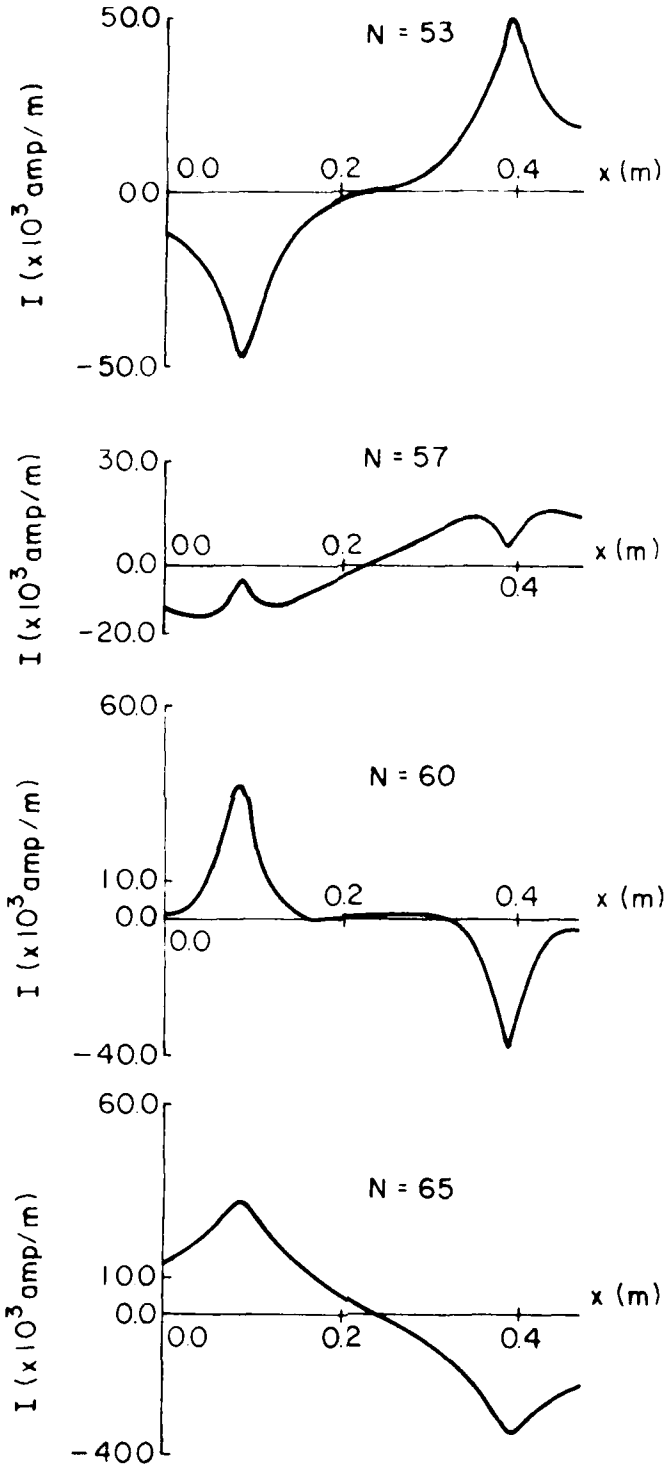

Figure 3.27 Eddy current distributions across the width of the plate in Figure 3.12 at various time steps for a continual sinusoidal exciting current.

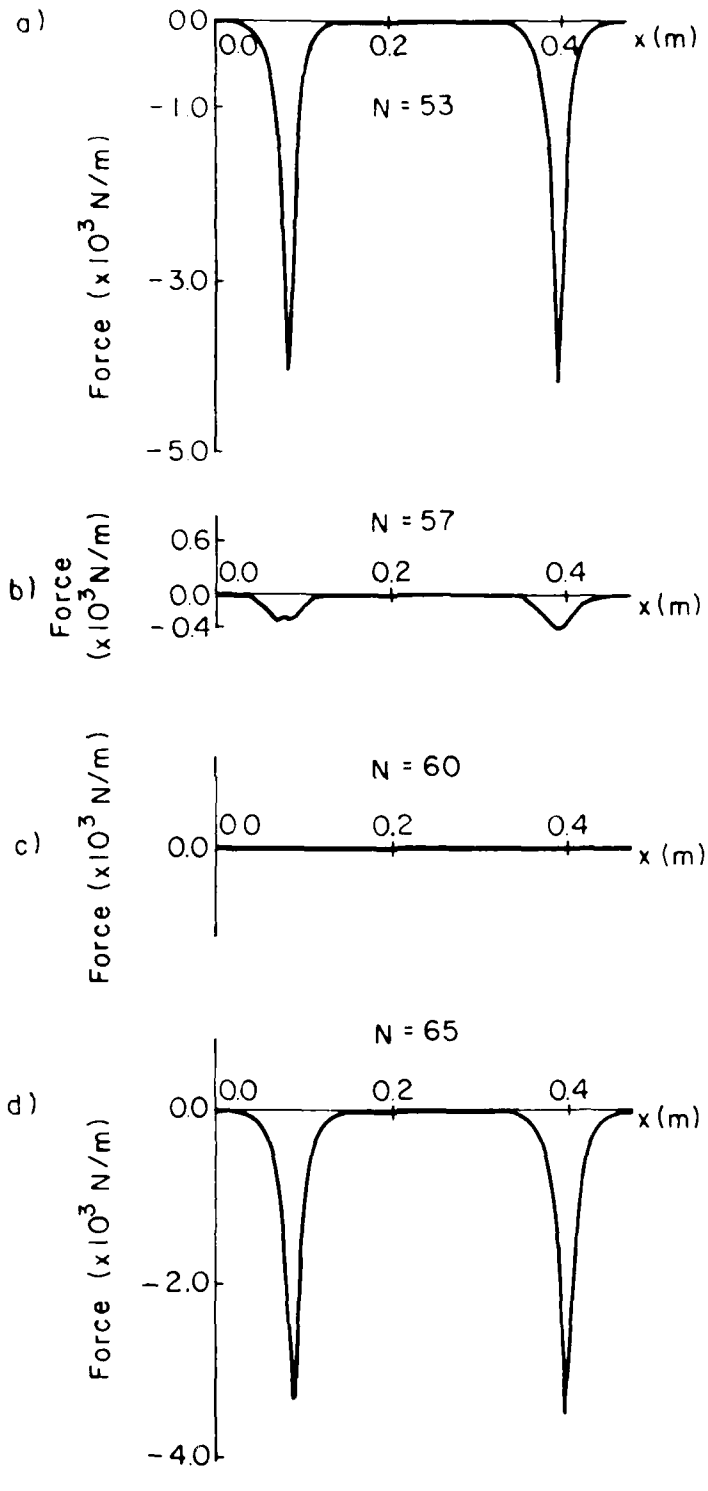

Figure 3.28 Magnetic force on the plate in Figure 3.12 at different time steps for a continual sinusoidal exciting current.

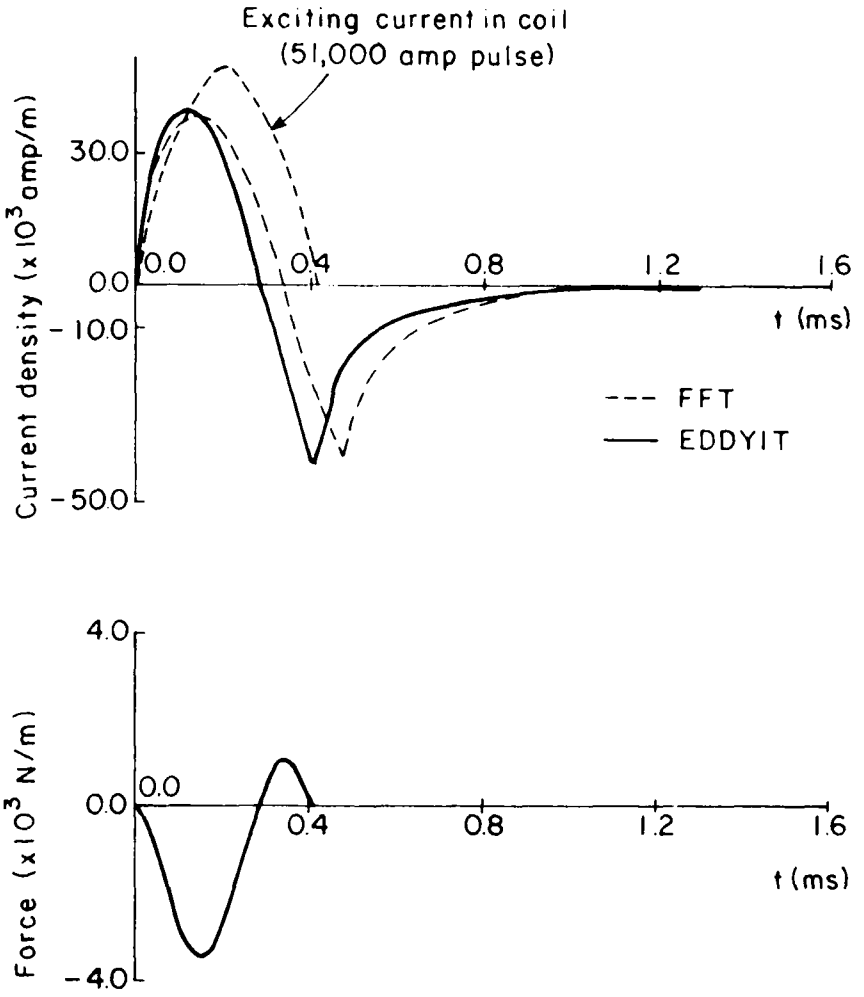

Figure 3.29 (a) Comparison of the FFT and EDDY1T results for transient eddy current at point G of Figure 3.12.

(b) Transient magnetic force at point G calculated by EDDY1T.

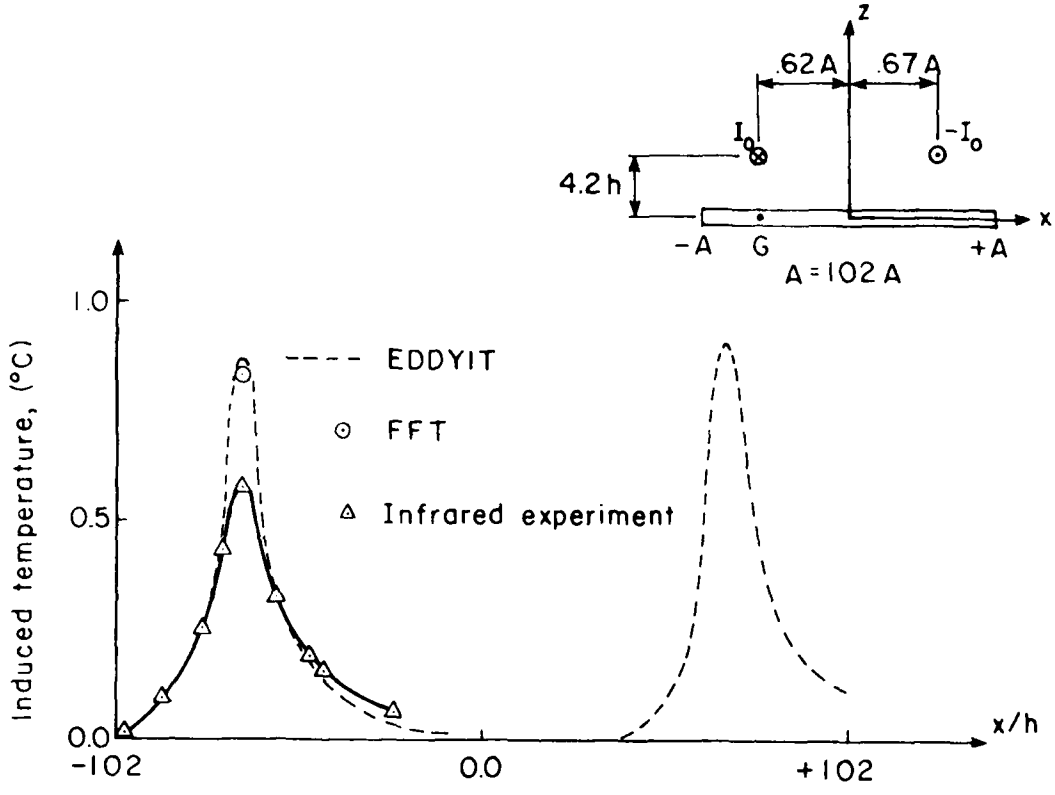

Figure 3.30 Comparison of the numerical and infrared experimental results of induced temperature rise.

shows more accurate time characteristics. This is evidenced by the late arrival of the second peak of the FFT result which should occur physically at the time when the driving current becomes zero. The correct arrival time of the second peak has been predicted by the EDDY1T result.

The induced temperature rise is shown in Figure 3.30 and compared with the infrared experimental results. The infrared picture is taken approximately 160 ms after the pulse is applied, as mentioned in connection with Figure 3.10. The prediction of the FFT result for the temperature is also shown for comparison.

d) Comparison of the Transient Solution and Experimental Measurements of Eddy Current Obtained with a Search Coil. A search coil technique has been used to measure the eddy current induced on an aluminum plate. The arrangement of the experiment is described schemetically in Figure 3.31. To simulate a one-dimensional plate, the measurements were taken along the central line of a rectangular plate with length/width ratio approximately equal to 4.2 (Ref. 101).

To measure the real induced current, the search coil readings at points A and B were first taken using a plastic dummy plate. The measurements were then made at points A and B for the conducting plate. The induced current densities are obtained by subtracting the readings obtained for the plastic plate from the readings for the real plate. The search coil readings obtained at point A underneath the wire are shown in Figure 3.32.

The induced current densities at points A and B so determined are compared with the numerical results obtained by using program EDDY1T in Figure 3.33. The qualitative agreement of the results are good at both points. Quantitatively some differences exist. These quantitative

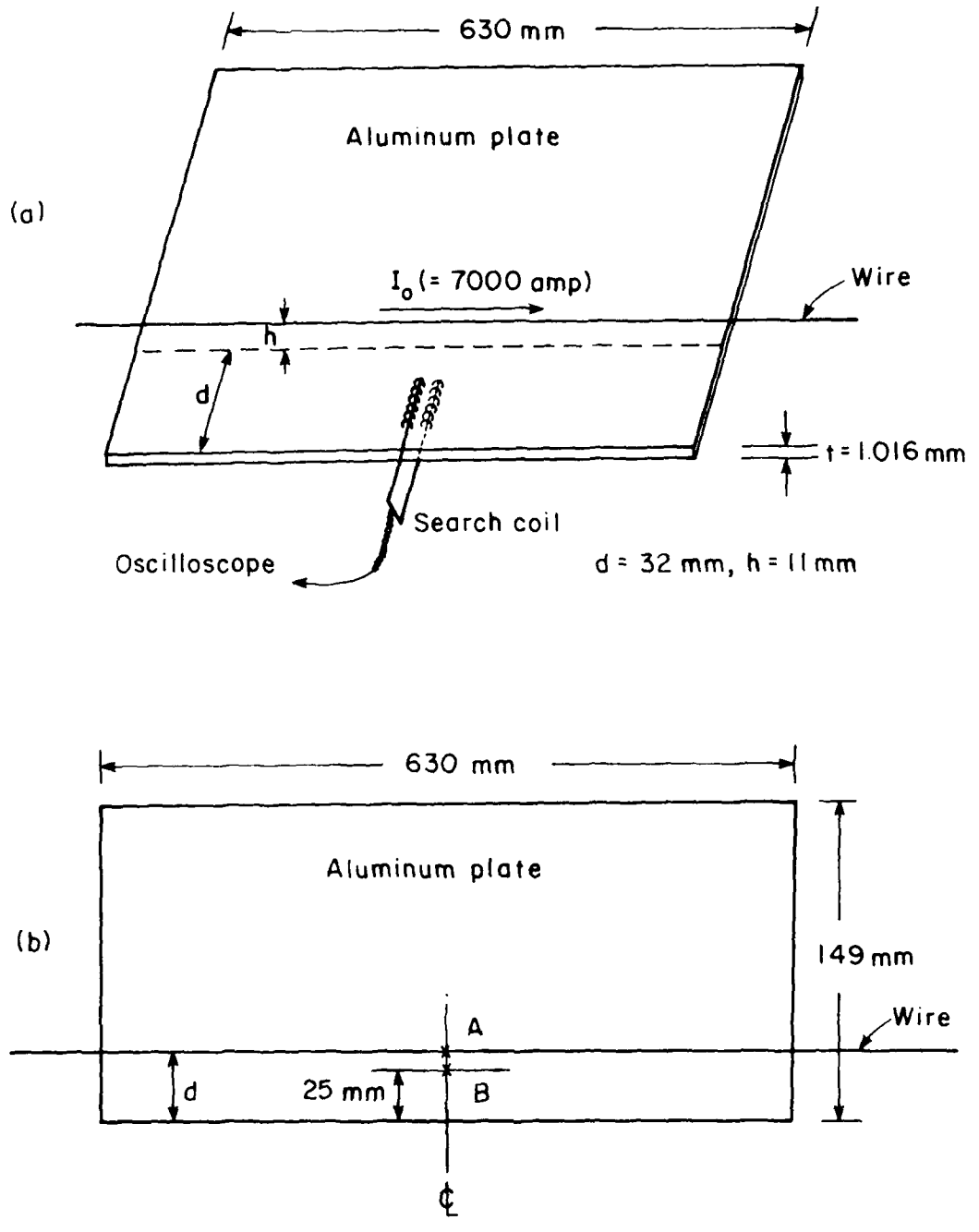

Figure 3.31 Arrangement of the search coil experiment for a long plate, (a) Isometric view, (b) Plan view.

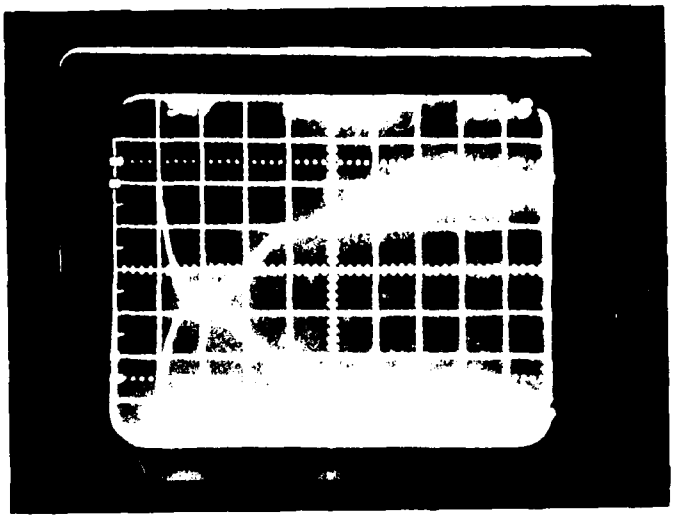

(a)

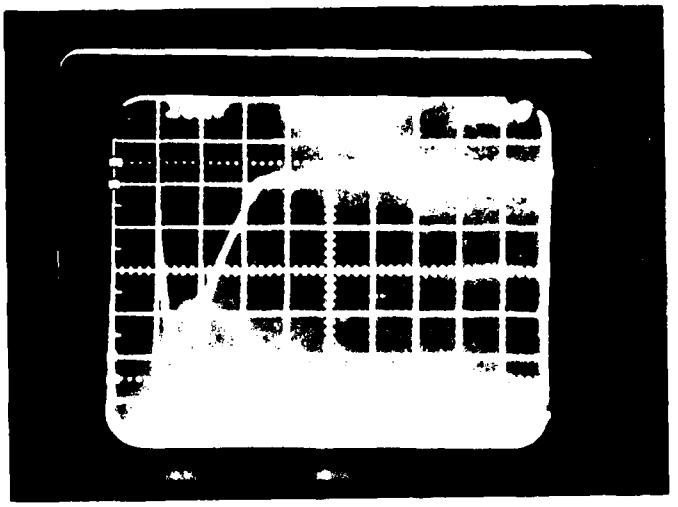

(b)

Figure 3.32 For the plate in Figure 3.31:

(a) Search coil reading at point A and the applied current with a plastic dummy plate,

(b) Search coil reading at point A and the applied current with an aluminum plate.

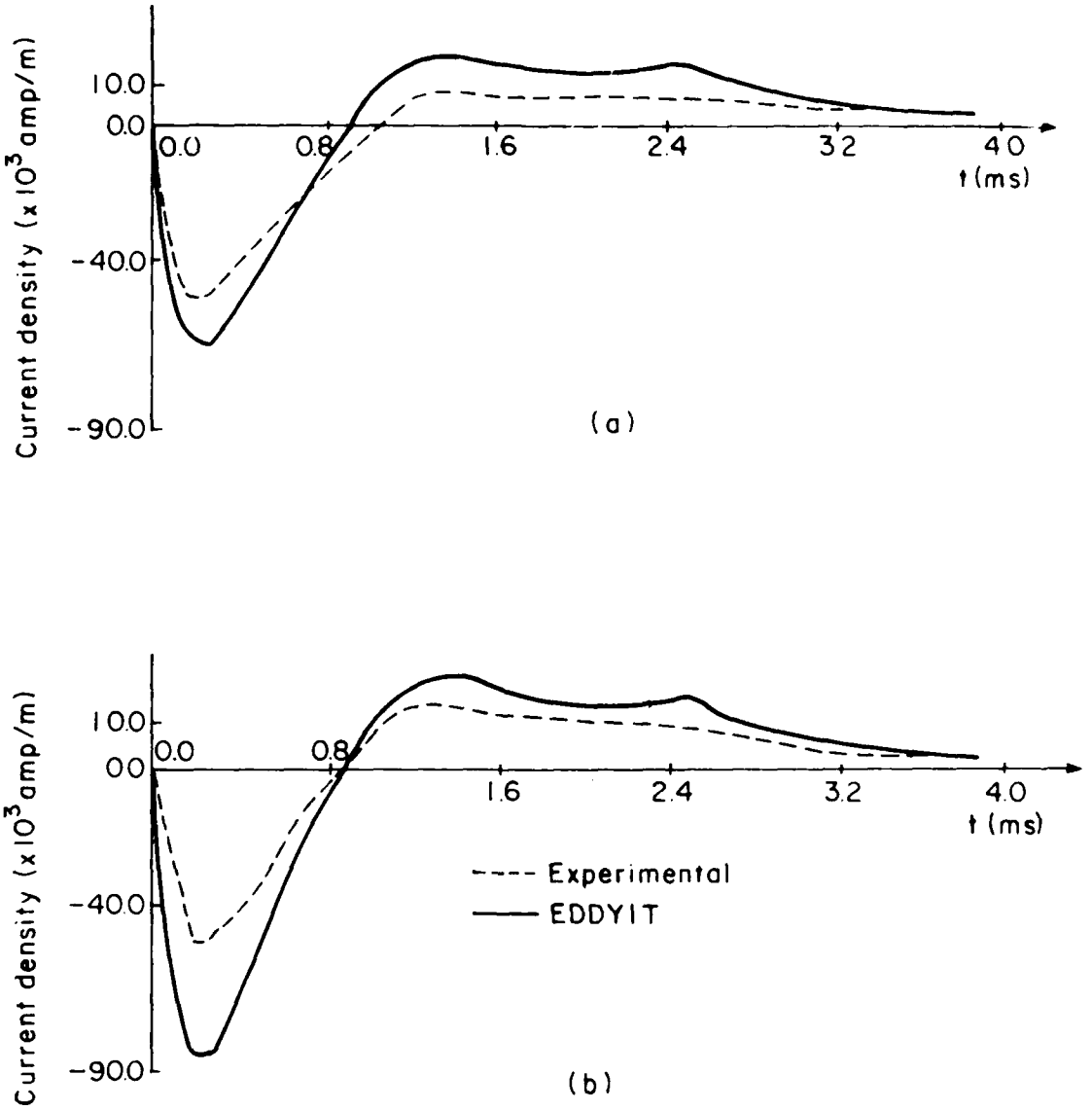

Figure 3.33 Numerical and search coil experimental results of the induced current density for the plate in Figure 3.31: (a) at point B, (b) under the wire at point A.

differences probably arise largely from the approximations involved in the experiment. Namely, each of the two search coils used has a finite length of about 10 mm and finite cross sectional dimension of about 10 mm. The dimension of the exciting wire itself is about 2 mm. The measurements obtained are therefore averaged values over the 10 mm length of the search coil. One example of this averaging effect in the experimental results can be seen from Figure 3.33. The two experimental curves have nearly the same peak value at points A and B, while in the infrared results and in all the numerical calculations, Figure 3.34, the induced current under the wire is definitely higher.

3.4 Eddy Current on Finite Plates

The finite element Galerkin formulation and the Fortran code EDDY2 for two-dimensional problems of steady state, harmonic currents in flat plates are presented in Section 3.4.1. The treatment of the nonlocal integral term is described in some detail. Some numerical results and their verifications are presented in Section 3.4.2.

3.4.1 Finite Element Formulation for Steady State Problems

The two-dimensional eddy current equation is obtained from Eq. (2.103) by dropping all the coupling terms. For steady state, harmonic currents in a flat plate, the equation may be nondimensionalized into the following form.

$$\nabla^2\phi - i2\pi R\phi + iR \int_{\text{area}} \frac{\phi(\xi,\eta)}{[(x-\xi)^2 + (y-\eta)^2 + 1]^{3/2}} d\xi d\eta = i2\pi R\theta(x,y) \tag{3.51}$$

in which the coordinates are nondimensionalized with respect to half the thickness $(\frac{h}{2})$; $\psi = (\frac{hR}{2\mu})\phi e^{i\omega t}$; $B_z^o = (\frac{B}{2})\theta e^{i\omega t}$; the magnetic Reynolds number

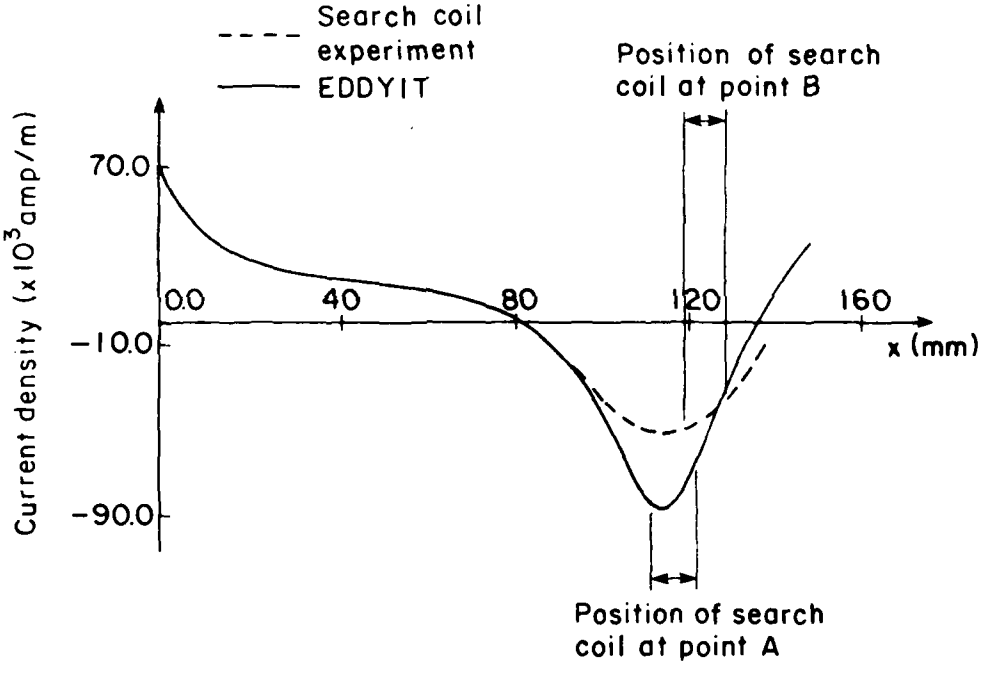

Figure 3.34 Current distribution across conducting plate at t = 0.2 ms for the plate in Figure 3.31

is $R = \frac{\omega\mu_0 h^2}{8\pi}$, which is related to skin depth δ through $R = \frac{1}{4\pi}\left(\frac{h}{\delta}\right)^2$; and B is the reference magnetic field.

The finite element Galerkin method is used to solve Eq. (3.51). ϕ is approximated globally and locally by

$$\phi = \sum_{k=1}^{G} M_k \phi_k \qquad \phi^E = \sum_{k=1}^{6} N_k^E \phi_k^E \tag{3.52a,b}$$

in which G is the total number of nodal points, E denotes the Eth element, M_k are the quadratic global interpolation functions generated from the local element shape functions N_k^E. Six-node triangular elements are used here. The local element shape functions are all quadratic in this case. The element algebraic equations are

$$\sum_{k=1}^{6} K_{jk}^E \phi_k + i \sum_{k=1}^{6} P_{jk}^E \phi_k + i \sum_{k=1}^{G} Q_{jk}^E \phi_k = iR_k^E \tag{3.53}$$

in which

$$K_{jk}^E = \sum_{i=1}^{6} \int_{A^E} N_{j,i}^E N_{k,i}^E \, dA^E \tag{3.54a}$$

$$P_{jk}^E = 2\pi R \int_{A^E} N_j^E N_k^E \, dA^E \tag{3.54b}$$

$$Q_{jk}^E = -R \int\int_{\text{area}} M_k(\xi,\eta) \, W_j^E(\xi,\eta) \, d\xi d\eta \tag{3.54c}$$

$$R_k^E = -2\pi R \int_{A^E} N_j^E \theta \, dA^E \tag{3.54d}$$

The weighting function W_j^E is given by

$$W_j^E(\xi,\eta) = \int_{A^E} \frac{N_j^E(x,y)}{[(x-\xi)^2 + (y-\eta)^2 + 1]^{3/2}}\, dxdy \qquad (3.55)$$

A change of the sequence of integrations in the Galerkin formulation of the integral term in Eq. (3.51) has been applied to obtain the weighting function W_j^E. Because of the numerical difficulty associated with the sharp variation of the kernal function in Eq. (3.55), the weighting function is calculated analytically within each element and numerically outside the element. Eq. (3.54c) is then integrated entirely by numerical quadrature.

The formulation in Eqs. (3.54c) and (3.55) is in terms of the global coordinates through the global position of the source point (ξ,η). To simplify the integration, each element is first mapped onto a standard triangle through a rigid body translation and rotation. A linear change of scales of the axes is then performed so that the standard triangle is independent of the coordinates of the nodes of the element being mapped, and the coordinates of the source point appear only as parameters in the analytical integration. The same form of the integrated result may then be used for all the elements in the finite element mesh.

Since N_j^E is quadratic, six basic integrations with numerators 1, x, y, x^2, xy, and y^2 in Eq. (3.55) need to be performed. These integrated results are used to form the weighting function. The six integrations, the weighting function W_j^E, and the element matrices $[K^E]$ and $[P^E]$ are detailed in Appendix B.

The resulting global matrix is again complex, nonsymmetric, and fully populated. Local, nonlocal, and image solutions can be calculated just as in the one-dimensional case. Eddy currents can be calculated through

numerical differentiation, and magnetic pressure and temperature evaluated after the stream function is solved.

A Fortran program EDDY2 has been developed based on the formulation of Eqs. (3.53) - (3.55). It calculates the local and nonlocal solutions of stream function, eddy current, temperature, and pressure. As of this writing, the image solution and two-dimensional graphic output capabilities remain to be implemented. Uniform magnetic field and fields due to any number of magnetic dipoles can be handled. Magnetic fields generated from other types of coils of interest can be added readily. The capability of analyzing for multiple frequencies also remains to be implemented.

The geometry of the plate and the description of the external magnetic field are the two basic forms of data needed by program EDDY2. The total numbers of nodal points, load cases, and elements need to be specified. Coordinate and boundary condition must be given for each input node. Intermediate nodes may be generated for any groups of nodal points that are uniformly spaced. Element information may also be generated. Although only six-node triangles are included in the present version of EDDY2, the program has been structured so that other types of elements may be added. Element group information and the master card for each element group therefore need to be input too.

The program allows for different orders of numerical integrations. Six- and seven-point formula are now provided. The order may be specified on the master element group card.

Presently two types of magnetic fields may be analyzed: the uniform field and the magnetic field due to any number of dipoles. For uniform field no other information is needed. For dipole field the positions and the relative strengths and senses of each magnetic dipole must be given

subsequently.

Values of the stream function, eddy current, temperature induced in a half cycle of the current, and time-averaged magnetic pressure are produced as output. The stream function is calculated at the nodes of the finite element mesh. Current, temperature, and pressure are evaluated at the centroid of each element. The stream function and current are calculated in complex form. The modulus and phase angle of the current are evaluated in the interest of spectral analysis for the calculation of transient currents.

3.4.2 Numerical Results and Experimental Verifications for Finite Plates

The two-dimensional finite element code EDDY2 has been verified for a limited number of problems involving uniform applied fields. The numerical results from EDDY2 have been checked with both analytic solutions and numerical calculations obtained from other methods. Infrared measurements are also used to verify the results qualitatively. More extensive verifications are needed to check the full capabilities, but comparison results for fields other than uniform are scarce except for low Reynolds number (local) cases.

The following objectives have been met with the program EDDY2 up to this writing.

a) Comparison of low Reynolds number results with the analytic solutions.

b) Comparison of low and intermediate Reynolds number results for long plate with the numerical results from program EDDY1.

c) Comparison of low Reynolds number results for a square plate with edge crack with the BIEM numerical results and infrared measurements (Ref. 102).

d) Dimensional analysis of the size effect of the width of a square plate.

Each of these is described separately below.

a) Comparison of Low Reynolds Number Results with the Analytic Solutions. In the low Reynolds number limit one may drop the nonlocal terms in Eq. (3.51) and obtain the local theory for the stream function in the two-dimensional case,

$$\nabla^2\phi = i2\pi R\theta(x,y) \tag{3.56}$$

The solution of the above Poisson equation is a common practice in many physical problems. For the uniform normal external magnetic field, the problem is analogous to the torsion of a shaft in the theory of elasticity, for example. For a square and rectangular plate in the low Reynolds number limit, the EDDY2 solution has been checked with the series solution for torsion of rectangular shafts. The agreement between the stream function and current density in one case and the stress function and shear stress in the other is excellent.

b) Comparison of Low and Intermediate Reynolds Number Results for Long Plate with the Numerical Results from Program EDDY1. For a long rectangular plate excited by a harmonic uniform field with the Reynolds number R = 0.0012, EDDY2 gives the stream function contour shown in Figure 3.35. Across the middle section of the long plate, the problem is essentially one-dimensional and may be approximated by an analysis with EDDY1. The close correlation between the two calculated induced currents across that section from EDDY2 and EDDY1 are shown in Figure 3.36.

For the intermediate Reynolds number case (R = 0.2 in EDDY1), the comparison between the stream functions calculated from EDDY1 and EDDY2

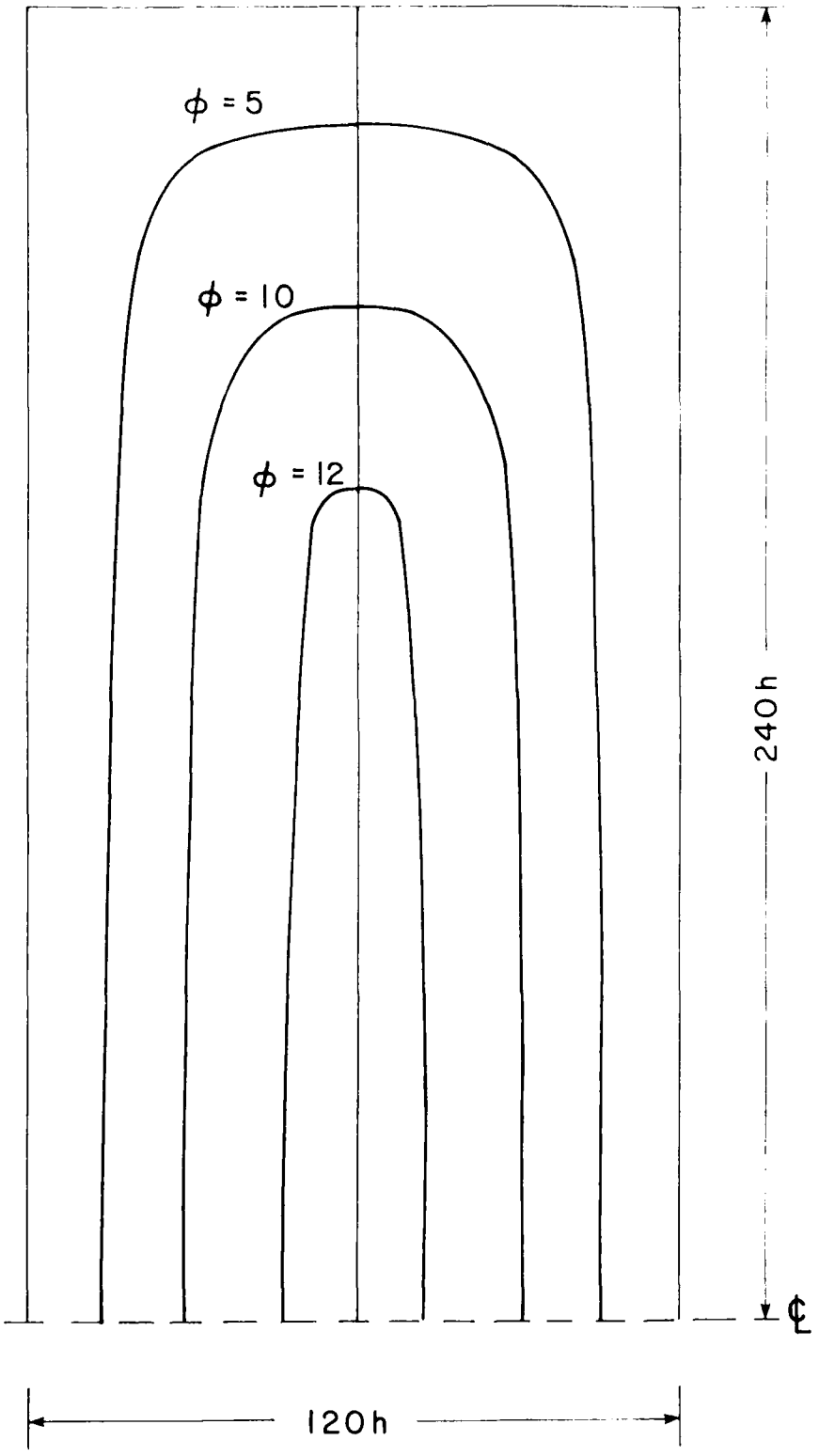

Figure 3.35 Stream function contours for a long rectangular plated excited by a harmonic uniform field (R = 0.0012).

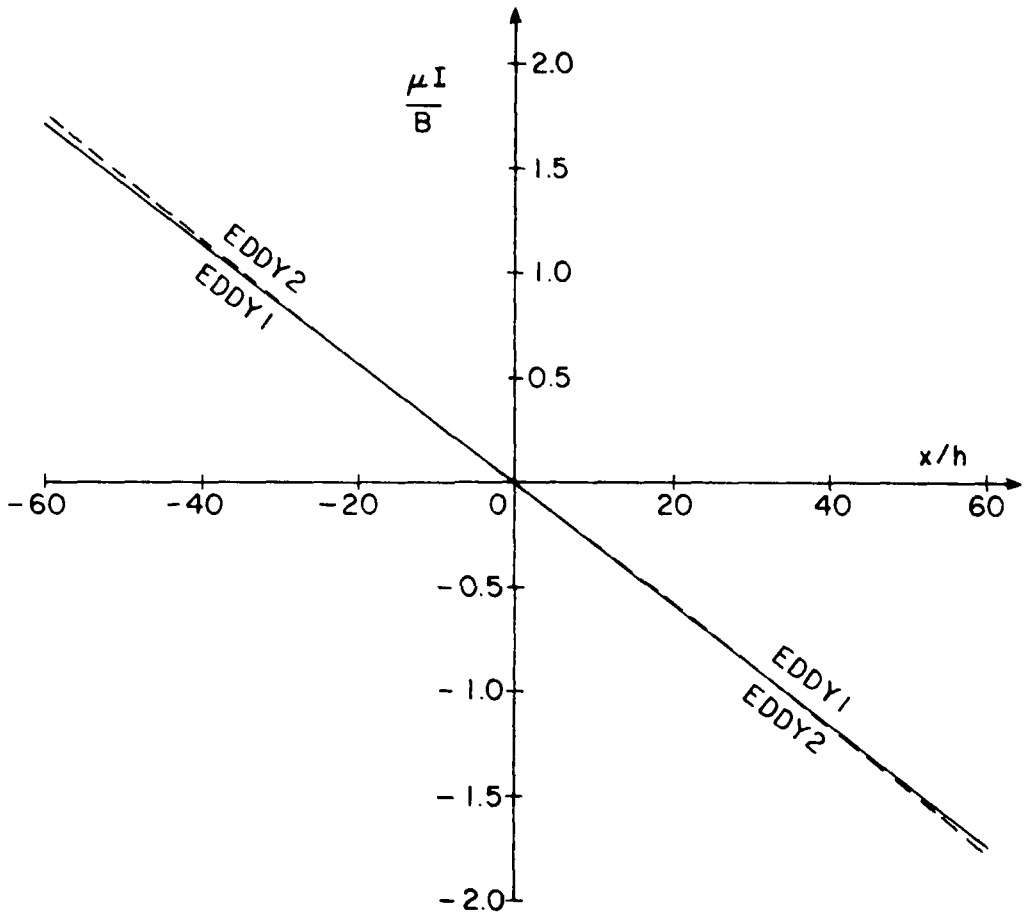

Figure 3.36 Comparison of one- and two-dimensional solutions of currents induced across the middle of a long rectangular plate by a harmonic uniform field (R = 0.03 in EDDY1).

are shown in Figure 3.37. The EDDY1 results are obtained with ten linear elements over the half-width of the plate, while the EDDY2 results are from a single quadratic element over the same distance,the agreement between the two should be therefore reasonable considering the difference in the discretization.

c) Comparison of Low Reynolds Number Results for a Square Plate with Edge Crack with the BIEM Numerical Results and Infrared Measurements. The flow of induced current around an edge crack in a square plate is calculated using the two-dimensional code in the large skin-depth limit for a few notch widths. A uniform applied magnetic field is assumed in these calculations. The stream function contours for one case are shown in Figure 3.38. These contours show the flow of current around the crack tip. Contours of constant temperature are also shown in Figure 3.39. The infrared measurements of the induced ohmic heating on the same plate but induced by a wire-source field are shown in Figure 3.40. The temperature or J^2 hot spot near the edge of the crack or slit is clearly shown. The same hot spot is predicted in the FE results, Figure 3.39, for the uniform magnetic field.

Quantitative comparison of the numerical and experimental results is difficult in this problem because of the difficulty in creating a uniform field within a sufficiently large region with the present experimental facilities. However, the FE results have been compared with the numerical results obtained from a boundary integral equation (BIE) code developed by Mukherjee (Ref. 84). This code has originally developed to solve for stresses around a crack. The comparison of the stream functions calculated is shown in Figure. 3.41. Close agreement is obtained between the two numerical results.

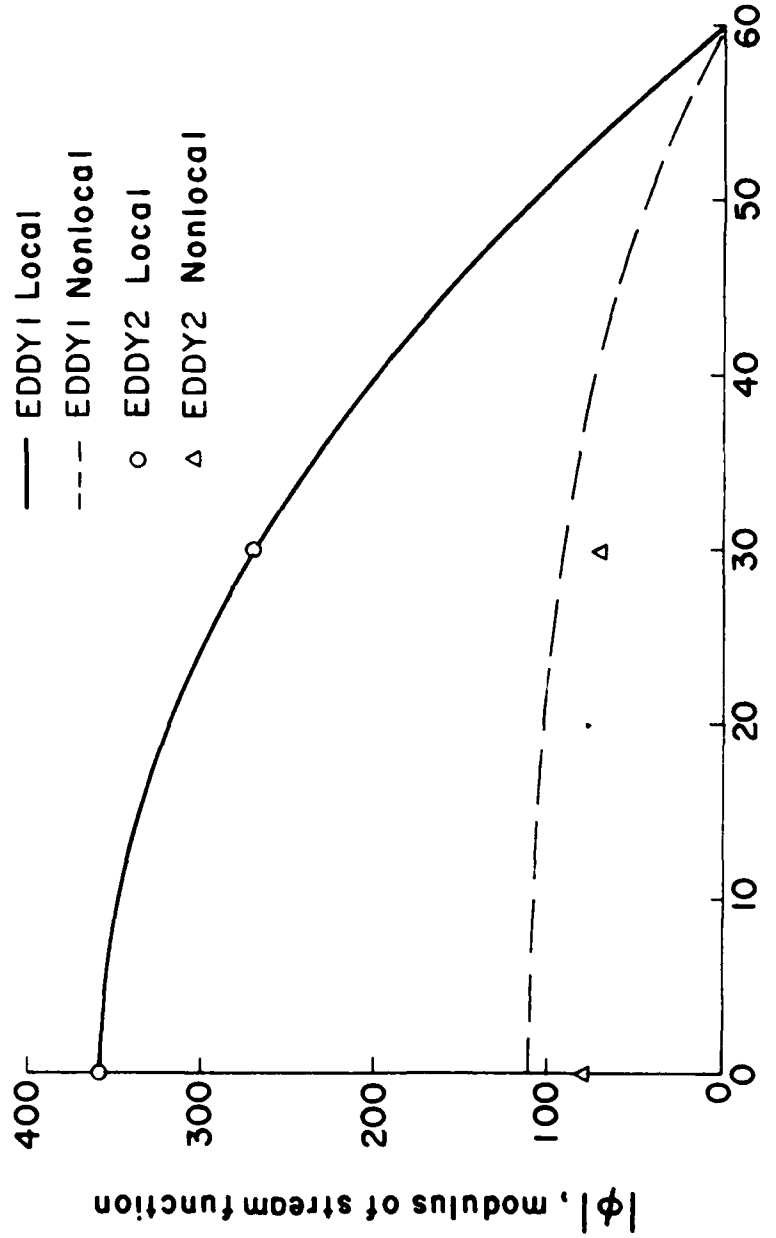

Figure 3.37 Eddy current stream function on the mid-length cross-section of a long rectangular plate (length:width = 4:1, R = 0.2).

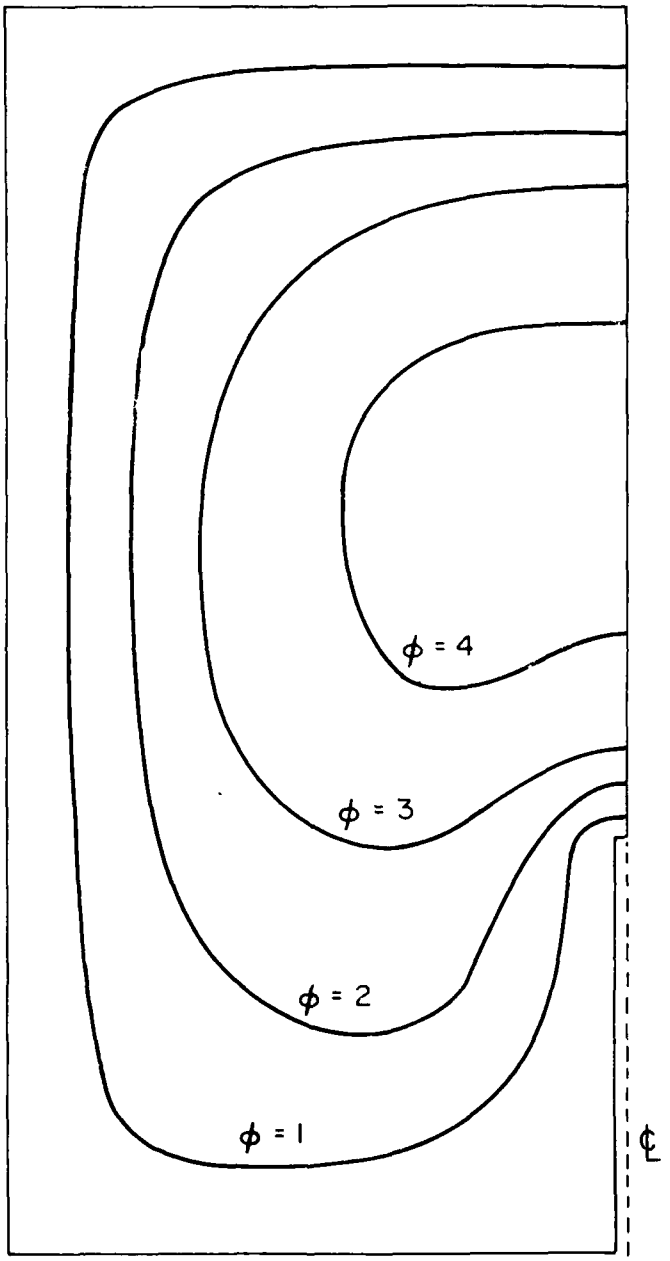

Figure 3.38 Stream function contours for a notched plate excited by a harmonic uniform field (notch-width = 2h, R = 0.001).

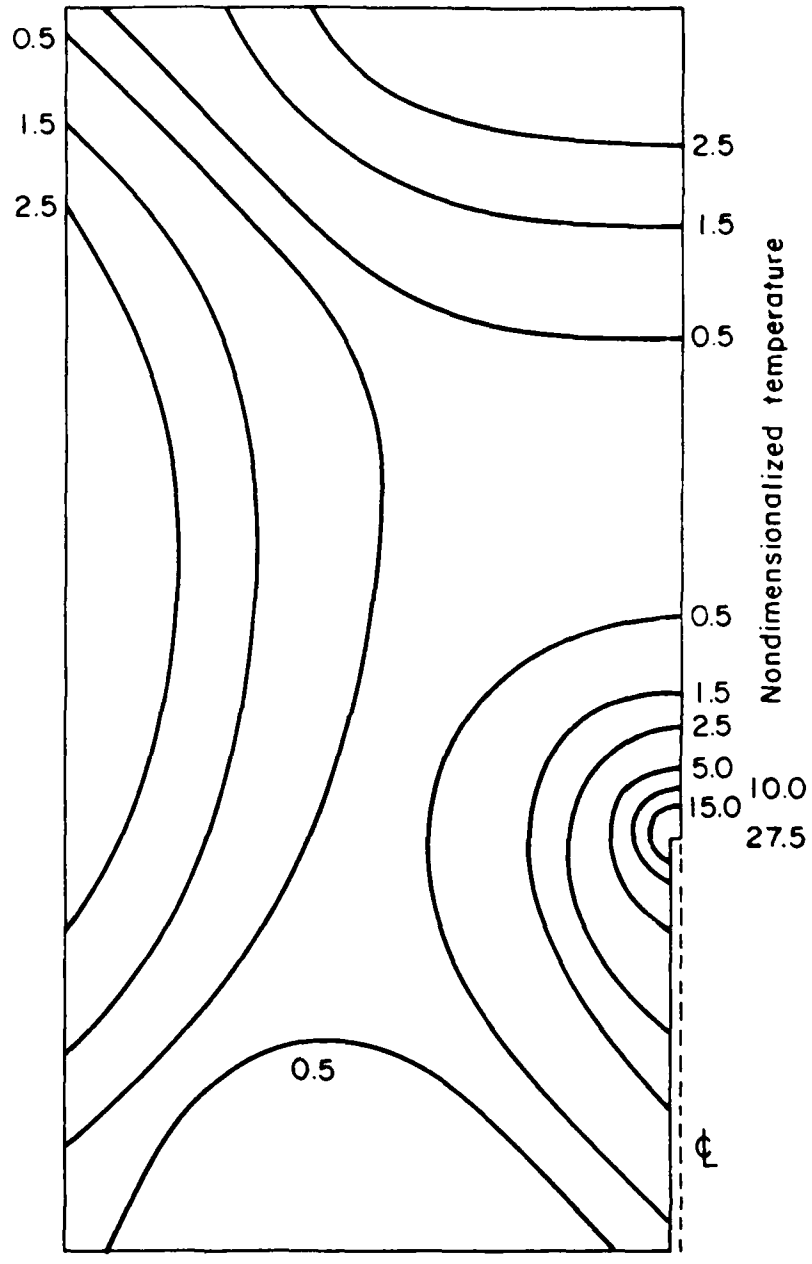

Figure 3.39 Isotherms for a notched plate excited by a harmonic uniform field (notchwidth = 2h, R = 0.001).

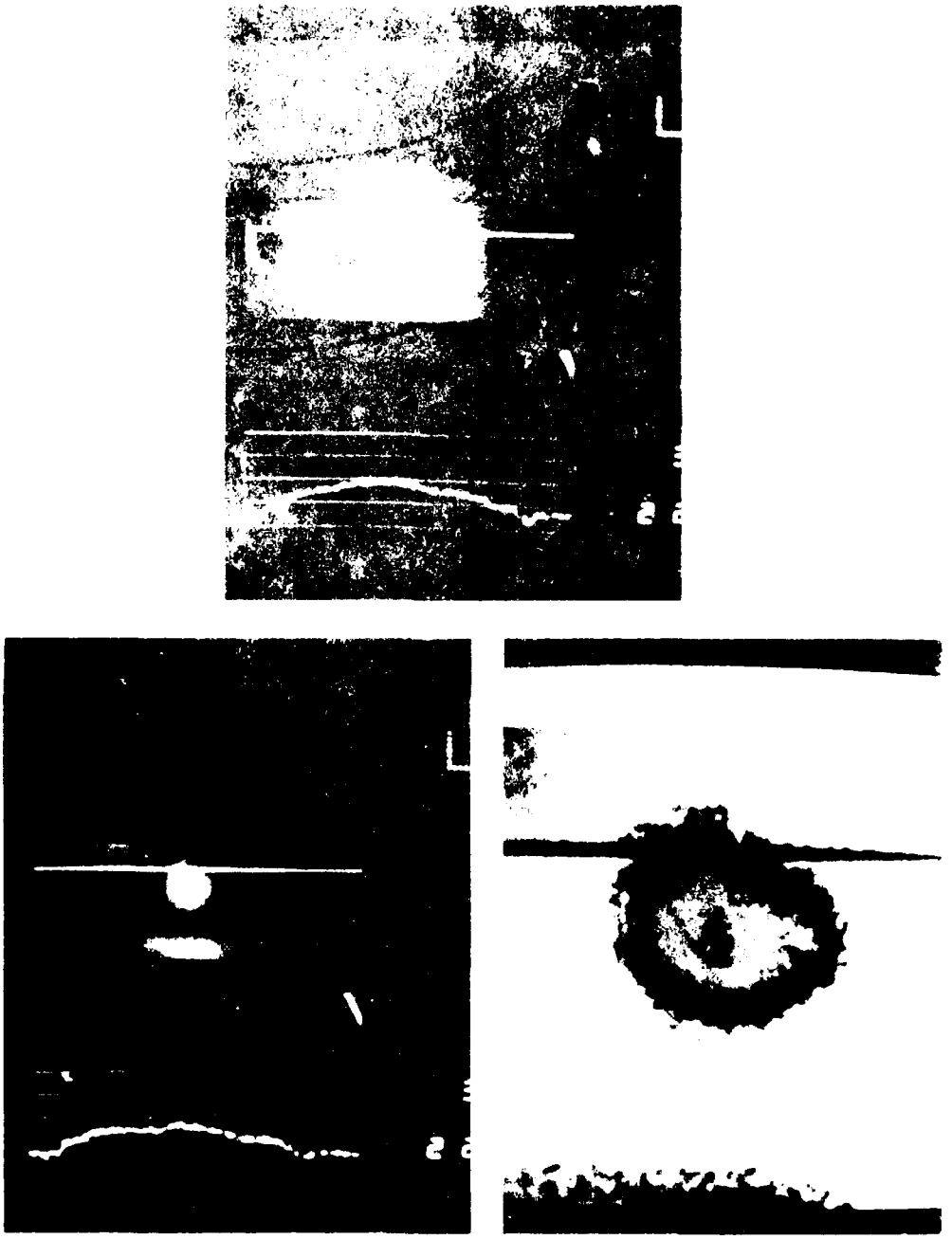

Figure 3.40 Infrared thermogram showing hot spots due to eddy current flow: (upper) plate without crack, (lower left) hot spot due to flow around a crack, (lower right) color quantized hot spot at top of crack (magnified).

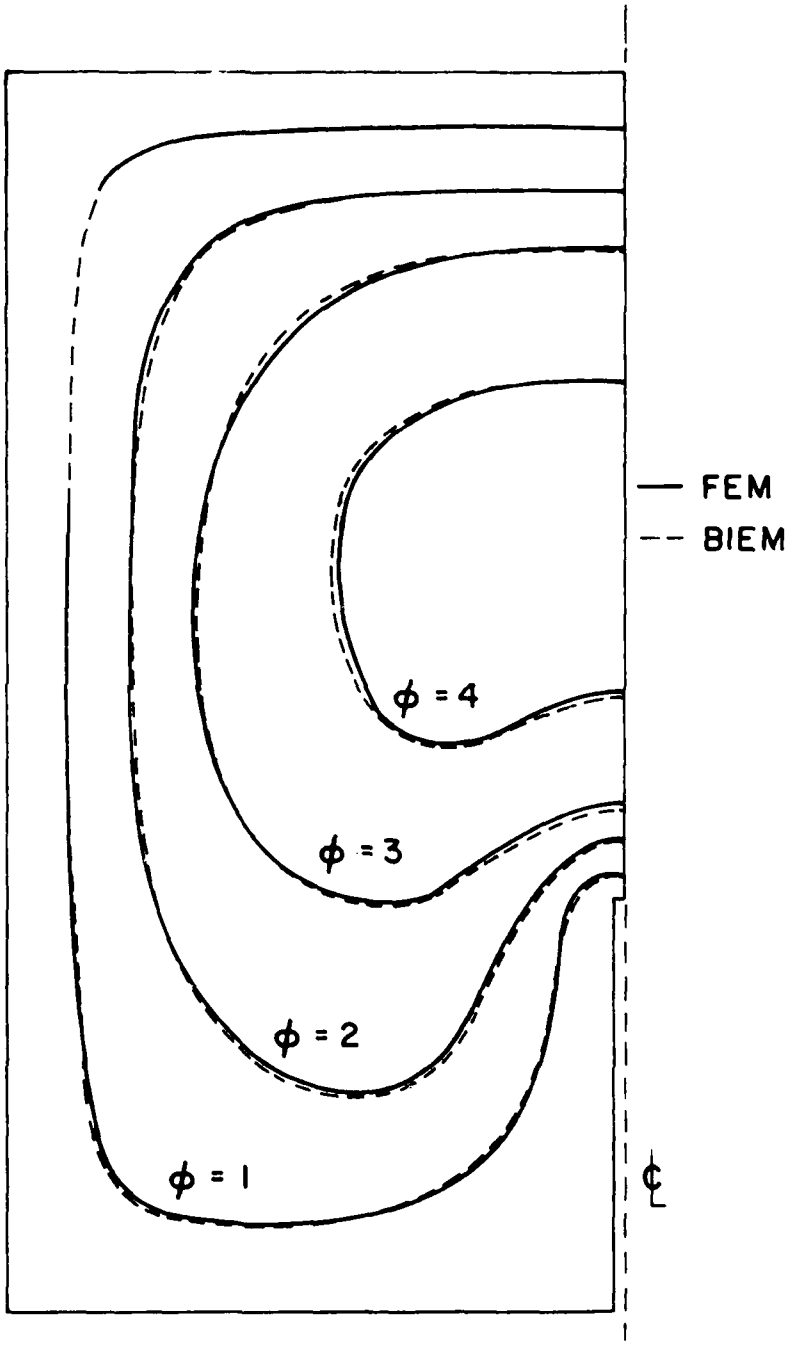

Figure 3.41 Comparison of eddy current stream lines for a notched square plate in a uniform field computed by boundary integral equation method (BIEM) and finite element method (FEM). (Notchwidth = 2h, notch length = 40h, plate length = 120h).

The BIEM code used in this problem basically solves the Poisson equation (3.56). Compared to the program EDDY2 in the low Reynolds number case, it has the advantage that only boundary elements need be used. This much reduces the number of equations to be solved. But the extension of the BIE method to include the nonlocal effect cannot be easily achieved.

d) Dimensional Analysis of the Size Effect of the Width of a Square Plate. For a square plate with different width/thickness (D/h) ratios, the program EDDY2 was run by Hara (Ref. 83). By using the original definition of the magnetic Reynolds number and the FE mesh shown in Figure 3.42, one obtains the relations between the modulus of the current at the centroidal points of the elements versus the parameter R for different D/h values. The exciting magnetic field is assumed uniform here. The moduli of the current at all centroid points of the elements therefore have the same value.

By using a different definition of the Reynolds number,

$$R^{I} = \left(\frac{D}{h}\right) R = \frac{1}{4\pi} \left(\frac{Dh}{\delta^2}\right) \tag{3.57}$$

one obtains the curves shown in Figure 3.43. At small R^{I} values these three curves correlate to each other well, but the differences begin to grow as the R^{I} values increase.

By using the same curves shown in Figure 3.42, but another definition of the magnetic Reynolds number R^{II},

$$R^{II} = \left(\frac{D}{h}\right)^2 R = \frac{1}{4\pi} \left(\frac{D}{\delta}\right)^2 \tag{3.58}$$

one obtains the curves shown in Figure 3.43, which show a much better correlation for the high R^{II} values. However, the agreement is still not as close as that obtained for the one-dimensional plate, Figure 3.20.

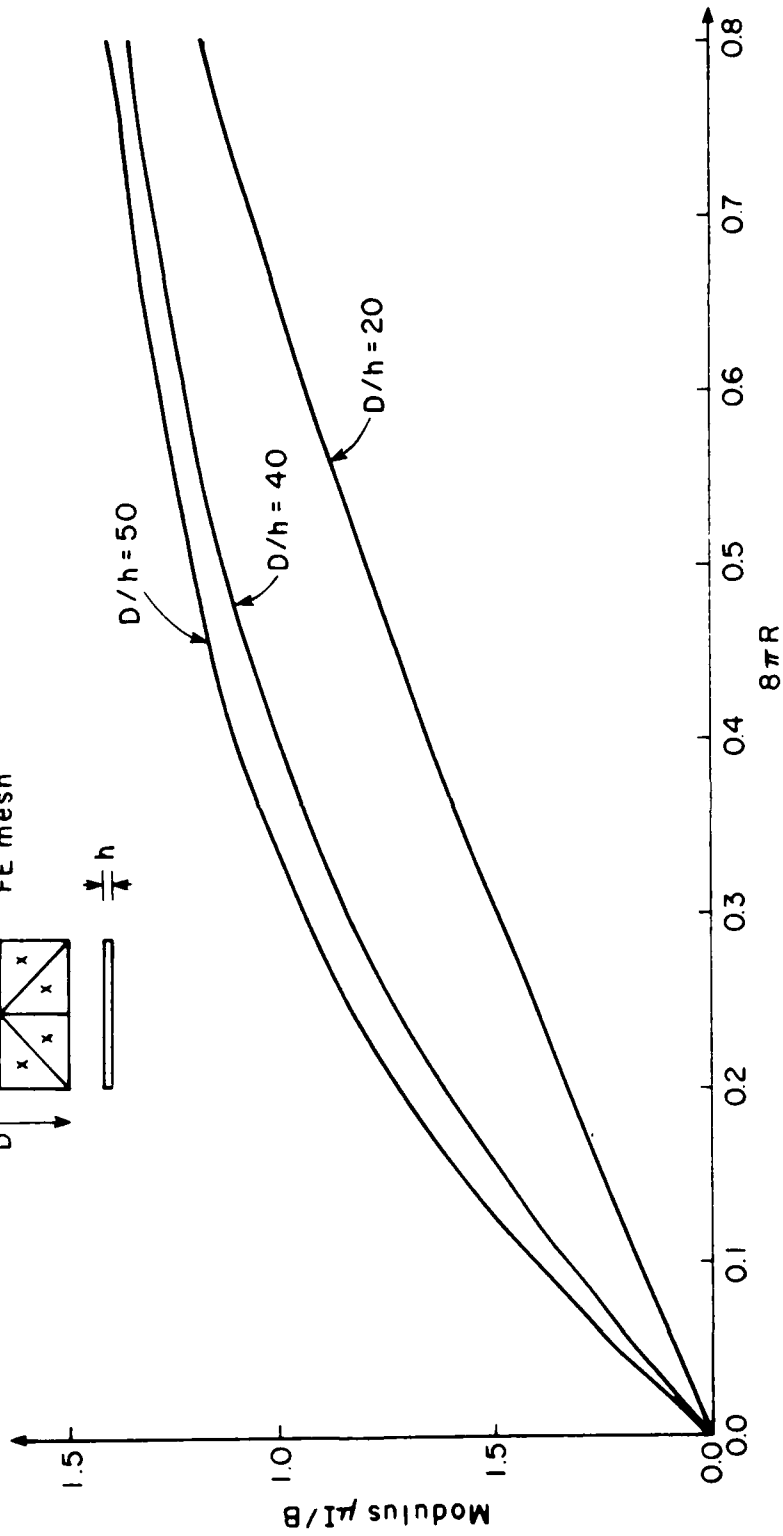

Figure 3.42 Modulus of the induced current density at the element centroids vs. the magnetic Reynolds number $R = (h/\delta)^2/4\pi$ for a square plate subject to a uniform transverse field.

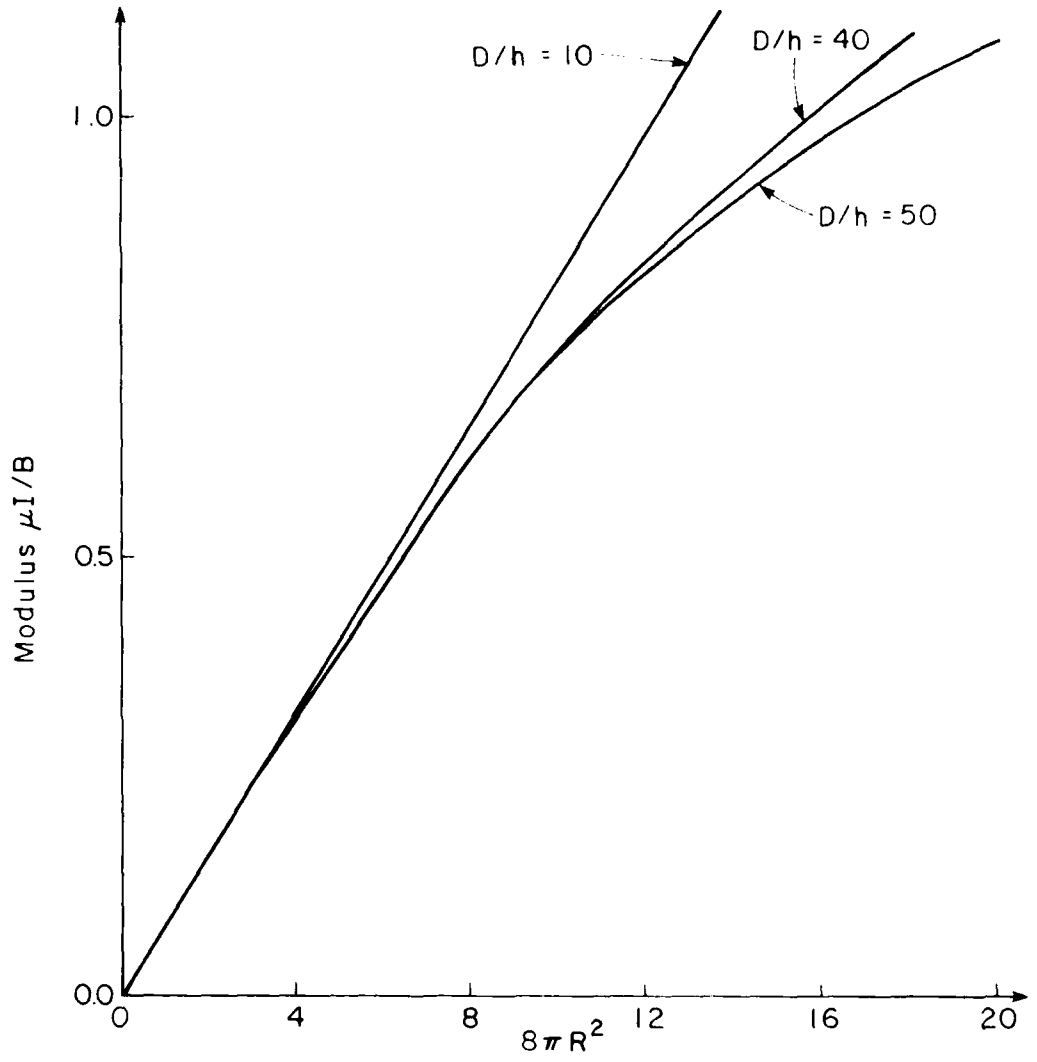

Figure 3.43 Modulus of the induced current density at the element centroids vs. the modified magnetic Reynolds number $R^I = (D/h)R = Dh/(4\pi\delta^2)$ for a square plate subject to a uniform transverse field.

This rough parameter study shows that the number of nondimensional parameters for the finite plate is more than one, and that they are probably related to each other in some fashion that cannot be revealed by the simple changes of parameter, Eq. (3.57) and (3.58). More detailed dimensional analysis is suggested to study the size effect of a two-dimensional plate.

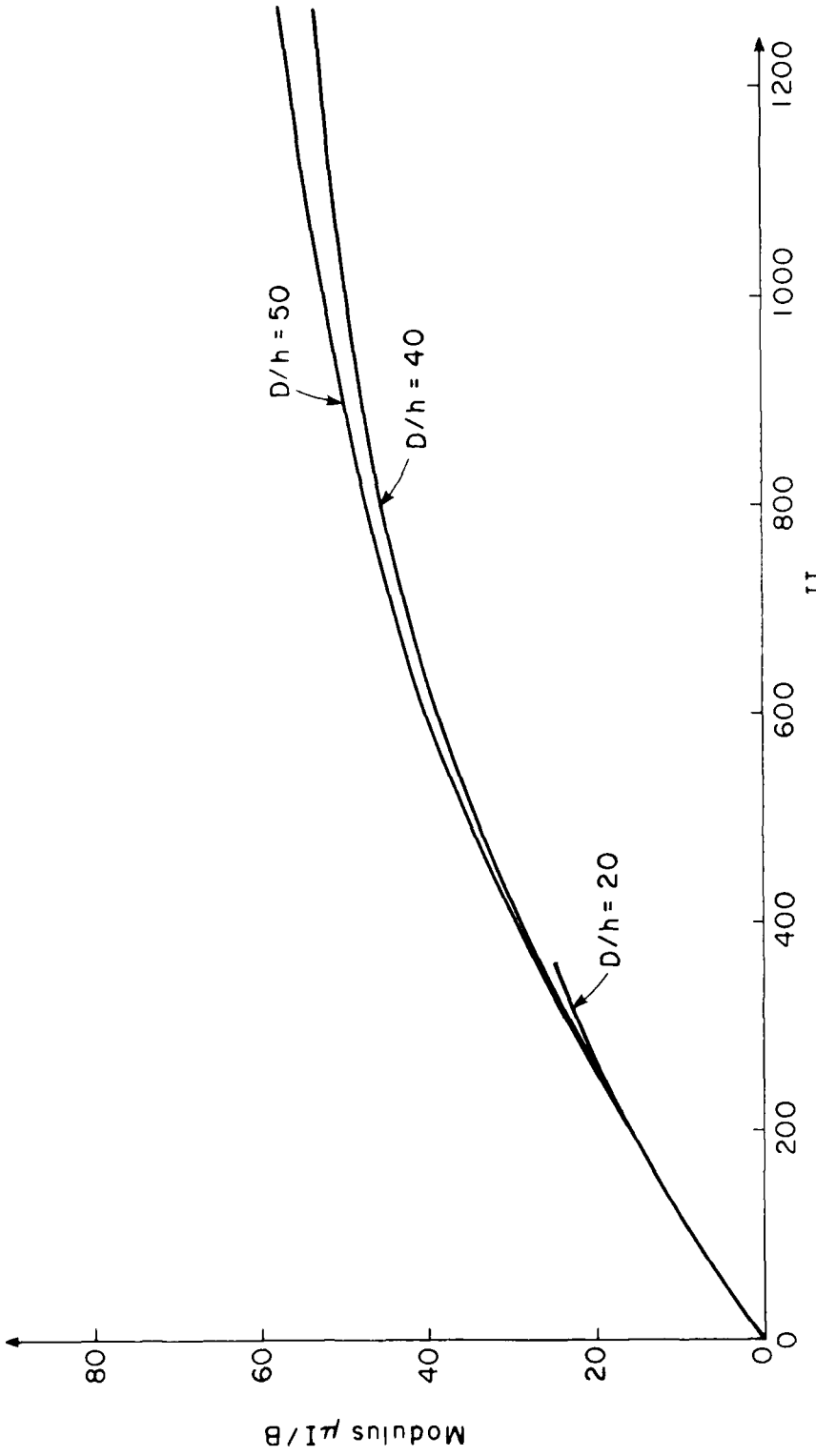

Figure 3.44 Modulus of the induced current density at the element centroids vs. the modified magnetic Reynolds number $RII = R(D/h)^2 = (D/\delta)^2/4\pi$ for a square plate subject to a uniform transverse field.

Chapter 4

LINEAR VIBRATION OF INFINITELY LONG MAGNETOELASTIC PLATES

The magnetically induced vibrations of infinitely long conducting plates are considered in this chapter. The plates have constant span ℓ along their infinite length. The exciting magnetic fields considered are invariant in space in the length direction. The equations governing the coupled system in this case are Equations (2.104) and (2.106). The finite element formulation used for analysis is presented in Section 4.1. The staggered transient analysis is applied to the two coupled equations. The computational procedure is described in Section 4.2. Numerical results and experimental verifications are presented in Section 4.3. The various coupling effects are discussed in Section 4.4.

The study described in this chapter has been limited so far to small transverse flexural motion of plates subjected to pulsed magnetic fields. The in-plane force effects are not included. The total coupling effects and the influence of static, uniform magnetic fields on the free vibrations of the plate are left for future investigations. The coupling effect through rotational motion is also left for further studies.

4.1 Basic Equations and Finite Element Formulation

The governing equations for infinitely long conducting plates subjected to exciting magnetic fields invariant in space in the length direction are derived in Chapter Two and are Eqs. (2.104) and (2.106). In this chapter the coupling effects in the induced vibrations are limited to the

transverse motion of the plate. The governing equations for this case are the following specialized versions of Eq. (2.104) and (2.106b):

$$\frac{\partial^2 \psi}{\partial x^2} - \sigma\mu_o \frac{\partial \psi}{\partial t} + \frac{\sigma\mu_o h}{2\pi} \int_0^{\ell} \frac{\frac{\partial}{\partial t} \psi\,(x')}{(x-x')^2 + \frac{h^2}{4}}\, dx'$$

$$= \sigma h \left[\frac{\partial B_z^o}{\partial t} - \frac{\partial}{\partial x} \left(\frac{\partial w}{\partial t} B_x^o\right)\right] \tag{4.1}$$

and

$$D \frac{\partial^4 w}{\partial x^4} + \rho h \frac{\partial^2 w}{\partial t^2} = \frac{\partial \psi}{\partial x} B_x^o \tag{4.2}$$

In both equations the coupling effects appear on the right-hand side only.

The same finite element formulation procedure as described in Chapter Three is applied to Eq. (4.1) and results in

$$\left\{ \frac{1}{\Delta t} [A] - (1-\theta)\,[s] \right\} \{\psi\}_{t+\Delta t}$$

$$= \left\{ \frac{1}{\Delta t} [A] + \theta\,[s] \right\} \{\psi\}_t + \theta\,\{R\}_t + (1-\theta)\,\{R\}_{t+\Delta t} \tag{4.3}$$

where $\{R\}$ is given by

$$R_j = \sigma h \int_E N_j^E \left[\frac{\partial B_z^o}{\partial t} - \frac{\partial}{\partial x} \left(\frac{\partial w}{\partial t} B_x^o\right)\right] dx \tag{4.4}$$

All the other finite element matrix and vectors are the same as defined in Section 3.3.

The transverse deflection w in Eq. (4.2) is approximated by the usual cubic model

$$w = \sum_{k=1}^{4} C_k^E w_k = \lfloor C^E \rfloor \{w\} \tag{4.5}$$

where

$$\{w\}^T = \lfloor w_1 \ \theta_1 \ w_2 \ \theta_2 \rfloor \tag{4.6}$$

and

$$C_1^E = 1 + 2\xi^3 - 3\xi^2 \qquad C_2^E = -x\,(\xi - 1)^2$$

$$C_3^E = 3\xi^2 - 2\xi^3 \qquad C_4^E = -x\,(\xi^2 - \xi) \tag{4.7}$$

with

$$\xi = x/L^E$$

The following matrix equation of motion is then obtained

$$[M]\,\{\ddot{w}\} + [K]\,\{w\} = \{F\} \tag{4.8}$$

in which

$$\{F\} = \int_E \{C\}\,\frac{\partial \psi}{\partial x}\,B_x^o\,dx \tag{4.9}$$

Using the Newmark integration scheme (Ref. 100), one has

$$[\hat{K}]\,\{w\}_{t+\Delta t} = \{\hat{F}\}_{t+\Delta t} \tag{4.10}$$

where

$$[\hat{K}] = a_o\,[M] + [K] \tag{4.11a}$$

$$\{\hat{F}\}_{t+\Delta t} = \{F\}_{t+\Delta t} + [M]\,(a_o\,\{w\}_t + a_2\,\{\dot{w}\}_t + a_3\,\{\ddot{w}\}_t) \tag{4.11b}$$

with

$$a_o = \frac{1}{\alpha \Delta t^2} \qquad a_1 = \frac{\delta}{\alpha \Delta t} \qquad a_2 = \frac{1}{\alpha \Delta t}$$

$$a_3 = \frac{1}{2\alpha} - 1,$$

$$\delta \geq 0.50 \qquad \alpha \geq 0.25\ (0.5 + \delta)^2$$

The trapezoidal rule is used for all the studies with $\alpha = \frac{1}{4}$ and $\delta = \frac{1}{2}$.

4.2 Staggered Transient Analysis and Computational Procedure

The equations (4.1) and (4.2) may be solved simultaneously in principle. In that case, the discretized equations will have the following form

$$[A]\ \{\dot{\psi}\} - [s]\ \{\psi\} = \{R\} - [D]\ \{\dot{w}\} \tag{4.12a}$$

$$[M]\ \{\ddot{w}\} + [K]\ \{w\} = [P]\ \{\psi\} \tag{4.12b}$$

where

$$\{R\} = \sigma h \int_E \{N^E\}\ \frac{\partial B_z^o}{\partial t}\ dx \tag{4.13a}$$

$$[D] = \sigma h \int_E \{N^E\}\ \left[\frac{\partial C^E}{\partial x}\right] B_x^o\ dx + \sigma h \int_E \{N^E\}\ [C^E]\ \frac{\partial B_x^o}{\partial x}\ dx \tag{4.13b}$$

$$[P] = \int_E \{C^E\}\ \left[\frac{\partial N^E}{\partial x}\right] B_x^o\ dx \tag{4.13c}$$

Define a state vector $\{\Delta\}$ with

$$\{\Delta\}^T = [\psi\ w] \tag{4.14}$$

Eq. (4.12) may then be put into the following form

$$[\bar{M}]\ \{\ddot{\Delta}\} + [\bar{D}]\ \{\dot{\Delta}\} + [\bar{K}]\ \{\Delta\} = \{\bar{R}\} \tag{4.15}$$

where

$$[\bar{M}] = \begin{bmatrix} 0 & 0 \\ 0 & M \end{bmatrix}, \quad [D] = \begin{bmatrix} A & D \\ 0 & 0 \end{bmatrix}, \quad [\bar{K}] = \begin{bmatrix} -s & 0 \\ -P & K \end{bmatrix}$$

$\{\bar{R}\}^T = [R\ 0]$

Eq. (4.15) may be integrated directly to give the solution simultaneously.

There are several disadvantages of the simultaneous solution scheme however. Besides the inefficiency of the solution of a larger, unsymmetric matrix equation, the same finite element mesh must be used for both subsystems for the treatment of the coupling terms. Since a finer mesh usually has to be used for the magnetic subsystem, this will result in an excessive number of structural elements for the coupled problems. The other consideration is the different time characteristics of the magnetic and mechanical subsystems. Since it is the structural response rather than the stress wave motion in the structure that is of interest in this study, one would like to know the range of the frequency of the field within which the mutual interactions are important. At higher frequency of the driving field, one may prefer different time steps for the two subsystems because the magnetic force will be more like an impulse to the structure. For these reasons a staggered solution scheme is attractive. Since the two governing equations are only weakly coupled, this approach is feasible and is adapted in this work. Different but conformable meshes are used for the two subsystems. The solution state of the coupled problem is advanced by sequentially executing Equations (4.3) and (4.10). The interaction terms appear in each as an external force effect. Temporal predictors may be used to calculate these force terms more accurately (Ref. 85). In the present study, no predictor is used. The accuracy is improved by using a smaller time step.

A Fortran program EDDYBEAM has been developed for the linear vibration of infinitely long plates. The computational scheme employed is basically a combination of the transient eddy current program EDDY1T and the struc-

tural analysis program BEAM. Different levels of coupling of these two programs may be specified in the input. The functions of these programs, which use different but conformable finite element meshes, is shown in Figure 4.1.

The first phase of the program is the initiation of the two subprograms EDDY1T and BEAM and the specification of the type of coupling. If the parameter LINK=0, the program provides the transient eddy current calculation only. If LINK=1, the magnetic force calculated on the rigid plate is used in the structural analysis program. The $\underset{\sim}{V}x\underset{\sim}{B}$ effect on the eddy current will not be considered. If LINK=2, two-way interactions are included and the solution corresponds to the coupled problem referred to the initial undeformed position of the plate. For LINK=3, the vector {R} in Eq. (4.4) is calculated on the deformed position of the plate at the previous time step using the unit normal vector of the undeformed plate. The magnetic force calculated is still applied to the original position of the plate for the analysis of the structural response. A limited follower force nature of the magnetic force is then obtained in the analysis. The results obtained from the different levels of coupling between the two subsystems serve to indicate the relative importance of the various interaction effects.

The major computational task is performed by the program EDDY1T. As shown in Figure 4.1, this computation consists of the time integration of the eddy current diffusion equation. At each time step, the induced current I_y and magnetic force F_z are calculated at each integration point. The magnetic forces are then transferred to the structural analysis program BEAM. The magnetic forces are integrated numerically and the effective consistent nodal force vector calculated to give the displacement at the

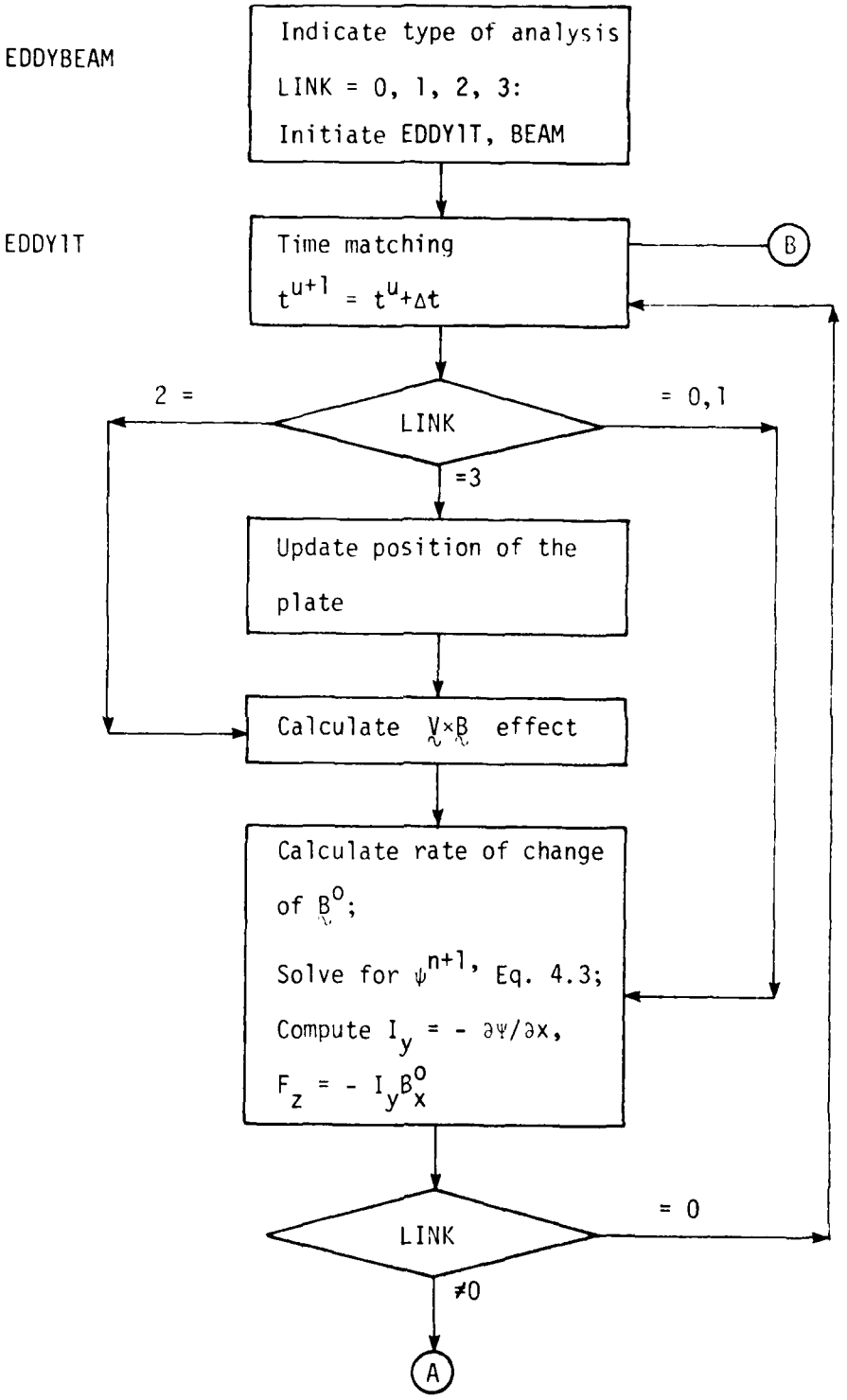

Figure 4.1 Computational Scheme of EDDYBEAM

BEAM

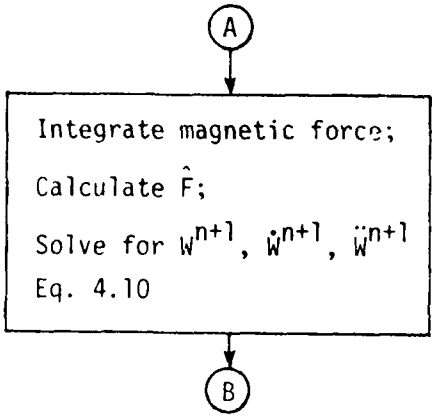

Figure 4.1 (Continued)

new time step. The $\nabla \times \underset{\sim}{B}$ values are then evaluated at the integration points by interpolation. If the change of distance between the plate and coil is considered (LINK=3), the calculation of $\nabla \times \underset{\sim}{B}$ is performed at the new position of the plate. The same alternative is applied to the calculation of the rate of change of the external magnetic field $\frac{\partial}{\partial t} \underset{\sim}{B}^{o}$. These calculated values are then used to begin the next time step.

In addition to the input information described in sub-subsection 3.3.1.b necessary for the transient eddy current calculation, geometric and material attributes for the structural problem must be input if LINK is not zero. Since a finer mesh usually is needed for an accurate calculation of the induced current and force, different but conformable meshes may be used for the magnetic and mechanical subsystems. The conformability of the two different finite element meshes is achieved by dividing each structural element into several equal-length field elements. The number of divisions may be different for each structural element and must be input as part of the mesh information.

The same size of time step is used for the calculation of both the magnetic and mechanical subsystems. A lumped mass matrix is used for the mechanical problem. Initial conditions and mechanical loads may be input to the program. Mesh generation and plotting capabilities for the time history and spatial variation of displacement and bending moment are provided as options.

The output from the EDDYIT portion of the program is described in Chapter Three. In addition, displacement velocity, and acceleration at each structural node together with the bending moment at specified points are produced as output of the subprogram BEAM. These are printed out after the output of the subprogram EDDYIT for each time step. Displacements and

bending moments may be plotted using a library subroutine if the plotting option is chosen.

4.3 Numerical Results and Experimental Verifications

The program EDDYBEAM has been applied to the magnetically induced vibrations of aluminum and stainless steel (SS 304) plates. The properties of these two materials are listed below.

Material	σ (Amp/Volt.m)	μ (N/Amp^2)	ρ (N·Sec^2/m^4)	E (N/m^2)	ν
aluminum	3.80×10^7	$4\pi \times 10^{-7}$	2.7×10^3	7.0×10^{10}	0.34
SS 304	1.39×10^6	$4\pi \times 10^{-7}$	8.0×10^3	2.0×10^{11}	0.30

The study so far has been limited to single pulsed currents. To have sufficient interaction time, the time characteristics of the electromagnetic and mechanical subsystems are compared below for cantilever plates. The information is used to design meaningful numerical and experimental tests.

Let f_n = frequency of vibration of the nth mode of the plate, and f^E = frequency of the driving current in the coil.

Then

$$f_n = \frac{1}{2\pi} K_n^2 \sqrt{\frac{EI}{m\ell^4}} = \frac{K_n^2}{2\pi} \sqrt{\frac{Eh^3}{\rho h \cdot 12\ell^4}}$$

$$= \frac{K_n^2}{2\pi\sqrt{12}} \sqrt{\frac{E}{\rho}} \left(\frac{h}{\ell^2}\right) \qquad (4.16)$$

in which E is the effective Young's modulus for long plates. Let the skin depth δ be N times the thickness of the plate h,

$$\delta^2 = N^2 h^2 = \frac{1}{\pi f^E \mu\sigma}$$

$$f^E = \frac{1}{\pi \mu\sigma N^2 h^2} \tag{4.17}$$

Matching the two frequencies, $f_n = f^E$, one obtains

$$\ell^2 = \frac{1}{2\sqrt{12}} N^2 K_n^2 \mu\sigma \sqrt{\frac{E}{\rho}} h^3 \tag{4.18}$$

The length and thickness of the plate for different combinations of mode and skin depth/thickness ratios are shown in Table 4.1. The following K_n values are used in the calculation of the tabled values (Ref. 86).

n	1	2	3	4	5	6	7	8
K_n	1.875	4.694	7.855	10.996	14.137	17.279	20.420	23.562

The frequencies and half-periods of the oscillations for both the magnetic field and the structure corresponding to the values in Table 4.1 are calculated in Table 4.2. The problem tested is determined by choosing suitable length and thickness so that the frequency of the driving current matches that of the vibrating beam for a selected mode.

The transient eddy current program EDDY1T has been verified in Chapter Three. The structural analysis program BEAM has also been tested for several dynamic problems. One problem tested is the free vibration of a simply supported beam subjected to a sinusoidal initial velocity shown in Figure 4.2. With four beam elements for half of the beam and integration by the trapezoidal rule version of the Newmark method, the results show good agreement with the theoretical solution for both choices of time step, although for $\Delta t = T/20$ some period elongation ($\tilde{\sim} 1\%$) is apparent.

The coupled problems studied have the general arrangement shown in Figure 4.3 with one exciting wire. One problem analyzed is for an aluminum

Table 4.1 Length and Thickness for Different Combinations of Mode Shape (n) and Skin Depth (N = δ/h)

Aluminum (Aℓ) : $\mu\sigma = 47.78$ Sec/m^2, $\sqrt{E/\rho} = 5090$ m/Sec

h (mm.)	N / n	ℓ (mm.)				
		1	2	3	4	5
1.0	1	11.11	22.22	33.33	44.44	55.55
	2	27.81	55.62	83.43	111.24	139.05
	3	46.54	93.08	139.62	186.16	232.70
1.5	1	20.41	40.82	61.23	81.63	102.04
	2	51.09	102.18	153.28	204.37	255.46
	3	85.50	171.00	256.49	341.00	427.49
2.0	1	31.42	62.84	94.26	125.68	157.10
	2	78.66	157.32	235.98	314.64	393.31
	3	131.63	263.27	394.90	526.53	658.16

SS 304 : $\mu\sigma = 1.8$ Sec/m^2, $\sqrt{E/\rho} = 5000$ m/Sec

h (mm.)	N / n	ℓ (mm.)				
		1	2	3	4	5
1.5	1	3.93	7.85	11.78	15.70	[illegible].63
	2	9.83	19.66	29.49	39.[illegible]	[illegible].14
	3	16.45	32.90	49.34	65.[illegible]	82.24
2.0	1	6.04	12.09	18.13	24.18	30.22
	2	15.13	30.26	45.40	60.53	75.66
	3	25.32	50.64	76.00	101.29	126.61
2.5	1	8.45	16.90	25.34	33.79	42.24
	2	21.15	42.30	63.44	84.59	105.74
	3	35.39	70.78	106.17	141.55	176.94

Table 4.2 Frequency and Half-period of Oscillation for Different Combinations of Thickness (h) and Skin Depth (N = δ/h)

Aluminum (Aℓ) : $\mu\sigma = 47.78\ \text{Sec/m}^2$

h (mm.)	N	f^* (1/sec) / $t_d{}^+$ (msec)				
		1	2	3	4	5
1.0	f	6.66×10^3	1.67×10^3	7.40×10^2	4.16×10^2	2.66×10^2
	t_d	0.075	0.300	0.675	1.201	1.876
1.5	f	2.96×10^3	7.40×10^2	3.29×10^2	1.85×10^2	1.18×10^2
	t_d	0.169	0.675	1.52	2.702	4.22
2.0	f	1.67×10^3	4.16×10^2	1.85×10^2	1.04×10^2	6.66×10^1
	t_d	0.300	1.200	2.702	4.803	7.505

SS 304 : $\mu\sigma = 1.8\ \text{m/Sec}^2$

h (mm.)	N	f^* (1/sec) / $t_d{}^+$ (msec)				
		1	2	3	4	5
1.5	f	4.44×10^5	1.11×10^5	4.94×10^4	2.78×10^4	1.78×10^4
	t_d	0.001	0.005	0.010	0.018	0.028
2.0	f	1.11×10^5	2.78×10^4	1.23×10^4	6.94×10^3	4.44×10^3
	t_d	0.005	0.018	0.041	0.072	0.113
2.5	f	2.83×10^4	7.07×10^3	3.14×10^3	1.77×10^3	1.13×10^3
	t_d	0.018	0.071	0.159	0.283	0.442

* $f = f^E$

\+ $t_d = \frac{1}{2f^E}$ = pulse duration

Note: f_n can be made equal to f by adjusting the length ℓ.

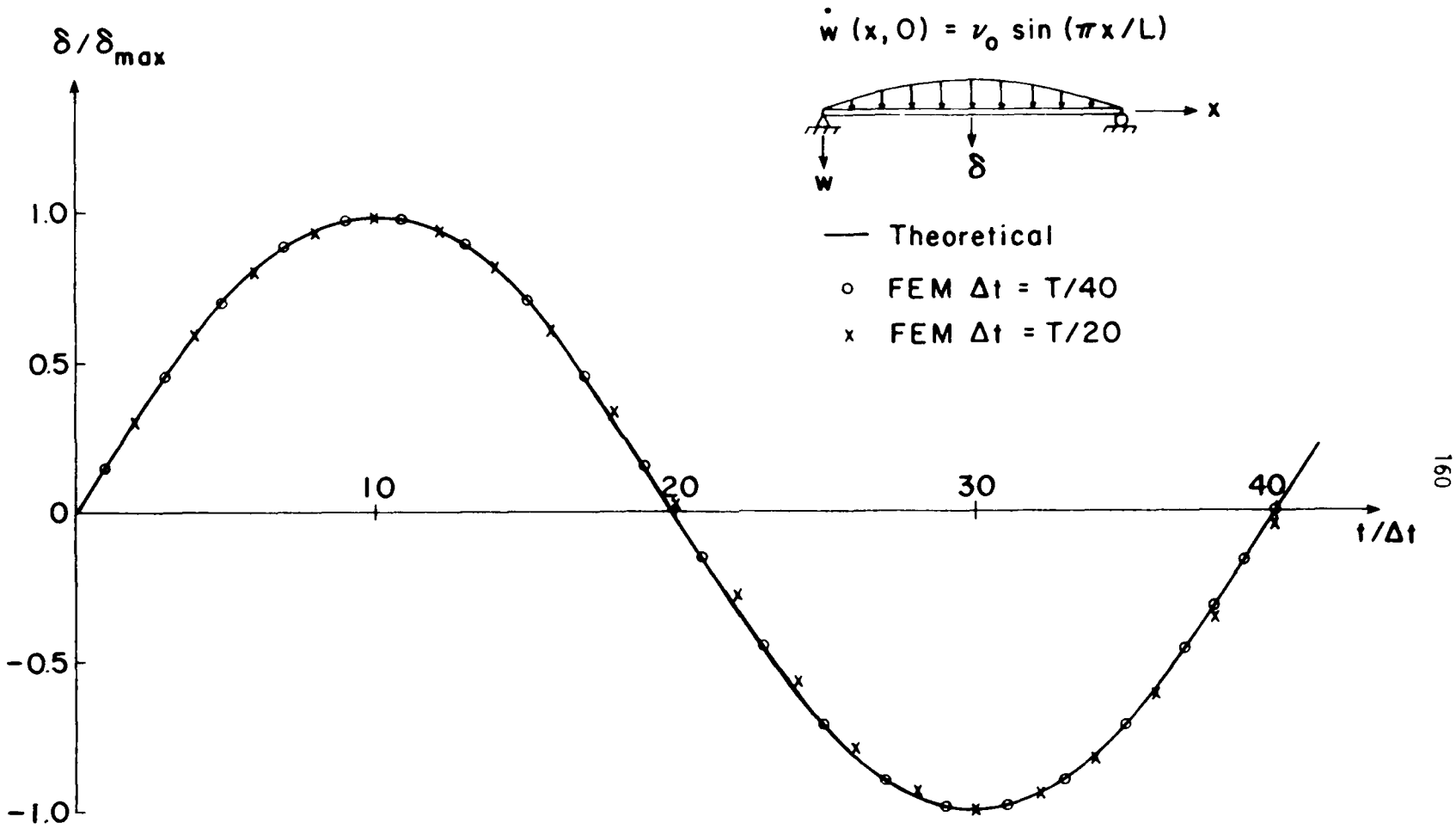

Figure 4.2 Comparison of theoretical and finite element method (FEM) results for linear transient vibration of a beam.

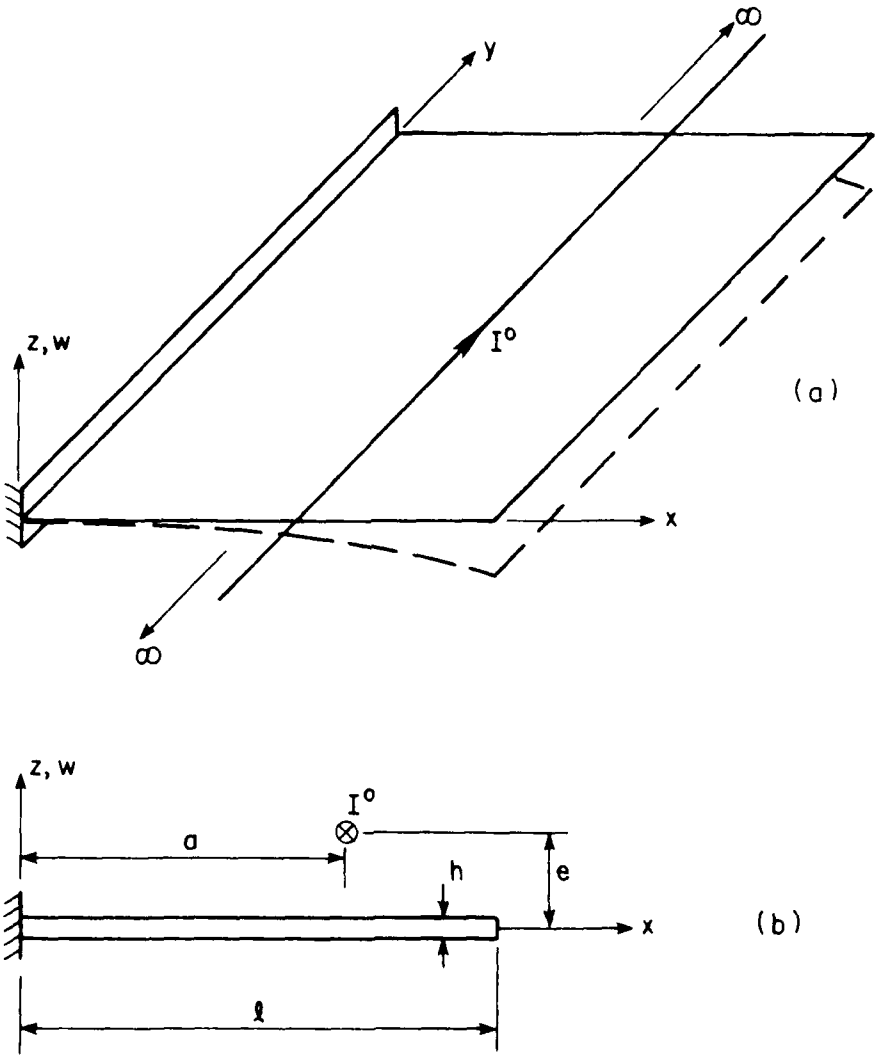

Figure 4.3 Long, cantilever conducting plate:
(a) Isometric view, single wire,
(b) Section, single-wire exciting coil.

plate with ℓ = 427 mm, a = 335 mm, h = 2.1 mm, and e = 8.1 mm. The exciting wire is purposely placed above the nodal point of the second vibration mode of the cantilever plate. Because of the much sharper variation of the electromagnetic field variables, more field elements than beam elements are used in the analysis. The meshes of the two subsystems are made conformable by dividing each beam element into several equal-length field elements as shown in Figure 4.4a. The frequencies and periods of the first three modes of the plate in this problem are:

N	1	2	3
f (1/sec)	9.51	59.60	166.87
T (sec)	0.1052	0.0168	0.0060

A half-sine pulse with 3 ms pulse duration and a 500 Amp driving current has been chosen. The pulse duration is made equal to half the period of the third mode of vibration. The results of the analysis are shown in Figures 4.5 and 4.6 and will be discussed in the next section.

Experimental verification has been attempted on a finite length beam plate with the same cross sectional properties and the arrangement of the exciting wire. This attempt failed, however, because of the small length-to-width ratio of the plate used in the experiment. The size effect on the eddy current distribution was investigated experimentally (Ref. 101). The affected distance from the ends of the plate was found to be about equal to the width of the plate. A new configuration that can be better simulated by the one-dimensional analysis was then designed. The numerical and experimental results for this second configuration are described below.

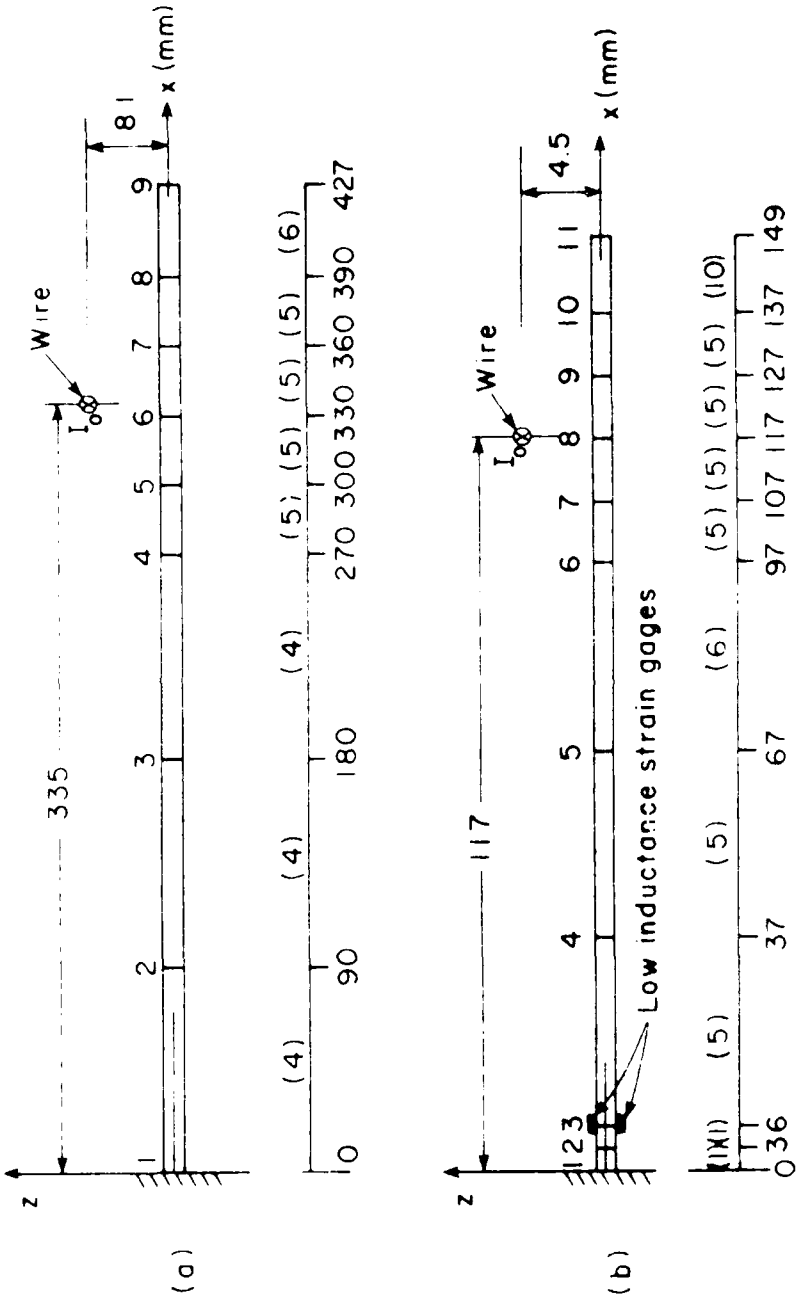

Figure 4.4 Arrangement and finite element meshes for the coupled problems. Numbers in parentheses indicate the number of field elements within each structural element.

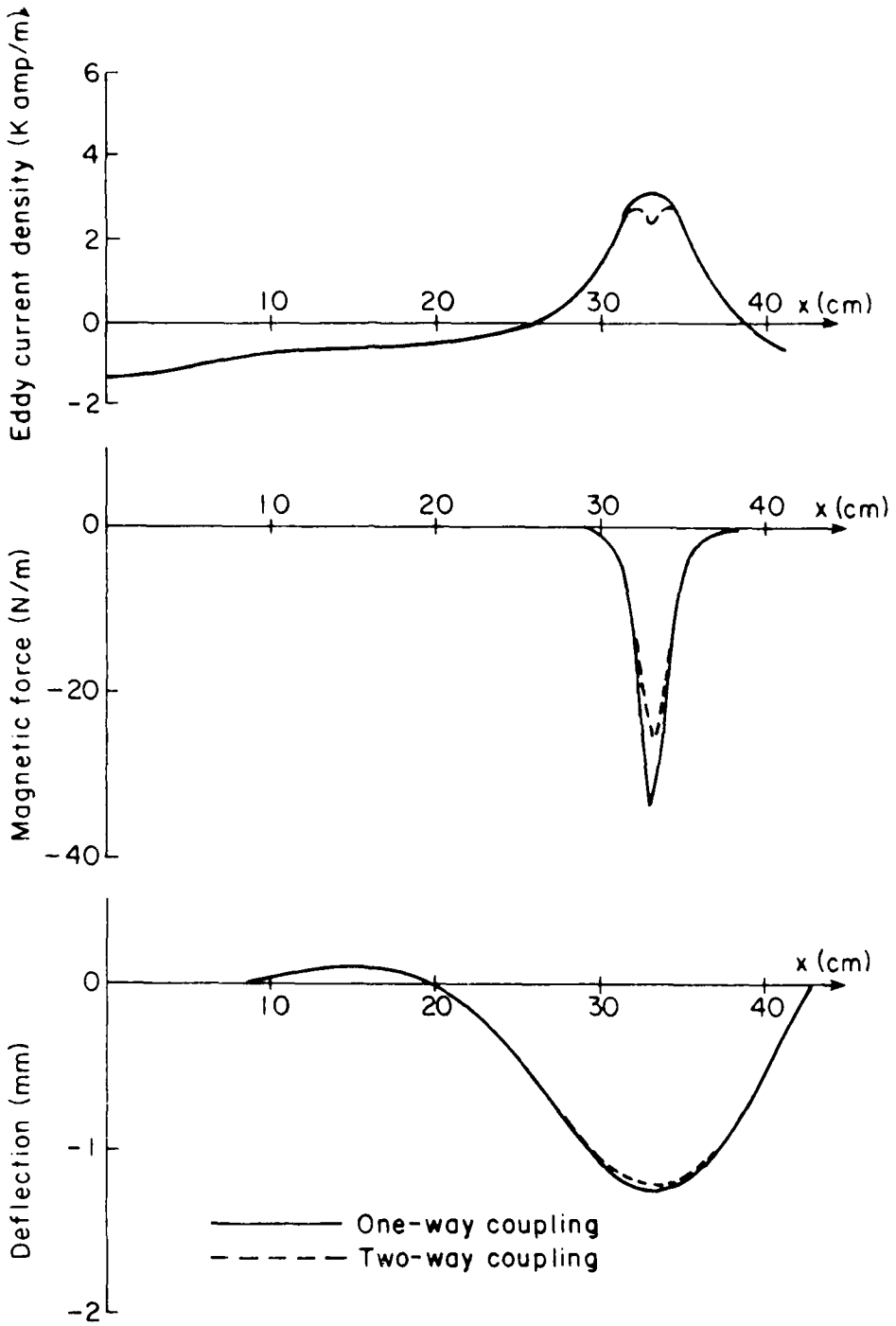

Figure 4.5 Nonlocal predictions of eddy current density, magnetic force, and transverse displacement at t = 0.9 ms for cantilever plate with single-wire exciting coil, Figure 4.4(a).

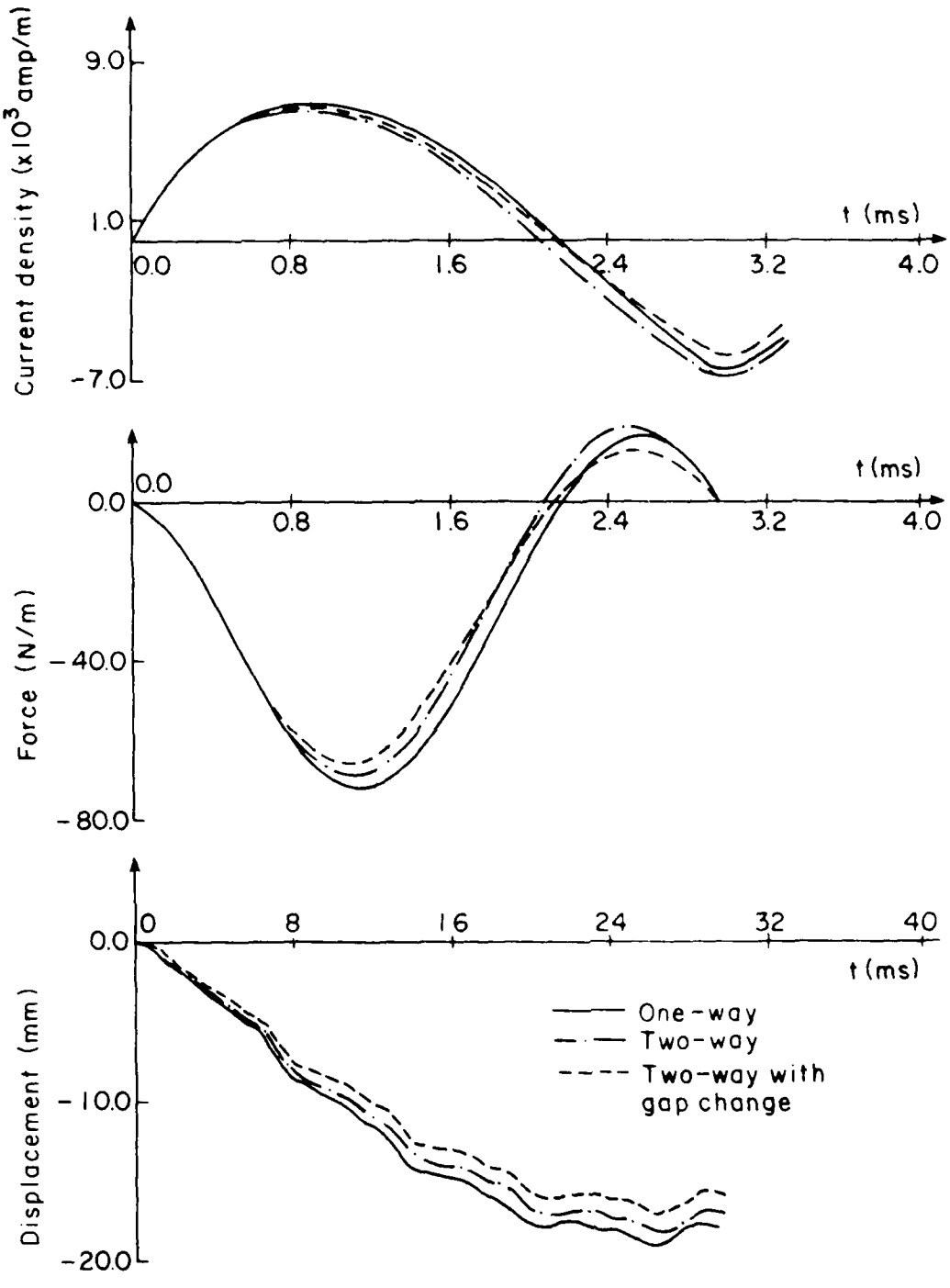

Figure 4.6 (a), (b) Induced current and force under the wire during the pulse duration, (c) vertical displacement at node 6 in Figure 4.4(a) during 1/4 the period of the first mode.

The new plate has a length/width ratio about 4.2 and is shown in Figure 3.31. The dimensions of the new configuration are ℓ = 149 mm, a = 117 mm, h = 1 mm, and e = 4.5 mm. The transient eddy current calculation is first verified for this new configuration using the search coil technique for e = 11 mm. The results have been presented in subsection 3.3.2. For the coupled problem, the finite element meshes shown in Figure 4.4b with e = 4.5 mm are used for analysis. In the experiment, two low inductance strain gages are applied at the position of node 3 in Figure 4.4b. The time history of the bending moment recorded is compared to the calculated result as an experimental verification.

The frequencies and periods of the first four modes of an infinitely long cantilever plate with this thickness are

N	1	2	3	4
f (1/sec)	37.6	236	660	1290
T (sec)	26.6×10^{-3}	4.24×10^{-3}	1.51×10^{-3}	0.77×10^{-3}

In the free vibration test of the actual finite-length plate, the same frequencies and periods have been observed.

Three different pulsed currents are used to study the induced motions of the plate. The study of pulsed problems has been motivated by potential applications in magnetic forming, pulsed electric magnets, and structural problems in high energy devices. The durations and currents of the driving pulses are

Pulse No.	1	2	3
I (Amps.)	2700	7000	8500
t_d (sec.)	5.0×10^{-3}	2.5×10^{-3}	1.2×10^{-3}

The actual pulsed currents are input numerically into the program EDDYBEAM. The calculated bending moments at the position of the strain gage are compared with the measured values for each case separately. Figures 4.7, 4.9, and 4.11 show the calculated bending moments for the first, second, and third pulse, respectively. Figures 4.8, 4.10, and 4.12 show the recorded voltage readings from the strain gages for each of the pulses used. These voltage readings have been calibrated and compared with the numerical results. The discussions of these numerical and experimental studies of the coupled problems are given in the next section.

4.4 Coupling and Nonlocal Effects

Because of the many geometric, material, and time parameters involved, the dimensional analysis of the transient coupled problem is more difficult than that of the steady-state problem and has not been attempted yet. However, from the limited number of problems studied in the last section, some conclusions about the various coupling and nonlocal effects may be drawn.

The results shown in Figure 4.6 for the first problem indicate that the velocity and displacement of the conducting plate both have a damping effect on the magnetic and mechanical subsystems. The magnitudes of the current, force, and displacement have been reduced and their phases changed, as can be seen in Figures 4.5 and 4.6. The damping also reduces the energy transfer from the magnetic subsystem to the mechanical subsystem. The efficiency of the energy transfer may be obtained by calculating the power supplied by the current source and the total kinetic and strain energies of the plate. An indication of the influences of various coupling effects on the energy transfer may be seen from Figure 4.6c which shows the long-

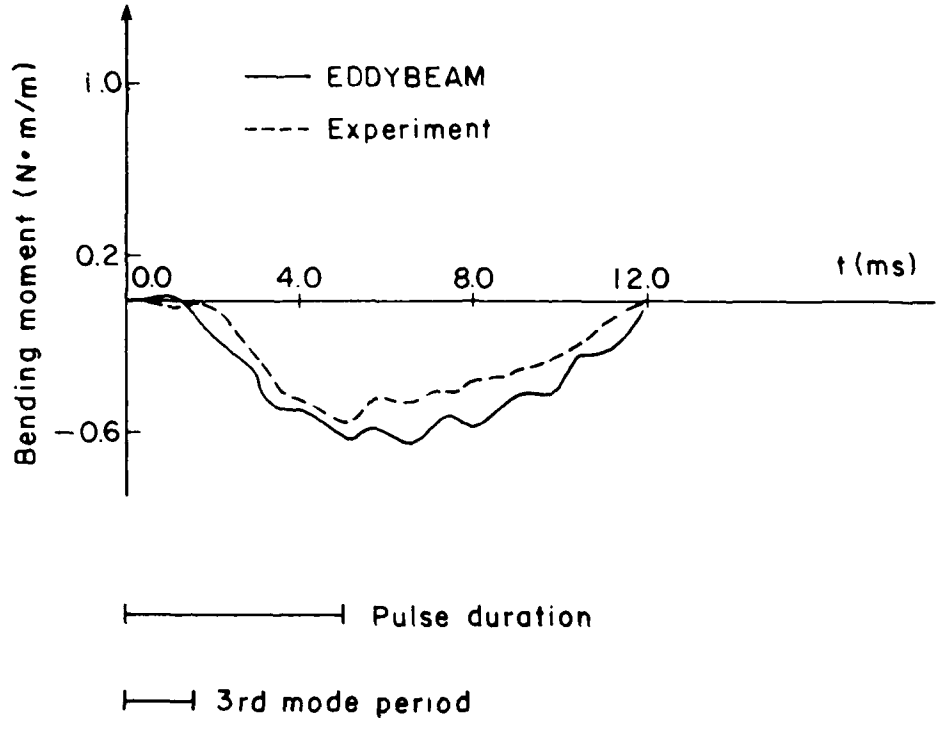

Figure 4.7 Comparison of the numerical and experimental results of the bending moment at node 3, Figure 4.4(b), for the 5 ms pulse.

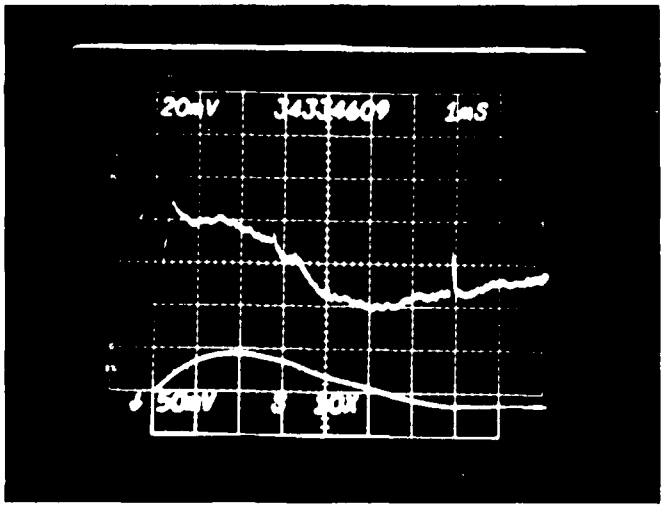

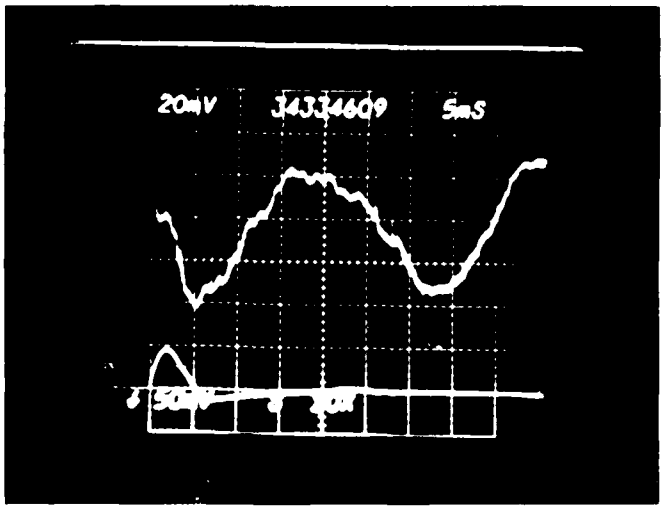

Figure 4.8 Low inductance strain gage readings for the 5 ms pulse for two different time scales.

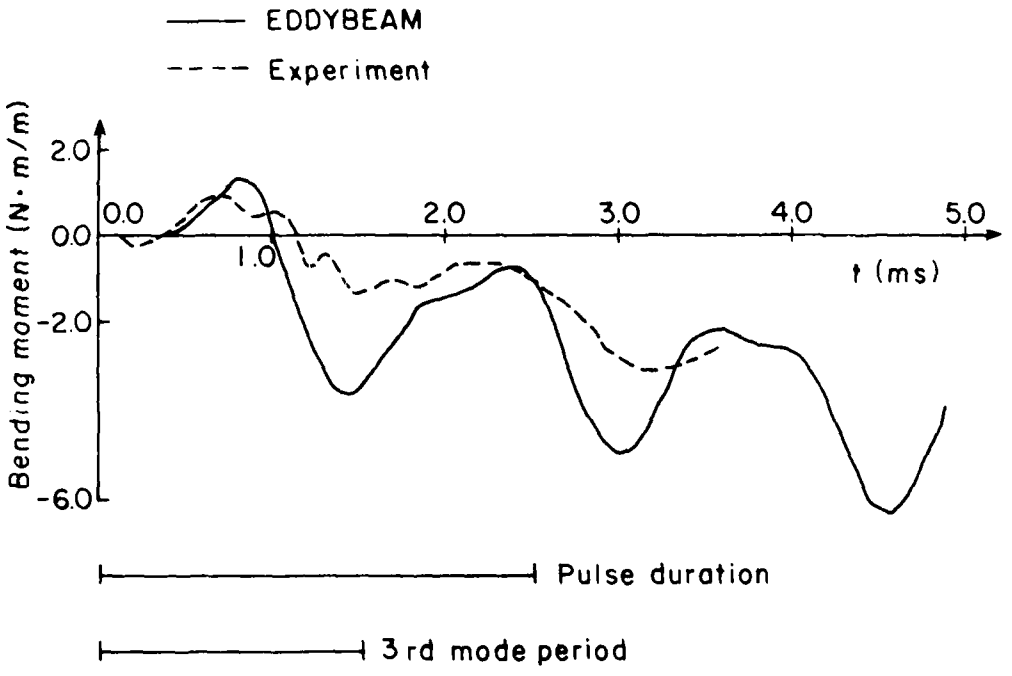

Figure 4.9 Comparison of the numerical and experimental results of the bending moment at node 3, Figure 4.4(b), for the 2.5 ms pulse.

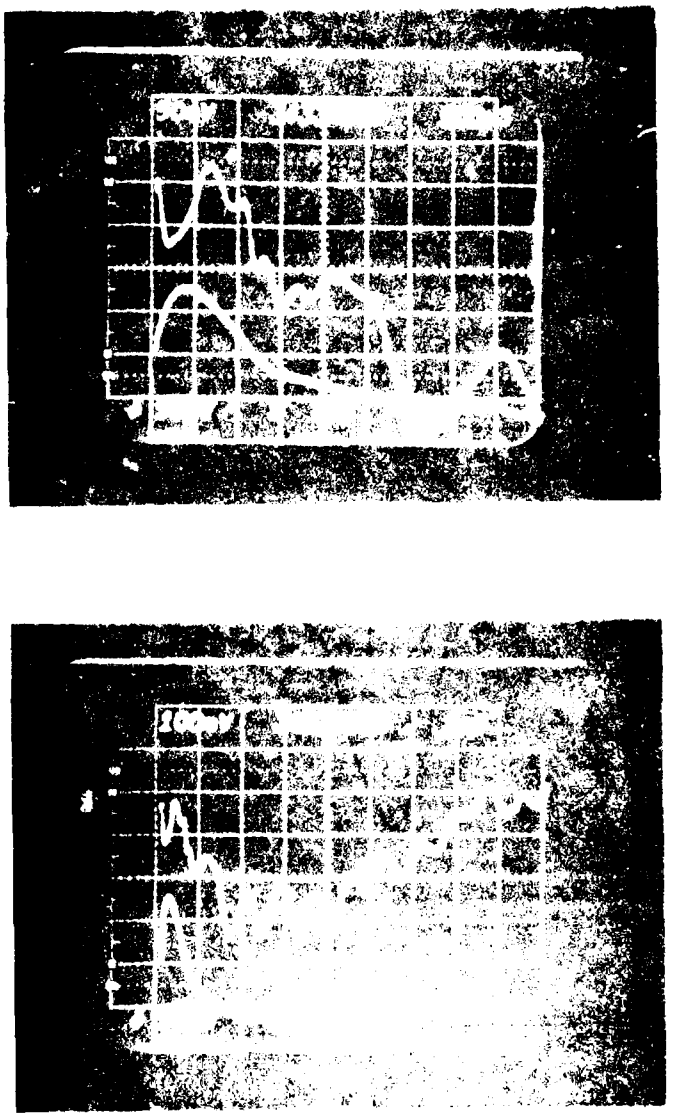

Figure 4.10 Low inductance strain gage readings for the 2.5 ms pulse for two different voltage and time scales.

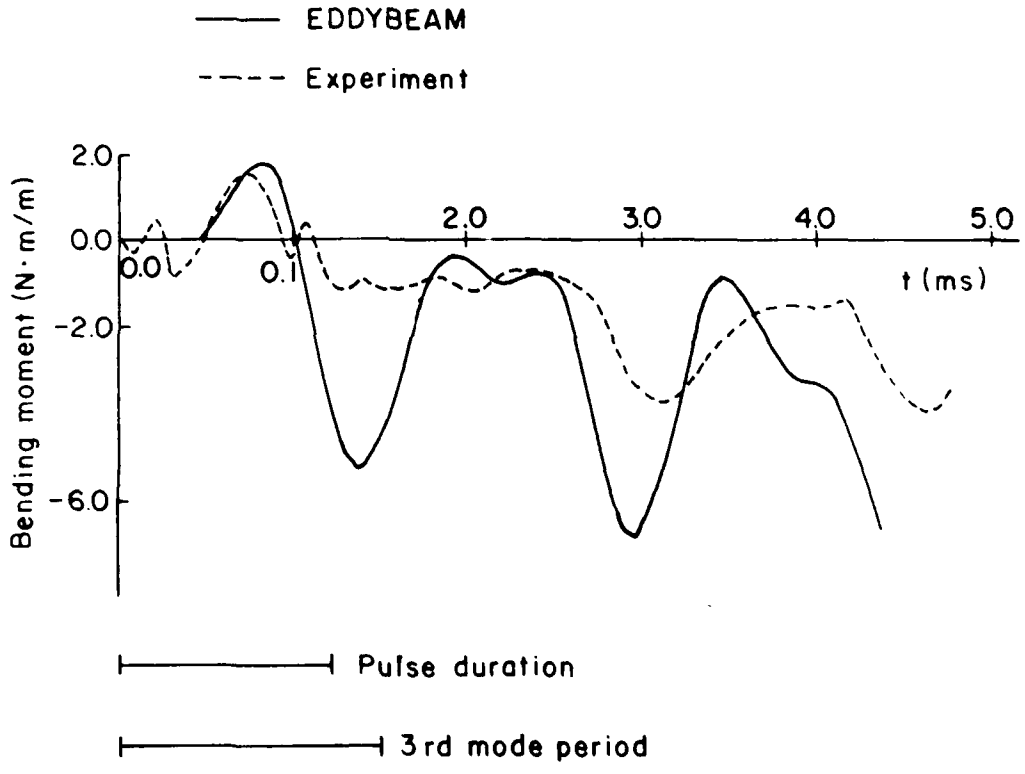

Figure 4.11 Comparison of the numerical and experimental results of the bending moment at node 3, Figure 4.4(b), for the 1.2 ms pulse.

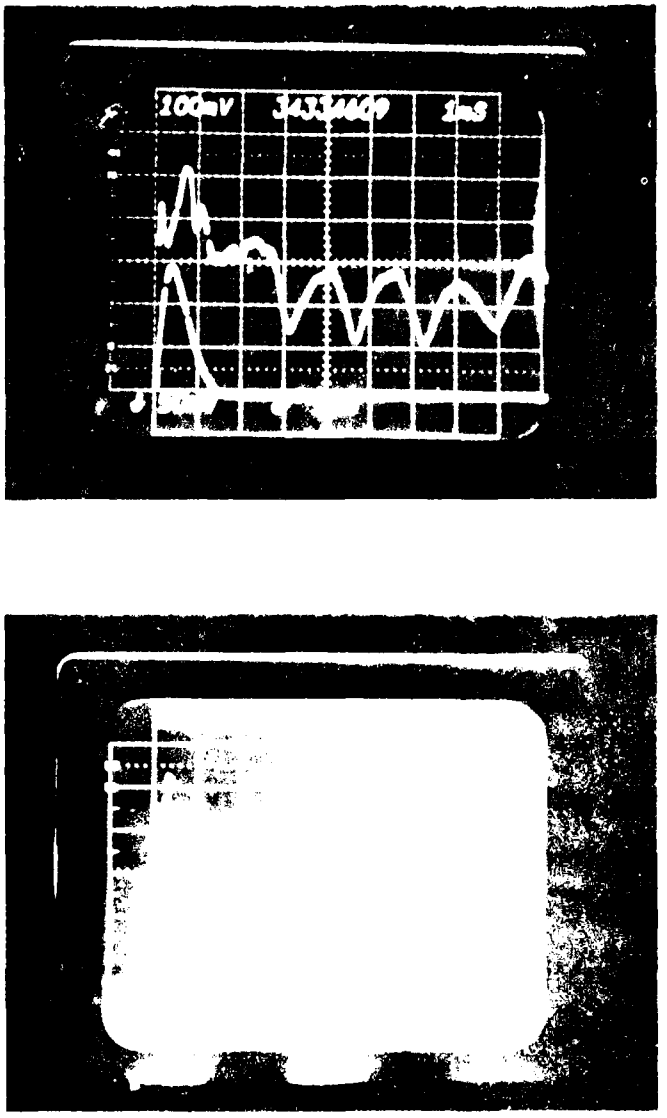

Figure 4.12 Low inductance strain gage readings for the 1.2 ms pulse for two different time scales.

time solutions of the displacement at node 6 (x = 330 mm). When the displacement reaches its maximum value, the energy density of the mechanical subsystem consists entirely of strain energy. The effects of the various couplings in reducing the total energy density at that point is obvious from the figure.

The gap distance between the wire and the mid-plane of the plate is approximately four times the thickness. The skin depth of a steady state current with the same period will be three times the thickness of the plate. The small gap distance and the nonlocal effects tend to concentrate the magnetic force at the nodal point of the second vibration mode. As a result, the induced motion of the plate consists mainly of the first and the third modes. The superposition of the third mode on the first mode is clearly shown in Figure 4.6c.

The nonlocal effect is still significant in this problem. The non-zero average pushing force can be easily seen from Figure 4.6b. A pulling force is developed close to the end of the pulse. Since the time variation of the magnetic field determines the induced current and force, it is possible to design a driving current to generate a large pulling force, instead of a pushing one, on the conductor.

Three different driving currents have been applied in the second problem. Since the position of the strain gage is far away from the wire, the effects of the various kinds of coupling are indistinguishable and only one curve is plotted for each case. Good quantitative agreement has been obtained in all cases. The quantitative difference is small in the long pulse duration case and larger in the shorter pulse duration cases. The differences may be partly caused by the flexibility of the clamped end support. The correlation between the numerical and experimental results

is considered acceptable in an experiment of this kind because of the end effects of the finite-length plate, the neglect of the structural and rotational magnetic damping, the finite size of the strain gage and the exciting wire, and the precision of the experimental measurements. These comparisons verify the model and the numerical results of the coupled problem.

The length of the pulse duration has an obvious effect on the mode of the induced vibration. In the 5 msec pulse duration case, mainly the first vibration mode is excited as can be seen from the oscillascope pictures, Figure 4.8. As the pulse duration decreases, the participation of the higher modes increases as shown in Figures 4.10 and 4.12 during half the period of the first mode of vibration. Note that in Figure 4.11 some higher frequency peaks in the experimental result cannot be represented in the numerical result. This is because the same finite element mesh is used for all three pulsed currents. To represent those higher frequency peaks more accurately, more beam elements would need to be included in the finite element mesh.

A schematic comparison of the pulse duration and the third mode period has been included in Figures 4.7, 4.9, and 4.11 to demonstrate this effect. More higher frequency modes will be excited as the pulse duration further decreases. The magnetic force in this case will act more like an impact. The nonlocal effect will also be more important as the short pulse includes more high frequency components. The nonzero averaged pushing force from the nonlocal effect during the pulse duration serves as the impact force in such a case.

A quantitative description of the effect of pulse duration on the induced vibration is difficult to draw from these studies presented. One

reason is that the current is voltage-controlled and a different amount of energy has been applied for each pulsed current. To study the effect of pulse duration on the distribution of energy transferred into different vibrational modes, the same electromagnetic energy should be input to the whole system, and the mutual inductance between the plate and wire considered. A parameter study of the effect of pulse duration can then be conducted through modal analysis of the vibrating plate.

An estimation of the effect of the difference between the time characteristics of the two subsystems on the induced vibration can be obtained in the following sense. The magnetic force may be integrated during the pulse duration and applied on the plate as an impact force. The mechanical energy in this case will be equal to the kinetic energy in the equivalent initial velocity problem. The mechanical energy in the coupled problem may be calculated from the kinetic and elastic energies of the plate after the pulse has been applied. Since in the very short pulse case the induced eddy current will screen the applied magnetic field out, the magnetic force will act more like a magnetic pressure as the pulse duration decreases. The comparison between the two mechanical energies thus calculated versus the ratio of pulse duration to various fundamental periods of vibration may indicate the effect of pulse duration on the induced vibrations. A more rigorous study of such effects should be based on the energy conversion between the magnetic and mechanical subsystems based on the same energy input, as described in the last paragraph.

The study of the coupled problems in this chapter has been limited to the case of one exciting wire. The various coupling and nonlocal effects are of course problem dependent and should be investigated for other types of applied field. Many different types of magnetic field,

AD-A111 012 CORNELL UNIV ITHACA N Y DEPT OF STRUCTURAL ENGINEERING F/G 12/1
FINITE ELEMENT ANALYSIS OF MAGNETOELASTIC PLATE PROBLEMS.(U)
AUG 81 K Y YUAN N00014-79-C-0224
UNCLASSIFIED 81-14 NL

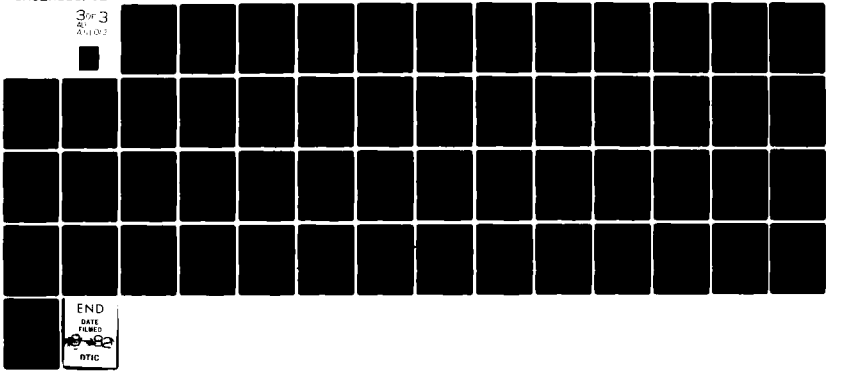

however, can be generated from superpositions of the one-wire fields. The study of the one-wire problem thus serves as a prototype for future studies.

Chapter 5

NONLINEAR VIBRATION OF INFINITELY LONG MAGNETOELASTIC PLATES

The magnetically induced vibrations of infinitely long conducting plates with finite deflections but small rotations are considered in this chapter. Beside the interest in studying the motion-dependent nature of magnetic forces, such studies may find applications in magnetic forming or in devices like magnetodynamic circuit breakers. Moreover, geometric nonlinearities must be included for investigations of structural stability.

The plate and the exciting magnetic field treated have the same general arrangement as in Chapter Four. The equations governing the coupled system now are Equations (2.102) and (2.66) to (2.67). The basic equations and the finite element formulation are presented in Section 5.1. An incremental-iterative procedure is suggested in Section 5.2 for the coupled nonlinear transient system. The implementation of the procedure in this study, however, met convergence problems because of the interaction between the time integration operator and the approximate solution procedure for the equations of motion. These difficulties are discussed in Section 5.3 together with some successful results obtained for static, nonlinear elastic problems.

5.1 Basic Equations and Finite Element Formulation

The linearized equations of motion governing the nonlinear mechanical system are

$$\int_{t_V} C_{\alpha\beta\gamma\delta}\, e_{\alpha\beta}\, \delta e_{\gamma\delta}\, {}^{t}dV + \int_{t_V} {}^{t}\tau_{\alpha\beta}\, \delta\, \eta_{\alpha\beta}\, {}^{t}dV = {}^{t+\Delta t}R - \int_{t_V} {}^{t}\tau_{\alpha\beta}\, \delta e_{\alpha\beta}\, {}^{t}dV \tag{2.66a}$$

$${}^{t+\Delta t}R = \int_{t_A} {}^{t+\Delta t}t_{\alpha}\, \delta\, u_{\alpha}\, {}^{t}dA + \int_{t_V} {}^{t}\rho\, ({}^{t+\Delta t}f_{\alpha} - \ddot{u}_{\alpha})\, \delta\, u_{\alpha}\, {}^{t}dV \tag{2.66b}$$

A nonlinear beam element developed by Bathe and Bolourchi (Ref. 87) is used for the updated Lagrangian (UL) finite element formulation. The components of displacement increment are approximated by

$$u_i = \sum_{k=1}^{6} h_k^i\, u_k \qquad i = 1,2 \tag{5.1}$$

in which the h_k^i are the interpolation function for the kth node in the element and the u_k are the nodal point displacement increments in the local axes at time t. Equation (5.1) is used to evaluate the linear and nonlinear parts of the strain tensor in Eq. (2.66) for each element. The formulation procedure results in the following incremental finite element stiffness equations

$$([{}^{t}K_L] + [{}^{t}K_{NL}])\, \{u\} = \{{}^{t+\Delta t}R\} - \{{}^{t}F\} \tag{5.2}$$

in which $[{}^{t}K_L]$, $[{}^{t}K_{NL}]$ are linear and nonlinear strain incremental stiffness matrices for the configuration at time t, $\{{}^{t+\Delta t}R\}$ is the vector of inertial effects and externally applied nodal loads at time $t+\Delta t$; and $\{{}^{t}F\}$ is the vector of nodal point forces equivalent to the element stresses at time t.

The linear stiffness matrix $[{}^{t}K_L]$ is computed as

$$[{}^{t}K_L] = \int_{t_V} [{}^{t}B_L]^T [C]\, [{}^{t}B_L]\, {}^{t}dV \tag{5.3}$$

in which $[{}^{t}B_L]$ is the linear strain-displacement transformation matrix for the configuration at time t, and [C] is the material property matrix. $[{}^{t}K_L]$

is the same as the usual linear beam stiffness matrix (Ref. 88).

The nonlinear stiffness matrix $[{}^{t}K_{NL}]$ accounts for the nonlinear effect of the stresses at time t and is calculated by

$$[{}^{t}K_{NL}] = \int_{{}^{t}V} [{}^{t}B_{NL}]^{T} [{}_{t}\tau] [{}^{t}B_{NL}] \, {}^{t}dV \tag{5.4}$$

in which $[{}^{t}B_{NL}]$ is the nonlinear strain-displacement transformation matrix, and $[{}_{t}\tau]$ is the matrix of Cauchy stresses in the configuration at time t.

The vector of nodal point forces $\{{}^{t}F\}$ accounts for the linear effects of the stresses at time t and is computed by

$$\{{}^{t}F\} = \int_{{}^{t}V} [{}^{t}B_{L}]^{T} \{\hat{{}_{t}\tau}\} \, {}^{t}dV \tag{5.5}$$

in which $\{\hat{{}_{t}\tau}\}$ is the vector of Cauchy stresses in the configuration at time t.

The vector of externally applied nodal loads $\{{}^{t+\Delta t}R\}$ for the configuration at time $t+\Delta t$ is obtained by the finite element evaluation of Eq. (2.44) using Eq. (2.66b). The deformation dependent nature of the force is proposed to be treated in an iterative way in the computational procedure. Details of the various element matrices and vectors are presented in Appendix C.

A moving curvilinear coordinate ζ is introduced on the mid-surface of the plate for the eddy current problem, Figure 5.1. As a first step in the study of the geometrically nonlinear coupled problem, the self-field effect is neglected. Eq. (2.102) in this case becomes for one-dimensional problems:

$$\frac{\partial^{2}\psi}{\partial\zeta^{2}} = \sigma h \left[\frac{\partial B_{n}^{o}}{\partial t} + \frac{\partial}{\partial\zeta} (\underset{\sim}{v}_{\zeta} \times \underset{\sim}{B}_{\zeta}^{o})_{z}\right] \tag{5.6}$$

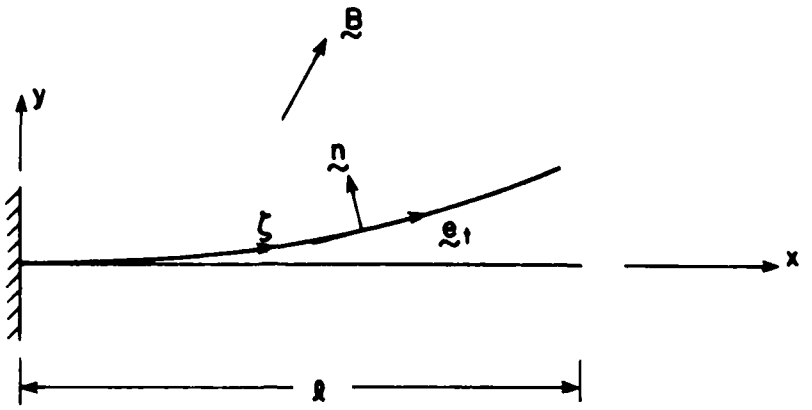

Figure 5.1 Fixed and moving coordinate systems on the mid-surface of a cantilever plate.

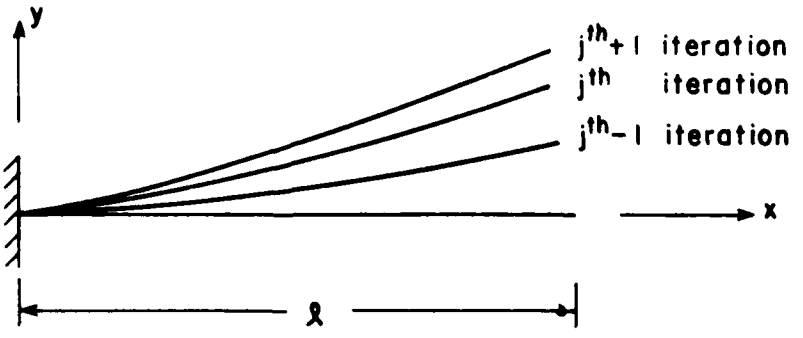

Figure 5.2 Configurations of a cantilever plate at three consecutive iteration steps.

in which n denotes the unit normal vector on the mid-surface of the deformed plate.

Using the Galerkin formulation and the linear shape function approximation

$$\psi^E = \sum_{k=1}^{2} N_k^E \psi_k, \tag{5.7}$$

one may discretize Eq. (5.6) into

$$- S_{jk}^E \psi_k = P_j^E \tag{5.8}$$

in which

$$S_{jk}^E = \int_E \frac{dN_j^E}{d\zeta} \frac{dN_k^E}{\partial\zeta} \, d\zeta \tag{5.9a}$$

$$P_j^E = \sigma_i \int_E N_j^E \left[B_n^o + \frac{\partial}{\partial\zeta} (\underset{\sim}{V}\times\underset{\sim}{B})_z \right] d\zeta \tag{5.9b}$$

After the stream function is solved, the magnetic body force is calculated from

$$t_\rho \, {}^{t+\Delta t}\underset{\sim}{f} = - \frac{\partial\psi}{\partial\zeta} B_n^o \, \underset{\sim}{e}_t + \frac{\partial\psi}{\partial\zeta} B_t^o \, \underset{\sim}{n} \tag{5.10}$$

This expression is used in Eq. (2.66b) for the calculation of the externally applied load vector $\{{}^{t+\Delta t}R\}$.

5.2 Staggered Transient Analysis and Computational Procedure

Except for the deformation- and velocity-dependent magnetic force, the solution of Eq. (5.2) may follow the standard incremental iterative pseudo-force procedure (Ref. 87). With an implicit time integration scheme, this involves a calculation of the unbalanced force and an iterative procedure to achieve the equilibrium among the internal element stresses, the

externally applied nodal point loads, and the inertia force at time $t+\Delta t$ (Ref. 89). For deformation-independent loads, such a procedure is straightforward. For some types of follower forces, such as pressure loadings, a load stiffness matrix may be added to the tangent stiffness matrix to account for the deformation-dependent nature of the force (Ref. 90). For the deformation- and velocity- dependent magnetic force, this approach is not applicable. In this work, an updated calculation of the magnetic force within each pseudo-force iteration step is suggested to achieve the simultaneous satisfaction of both the eddy current equation and the equations of motion. The procedure for this calculation is described below.

Consider the state of motion of the plate at j-th iteration shown in Figure 5.2. The magnetic force has been calculated based on the motion of the plate at the j-1st iterative step and applied to the configuration of the plate at that step. If the unbalanced force calculated is such that a prescribed convergence tolerance is violated (Ref. 89), the eddy current equation is solved again based on the motion and position at the j-th iterative step. The unbalanced force is recalculated with this newly calculated magnetic force and applied to the configuration at the j-th iterative step. The same nonlinear stiffness matrix $[{}^{t}K_{NL}]$ and nodal force vector $\{{}^{t}F\}$ are employed in each iteration. The procedure is continued until the tolerance is satisfied, i.e., until the error in equilibrium or the change in incremental energy is acceptably small (Ref. 89).

The trapezoidal rule version of the Newmark method (Ref. 100) is used to integrate the equations of motion. A quasi-Newton method is used for the iterative procedure (Ref. 89). A force and/or energy tolerance is used for convergence checks (Ref. 89). The incremental iterative computational procedure is summarized in Table 5.1.

Table 5.1 Summary of Incremental-Iterative Integration Procedure

Initial Calculations

1. Form the linear stiffness matrix $[K_L]$ and mass matrix $[M]$; initialize $\{{}^{0}u\}$, $\{{}^{0}\dot{u}\}$, $\{{}^{0}\ddot{u}\}$; form the field matrix $[s]$.
2. Calculate the time-integration constants and convergence-tolerance constants. **Newmark method: θ=1.0, δ=0.5, α=0.25**

   $a_0 = 1/(\alpha\Delta t^2)$ $\quad a_1 = \delta/(\alpha\Delta t)$ $\quad a_2 = 1/(\alpha\Delta t)$ $\quad a_3 = 1/(2\alpha)-1$

   $a_4 = \delta/\alpha - 1$ $\quad a_5 = \Delta t(\delta/\alpha - 2)/2$ $\quad a_6 = a_0$ $\quad a_7 = -a_2$

   $a_8 = -a_3$ $\quad a_9 = \Delta t(1-\delta)$ $\quad a_{10} = \delta\Delta t$.

   Force tolerance : ftol = 0.1 (unless otherwise noted)

   Energy tolerance : etol = 0.001 (unless otherwise noted)
3. Form the effective linear coefficient matrix $[\hat{K}] = [K_L] + a_0 [M]$.

For Each Time Step

1. Calculate the magnetic field at the new position and form the field vector $\{{}^{t+\Delta t}p\}$; calculate the vector of nodal point forces $\{{}^{t}F\}$.
2. Solve the eddy current equation (5.8) and calculate the induced current and force on the plate.
3. Integrate and transfer the magnetic force to the structural program and form the load vector $\{{}^{t+\Delta t}R\}$.
4. Update $[\hat{K}]$ for nonlinear stiffness effects to obtain $[{}^{t}\hat{K}] = [\hat{K}] + [{}^{t}K_{NL}]$, and triangularize $[{}^{t}\hat{K}]$: $[{}^{t}\hat{K}] = [L]\,[D]\,[L]^T$.
5. Form the effective load vector $\{{}^{t+\Delta t}R\}$:

   $\{{}^{t+\Delta t}R\} = \{{}^{t}R\} + \theta\,(\{{}^{t+\Delta t}R\} - \{{}^{t}R\}) + [M]\,(a_1\,\{{}^{t}\dot{u}\} + a_2\,\{{}^{t}\ddot{u}\}) - \{{}^{t}F\}$.

6. Solve for the displacement increment $\{u\}$.

7. If required, iterate for equilibrium as follows:

   (a) initialize: $j=0$, $\{u^{(o)}\}= \{u\}$

   (b) $j = j+1$

   (c) interpolate the new displacement and velocity and transfer to eddy current program,

   (d) calculate the magnetic field at the new position at the same time step and solve for the magnetic force,

   (e) integrate and transfer the magnetic force to the structural program to form the unbalanced load vector $\{\Delta\ {}^{t+\Delta t}\hat{R}^{(j)}\}$

   (f) solve for the j-th correction to the displacement increment $\{\Delta\ u^{(j)}\}$ and update the displacement increment $\{u^{(j)}\} = \{u^{(j-1)}\} + \{\Delta\ u^{(j)}\}$

   (g) check iteration convergence: $\| \{\Delta\ {}^{t+\Delta t}\hat{R}^{(j)}\} \|_2 \Big/ \| \{\hat{R}\} \|_2^{max} \leq$ ftol,

   and/or $\{\Delta\ u^{(j)}\}^T \{\Delta\ {}^{t+\Delta t}\hat{R}^{(j-1)}\} \Big/ \{\Delta\ u^{(1)}\}^T \{{}^{t+\Delta t}\hat{R}^{(1)}\} \leq$ etol,

   (h) if convergence $\{u\} = \{u^{(j)}\}$ and go to 8;
   if no convergence and limit on number of iterations not exceeded, go to (b); otherwise, stop the program with a message to restart using a smaller time step size.

8. Calculate new displacements, velocities, and accelerations

$$\{{}^{t+\Delta t}\ddot{u}\} = a_6 \{u\} + a_7 \{{}^{t}\dot{u}\} + a_8 \{{}^{t}\ddot{u}\}$$

$$\{{}^{t+\Delta t}\dot{u}\} = \{{}^{t}\dot{u}\} + a_9 \{{}^{t}\ddot{u}\} + a_{10} \{{}^{t+\Delta t}\ddot{u}\}$$

$$\{{}^{t+\Delta t}u\} = \{{}^{t}u\} + \{u\}$$

9. If required number of time steps have been calculated, stop; otherwise, go to 1.

A Fortran program BEAMNL has been developed for the mechanical part of the problem based on the formulation and computational procedure presented. Some geometrically nonlinear static problems have been solved successfully using the program BEAMNL, but the iteration procedure for geometrically nonlinear dynamic problems experienced some convergence difficulties. This convergence problem and some limited results obtained are discussed and presented in the next section. The present version of the program BEAMNL is briefly described below.

BEAMNL is designed to analyze linear and geometrically nonlinear static and dynamic problems of a linear elastic beam plate. The type of analysis may be specified by the input parameter NANTY. For nonlinear problems, the Newton Cotes quadrature formula is used to calculate the element stress vectors $\{^{t}F\}$. The order of the quadrature formula may be specified in the input data. One load case for a single type of analysis is handled at each run.

Geometric, material, and load information need to be input to the program. The number of incremental solutions and number of iterations allowed must also be specified for the nonlinear problems. Time integration constants and convergence parameters also need to be input. The initial conditions may be specified, if any, (input data IGIVN≠0) for the dynamic problems.

Displacements, velocities, and accelerations are produced as output of the program. The number of iterations at each incremental step is also printed out for reference. No plotting capabilities are incorporated yet.

5.3 Convergence Problems and Some Limited Results

The linear part and nonlinear static part of the program BEAMNL have been tested and verified through comparisons with analytical and experimental results. One of the nonlinear static problems studied is the large deformation analysis of a cantilever subjected to an end moment, shown in Figure 5.3 (Ref. 87). Five beam elements are used for this problem with Newton Cotes formula of order three in both the length and the thickness direction of the element. Seventy incremental steps are used with equilibrium iteration. The force and energy tolerance used are 0.1 and 0.001, respectively. The calculated response compares well with the analytical solution within the range of the moment parameter η shown in the figure. Good agreement with the analytical result is expected for even larger values of η. Note that in this problem there is no coupling between the axial force and the flexural deformation since it is a pure bending problem.

The second problem studied is the large deformation analysis of a cantilever subjected to an end load, Figure 5.4. Seven beam elements are used with the mesh finer in the region closer to the support. The deflections of the beam at different load levels are shown in Figure 5.4. The curvature at the root of the cantilever beam is shown as a function of load in Figure 5.5. The theoretical and experimental results are from an unpublished study by Pao and Moon of Cornell University. The FE analysis predicts deflections accurately for tip deflections up to about 60% of the cantilever span, corresponding to a loading parameter f of nearly 2.0. The curvature is accurate up to about $f = 4.0$. Note that in the analytic results the beam is assumed inextensible, while in the FE results the effect of axial deformation is included.

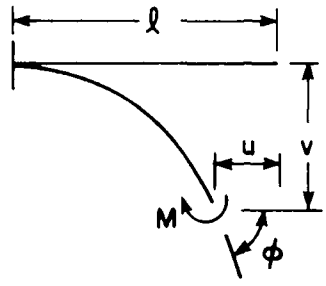

L = 100 in
I = 0.01042 in
A = 0.5 in^2
E = 1.2 x 10^4 psi
M = Concentrated end movement

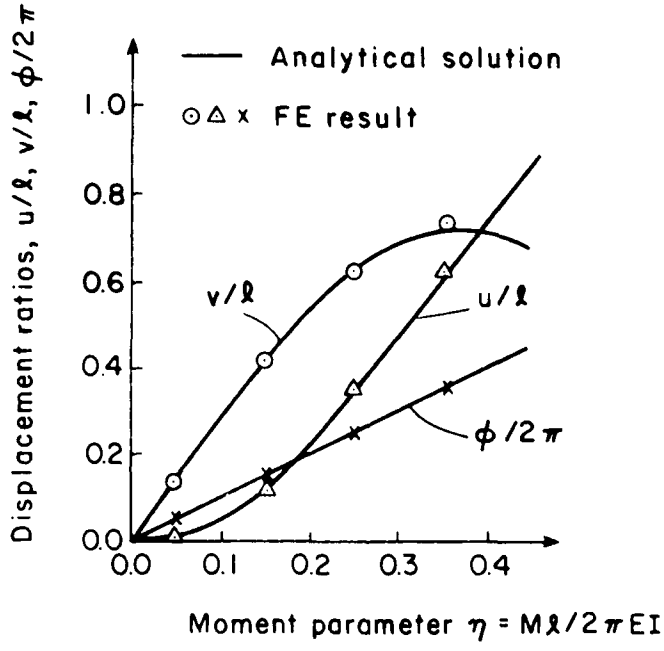

Figure 5.3 Moment deflection curve of an elastic cantilever plate loaded by a moment at its tip.

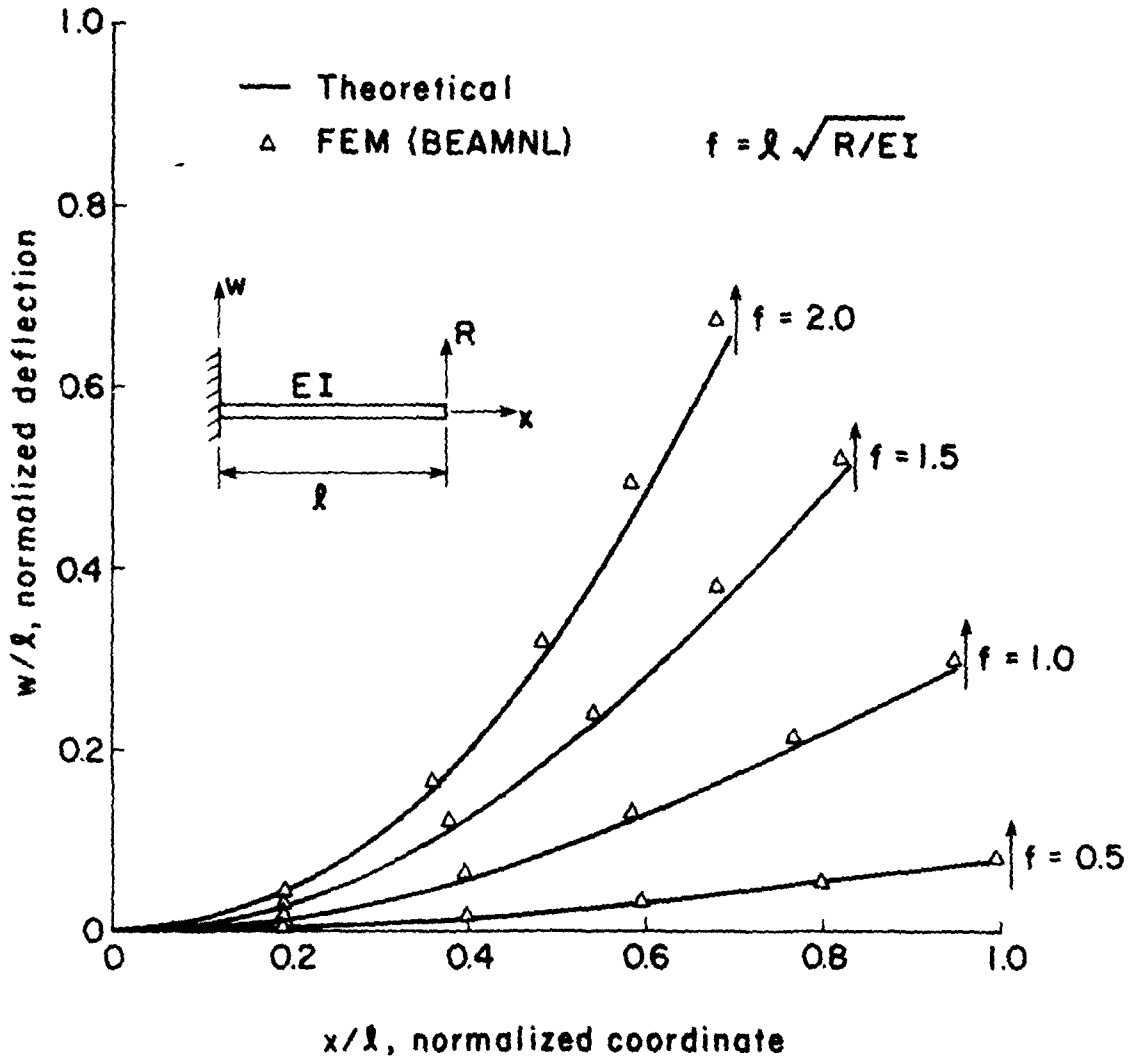

Figure 5.4 Comparison of FE and theoretical predictions of the nonlinear elastic bending deflections of a tip-loaded cantilever beam.

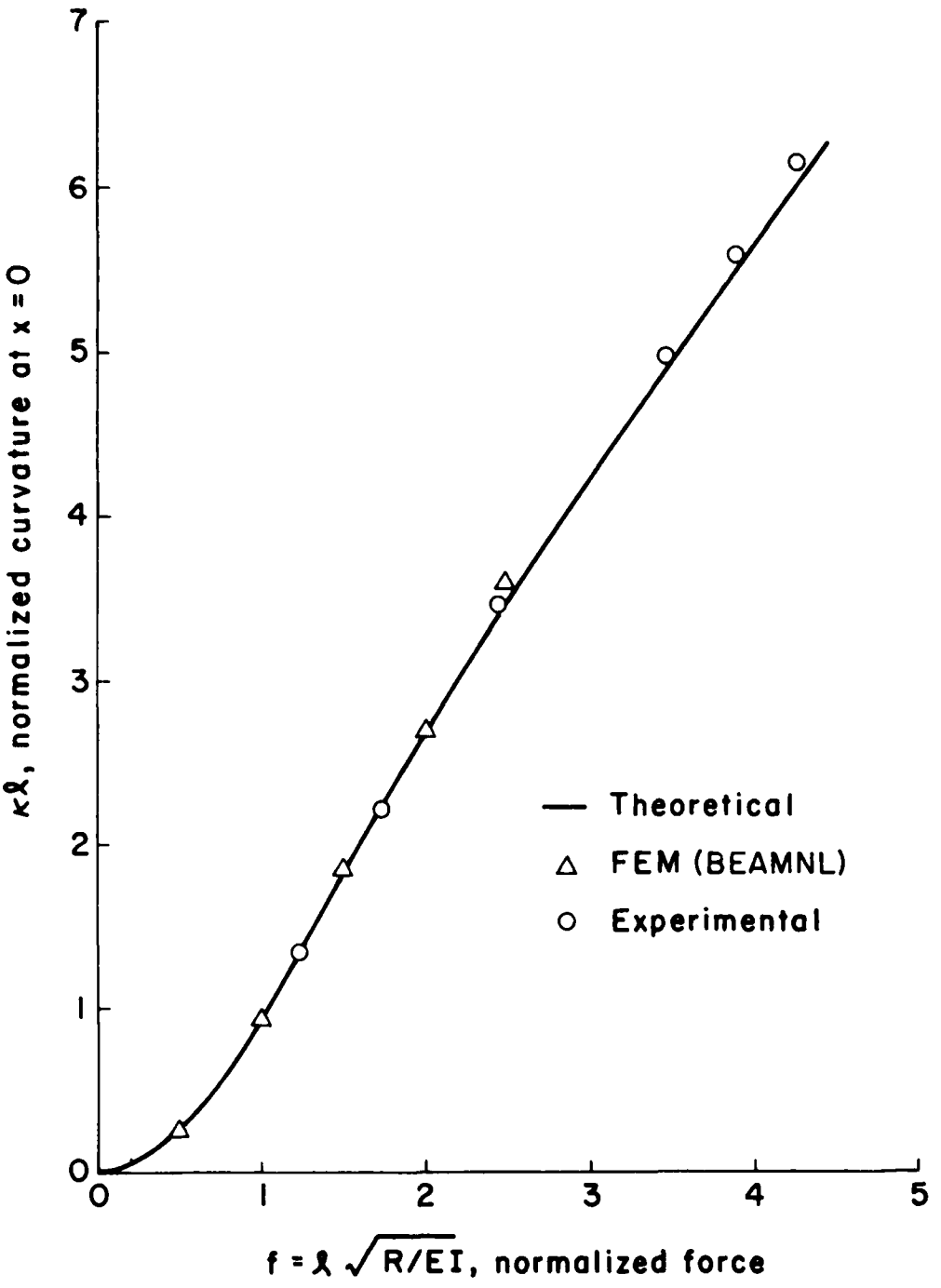

Figure 5.5 Comparison of theoretical, experimental, and FE results for the curvature at the root of the cantilever beam shown in Figure 5.4.

Strong coupling between the axial force and the flexure deformation exists in this problem. When the loading parameter f becomes greater than 2.5, the behavior of the deflected beam becomes more like an arch. Slow convergence of the iteration scheme occurs for this situation. At larger values of f, convergence fails with the present quasi-Newton method. Stronger convergence tolerances with ftol = $1x10^{-4}$ and etol = $1x10^{-6}$ have been used for this structural stiffening problem, and a small time step is needed for convergence (Ref. 89).

Geometrically nonlinear analysis has been attempted for the large amplitude free vibrations of a simply supported beam. The purpose of the analysis is to establish the frequency-amplitude relationship of the beam and to compare it with the analytical result (Refs. 91, 92). This study is not successful because the iteration scheme fails to converge within each time step. The numerical experience shows that the lack of convergence arises from the high frequency axial vibrations of the beam element. The large axial forces developed from these axial vibrations cause an increase of the unbalanced force during the iterative procedure. Attempts have been made to separate the inertia force effect and the effect of the linear approximation to the nonlinear equations in the calculations of the unbalanced forces, but with the present quasi-Newton scheme all the attempts failed because of the intrinsic interaction of the time integration method with the approximate solution procedure for the equations of motion.

A quasi-Newton method and structural (i.e., one-dimensional) beam elements are used in the nonlinear dynamic analysis in this work. A literature survey reveals that for transient nonlinear analysis all the works surveyed (Refs. 93 - 96) which use continuum (i.e., two-dimensional plane stress) elements adopt either a quasi-Newton or the full Newton

method for iteration. Transient nonlinear analyses using structural elements usually employ explicit time integration schemes (Ref. 97, 98). Studies which use structural elements together with an implicit integration scheme and quasi-Newton method for iteration have not been found.

In transient nonlinear analysis the dynamic properties of different types of elements have a definite effect on the success of a particular solution method used. Efforts to use implicit integration schemes with a quasi-Newton method for iteration appear to be futile. It is suggested that the full Newton or the BFGS method (Ref. 99) be used for the iterative procedure in the future.

Chapter 6

CONCLUSION

This thesis has presented an integrated study of the magnetically induced vibrations of nonferrous conducting plates. The continuum mechanics basis, the stream function modelling of the coupled problem, the intermediate eddy current calculations on rigid flat plates, and the linear vibrations of infinitely long plates have been discussed in some detail. Some preliminary studies of the coupled nonlinear problems of infinitely long plates have also been presented. A summary of the work presented in this thesis is given below. Conclusions from the present study are then drawn. Some suggestions for further research are made at the end of the chapter.

6.1 Summary

The thesis contains three main phases: theoretical modelling of the magnetoelastic plate, finite element eddy current calculations on rigid plates, and finite element numerical studies of coupled magnetoelastic problems. The numerical results obtained have been compared with analytic and experimental results at each stage of the study. The physics and continuum mechanics background of the problem has been presented in Chapter Two. The magnetic force-field method has been chosen to formulate the coupled problems. The magnetic force-energy method (Ref. 25) has not been emphasized, although the energy transfer between the magnetic and mechanical subsystems has been briefly mentioned in Chapter Two, and the

magnetic energy-circuit method for eddy current calculation discussed in Chapter Three.

The modelling of plate problems by the stream function method has been presented in Section 2.3. All the simplifying assumptions have been carefully examined and the limitations of the stream function method in the large deformation cases analyzed. The governing equations for the magnetic and mechanical subsystems have been derived and the various coupling effects discussed. The assumption of constant magnetic body force across the thickness of the plate and the neglect of the magnetic damping moment have also been discussed. Both linear and nonlinear problems have been studied. All the equations have been linearized to the first order of the various unknown variables. The updated Lagrangian description of the magnetic subsystem and the approximations involved in the linearization procedure have been given special attention.

Eddy current calculations on rigid conducting plates have been presented in Chapter Three. The FE Galerkin formulations and the treatment of the integral terms in the eddy current equations have been presented in detail. Comparisons of the numerical results with the infrared and search coil experimental results have been made. Analytical solutions in the low and high magnetic Reynolds number limits have also been employed to verify the numerical results. Detailed studies including some dimensional analysis have been carried out for the steady state and transient eddy current problems on infinitely long plates. For finite plates, only the steady state analysis has been formulated and performed.

Chapter Four treats the linear vibrations of infinitely long conducting plates excited by single pulsed currents. The types of coupling studied have been limited to the effects of the transverse motions of the

plates. The staggered transient analysis and the computational procedure have been presented in detail. The calculated moments have been compared to experimental values obtained with low inductance strain gage readings. The effect of pulse duration on the induced vibrations and energy transfers have been demonstrated through the three pulsed currents studied. The results show that as the pulse duration decreases, the nonlocal effect becomes more important and the magnetic force acts more like an impact load. A quantitative description of the effect of pulse duration on the induced vibration has not been presented because the control condition of the driving currents does not readily permit equivalence of the input energies in the three problems studied. A rough method has been suggested to estimate the effect of pulse duration on the contribution of nonlocal pushing force in the mechanical energy converted. The effect of the difference in the time characteristics of the two subsystems on the induced vibration may then be represented quantitatively.

The induced nonlinear vibrations of infinitely long plates have been formulated in Chapter Five based on the linearized equations for the updated incremental analysis procedure. The staggered transient analysis and the computational scheme have been presented. An iterative procedure has been proposed for the motion-dependent magnetic load. Some preliminary results for the nonlinear static problems have been presented. The convergence difficulties in the nonlinear dynamic problems have been discussed and some suggestions made for the improvement of the iteration scheme used.

6.2 Conclusions

The following conclusions may be drawn from the work presented:

1. The stream function method presents a useful tool for the eddy current calculations on thin nonferrous conducting plates in the low and intermediate frequency cases. The capability of this method for curved surfaces is limited to small curvature situations. This method has a close relationship with other eddy current circuit models. The advantages and disadvantages of the different methods need further comparative studies.

2. From the experience of using the Fortran programs developed, the EDDY1 and EDDY1T codes appear to be reasonably efficient. The EDDY2 code takes more computation time because of the complicated forms of the weighting functions for the six-node triangular elements. The efficiency of the EDDY2 code can be greatly improved by using rectangular elements and/or linear triangular elements. The weighting functions for these elements can be easily integrated or obtained from the weighting functions for the six-node triangular elements presented in Appendix B.

3. The modelling and formulations for the linear coupled problem in Chapter Four have been verified satisfactorily through comparisons with low inductance strain gage experiments. The velocity and displacement have a damping effect on the coupled problem. The total energy transferred to the conducting plate is reduced because of these motional effects, but their influence seems to be small for the problems studied. The pulse duration has an effect on both the magnetic force and the induced vibrations. For the short pulse an impact approximation based on the nonlocal pushing force will be reasonable.

4. The quasi-Newton method cannot be used in the iterative procedure together with the structural elements in the transient nonlinear problems. The fictitious in-plane deformation caused by the simplifying assumptions in the structural theory creates large in-plane inertia forces which make

the convergence of equilibrium iteration difficult when the quasi-Newton method is used. The simplifying kinematic assumptions in the structural elements have a definite influence on their performance in transient nonlinear analysis. The full Newton or a BFGS method should be used for these problems if structural elements are to be used. The study of the induced nonlinear vibrations of conducting plates cannot proceed until these numerical problems are solved.

6.3 Suggestions for Further Research

The following suggestions are made for future work:

1. For the immediate continuation of the present work, it is suggested that linear elements be implemented in the program EDDY2 to achieve better efficiency of the computation; that the effect of pulse duration on the energy transfer and induced vibration of infinitely long plates be studied in more depth; and that the full Newton and BFGS methods be tested for the transient nonlinear problems to enable the continuation of the study for the induced nonlinear vibrations of conducting plates.
2. The eddy current circuit nature of the stream function formulation should be explored to enable a modal analysis of the eddy current and the coupled problems. The magnetic energy stored in various eddy current modes and its conversion into mechanical energies in different vibrational modes of the plate should be calculated in such a modal theory for the coupled problems. The modal study of the coupled problem described basically is equivalent to the magnetic force-energy method discussed in Reference 25.
3. The in-plane force and the magnetic damping moment should be included, and their effect on the induced vibrations and stability of the conductors studied. Different types of magnetic fields, such as transverse or inclined

uniform fields, should also be investigated.

4. Cyclically pulsed currents and their effect on induced vibrations should be studied for possible magneto-flutter effects. Heat conduction and thermoelastic coupling in such cases may be important and may need to be included in the analysis.

APPENDIX A

MATRICES AND NONLOCAL INTEGRATIONS FOR ONE-DIMENSIONAL PLATES

This appendix presents explicit finite element matrices including the analytic expressions for the nonlocal integration terms described in sub-subsection 3.3.1.b for the transient one-dimensional problems. The matrices and expressions for the steady state problems described in sub-subsection 3.3.1.a may be obtained from these by setting $h = 1$, $\sigma\mu = R$, and by replacing X and X' by the nondimensionalized quantites x and ξ.

$$[S^E] = \frac{1}{L^E}\begin{bmatrix} 1 & -1 \\ -1 & 1 \end{bmatrix} \tag{A.1}$$

$$[P^E] = \sigma\mu\, L^E \begin{bmatrix} 1/3 & 1/6 \\ 1/6 & 1/3 \end{bmatrix} \tag{A.2}$$

$$W_1^E = \frac{h}{2L^E}\{\ell n\,[(X'-X_1^E)^2 + \tfrac{1}{4}h^2] - \ell n\,[(X'-X_2^E)^2 + \tfrac{1}{4}h^2]\} + \tag{A.3a}$$

$$- \frac{2}{L^E}(X'-X_2^E)\{\tan^{-1}[\tfrac{2}{h}(X'-X_1^E)] - \tan^{-1}[\tfrac{2}{h}(X'-X_2^E)]\}$$

$$W_2^E = -\frac{h}{2L^E}\{\ell n\,[(X'-X_1^E)^2 + \tfrac{1}{4}h^2] - \ell n\,[(X'-X_2^E)^2 + \tfrac{1}{4}h^2]\} + \tag{A.3b}$$

$$+ \frac{2}{L^E}(X'-X_1^E)\{\tan^{-1}[\tfrac{2}{h}(X'-X_1^E)] - \tan^{-1}[\tfrac{2}{h}(X'-X_2^E)]\}$$

in which the superscript E denotes the Eth element, L^E the length of the element, and X_1^E and X_2^E the coordinates of the two end nodes of element E, as shown in Figure A.1.

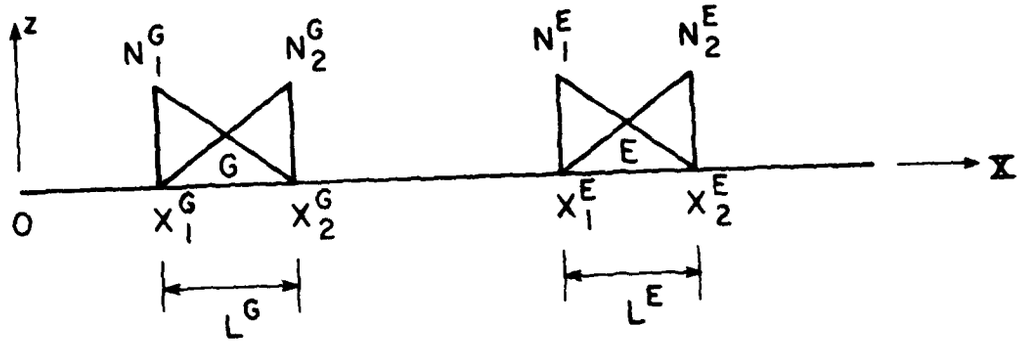

Figure A.1 Notations used in nonlocal integrations for one-dimensional plates.

The nonlocal integration Eq. (3.41) is performed element-wise and calculated over all the elements for each element E. For any element G, the contributions to the nonlocal integration of element E are, Figure A.1,

$$Q_{jk}^{EG} = \frac{\sigma\mu}{2\pi} \int_{x_1^G}^{x_2^G} N_k^G (x') W_j^E (x') dx', \qquad j, k=1,2 \tag{A.4}$$

The resulting analytical expressions of these integrations are:

$$Q_{11}^{EG} = \frac{1}{4\pi} \frac{\sigma\mu}{L^E L^G} \{ 2hL^E L^G +$$

$$+ \frac{h}{6} [- (x_1^G-x_1^E)^2 + (x_1^G-x_2^E)^2 + (x_2^G-x_1^E)^2 - (x_2^G-x_2^E)^2] +$$

$$+ \frac{h}{2} [\frac{h^2}{12} + (x_1^G-x_1^E)^2 - 2 (x_2^G-x_1^E) (x_1^G-x_2^E)] \ln [(x_1^G-x_1^E)^2 + \frac{h^2}{4}] +$$

$$+ \frac{h}{2} [-\frac{h^2}{12} - (x_1^G-x_2^E)^2 + 2 (x_2^G-x_2^E) (x_1^G-x_2^E)] \ln [(x_1^G-x_2^E)^2 + \frac{h^2}{4}] +$$

$$+ \frac{h}{2} [-\frac{h^2}{12} + (x_2^G-x_1^E)^2 - 2 L^E (x_2^G-x_1^E)] \ln [(x_2^G-x_1^E)^2 + \frac{h^2}{4}] +$$

$$+ \frac{h}{2} [\frac{h^2}{12} - (x_2^G-x_2^E)^2] \ln [(x_2^G-x_2^E)^2 + \frac{h^2}{4}] +$$

$$+ [\frac{2}{3} (x_1^G-x_1^E)^3 + 2 (L^E+ L^G) (x_1^G-x_1^E)^2 - 4 L^E (x_2^G-x_1^E)(x_1^G-x_1^E) -$$

$$- \frac{h^2}{2} (x_2^G-x_2^E)] \tan^{-1} (\frac{2}{h}) (x_1^G-x_1^E) +$$

$$+ [- \frac{2}{3} (x_1^G-x_2^E)^3 - 2 L^G (x_1^G-x_2^E)^2 + \frac{h^2}{2} (x_2^G-x_2^E)] \tan^{-1} (\frac{2}{h}) (x_1^G-x_2^E) +$$

$$+ \left[\frac{4}{3}(x_2^G-x_1^E)^3 - 2(x_2^G-x_1^E)^2(x_2^G-x_2^E) + \frac{h^2}{2}(x_2^G-x_2^E)\right]\tan^{-1}\left(\frac{2}{h}\right)(x_2^G-x_1^E) +$$

$$+ \left[\frac{2}{3}(x_2^G-x_2^E)^3 - \frac{h^2}{2}(x_2^G-x_2^E)\right]\tan^{-1}\left(\frac{2}{h}\right)(x_2^G-x_2^E)\ \}$$

$$Q_{12}^{EG} = \frac{1}{4\pi}\frac{\sigma\mu}{L^E L^G}\ \{ - 2hL^E L^G +$$

$$+ \frac{h}{6}\left[(x_1^G-x_1^E)^2 - (x_1^G-x_2^E)^2 - (x_2^G-x_1^E)^2 + (x_2^G-x_2^E)^2\right] +$$

$$+ \frac{h}{2}\left[-\frac{h^2}{12} + (x_1^G-x_1^E)^2 - 2L^E(x_1^G-x_1^E)\right]\ln\left[(x_1^G-x_1^E)^2 + \frac{h^2}{4}\right] +$$

$$+ \frac{h}{2}\left[\frac{h^2}{12} - (x_1^G-x_2^E)^2\right]\ln\left[(x_1^G-x_2^E)^2 + \frac{h^2}{4}\right] +$$

$$+ \frac{h}{2}\left[\frac{h^2}{12} + (x_2^G-x_1^E)^2 - 2(x_1^G-x_1^E)(x_2^G-x_2^E)\right]\ln\left[(x_2^G-x_1^E)^2 + \frac{h^2}{4}\right] +$$

$$+ \frac{h}{2}\left[-\frac{h^2}{12} - (x_2^G-x_2^E)^2 + 2(x_2^G-x_2^E)(x_1^G-x_2^E)\right]\ln\left[(x_2^G-x_2^E)^2 + \frac{h^2}{4}\right] +$$

$$+ \left[-\frac{2}{3}(x_1^G-x_1^E)^3 + 2L^E(x_1^G-x_1^E)^2 + \frac{h^2}{2}(x_1^G-x_2^E)\right]\tan^{-1}\left(\frac{2}{h}\right)(x_1^G-x_1^E) +$$

$$+ \left[\frac{2}{3}(x_1^G-x_2^E)^3 - \frac{h^2}{2}(x_1^G-x_2^E)\right]\tan^{-1}\left(\frac{2}{h}\right)(x_1^G-x_2^E) +$$

$$+ \left[\frac{2}{3}(x_2^G-x_1^E)^3 + 2(L^E-L^G)(x_2^G-x_1^E)^2 - 4L^E(x_1^G-x_1^E)(x_2^G-x_1^E) -\right.$$

$$\left. - \frac{h^2}{2}(x_1^G-x_2^E)\right]\tan^{-1}\left(\frac{2}{h}\right)(x_2^G-x_1^E) +$$

$$+ \left[\frac{4}{3}(x_2^G-x_2^E)^3 - 2(x_2^G-x_2^E)^2(x_1^G-x_2^E) + \frac{h^2}{2}(x_1^G-x_2^E)\right]\cdot$$

$$\cdot\ \tan^{-1}\left(\frac{2}{h}\right)(x_2^G-x_2^E)\ \}$$

$$Q_{21}^{EG} = \frac{1}{4\pi}\frac{\sigma\mu}{L^E L^G}\Big\{ - 2hL^E L^G +$$

$$+ \frac{h}{6}\left[(x_1^G-x_1^E)^2 - (x_1^G-x_2^E)^2 - (x_2^G-x_1^E)^2 + (x_2^G-x_2^E)^2\right] +$$

$$+ \frac{h}{2}\left[-\frac{h^2}{12} - (x_1^G-x_1^E)^2 + 2\,(x_1^G-x_1^E)(x_2^G-x_1^E)\right] \ln\left[(x_1^G-x_1^E)^2 + \frac{h^2}{4}\right] +$$

$$+ \frac{h}{2}\left[\frac{h^2}{12} + (x_1^G-x_2^E)^2 - 2\,(x_1^G-x_1^E)(x_2^G-x_2^E)\right] \ln\left[(x_1^G-x_2^E)^2 + \frac{h^2}{4}\right] +$$

$$+ \frac{h}{2}\left[\frac{h^2}{12} - (x_2^G-x_1^E)^2\right] \ln\left[(x_2^G-x_1^E)^2 + \frac{h^2}{4}\right] +$$

$$+ \frac{h}{2}\left[-\frac{h^2}{12} + (x_2^G-x_2^E)^2 + 2\,L^E\,(x_2^G-x_2^E)\right] \ln\left[(x_2^G-x_2^E)^2 + \frac{h^2}{4}\right] +$$

$$+ \left[\frac{4}{3}(x_1^G-x_1^E)^3 - 2\,(x_1^G-x_1^E)^2\,(x_2^G-x_1^E) + \frac{h^2}{2}(x_2^G-x_1^E)\right]\tan^{-1}\left(\frac{2}{h}\right)(x_1^G-x_1^E) +$$

$$+ \left[\frac{2}{3}(x_1^G-x_2^E)^3 - 2\,(L^E-L^G)\,(x_1^G-x_2^E)^2 + 4\,L^E\,(x_1^G-x_2^E)(x_2^G-x_2^E) -\right.$$

$$\left. - \frac{h^2}{2}(x_2^G-x_1^E)\right]\tan^{-1}\left(\frac{2}{h}\right)(x_1^G-x_2^E) +$$

$$+ \left[\frac{2}{3}(x_2^G-x_1^E)^3 - \frac{h^2}{2}(x_2^G-x_1^E)\right]\tan^{-1}\left(\frac{2}{h}\right)(x_2^G-x_1^E) +$$

$$+ \left[-\frac{2}{3}(x_2^G-x_2^E)^3 - 2\,L^E\,(x_2^G-x_2^E)^2 + \frac{h^2}{2}(x_2^G-x_1^E)\right]\tan^{-1}\left(\frac{2}{h}\right)(x_2^G-x_2^E)\Big\}$$

$$Q_{22}^{EG} = \frac{1}{4\pi} \frac{\sigma\mu}{L^E L^G} \{ 2hL^E L^G +$$

$$+ \frac{h}{6} [- (x_1^G - x_1^E)^2 + (x_1^G - x_2^E)^2 + (x_2^G - x_1^E)^2 - (x_2^G - x_2^E)^2] +$$

$$+ \frac{h}{2} [\frac{h^2}{12} - (x_1^G - x_1^E)^2] \ln [(x_1^G - x_1^E)^2 + \frac{h^2}{4}] +$$

$$+ \frac{h}{2} [- \frac{h^2}{12} - (x_1^G - x_2^E)^2 + 2 L^E (x_1^G - x_2^E)] \ln [(x_1^G - x_2^E)^2 + \frac{h^2}{4}] +$$

$$+ \frac{h}{2} [- \frac{h^2}{12} - (x_2^G - x_1^E)^2 + 2 (x_1^G - x_1^E)(x_2^G - x_1^E)] \ln [(x_2^G - x_1^E)^2 + \frac{h^2}{4}] +$$

$$+ \frac{h}{2} [\frac{h^2}{12} + (x_2^G - x_2^E)^2 - 2 (x_1^G - x_2^E)(x_2^G - x_1^E)] \ln [(x_2^G - x_2^E)^2 + \frac{h^2}{4}] +$$

$$+ [\frac{2}{3} (x_1^G - x_1^E)^3 - \frac{h^2}{2} (x_1^G - x_1^E)] \tan^{-1} (\frac{2}{h}) (x_1^G - x_1^E) +$$

$$+ [\frac{4}{3} (x_1^G - x_2^E)^3 - 2 (x_1^G - x_2^E)^2 (x_1^G - x_1^E) + \frac{h^2}{2} (x_1^G - x_1^E)] \cdot$$

$$\cdot \tan^{-1} (\frac{2}{h})(x_1^G - x_2^E)$$

$$+ [- \frac{2}{3} (x_2^G - x_1^E)^3 + 2 L^G (x_2^G - x_1^E)^2 + \frac{h^2}{2} (x_1^G - x_1^E)] \tan^{-1} (\frac{2}{h}) (x_2^G - x_1^E) +$$

$$+ [\frac{2}{3} (x_2^G - x_2^E)^3 - 2 (L^E + L^G) (x_2^G - x_2^E)^2 + 4 L^E (x_1^G - x_2^E)(x_2^G - x_2^E) -$$

$$- \frac{h^2}{2} (x_1^G - x_1^E)] \tan^{-1} (\frac{2}{h}) (x_2^G - x_2^E) \}$$

APPENDIX B

MATRICES AND NONLOCAL INTEGRATIONS FOR TWO-DIMENSIONAL PLATES

This appendix presents the finite element matrices and the analytic expressions of the nonlocal weighting functions described in subsection 3.4.1 for the steady state two-dimensional eddy current problems. The nondimensionalized finite element equations are those presented in Eq. (3.53).

By using the natural coordinates L_1, L_2, L_3 for the six-node triangular element shown in Figure B.1, one may write the shape functions N_i as:

$$\begin{aligned} N_1 &= L_1(2L_1-1) & N_4 &= 4L_1L_2 \\ N_2 &= L_2(2L_2-1) & N_5 &= 4L_2L_3 \\ N_3 &= L_3(2L_3-1) & N_6 &= 4L_3L_1 \end{aligned} \tag{B.1}$$

in which

$$\begin{Bmatrix} L_1 \\ L_2 \\ L_3 \end{Bmatrix} = \frac{1}{2A} \begin{bmatrix} a_1 & b_1 & c_1 \\ a_2 & b_2 & c_2 \\ a_3 & b_3 & c_3 \end{bmatrix} \begin{Bmatrix} 1 \\ x \\ y \end{Bmatrix} \tag{B.2}$$

$$\left.\begin{aligned} a_i &= x_{i+1}\, y_{i+1} - x_{i+2}\, y_{i+1} \\ b_i &= y_{i+1} - y_{i+2} \\ c_i &= x_{i+2} - x_{i+1} \end{aligned}\right\} \quad i = 1,2,3 \tag{B.3}$$

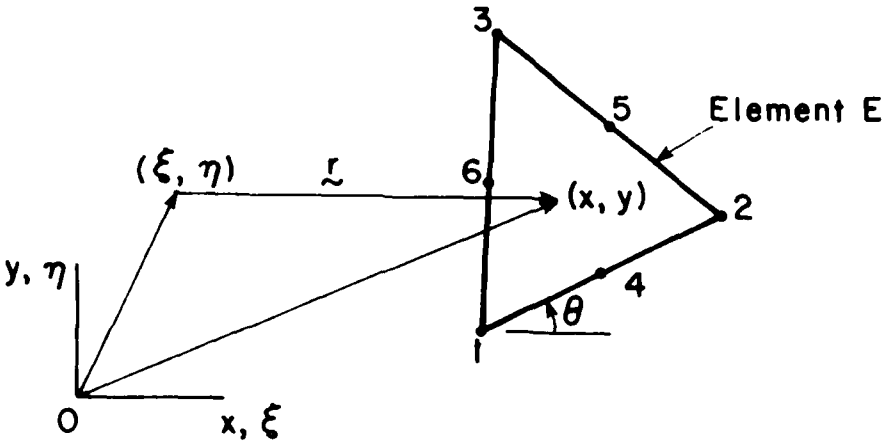

Figure B.1 Six-node triangular element in global coordinates.

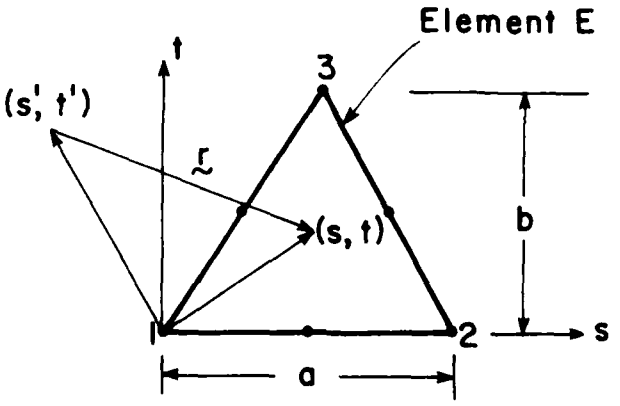

Figure B.2 Translated and rotated coordinates used in nonlocal integration.

$$A = \frac{1}{2}\left(X_2Y_3 + X_3Y_1 + X_1Y_2 - X_2Y_1 - X_3Y_2 - X_1Y_3\right) \tag{B.4}$$

The matrices [K] and [P] in Eq.(3.53) may then be integrated to obtain

$$[P] = \frac{\pi RA}{90}\begin{bmatrix} 6 & & & & & \\ -1 & 6 & & & \text{symm.} & \\ -1 & -1 & 6 & & & \\ 0 & 0 & -4 & 32 & & \\ -4 & 0 & 0 & 16 & 32 & \\ 0 & -4 & 0 & 16 & 16 & 32 \end{bmatrix} \tag{B.5}$$

and

$$[K] = -\frac{1}{A}$$

$-\frac{1}{4}(b_1^2 + c_1^2)$		
$\frac{1}{12}(b_1b_2 + c_1c_2)$	$-\frac{1}{4}(b_2^2 + c_2^2)$	Symmetric
$\frac{1}{12}(b_1b_3 + c_1c_3)$	$\frac{1}{12}(b_2b_3 + c_2c_3)$	$-\frac{1}{4}(b_3^2 + c_3^2)$
$-\frac{1}{3}(b_1b_2 + c_1c_2)$	$-\frac{1}{3}(b_1b_2 + c_1c_2)$	0
0	$-\frac{1}{3}(b_2b_3 + c_2c_3)$	$-\frac{1}{3}(b_2b_3 + c_2c_3)$
$-\frac{1}{3}(b_1b_3 + c_1c_3)$	0	$-\frac{1}{3}(b_1b_3 + c_1c_3)$

$$
\begin{bmatrix}
-\frac{2}{3}\left[b_1^2 + b_2^2 + b_1 b_2 + c_1^2 + c_2^2 + c_1 c_2\right] & & \\
-\frac{1}{3}\left[b_2\,(b_1+b_2+b_3) + c_2\,(c_1+c_2+c_3) + 2\,(b_1 b_3 + c_1 c_3)\right] & -\frac{2}{3}\left[b_2^2 + b_3^2 + b_2 b_3 + c_2^2 + c_3^2 + c_2 c_3\right] & \\
-\frac{1}{3}\left[b_1\,(b_1+b_2+b_3) + c_1\,(c_1+c_2+c_3) + 2\,(b_2 b_3 + c_2 c_3)\right] & -\frac{1}{3}\left[b_3\,(b_1+b_2+b_3) + c_3\,(c_1+c_2+c_3) + 2\,(b_1 b_2 + c_1 c_2)\right] & -\frac{2}{3}\left[b_1^2 + b_3^2 + b_1 b_3 + c_1^2 + c_3^2 + c_1 c_3\right]
\end{bmatrix}
$$

(B.6)

To integrate the weighting functions W_j^E in Eq. (3.55), the element is referred to a new coordinate system (s, t) obtained by the following relationship, Figure B.2,

$$\begin{Bmatrix} s \\ t \end{Bmatrix} = \begin{bmatrix} \cos\theta & \sin\theta \\ -\sin\theta & \cos\theta \end{bmatrix} \begin{Bmatrix} x-x_1^E \\ y-y_1^E \end{Bmatrix} \tag{B.7}$$

$$\begin{Bmatrix} x \\ y \end{Bmatrix} = \begin{bmatrix} \cos\theta & -\sin\theta \\ \sin\theta & \cos\theta \end{bmatrix} \begin{Bmatrix} s \\ t \end{Bmatrix} + \begin{Bmatrix} x_1^E \\ y_1^E \end{Bmatrix} \tag{B.8}$$

Under this transformation,

$$[(x-\xi)^2 + (y-n)^2 + 1]^{3/2} = [(s-s')^2 + (t-t')^2 + 1]^{3/2}$$

$$L_1 = 1-u-(1-c)v, \quad L_2 = u-cv, \quad L_3 = v \tag{B.9}$$

in which

$$u = s/a, \quad v = t/b, \quad c = s_3/a \tag{B.10}$$

The six weighting functions W_j^E may then be written as

$$W_1^E = ab\,[I_1 - 3\,I_u - 3(1-c)\,I_v + 2\,I_{uu} + 4(1-c)\,I_{uv} + 2(1-c)^2\,I_{vv}]$$

$$W_2^E = ab\,[-\,I_u + c\,I_v + 2\,I_{uu} - 4c\,I_{uv} + 2c^2\,I_{vv}]$$

$$W_3^E = ab\,[-\,I_v + 2\,I_{vv}]$$

$$W_4^E = 4ab\,[I_u - c\,I_v - I_{uu} + (2c-1)\,I_{uv} + c(1-c)\,I_{vv}]$$

$$W_5^E = 4ab\,[I_{uv} - c\,I_{vv}]$$

$$W_6^E = 4ab\,[I_v - I_{uv} - (1-c)\,I_{vv}] \qquad (B.11)$$

in which the six basic integrations I_1, I_u, I_v, I_{uu}, I_{uv}, and I_{vv} are:

$$I_1 = \iint_A \frac{dA}{[a^2(u-u')^2+b^2(v-v')^2+1]^{3/2}}$$

$$= \frac{1}{ab} \left\{ \tan^{-1}\,[b^2(1-v')(u'-cv')+c] \cdot \right.$$

$$\cdot \sqrt{\frac{a^2b^2(u'-cv')^2+a^2c^2}{b^2[b^2(1-v')(u'-cv')+c]^2+b^2(u'-c)^2[a^2b^2(u'-cv')^2+a^2c^2+b^2]}} +$$

$$+ \tan^{-1}\,[b^2v'(u'-cv')-c] \cdot$$

$$\cdot \sqrt{\frac{a^2b^2(u'-cv')^2+a^2c^2}{b^2[c-b^2v'(u'-cv')]^2+b^2u'^2[a^2b^2(u'-cv')^2+a^2c^2+b^2]}} +$$

$$+ \tan^{-1}\,\{b^2(1-v')[1-u'-(1-c)v']+(1-c)\} \cdot$$

$$\cdot \sqrt{\frac{a^2b^2[1-u'-(1-c)v']^2+a^2(1-c)^2}{b^2\{b^2(1-v')[1-u'-(1-c)v']+(1-c)\}^2+b^2(c-u')^2\{a^2b^2[1-u'-(1-c)v']^2+a^2(1-c)^2+b^2\}}} +$$

$$+ \tan^{-1}\,\{b^2v'[1-u'-(1-c)v']-(1-c)\} \cdot$$

$$\left. \cdot \sqrt{\frac{a^2b^2[1-u'-(1-c)v']^2+a^2(1-c)^2}{b^2\{(1-c)-b^2v'[1-u'-(1-c)v']\}^2+b^2(1-u')^2\{a^2b^2[1-u'-(1-c)v']^2+a^2(1-c)^2+b^2\}}} \right\}$$

(B.12)

$$I_u = \iint_A \frac{u\ dA}{[a^2(u-u')^2+b^2(v-v')^2+1]^{3/2}} =$$

$$= u'I_1 + \frac{1}{a^2\sqrt{a^2c^2+b^2}} K_1 - \frac{1}{a^2\sqrt{a^2(1-c)^2+b^2}} K_2 \qquad (B.13)$$

$$I_v = \iint_A \frac{v\ dA}{[a^2(u-u')^2+b^2(v-v')^2+1]^{3/2}} =$$

$$= v'I_1 - \frac{c}{b^2\sqrt{a^2c^2+b^2}} K_1 - \frac{1-c}{b^2\sqrt{a^2(1-c)^2+b^2}} K_2 + \frac{1}{ab^2} K_3 \qquad (B.14)$$

$$I_{uu} = \iint_A \frac{u^2\ dA}{[a^2(u-u')^2+b^2(v-v')^2+1]^{3/2}} =$$

$$= (u' - \frac{1}{a^2})\ I_1 + \frac{2(a^2c^2+b^2)u'+a^2c^2(u'-cv')}{a^2(a^2c^2+b^2)\sqrt{a^2c^2+b^2}} K_1 +$$

$$+ \frac{-2[a^2(1-c)^2+b^2]u'+a^2(1-c)^2[1-u'-(1-c)v']}{a^2[a^2(1-c)^2+b^2]\sqrt{a^2(1-c)^2+b^2}} K_2 +$$

$$+ [\frac{u'}{a^2b} + \frac{v'}{a^3}]\ K_3 + \frac{c}{a^2(a^2c^2+b^2)} K_4 + \frac{1-c}{a^2[a^2(1-c)^2+b^2]} K_5 \qquad (B.15)$$

$$I_{uv} = \iint_A \frac{uv\ dA}{[a^2(u-u')^2+b^2(v-v')^2+1]^{3/2}} =$$

$$= u' I_v + \frac{a^2cu'+b^2v'}{a^2(a^2c^2+b^2)\sqrt{a^2c^2+b^2}} K_1 - \frac{a^2(1-c)(1-u')+b^2v'}{a^2[a^2(1-c)^2+b^2]\sqrt{a^2(1-c)^2+b^2}} K_2 +$$

$$+ \frac{1}{a^2(a^2c^2+b^2)} K_4 - \frac{1}{a^2[a^2(1-c)^2+b^2]} K_5 \qquad (B.16)$$

$$I_{vv} = \iint_A \frac{v^2\, dA}{[a^2(u-u')^2+b^2(v-v')^2+1]^{3/2}} =$$

$$= (v'^2 - \frac{1}{b^2})\, I_1 + \frac{b^2(u'-cv')-2(a^2c^2+b^2)cv'}{b^2(a^2c^2+b^2)\sqrt{a^2c^2+b^2}} K_1 +$$

$$+ \frac{b^2[1-u'-(1-c)v']-2[a^2(1-c)^2+b^2](1-c)v'}{b^2[a^2(1-c)^2+b^2]\sqrt{a^2(1-c)^2+b^2}} K_2 +$$

$$+ \frac{2v'}{ab^2} K_3 - \frac{c}{b^2(a^2c^2+b^2)} K_4 - \frac{1-c}{b^2[a^2(1-c)^2+b^2]} K_5 \qquad (B.17)$$

in which

$$K_1 = \ln \left| \frac{\sqrt{(a^2c^2+b^2)[a^2(u'-c)^2+b^2(v'-1)^2+1]} - a^2c(u'-c)-b^2(v'-1)}{\sqrt{(a^2c^2+b^2)(a^2u'^2+b^2v'^2+1)} - a^2cu'-b^2v'} \right| \qquad (B.18)$$

$$K_2 = \ln \left| \frac{\sqrt{[a^2(1-c)^2+b^2][a^2(u'-c)^2+b^2(v'-1)^2+1]} + a^2(1-c)(u'-c)-b^2(v'-1)}{\sqrt{[a^2(1-c)^2+b^2][a^2(1-u')^2+b^2v'^2+1]} - a^2(1-c)(1-u')-b^2v'} \right| \qquad (B.19)$$

$$K_3 = \ell n \left| \frac{\sqrt{a^2(u'-1)^2+b^2v'^2+1} - a(u'-1)}{\sqrt{a^2u'^2+b^2v'^2+1} - au'} \right| \tag{B.20}$$

$$K_4 = \sqrt{a^2(u'-c)^2+b^2(v'-1)^2+1} - \sqrt{a^2u'^2+b^2v'^2+1} \tag{B.21}$$

$$K_5 = \sqrt{a^2(1-u')^2+b^2v'^2+1} - \sqrt{a^2(c-u')^2+b^2(v'-1)^2+1} \tag{B.22}$$

The nonlocal matrix [Q] is calculated numerically by using these six analytic expressions of the weighting function W_j^E within each element. Pure numerical integrations are used to evaluate the nonlocal integrations for (u',v') outside the element.

APPENDIX C

MATRICES AND VECTORS FOR NONLINEAR DYNAMIC ANALYSIS

This appendix summarizes the matrices and vectors for the finite element UL transient nonlinear analysis described in Section 5.1. Details of the derivations are given by Bathe and Bolourchi (Ref. 87).

The interpolation functions for the components of displacement increment in Eq. (5.1) are

$$\begin{Bmatrix} u_1 \\ u_2 \end{Bmatrix} = \begin{vmatrix} 1-\frac{r}{L} & 6\frac{s}{L}\psi_1 & -s\psi_2 & \frac{r}{L} & -6\frac{s}{L}\psi_1 & s\psi_3 \\ 0 & \psi_4 & L\psi_5 & 0 & \psi_6 & -r\psi_1 \end{vmatrix} \{u\} \tag{C.1}$$

in which

$$\{u\} = \lfloor u_1 \; u_2 \; u_3 \; u_4 \; u_5 \; u_6 \rfloor^T \tag{C.2}$$

$$\psi_1 = \frac{r}{L} - \left(\frac{r}{L}\right)^2, \qquad \psi_2 = 1 - 4\frac{r}{L} + 3\left(\frac{r}{L}\right)^2$$

$$\psi_3 = 2\frac{r}{L} - 3\left(\frac{r}{L}\right)^2, \qquad \psi_4 = 1 - 3\left(\frac{r}{L}\right)^2 + 2\left(\frac{r}{L}\right)^3 \tag{C.3}$$

$$\psi_5 = \frac{r}{L} - 2\left(\frac{r}{L}\right)^2 + \left(\frac{r}{L}\right)^3, \qquad \psi_6 = 3\left(\frac{r}{L}\right)^2 - 2\left(\frac{r}{L}\right)^3 ;$$

and in which L is the length of the beam element, r, s are the beam convected coordinates, Figure C.1. The shear deformation is not included in this approximation.

The linear strain-displacement transformation matrix $[{}^tB_L]$ relates the linear part of the strain components to the nodal degrees of freedom

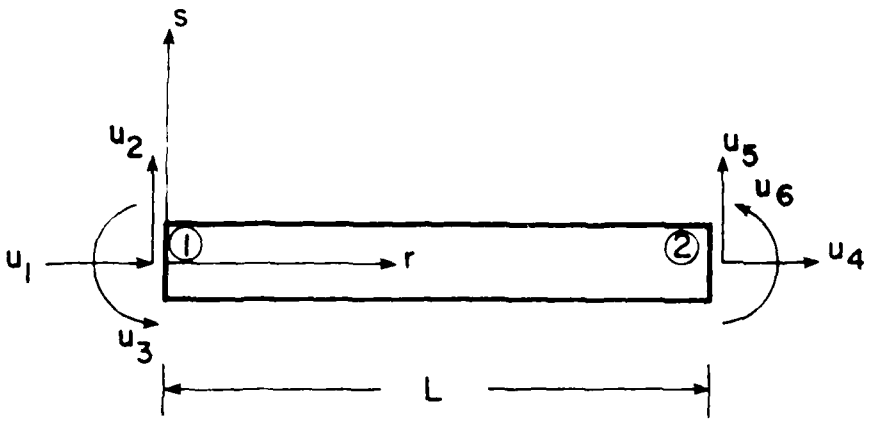

Figure C.1 Convected coordinates and degrees of freedom of beam element.

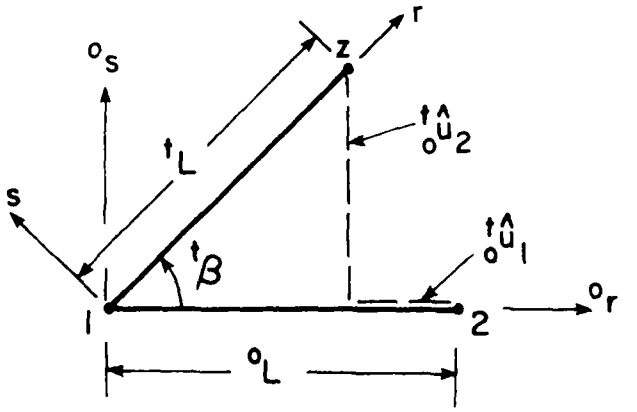

Figure C.2 Current and original local coordinates of beam element.

$$\begin{Bmatrix} e_{11} \\ 2e_{12} \end{Bmatrix} = [{}^{t}B_L] \{u\}, \tag{C.4}$$

and is

$$[{}^{t}B_L] = \begin{bmatrix} -\frac{1}{L} & 6\frac{s}{L^2} & -12\frac{rs}{L^3} & 4\frac{s}{L} & -6\frac{rs}{L^2} & \frac{1}{L} & -6\frac{s}{L^2} & +12\frac{rs}{L^3} & 2\frac{s}{L} & -6\frac{rs}{L^2} \\ 0 & 0 & 0 & 0 & 0 & 0 \end{bmatrix} \{u\} \tag{C.5}$$

The linear stiffness matrix $[{}^{t}K_L]$ is calculated from Eq. (5.3) using $[{}^{t}B_L]$ given above and is the same as the usual linear beam stiffness matrix:

$$[{}^{t}K_L] = E \begin{bmatrix} \frac{A}{L} & & & & & \\ 0 & \frac{12I}{L^3} & & \text{Symm.} & & \\ 0 & \frac{6I}{L^2} & \frac{4I}{L} & & & \\ -\frac{A}{L} & 0 & 0 & \frac{A}{L} & & \\ 0 & -\frac{12I}{L^3} & -\frac{6I}{L^2} & 0 & \frac{12I}{L^3} & \\ 0 & \frac{6I}{L^2} & \frac{2I}{L} & 0 & -\frac{6I}{L^2} & \frac{4I}{L} \end{bmatrix} \tag{C.6}$$

The matrix of Cauchy stresses $[{}_{t}\tau]$ in Eq. (5.4) in this case is

$$[{}_{t}\tau] = \begin{bmatrix} \tau_{11} & 0 & 0 \\ 0 & \tau_{11} & 0 \\ 0 & 0 & 0 \end{bmatrix} \tag{C.7}$$

The nonlinear strain-displacement transformation matrix $[{}^{t}B_{NL}]$ is

$$[{}^{t}B_{NL}] = [b_{ij}]_{3\times 6}$$

$$= \begin{bmatrix} -\frac{1}{L} & 6\frac{s}{L^2} & -12\frac{rs}{L^3} & 4\frac{s}{L} & -6\frac{rs}{L^2} & \frac{1}{L} & -6\frac{s}{L^2} & +12\frac{rs}{L^3} & 2\frac{s}{L} & -6\frac{rs}{L^2} \\ 0 & -6\frac{r}{L^2} & +6\frac{r^2}{L^3} & 1 & -4\frac{r}{L} & +3\frac{r^2}{L^2} & 0 & 6\frac{r}{L^2} & -6\frac{r^2}{L^3} & -2\frac{r}{L} & +3\frac{r^2}{L^2} \\ 0 & 6\frac{r}{L^2} & -6\frac{r^2}{L^3} & -1 & +4\frac{r}{L} & -3\frac{r^2}{L^2} & 0 & -6\frac{r}{L^2} & +6\frac{r^2}{L^3} & 2\frac{r}{L} & -3\frac{r^2}{L^2} \end{bmatrix} \qquad (C.8)$$

The nonlinear stiffness matrix $[{}^{t}K_{NL}]$ in Eq. (5.4) is obtained using $[{}^{t}B_{NL}]$ given above and is shown in Eq. (C.9). The Newton-Cotes quadrature formula is used to integrate $[{}^{t}K_{NL}]$ numerically.

$$[{}^{t}K_{NL}] = \int_{v}$$

$\tau_{11}(b_{11}^2 + b_{21}^2)$		
$\tau_{11}(b_{11}b_{12} + b_{21}b_{22})$	$\tau_{11}(b_{12}^2 + b_{22}^2)$	
$\tau_{11}(b_{11}b_{13} + b_{21}b_{23})$	$\tau_{11}(b_{12}b_{13} + b_{22}b_{23})$	$\tau_{11}(b_{13}^2 + b_{23}^2)$
$\tau_{11}(b_{11}b_{14} + b_{21}b_{24})$	$\tau_{11}(b_{12}b_{14} + b_{22}b_{24})$	$\tau_{11}(b_{13}b_{14} + b_{23}b_{24})$
$\tau_{11}(b_{11}b_{15} + b_{21}b_{25})$	$\tau_{11}(b_{12}b_{15} + b_{22}b_{25})$	$\tau_{11}(b_{13}b_{15} + b_{23}b_{25})$
$\tau_{11}(b_{11}b_{16} + b_{21}b_{26})$	$\tau_{11}(b_{12}b_{16} + b_{22}b_{26})$	$\tau_{11}(b_{13}b_{16} + b_{23}b_{26})$

Symmetric

$$\begin{bmatrix} \tau_{11}(b_{14}^2 + b_{24}^2) & & \\ \tau_{11}(b_{14}b_{15} + b_{24}b_{25}) & \tau_{11}(b_{15}^2 + b_{25}^2) & \\ \tau_{11}(b_{14}b_{16} + b_{24}b_{26}) & \tau_{11}(b_{15}b_{16} + b_{25}b_{26}) & \tau_{11}(b_{16}^2 + b_{26}^2) \end{bmatrix} dV \qquad (C.9)$$

The vector of Cauchy stresses $\{{}_t\hat{\tau}\}$ in Eq. (5.5) is

$$\{{}_t\hat{\tau}\} = \lfloor \tau_{11} \; \tau_n \rfloor^T \tag{C.10}$$

in which τ_{12} has been set to zero. The Newton-Cotes formula is also used to integrate the vector of nodal point forces $\{{}^tF\}$ given below.

$$\{{}^tF\} = \int_V \begin{vmatrix} \tau_{11}(-\frac{1}{L}) \\ \tau_{11}(6\frac{s}{L^2} - 12\frac{rs}{L^3}) \\ \tau_{11}(4\frac{s}{L} - 6\frac{rs}{L^2}) \\ \tau_{11}(\frac{1}{L}) \\ \tau_{11}(-6\frac{s}{L^2} + 12\frac{rs}{L^3}) \\ \tau_{11}(2\frac{s}{L} - 6\frac{rs}{L^2}) \end{vmatrix} dV \tag{C.11}$$

The element stiffness equations must be transformed to global coordinates before they are assembled into a set of global equations. The transformation matrix from local to global coordinates is

$$[{}^tR] = [{}^t\bar{R}] \; [{}^0R] \tag{C.12}$$

in which $[{}^0R]$ is the transformation matrix from the original local coordinates of the element to the global coordinates, and $[{}^t\bar{R}]$ is the transformation matrix from the current to the original local coordinates of the beam element. $[{}^t\bar{R}]$ is given by

$$[{}^t\bar{R}] = \begin{vmatrix} {}^t\hat{R} & 0 \\ 0 & {}^t\hat{R} \end{vmatrix} \tag{C.13}$$

in which

$$[{}^{t}\hat{R}] = \begin{vmatrix} \cos{}^{t}\beta & \sin{}^{t}\beta & 0 \\ -\sin{}^{t}\beta & \cos{}^{t}\beta & 0 \\ 0 & 0 & 1 \end{vmatrix} \tag{C.14}$$

with

$$\sin{}^{t}\beta = {}^{t}_{o}\hat{u}_2/{}^{t}L$$

$${}^{t}L = [({}^{o}L + {}^{t}_{o}\hat{u}_1)^2 + ({}^{t}_{o}\hat{u}_2)^2]^{1/2} \tag{C.15}$$

as shown in Figure C.2.

The element matrices and vectors in global coordinates are $[{}^{t}R]^T[{}^{t}K][{}^{t}R]$, $[{}^{t}R]^T\{{}^{t}F\}$, and $[{}^{t}R]^T\{u\}$, respectively, in which

$$[{}^{t}K] = [{}^{t}K_L] + [{}^{t}K_{NL}].$$

The element stress increments are calculated by using the following strain increment

$$e_{11} = \sum_{\substack{j=2 \\ j\neq 4}}^{6} {}^{t}B_{L_{1j}}\, u_j + \frac{1}{{}^{o}L}\,({}^{t}L - {}^{t-\Delta t}L) \tag{C.16}$$

The total element stresses are updated by using

$${}^{t+\Delta t}\tau_{11} = {}^{t}\tau_{11} + E\, e_{11} \tag{C.17}$$

REFERENCES

1. Brown, W. F., Magnetoelastic Interactions. Springer-Verlag, New York, 1966.

2. Toupin, R. A.,The Elastic Dielectric, J. Rational Mechanics and Analysis. Vol. 5, 1956, p. 849-915.

3. Toupin, R. A.,A Dynamic Theory of Elastic Dielectrics, Int. J. Engineering Science. Vol. 1, 1963, p. 101-126.

4. Tiersten, H. F., Coupled Magnetomechanical Equations for Magnetically Saturated Insulators, J. Mathematical Physics. Vol. 5, 1964, p. 1298-1318.

5. Tiersten. H. F., Variational Principle for Saturated Magnetoelastic Insulators, J. Mathematical Physis. Vol. 6, 1965, p. 779-787.

6. Pao, Y. H., Electromagnetic Forces in Deformable Continua, Mechanics Today. Vol. 4, S. Nemat-Nasser (ed.), Pergamon Press, 1978.

7. Penfield, P., and Hans, H. A., Electrodynamics of Moving Media. MIT Press, Cambridge, Mass., 1967.

8. Truesdell, C., and Toupin, R. A., The Classical Field Theories, Handbuchder Physik. Vol. III/1, S. Flügge (ed.), Springer-Verlag, Berlin, 1960.

9. Parkus, H., Variational Principles in Thermo- and Magneto-elasticity, CISM Course 58, Springer-Verlag, Wien, 1970.

10. Parkus, H., Magneto- Thermoelasticity. CISM Course 118, Springer-Verlag, Wien, 1972.

11. Parkus, H.,(ed.). Electromagnetic Interactions in Elastic Solids. CISM Course 257, Springer-Verlag, Wien, 1979.

12. Hutter, K., and Van de Ven, A. A. F., Field Matter Interaction in Thermoelastic Solids. (Lecture Notes in Physics: Vol. 88), Springer-Verlag, 1979.

13. Alblas, J. B., Electro- Magneto- Elasticity, Topics in Applied Continuum Mechanics. Zeman, J. L., and Ziegler, F. (eds.), Springer-Verlag, Wien, 1974.

14. Eringen, A. C.,(ed.). Continuum Physics. 4 Volumes, Academic Press, Vol. 1, 1971; Vol. 2, 1975; Vol. 3, 1976; Vol. 4, 1976.

15. Knopoff, L., The Interaction between Elastic Wave Motions and a Magnetic Field in Electric Conductors, J. Geophysical Research. Vol. 60, 1955, p. 441.

16. Wilson, A. J., The Propogation of Magnetothermoelastic Plane Waves, Proc. Camb. Phil. Soc. Vol. 59, 1963, p. 483.

17. Kaliski, S., and Petykiewicz, J., Dynamical Equations of Motion and Solving Functions for Elastic and Inelastic Anisotropic Bodies in the Magnetic Field, Proc. Vibration Problems. No. 2, Vol. 1, 1959/1960, p. 15-35.

18. Dunkin, J. W., and Eringen, A. C., On the Propogation of Waves in an Electromagnetic Elastic Solid, Int. J. Engineering Science. Vol. 1, 1963, p. 461-495.

19. Paria, G., Magnetoelasticity and Magnetothermoelasticity, Advances in Applied Mechanics. Vol. 10, Kuerti, G. (ed.), Academic Press, N.Y., 1967, p. 73-112.

20. Montgomery, D.B., Solenoid Magnet Design. Wiley-Interscience, N.Y., 1969.

21. Brechna, Superconducting Magnet Systems. Springer-Verlag, N.Y., 1973.

22. Woodson, H. H., and Melcher, J. R., Electromechanical Dynamics, Parts I, II, III, John Wiley & Sons, N.Y., 1968.

23. Melcher, J. R., Continuum Electromechanics. MIT Press, 1981.

24. Becker, E. B., and Pillsbury, R. D., Finite Element Analysis of Coupled Electric, Magnetic, and Dynamic Problems, Formulations and Computational Algorithms in Finite Element Analysis. Bathe, K. J., et. al. (eds.), MIT Press, 1977, p. 1059-1083.

25. Moon, F. C., Problems in Magneto-Solid Mechanics, Mechanics Today. Nemat-Nasser, S., (ed.), American Academy of Mechanics, Nov. 1977.

26. Moon, F. C., and Swanson, C., Experiment on Buckling and Vibration of Superconducting Coils, ASME Paper No. 77-WA/APM-28, J. Applied Mechanics, Dec. 1977.

27. Moon, F. C., and Swanson, C., Vibration and Stability of a Set of Superconducting Toroidal Magnets, J. Applied Physics. Vol. 47, No. 3, March 1976, p. 914-919.

28. Miya, K., An, S., Ando, Y., Ohta, M., and Suzuki, Y., Application of Finite Element Method to Electro-Magneto-Mechanical Dynamics of Superconducting Magnet Coil and Vacuum Vessel, Proc. 6th Symp. of Engineering Problems of Fusion Research. Nov. 1975, Publ. IEEE, N.Y., 1976, p. 927-934.

29. Moon, F. C. (ed.), Mechanics of Superconducting Structures. ASME Applied Mechanics Symposia Series, AMD-Vol. 41, ASME, 1980.

30. Hutter, K., and Pao, Y. H., A Dynamic Theory for Magnetizable Elastic Solids With Thermal and Electrical Conduction, J. Elasticity. Vol. 4, 1974, p. 89.

31. Hutter, K., Electrodynamics of Deformable Continua, Ph.D. Thesis, Cornell University, Ithaca, N.Y., 1973.

32. Jackson, J. D., Classical Electrodynamics. John Wiley & Sons, N.Y., 1962.

33. Landau, E., and Lifshitz, M., Electrodynamics of Continuous Media. Pergaman Press, 1960.

34. Bathe, K. J., and Ramm, E. L., Finite Element Formulations for Large Deformation Dynamic Analysis, Int. J. Numerical Methods in Engineering. Vol. 9, 1975, p. 353-386.

35. Van de Ven, A. A. F., Interaction of Electromagnetic and Elastic Fields in Solids, Dr. of Science Thesis, Technische Hogeschool Eidenhoven, The Netherlands, 1975.

36. Ambartsumyan, S. A., Bagdasaryan, G. E., and Belubekyan, M. V., Magnetoelasticity of Thin Shells and Plates, (in Russian), Fizmatgiz, Moscow, 1977.

37. Moon, F. C., Vibrations of Current Carrying Plates, Reseach Report 974-AMS, Dept. of Aerospace and Mechanical Sciences, Princeton University, March, 1971.

38. Malvern, L. E., Introduction to the Mechanics of a Continuous Medium. Prentice-Hall, Englewood Cliffs, N.J., 1969.

39. Panovko, Y. G., and Gubanova, I. I., Stability and Oscillations of Elastic Systems. (English translation of Russian), Consultants Bureau, N.Y., 1965.

40. Moon, F. C., and Pao, Y. H., Magnetoelastic Buckling of a Thin Plate, J. Applied Mechanics. Vol. 35, No. 1, 1968, p. 53-58.

41. Pao, Y. H., and Yeh, C. S., A Linear Theory for Soft Ferromagnetic Elastic Solids, Int. J. Engineering Science. Vol. 11, No. 4, April 1973, p. 415.

42. Kaliski, S., Quasi-static Approximation to the Equation of Elastic Vibration in a Ferromagnetic Plate under the Action of a Transverse Magnetic Field, Bull. de l'Academic Polonaise des Sci. Vol. XVII, No. 9, 1969, p. 411-418.

43. Moon, F. C., and Pao, Y. H., Vibration and Dynamic Instability of a Beam-Plate in a Transverse Magnetic Field, J. Applied Mechanics. Vol. 36, No. 1, 1969, p. 92-100.

44. Moon, F. C., The Mechanics of Ferroelastic Plates in a Uniform Magnetic Field, J. Applied Mechanics. Vol. 37, No. 1, 1970, p. 153-158.

45. Srinivasan, S., Vibration and Stability of Beams and Plates in the Presence of Electromagnetic Fields, Ph.D. Thesis, Ohio State University, Columbus, Ohio, 1970.

46. Ambartsumyan, S. A., On the Problem of Oscillations of the Electro-conductive Plates in the Transverse Magnetic Field, Theory of Shells. Koiter, W. T., and Mikhailov, G. K. (eds.), North-Holland Publishing Company, 1980,

47. Ambartsumyan, S. A., Theory of Anisotropic Plates. (English translation of Russian), Technomic Publishing Company, Inc., 1970.

48. Edelen, D. G. B., Nonlocal Variational Mechanics, I-VIII, Int. J. Engineering Science. Vol. 7, 1969.

49. Sommerfeld, A., Electrodynamics. Lectures on Theoretical Physics, Vol. III, Academic Press, 1952.

50. Williams, L. P., The Origins of Field Theory. Random House, N.Y., 1966.

51. Smythe, W. R., Static and Dynamic Electricity. Third Edition, McGraw Hill, Chapter X, 1968.

52. Stoll, R. L., The Analysis of Eddy Currents. Clarendon Press, Oxford, 1974.

53. Lammerauer, J., and Stasl, M., Eddy Currents. Illiffe Book Ltd., London, 1966.

54. Chari, M. V. K., and Silvester, P. P. (eds.), Finite Elements in Electrical and Magnetic Field Problems. John Wiley and Sons, N.Y., 1980.

55. Silvester, P., and Haslam, C. R. S., Magnetotelluric Modelling by the Finite Element Method, Geophysical Prospecting. Vol. 20, 1972, p. 872-891.

56. Chari, M. V. K., Finite Element Solution of the Eddy Current Problem in Magnetic Structures, IEEE Trans., Vol. PAS-93, No. 1, 1973.

57. Salon, S. J., and Schneider, J. M., The Application of a Finite Element Formulation of the Electric Vector Potential to Eddy Current Losses, IEEE Paper A79-545-5, 1979.

58. Salon, S. J., and Schneider, J. M., A Comparison of Boundary Integral and Finite Element Formulations of the Eddy Current Problems, IEEE Paper 80 SM 526-4, 1980.

59. Silvester, P., Eddy Current Modes in Linear Solid-Iron Bars, Proc. IEE (London). Vol. 112, No. 8, August 1965, p. 1589-1594.

60. Silvester, P., Modal Network Theory of Skin Effect in Flat Conductors, Proc. IEEE. Vol. 54, No. 9, Sept. 1966, p. 1147-1151.

61. Silvester, P., Wong, S. K., and Burke, P. E., Modal Theory of Skin Effect in Single and Multiple Turn Coils, IEEE Trans., Vol. PAS-91, 1972, p. 29-34.

62. Konrad, A., Coulomb, J. L., Sabonnadiere, J. C., and Silvester, P., Finite Element Analysis of Steady-State Skin Effect in a Slot-embedded Conductor, IEEE Winter Meeting, N.Y., Paper No. A 76 189-1, 1976.

63. Silvester, P., and Popovic, B. D., The Integral Equations of Superconduction Levitation Systems, Digests of the Intermag. Conf. Int. Magnetics Conf., IEEE, Toronto, Canada, May 1974, p. 19.9

64. Schaffer, G., and Banderet, P., Skin Effect in Heavy-Current Conductor Bars, Brown Boveri Rev. Vol. 52, 1965, p. 623-628.

65. Silvester, P., Dynamic Resistance and Inductance of Slot-embedded Conductors, IEEE Trans., Vol. PAS-87, 1968, p. 250-256.

66. Gopinath, A., and Silvester, P., Calculation of Inductance of Finite-Length Strips and Its Variation with Frequency, IEEE Trans., Vol. MIT-21, 1973, p. 380-386.

67. Biddlecombe, C. S., Collie, C. J., Simkin, J., and Trowbridge, C. W., The Integral Equation Method Applied to Eddy Currents, RL-76-043, Rutherford Laboratory. Also Proc. COMPUMAG Conf., Oxford, 1976.

68. Donea, J., Giuliani, S., and Philippe, A., Finite Elements in the Solution of Electromagnetic Induction Problems, Int. J. Numerical Methods in Engineering. Vol. 8, 1974, p. 359-367.

69. Palanisamy, R., and Lord, W., Finite Element Modelling of Electro-Magnetic NDT Phenomena, IEEE Trans. on Magnetics. Vol. Mag-15, No. 6, 1979, p. 1479-1481.

70. Nehl, T. W., and Demerdash, N. A., Application of Finite Element Eddy Current Analysis to Nondestructive Detection of Flaws in Metallic Structures, Proc. of INTERMAG 80, N.Y., 1980.

71. Lord, W., and Hwang, J. H., Finite Element Modelling of Magnetic Field/Defect Interactions, ASTM J. Testing and Evaluation, 3:21, 1975.

72. Turner, L. R., An Integral Equation Approach to Eddy Current Calculation, IEEE Trans. Mag., MAG-13, 1978, p. 1119.

73. Turner, L. R., and Lari, R. J., Developments of the Eddy Current Program EDDYNET, Proc. COMPUMAG Conf. on the Computation of Magnetic Fields, Grenoble, 1978.

74. Turner, L. R., Lari, R.J., and Sandy, G. L., Eddy Current Simulation in Prisms, Plates, and Shells with the Program EDDYNET, Symp. on Eddy Current Characterizations of Materials and Structures. Gaithersburg, MD, 1979.

75. Kameari, A., and Suzuki, Y., Eddy Current Analysis by the Finite Element Circuit Method, Proc. 7th Symp. on Engineering Problems of Fusion Research. Knoxville, Tenn., USA, 1977, p. 1386-1392.

76. Compter, J.C., and Hamels, D., Analysis of an Actuator System Consisting of a Coil and a Movable Conducting Disk, Using Network Representations, Electric Machines and Electromechanics. Vol. 5, 1980, p. 257-271.

77. Carpenter, C. J., Finite Element Network Models and Their Application to Eddy Current Problems, Proc. IEE. Vol. 122, No. 4, 1975.

78. Carpenter, C. J., and Djurovic, M., Three-Dimensional Numerical Solution of Eddy Currents in Thin Plates, Proc. IFE. Vol. 122, No. 6, 1975.

79. Hammond, P., and Penman, J., Calculation of Eddy Currents by Dual Energy Methods, Proc. IEE. Vol. 125, No. 7, 1978.

80. De Mey, G., A Method for Calculating Eddy Currents in Plates of Arbitrary Geometry, Archiv. für Elektrotechnik. Vol. 56, 1974, p. 137-140.

81. Lachat, J. C., and Watson, J. O., Effective Numerical Treatment of Boundary Integral Equations: A Formulation for Three-Dimensional Elastostatics, Int. J. Numerical Methods in Engineering. Vol. 10, 1976, p. 991-1005.

82. Jeng, G., and Wexler, A., Isoparametric, Finite Element, Variational Solution of Integral Equations for Three-Dimensional Fields, Int. J. Numerical Methods in Engineering. Vol. 11, 1977, p. 1455-1471.

83. Hara, K., Parameter Study on Eddy Current Problems, Size Effect on Induced Current, Term Project Report in Course CEE G713-Finite Element Analysis, Cornell University, Ithaca, N.Y., Spring, 1981.

84. Mukherjee, S., and Morjaria, M., Boundary Element Analysis of Time-Dependent Inelastic Deformation of Cracked Plates Loaded in Anti-Plane Shear, Theoretical and Applied Mechanics Report, Cornell University to Dept. of Energy (No. C00-2733-28), July 1980.

85. Felippa, C. A., and Park, K. C., Staggered Transient Analysis Procedures for Coupled Mechanical Systems: Formulation, Computer Methods in Applied Mechanics and Engineering. Vol. 24, 1980, p. 61-111.

86. Bishop, R. E. D., and Johnson, D. C., Vibration Analysis Tables. Cambridge University Press, 1956.

87. Bathe, K. J., and Bolourchi, S., Large Displacement Analysis of Three-Dimensional Beam Structures, Int. J. Numerical Methods in Engineering. Vol. 14, 1979, p. 961-986.

88. McGuire, W., and Gallagher, R. H., Matrix Structural Analysis. John Wiley and Sons, 1979.

89. Bathe, K. J., and Cimento, A. P., Some Practical Procedures for the Solution of Nonlinear Finite Element Equations, Computer Methods in Applied Mechanics and Engineering. Vol. 22, 1980, p. 59-85.

90. Hibbitt, H. D., Some Follower Forces and Load Stiffness, Int. J. Numerical Methods in Engineering. Vol. 14, 1979, p. 937-941.

91. Burgreen, D., Free Vibrations of a Pin-Ended Column With Constant Distance Between Pin Ends, J. Applied Mechanics. Vol. 72, No. 6, 1951, p. 135-139.

92. Woinowsky-Krieger, S., The Effect of an Axial Force on the Vibration of Hinged Bars, J. Applied Mechanics. Vol. 72, No. 3, 1950, p. 35-36.

93. Belytschko, T., Osias, J. R., and Marcal, P. V. (eds.), Finite Element Analysis of Transient Nonlinear Structural Behavior, ASME Applied Mechanics Symposia Series, AMD - Vol. 14, ASME, 1975.

94. McNamara, J. F., Solution Schemes for Problems of Nonlinear Structural Dynamics, J. Pressure Vessel Technology, ASME, Vol. 96, No. 2, May 1974, p. 96-102.

95. Belytschko, T., and Schoeberle, D. T., On the Unconditional Stability of an Implicit Algorithm for Nonlinear Structural Dynamics, J. Applied Mechanics. Dec. 1975, p. 865-869.

96. Adeli, H., Gere, J. M., Weaver, W., Algorithms for Nonlinear Structural Dynamics, J. Structural Division, ASCE, No. ST2, Feb. 1978, p. 263-280.

97. Belytschko, T., and Hsieh, B. J., Nonlinear Transient Finite Elements Analysis With Convected Coordinates, Int. J. Numerical Methods in Engineering. Vol. 17, 1973, p. 255-271.

98. Braekhus, J., and Aasin, J. O., Experiments with Direct Integration Algorithms for Ordinary Differential Equations in Structural Dynamics, Computer and Structures. Vol. 13, 1981, p. 91-96.

99. Matthies, H., and Strang, G., The Solution of Nonlinear Finite Element Equations, Int. J. Numerical Methods in Engineering. Vol. 14, 1979, p. 1613-1626.

100. Bathe, K. J., and Wilson, E. L., Numerical Methods in Finite Element Analysis. Prentice-Hall, Inc., 1976.

101. Hara, K., and Moon, F. C., Unpublished experimental results to appear in technical report to be submitted to ONR.

102. Yuan, K. Y., Moon, F. C., and Abel, J. F., Numerical Solutions for Coupled Magnetomechanics, Department of Structural Engineering Report Number 80-5, Cornell University, February 1980.

COMPOSITE LIST OF TECHNICAL REPORTS

TO THE

OFFICE OF NAVAL RESEARCH

NUMERICAL SOLUTIONS FOR COUPLED MAGNETOTHERMOMECHANICS

Task Number NR 064-621

Departments of Structural Engineering and
Theoretical and Applied Mechanics,
Cornell University,
Ithaca, New York 14853

1. K.Y. Yuan, F.C. Moon, and J.F. Abel, "Numerical Solutions for Coupled Magnetomechanics", Department of Structural Engineering Report Number 80-5, February 1980.

2. F.C. Moon and K. Hara, "Detection of Vibrations in Metallic Structures Using Small Passive Magnetic Fields", January 1981.

3. S. Mukherjee, M.A. Morjaria, and F.C. Moon, "Eddy Current Flows Around Cracks in Thin Plates for Nondestructive Testing", March 1981.

4. K.Y. Yuan, F.C. Moon, and J.F. Abel, "Finite Element Analysis of Coupled Magnetomechanical Problems of Conducting Plates", Department of Structural Engineering Report Number 81-10, May 1981.

5. F.C. Moon, "The Virial Theorem and Scaling Laws for Superconducting Magnet Systems", May 1981.

6. K.Y. Yuan, "Finite Element Analysis of Magnetoelastic Plate Problems", Department of Structural Engineering Report Number 81-14, August 1981.

7. K.Y. Yuan et al., "Two Papers on Eddy Current Calculations in Thin Plates", September 1981.

END

DATE
FILMED

3-82

DTIC